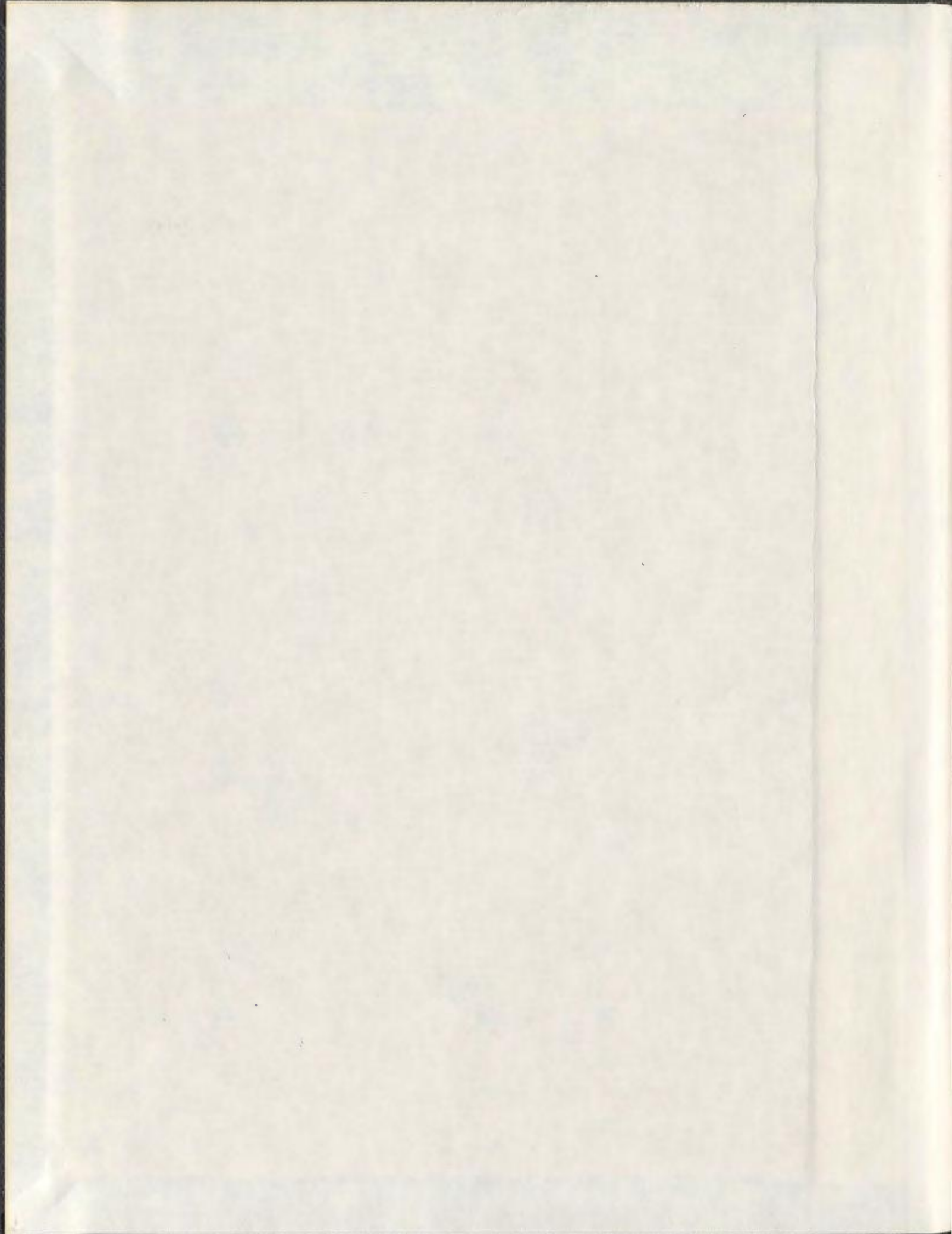


ELASTODYNAMIC AND FINITE ELEMENT
ANALYSIS OF COUPLED LATERAL-AXIAL VIBRATION
OF A DRILLSTRING WITH A DOWNHOLE VIBRATION
GENERATOR AND SHOCK SUB

AHMAD GHASEMLOONIA



**Elastodynamic and Finite Element Analysis of Coupled Lateral-Axial Vibration of a
Drillstring with a Downhole Vibration Generator and Shock Sub**

by

© Ahmad Ghasemloonia

A Dissertation submitted to the

School of Graduate Studies

in partial fulfillment of the requirements for the degree of

Doctor of Philosophy

Faculty of Engineering and Applied Science

Memorial University of Newfoundland

August 2013

St. John's

Newfoundland

ABSTRACT

Axial vibration generators improve oilwell drilling efficiency by reducing drillstring-wellbore friction. However, tool vibration can cause unwanted vibrations of the drillstring, and thus premature failure of components. The only effective way to benefit from the positive consequences of these tools is to develop vibration models to predict the vibration pattern of the drillstring for any mode of interest, and implement suppression tools, such as a shock sub to isolate the imposed vibration from the rest of the drillstring.

Transverse vibration, which is coupled to axial vibration, is the main cause of premature failure of drillstrings. Nonlinear coupled axial-transverse vibration of a drillstring with a downhole vibration generator and shock sub is investigated. Analytical elastodynamic and finite element models are developed.

The Newtonian approach and the “Bypassing PDEs” method were implemented in developing the analytical models and the ABAQUS *Explicit* solver package[®] was used to develop finite element method (FEM) models. The bottom-hole assembly was assumed as a multi-span bottom-hole assembly (BHA) and realistic boundary conditions were assumed. The lateral comparison functions for a multi-span BHA and axial comparison functions for a system of hybrid continuous (step-beam drillstring) and discrete elements (springs and dampers of the shock sub and the equivalent top boundary condition) were developed analytically. The effects of mud damping, spatially varying axial force along the drillstring, bit-rock interaction and lateral contacts were included. Nonlinearities due

to strain energy, geometry, axial stiffening and Hertzian contact forces were also captured in the models.

The simulation results were used to extract modal characteristics and analyze the downhole vibration trends of a drillstring with a shock sub and vibrating tool installed on the BHA. Multi-mode analysis in the expanded Galerkin's method with accurate comparison functions enabled a multi-point contact analysis, multi mode modal dynamic analysis, and prediction of more realistic critical rotary speeds. A simulated shock sub effectively isolated the vibrating tool from the drillstring, while amplifying the tool force at the bit. Analytical and FEM models showed excellent agreement. The models in their current form can be used to guide the design of drillstrings and to predict drilling parameters such as speed and weight-on-bit (WOB) that will result in acceptable vibration levels.

ACKNOWLEDGEMENTS

I would like to express profound gratitude to my supervisors, Dr. Geoff Rideout and Dr. Stephen Butt, for their expert guidance, encouragement and supports throughout this research work. I gratefully acknowledge their technical expertise, as well as their immense patience, which enabled me to complete my Ph.D. successfully. I am also grateful to the remaining member of my doctoral committee, Dr. Katna Munaswamy for his valuable comments and suggestions. In addition, I would like to acknowledge the valuable comments for development of the analytical model made by Dr. Neil Hookey, Dr. Seshu Adluri, Dr. Yuri Muzychka at Memorial University and Dr. Ali Hajnayeb at Chamran University.

In my daily work, I have been blessed with friendly and cheerful fellow students at the Advanced Drilling Group whom I would also like to gratefully acknowledge especially the project manager Farid Arvani for his support and encouragements.

I would also like to thank Husky Energy, Suncor Energy, The Atlantic Canada Opportunities Agency and The Research, Mitacs and Development Corporation of Newfoundland and Labrador (AIF Contract No. 781-2636-1920044) for funding this research over the past four and a half years. Additionally, I would like to acknowledge the financial support provided by the School of Graduate Studies at Memorial University.

Last but not least, I am as ever, indebted to my mother Narjes, my brother Amir, and my sister Nahid, to whom I owe much of what I have become. I thank them for their love,

support and confidence throughout my life. They taught me to value honesty and humility above all other virtues.

Philosophy is written in this grand book — I mean the universe — which stands continually open to our gaze, but it cannot be understood unless one first learns to comprehend the language and interpret the characters in which it is written. It is written in the language of mathematics, and its characters are triangles, circles, and other geometrical figures, without which it is humanly impossible to understand a single word of it; without these, one is wandering around in a dark labyrinth.

Galileo Galilei, 1623

Table of Contents

ABSTRACT.....	ii
ACKNOWLEDGEMENTS.....	iv
Table of Contents.....	vii
List of Tables.....	xiv
List of Figures.....	xv
List of Appendices.....	xxi
1 Introduction and Problem Statement.....	1
1.1 Introduction.....	1
1.2 Statement of the Problem.....	2
1.3 Thesis Statement.....	6
1.4 Research Plan and Objectives.....	8
1.5 References.....	14
2 Technical Background.....	16
2.1 Introduction.....	16
2.2 Drilling Engineering.....	16
2.3 Drilling Enhancement Techniques: Percussion Drilling.....	18
2.4 Drilling Enhancement Techniques: Vibration-Assisted Rotary Drilling.....	20
2.5 Fundamentals of Oilwell Drilling and Drilling Tools.....	23

vii

2.6	The Vibration Behavior of the Drillstring	27
2.6.1	Axial vibration of the drillstring	29
2.6.2	Torsional Vibration of the Drillstring	35
2.6.3	Transverse Vibration of the Drillstring	39
2.6.4	Coupled Modes of the Drillstring Vibration	44
2.7	Vibration Isolation Methods for the Drillstring	47
2.8	Formulation of Equations of Motion: Newtonian and Energy Variational Approaches	49
2.9	The “Bypassing PDEs” Method	53
2.10	Solution Methods of Drillstring Analytical Models	54
2.11	Dynamic Finite Element Analysis (FEA) of the Drillstring	59
2.12	References	63
3	The Effect of Weight on Bit on the Contact Behavior of Drillstring and Wellbore .	79
3.1	Abstract	79
3.2	Introduction	80
3.3	Analytical Overview of the Problem	82
3.4	Bond Graph Modeling of the Drillstring	85
3.5	Modeling Results	88
3.6	Conclusions	92

3.7	References	93
3.8	Biography	94
3.9	Appendix 3.1	96
4	Coupled Transverse Vibration Modeling of Drillstrings Subjected to Torque and Spatially Varying Axial Load	97
4.1	Abstract	97
4.2	Introduction	98
4.3	Literature Review	101
4.4	Derivation of Governing Equations	103
4.5	Analytical Solution of the Equations	108
4.6	Application of the FEM Method to the Transverse Vibration of the Drillstring	117
4.7	Determination of Appropriate Model Order	120
4.8	Conclusions	123
4.9	Funding Acknowledgment	124
4.10	References	124
4.11	Appendix 4.1: Nomenclature	128
4.12	Appendix 4.2: Analytical Equations	128
4.13	Appendix 4.3: Axial Force in the Collar Section	131

5	Analysis of Multi-Mode Nonlinear Coupled Axial-Transverse Drillstring Vibration in Vibration Assisted Rotary Drilling	133
5.1	Abstract	133
5.2	Introduction	135
5.3	Literature Review	137
5.4	Derivation of Governing Equations	144
5.4.1	Energy Equations for the BHA and the Pipe Sections.....	147
5.4.2	Eigenfunctions and Eigenfrequencies of a Three Span Beam with Different Lengths	152
5.5	Lagrangian and Equations of Motion.....	155
5.6	Numerical Results	156
5.7	Conclusions	169
5.8	Acknowledgment	170
5.9	References	170
6	Vibration Analysis of a Drillstring in Vibration-Assisted Rotary Drilling-Finite Element Modeling With Analytical Validation	175
6.1	Abstract	175
6.2	Introduction	177
6.3	Literature Review	179

6.4 Review of the Analytical Drillstring Model- Deriving the Governing Equations ..	187
6.5 Dynamic Finite Element Model of the Drillstring	191
6.5.1 Appropriate Model Order and Mesh Sensitivity Analysis (h-method).....	198
6.6 Numerical Results and Discussion.....	200
6.6.1 Modal Order Detection and Mesh Sensitivity Analysis Results.....	210
6.7 Conclusions	213
6.8 Acknowledgment	215
6.9 References	215
6.10 Appendix 6.1: Energy terms for the first span of the BHA.....	220
6.11 Appendix 6.2: Energy terms for the pipe section.....	222
6.12 Appendix 6.3: Lagrangian of the BHA and the pipe section	222
6.13 Appendix 6.4: Eigenfunctions and eigenfrequencies of a three span beam with different lengths	224
6.14 Nomenclature	226
7 Elastodynamic and Finite Element Vibration Analysis of a Drillstring with a Downhole Vibration Generator Tool and a Shock Sub	228
7.1 Abstract	228
7.2 Introduction	230
7.3 Literature Review	234

7.3.1	Downhole Vibration Generator Tools.....	234
7.3.2	Shock Subs and Drillstring Axial Vibration Decoupling.....	236
7.3.3	Analytical Modeling	237
7.3.4	Dynamic Finite Element Modeling (FEM).....	243
7.4	Analytical Modeling: Derivation of Governing Equations	246
7.4.1	Eigenfunctions and Eigenfrequencies of the Axial Motion of the Drillstring 255	
7.4.2	The Lagrange's Equation and Equations of Motion.....	260
7.5	Dynamic Finite Element Model of the Drillstring	262
7.6	Numerical Results and Discussion.....	267
7.7	Conclusions	282
7.8	Acknowledgment	284
7.9	References	285
7.10	Nomenclature	292
8	Concluding Remarks.....	294
8.1	Summary	294
8.2	Concluding Remarks	295
8.3	Dissertation Highlights and Contributions	299
8.4	Future Research Recommendations	301

Appendix 1: Buoyant Force Treatment in the Drillstring	304
Appendix 2: Hamilton's Principle and Lagrange's Equation	310
Appendix 3: Hamilton's Principle versus the "Bypassing PDEs" Method for Continuous Systems- A Case Study	317
Appendix 4: FEM Modeling of the Drillstring-A Case Study	323
Appendix 5: List of Assumptions in the Developed Models	328

List of Tables

Table 3.1: Drillstring properties	96
Table 3.2: Bond graph model properties	96
Table 4.1: Dimensions and characteristics of the drillstring and collar section	112
Table 5.1: Parameters used in the simulations	157
Table 5.2: The first four natural frequencies for coupled axial-transverse-transverse modes	158
Table 6.1: Parameters used in the simulations	200
Table 6.2: Extracted resonance rotary speeds	202
Table 7.1: Nomenclature of motion and comparison functions for each section of the drillstring	248
Table 7.2: Numerical values used in the simulations	261
Table 7.3: Extracted resonance rotary speeds	268
Table A1-1: Abbreviations used in Figure A1.2	306

List of Figures

Figure 2.1: Schematic of a typical rotary drill rig	26
Figure 2.2: Different types of stabilizer	26
Figure 2.3: The primary modes of the drillstring vibration	28
Figure 2.4: Axial vibration of the drillstring and bit bounce	30
Figure 2.5: A simple model for the axial vibration of the drillstring	32
Figure 2.6: Geometric configuration of the axial vibration of the drillstring	32
Figure 2.7: Torsional vibration of the drillstring	35
Figure 2.8: Varying downhole rotary speed vs. the input rotary speed at the surface (stick-slip state)	36
Figure 2.9: A model for the torsional vibration of the drillstring	38
Figure 2.10: Drillstring in the transverse vibration state	40
Figure 2.11: Schematic of the drillstring with shock sub	48
Figure 3.1: Schematic view of drillstring and stabilizer	83
Figure 3.2: Schematic of drillstring under weight on bit and corresponding element	84
Figure 3.3: Bond graph model of drillstring with wellbore contact point at stabilizer	88
Figure 3.4: Transverse displacement (w), velocity and contact force at the point of contact between drillstring and wellbore for 150 kN weight on bit	89
Figure 3.5: Behavior of Hertzian contact element	89
Figure 3.6: Phase plane for WOB = 150 kN	90
Figure 3.7: Contact force versus position of drillstring	90
Figure 3.8: Phase plane for WOB = 350 kN	91

Figure 3.9: Contact force versus position of drillstring	92
Figure 3.10: Transverse displacement (w), velocity and contact force at the point of contact between drillstring and wellbore for 350 kN weight on bit	92
Figure 4.1: Schematic diagram of the drillstring in the wellbore	104
Figure 4.2: Drillstring elements between two stabilizers a) The uz plane b) the vz plane	105
Figure 4.3: Torque in the z direction decomposed to tangential and normal components	106
Figure 4.4: The profile of axial load along drillstring	108
Figure 4.5: The function $p(t)$ for the first five modes (the u direction)	112
Figure 4.6: The function $q(t)$ for the first five modes (the v direction)	113
Figure 4.7: The function $q(t)$ for the second mode to the fifth mode	114
Figure 4.8: The natural frequency in the u and v directions for the first five modes by the analytical model	115
Figure 4.9: The effect of WOB on the natural frequency in the u direction	116
Figure 4.10: The effect of torque on the natural frequency in the u direction	117
Figure 4.11: The deformed shape of the drillstring in different modes	119
Figure 4.12: Comparison of the natural frequencies in the u and v directions for the FEM and the expanded Galerkin method	120
Figure 4.13: Effective mass in the “ u ” direction	121
Figure 4.14: Effective mass in the “ v ” direction	122
Figure 4.15: Force profile along the collar section	132

Figure 5.1: Schematic of the multi span drillstring under the effect of the VARD tool	145
Figure 5.2: Spatially varying axial force along an 860 m drillstring	146
Figure 5.3: Schematic of a 3 span BHA	152
Figure 5.4: The first four mode shapes of a three span beam	155
Figure 5.5: Axial deflection near the hook point	158
Figure 5.6: Axial deflection, midpoint on span 1 of the BHA	159
Figure 5.7: Axial deflection, midpoint on span 2 of the BHA	159
Figure 5.8: Axial deflection, a point close to the bit on span 3 of the BHA	160
Figure 5.9: Axial velocity, a point close to the bit on span 3 of the BHA	161
Figure 5.10: Phase plane, a point close to the bit on span 3 of the BHA	161
Figure 5.11: Lateral deflection and velocities, a no-contact point on the top span of the BHA	162
Figure 5.12: Lateral phase planes, trajectory and radial deflection, a no-contact point on the top span of the BHA	163
Figure 5.13: Radial deflection of the contact point, first span of the BHA	164
Figure 5.14: Phase portrait of the contact point on the first span of the BHA	165
Figure 5.15: Radial deflection of the contact point, second span of the BHA	166
Figure 5.16: Phase portrait of the contact point on the second span of the BHA	167
Figure 5.17: Radial deflection of the contact point, last span of the BHA	168
Figure 5.18: Phase portrait of the contact point on the last span of the BHA	168
Figure 6.1: Schematic of the multi span drillstring under the effect of the VARD	187

tool

Figure 6.2: Schematic of a 3 span BHA	188
Figure 6.3: Spatially varying axial force along the drillstring	189
Figure 6.4: Axial deflection near the hook point	202
Figure 6.5: Axial deflection of a point on the top span	203
Figure 6.6: Axial deflection of a point on the middle span	203
Figure 6.7: Axial deflection of a point on the last span, close to the bit	204
Figure 6.8: Axial velocity of a point on the last span, close to the bit	204
Figure 6.9: Phase plane, a point on the last span, close to the bit	205
Figure 6.10: Lateral deflection and velocities for a point on the pipe section	206
Figure 6.11: Phase plane, phase trajectory and radial deflection for a point on the pipe section	208
Figure 6.12: Radial deflection of the contact point, first span	208
Figure 6.13: Radial deflection of the contact point, second span	209
Figure 6.14: Radial deflection of the contact point, third span	209
Figure 6.15: Lateral velocities of a point on the top span	210
Figure 6.16: Normalized total effective mass in each direction	211
Figure 6.17: Mesh sensitivity analysis, pipe section	212
Figure 6.18: Mesh sensitivity analysis, collar section	213
Figure 6.19: The first four mode shapes of a three span BHA	226
Figure 7.1: Schematic of the drillstring inside the wellbore	248
Figure 7.2: Normalized lateral mode shapes for the entire drillstring	255

Figure 7.3: Schematic of the drillstring in the axial motion	257
Figure 7.4: Normalized axial mode shapes of the entire drillstring	260
Figure 7.5: Axial displacement above the shock sub (with and without shock sub)	269
Figure 7.6: Sensitivity analysis of the shock sub to the stiffness value (transmitted axial displacement)	270
Figure 7.7: Transmitted axial force above the shock sub	271
Figure 7.8: Sensitivity analysis of the shock sub to the stiffness value (transmitted axial force)	272
Figure 7.9: Axial displacement near the rig floor (with and without shock sub)	273
Figure 7.10: Sensitivity analysis of the shock sub to the stiffness value (axial displacement near the rig floor)	274
Figure 7.11: Sensitivity analysis of the shock sub to the drillstring rotary speed (axial force above the shock sub)	275
Figure 7.12: Sensitivity analysis of the shock sub to the drillstring rotary speed (axial displacement above the shock sub)	276
Figure 7.13: Developed cutting force at the bit due to the downhole vibration generator (without shock sub)	277
Figure 7.14: Developed cutting force at the bit due to the downhole vibration generator (with shock sub)	277
Figure 7.15: Developed cutting force at the bit due to the downhole vibration generator tool (with and without shock sub)	278
Figure 7.16: Radial deflection at the contact point, first span of the BHA	279

Figure 7.17: Radial deflection at the contact point, second span of the BHA	280
Figure 7.18: Radial deflection at the contact point, last span of the BHA	281
Figure 7.19: Radial deflection at the contact point in the resonance, top span of the BHA	282
Figure A1.1: Free body diagram of the drillstring	306
Figure A1.2: Free body diagram of the drillstring	307
Figure A3.1: Simply supported beam in transverse motion	317
Figure A4.1: Generalized coordinates	323
Figure A4.2: Rotation angles	324

List of Appendices

Appendix 1: Buoyant Force Treatment in the Drillstring	304
Appendix 2: Hamilton's Principle and Lagrange's Equation	310
Appendix 3: Hamilton's Principle versus the "Bypassing PDEs" Method for Continuous Systems- A Case Study	317
Appendix 4: FEM Modeling of the Drillstring-A Case Study	323
Appendix 5: List of Assumptions in the Developed Models	328

1 Introduction and Problem Statement

1.1 Introduction

As the consumption of energy increases across the globe, the demand for a more efficient and safer exploration and exploitation techniques is increasing. Drilling is one of the most costly and risky activities in oil and gas reservoirs exploration and field development.

Drilling techniques have rapidly evolved to increase production rates while decreasing the cost. Vibration-assisted rotary drilling (VARD) is an emerging technology that enhances rotary drilling by adding vibrations at the bit or elsewhere in the "Bottomhole Assembly" (BHA). VARD can be defined as the intentional introduction of controlled vibration into the drillstring to increase drilling performance. Recently, high frequency downhole vibration generator tools, such as agitators are installed in the BHA, which is demonstrated to increase the rate of penetration in drilling wells. The drillstring is one of the major parts of any drill rig and many important drilling parameters are controlled through the drillstring. This long rotary structure has a complex-nonlinear-coupled vibration behavior.

However, with the implementation of sophisticated downhole vibration generators, several catastrophic failures of the drillstring, bit and "measurement while drilling" (MWD) tools are reported by industry. This is due to the fact that the vibration generator tool acts as an excitation source for the drillstring vibration, or their working parameters are not compatible with the drillstring configuration. Therefore, the unwanted excited

vibration waves are propagating along the drillstring and drill rig, which is a potential disadvantage of this technique.

The only effective way to benefit from the positive consequences of these tools is to isolate the imposed vibration above the bit from the rest of the drillstring. Effective low-priced methods to achieve this goal are to develop and implement vibration decoupling tools and operational guidelines, while vibration generator tools are in use. The only effective way to develop decoupling tools and operational guidelines is through vibration modeling of the drillstring inside the wellbore. In the present research, analytical and numerical models of drillstring vibrations, under the effect of downhole vibration generator tools, are developed and tuned, and isolation methods and operational guidelines are proposed

1.2 Statement of the Problem

Drilling is one of the most costly and risky activities for both exploration and development of oil fields. The oil and gas industry is actively researching technologies to improve drilling technology and efficiency. Enhanced drilling techniques, such as "vibration-assisted rotary drilling" have been emerging in the last decade and are now considered as conventional technology. This technique is based on introducing high frequency axial vibration in the BHA through a downhole vibration generator tool for the purpose of reducing drillstring-wellbore friction and thus enhancing the penetration rate by improved weight transfer [1,2]. Reducing the probability of stick-slip, controlled reaction torque, improved steering, more efficient cutting removal and improved load

buckling capacity are other potential enhancements of these axial vibratory tools.

Nevertheless, implementing vibration generator tools in the rotary drilling raises concerns about the unfavourable side effects on the drill rig itself and, in particular, on the drillstring.

Contrary to the improving effect on the rate of penetration (ROP) and efficiency, the implementation of downhole vibration generators in the BHA adds a vibration excitation source on the drillstring. Although this is an axial excitation, other modes are also affected by this source due to the vibration coupling nature in the drillstring. This results in unwanted vibration waves propagating along the drillstring. The undesired vibration of the drillstring increases the risk of hole deviation, wellbore washout, and most importantly premature failure of the BHA and its components, including MWD tools. Moreover, as a result of exciting unwanted vibration modes of the drillstring, a large portion of the provided power at the surface is lost. The problem worsens if the working parameters of the vibration generator (load and frequency) are not compatible with the configuration of the drillstring and formation. It is of great interest to the oil and gas industry to investigate methods to benefit from potential advantages of the downhole vibration generator tool and avoid the negative consequences. From a practical point of view, the solution of this problem is to decouple the vibrations induced by the tool from the rest of the drillstring. This consists of designing vibration suppression tools, such as shock subs, developing drilling guidelines and designing a drillstring configuration which is compatible with the vibration generator tool. The only way to achieve the above goals is to investigate the vibration pattern of the drillstring and its dynamic behavior, either in

the frequency domain or the time domain, under the effect of the downhole vibration tool. The first essential step to study the dynamic behavior of the drillstring is to investigate the mechanics of the drillstring, its vibration behavior and develop models to recognize its vibration pattern for any mode of interest.

The drillstring is one of the major components of any type of drill rig. It is a tool used to transfer energy and rotation to the bit. This long rotary, slender structure plays one of the most important roles in overall drilling efficiency. It consists of a lower heavier section called the collars and a lighter upper section called the pipes. The collar section is constrained with multiple stabilizers inside the wellbore, which are used to increase the load carrying capacity of the drillstring and control well trajectories. The annulus between the BHA and the wellbore is filled with drilling mud, which cools the bit and flushes the cuttings out of the hole and helps to overcome formation pressure. Moreover, the mud has a significant vibration damping role in certain modes. A driving torque is applied to the top part of the drillstring. The drillstring on top is attached to the hoisting system and on the bottom the attached bit is in contact with the rock. The effects of the hook load, mud hydrostatic forces (upward at the bit location and downward at the pipe-collar junction) and self weight are presented as a spatially varying axial force along the drillstring. This load changes from compression in the collars to tension in the pipes. At the bit, besides an upward hydrostatic force, there is another force called the "weight-on-bit (WOB)", which is the primary cutting load.

This beam-like structure is under three primary states of vibration simultaneously: axial, transverse and torsional. Moreover, these modes are coupled due to axial stress distribution along the drillstring from compression to tension, the coupling nature of the bit-rock interaction, driving torque, axial stiffening due to the gravitational field and the curvature of the drillstring. Also, the vibration trend of the drillstring is nonlinear due to the sources of nonlinearity, such as drillstring-wellbore impact and bit rock interaction force. The axial bit displacement, multiple lateral contacts and the frictional torque fluctuations at the bit are major excitation sources for axial, lateral and torsional modes, respectively. Among the primary modes, the transverse mode is the most destructive mode and is responsible for most of the drillstring and BHA failures [3,4,5]. In the case of implementing downhole axial force generators, axial vibration behavior is also of great interest. This is due to the intentional axial excitation of the drillstring and therefore, the source in the axial direction should be decoupled. Also, the introduced axial force by the downhole vibration generator creates lateral excitation, and thus, lateral instabilities [6]. Also, axial and transverse vibrations are more violent compared to torsional vibrations of the drillstring in vertical wells [7]. As a result, investigation of the coupled axial-lateral mode of the drillstring, with the vibration generator tool in use, is the key towards understanding the vibration pattern of the drillstring and development of vibration isolators and operational drilling guidelines. Capturing the torsional mode is beyond the scope of this thesis.

Due to the nonlinearity, coupling nature and complex boundary conditions, vibration modeling of the drillstring coupled modes is a challenging problem. Therefore, classical

beam vibration theories are not accurate enough to model the dynamic behavior of the drillstring. Modeling the contact behavior and mud hydrostatic damping are other challenges in drillstring vibration modeling. In order to precisely model this complex behavior, it is essential to develop specific dynamic models for the modes of interest. Analytical elastodynamic modeling (energy variational or Newtonian approaches) and finite element modeling schemes are extensively used in the literature for deriving the governing dynamic equations. As a result of the above mentioned complex phenomena, a closed form solution of the governing equations is not also feasible. Therefore, classical approximation techniques must be implemented to analyze the dynamics and the motion trend of the drillstring inside the wellbore. This also enables a sensitivity study of the effect of controllable parameters on the motion trend of the drillstring. The frequency characteristics of the drillstring, the trajectory of drillstring motion inside the wellbore, the drillstring-wellbore contact behavior and developed dynamic reaction forces are deliverables of the developed models.

1.3 Thesis Statement

Currently there has been no formal investigation of the effect of the vibration induced by downhole tools on the nonlinear coupled axial-transverse vibration of oilwell drillstrings. Moreover, there is no model showing the effect of vibration isolators on the dynamic response of drillstrings with vibrating tools. The effect of vibration generator tools on the developed cutting force has not been addressed in the literature. There are no reported nonlinear coupled vibration models that allow designing and tuning a shock sub to decouple the imposed vibration on the bit from the rest of the drillstring, or the

development of operational guidelines so that unwanted drillstring vibration is suppressed.

This thesis studies the coupled axial-transverse (with two orthogonal lateral directions) dynamic behavior of the drillstring in the presence of the downhole vibration generator tool and vibration isolator. A non-linear, multi-mode, mathematical elastodynamic model of the vertical drillstring capturing a multi-span BHA is developed and validated with a coupled nonlinear axial-transverse finite element model (FEM). Both models capture the effects of mud damping, driving torque, multi-span contact, spatially varying axial load, bit-formation interaction, gyroscopic rotary effect and axial stiffening. The governing equations in the analytical model are obtained by implementing the Newtonian approach or the "Bypassing PDEs" method on the Lagrangian of the system in conjunction with the expanded Galerkin's method, with the most highly contributing modes identified and retained in the analysis. The analytical model is capable of extracting the critical rotary speeds as well as dynamic time response of any point on the drillstring. The dynamic FEM model is developed through the ABAQUS FEM *Explicit* solver package with the "kinematic friction contact" algorithm. The FEM model is capable of modal characteristic extraction as well as dynamic analysis of the entire drillstring. A mesh sensitivity analysis is conducted to reduce computational time of the FEM model. The accuracy of the retained modes in the analytical equations is verified by extracting the total effective mass derived by the FEM model. Simulation results of both models are used to extract and compare the critical rotary speeds, conduct a qualitative contact analysis and develop the phase portrait of motion trajectories of the drillstring inside the wellbore. Moreover, the

effect of incorporating the shock sub on the decoupling and isolation of the imposed vibration at the bit from the rest of the drillstring in a range of the drillstring rotary speed is investigated. At last, the enhancing effect of the vibration generator tool on the developed cutting force is studied. Fast running time and symbolic solution are the major advantages of the analytical model, which enables sensitivity analysis of the controllable drilling parameters. On the other hand, the FEM model enables easy reconfiguration and future extensions of model geometry, interactions, and modified BHA configurations.

1.4 Research Plan and Objectives

Due to the complexity of vibration modeling of the drillstring as stated in section 1-2, the modeling task in this research is performed in multiple modeling steps. It starts with preliminary simple models (e.g. non-rotating BHA models) and with the advancement of the modeling task, more complexity will be added. This helps towards better visualization of each interacting parameter and its role on the vibration trend of the drillstring. The following research plan is defined in this study:

1. The effect of weight on bit on the contact behavior of the drillstring and wellbore

In this step, the single plane lateral vibration behavior of the BHA section under a constant compressive axial load is studied. The BHA has the dominant role in the vibration of the drillstring compared to the pipe section. It is desired to study the contact behavior of the drillstring and wellbore for the WOB values and investigate the effect of increasing the WOB to the buckling limit of the BHA section on the contact behavior.

The BHA is modeled as a simply supported, single span beam under a constant load. The

governing analytical equations are derived using the Newtonian approach for a beam element under a compressive load. The resulting partial differential equation (PDE) is solved analytically using the method of separation of variables and the natural frequency and mode shapes equations are derived. Then, a bond graph model of the drillstring at the contact location is developed, using the modal expansion method. The modal mass and the modal stiffness values are computed based on the mode shape and natural frequencies for the first five modes. In the modal expansion method, the lateral response is an infinite sum of a linear combination of individual mode shapes. At the point of contact between the drillstring and the wellbore, the Hertzian contact force is defined to model the impact force on the drillstring. Phase planes at the contact points are generated for WOB values below and above the buckling limit and the severity of the contact are studied qualitatively. Also, the developed contact force are determined.

This preliminary model is capable of qualitative analysis of the contact behavior. Since the lateral modes are in two coupled orthogonal planes, and the axial force is not constant along the BHA section, it is required to develop a model which captures these relevant real-world phenomena. Therefore, the next modeling step is as follows.

2. Coupled transverse vibration modeling of drillstrings subjected to torque and spatially varying axial load

In this step, the coupled lateral vibrations of the BHA in the presence of the top driving torque and spatially varying axial load is investigated. The lateral modes are coupled via the tangential components of the torque in the curved BHA, which create bending

moment components on the beam element about two orthogonal axes in the transverse direction. The analytical equations for spatially varying force in the collar section due to the mud hydrostatic effect, self weight and hydrostatic force at the mismatch area of the pipe-collar junction is derived and implemented in the equations. In this step, the Newtonian approach is used to derive the equations of motion. The rotation of the drillstring and gyroscopic effect are neglected, because the BHA could be assumed as a low speed rotor. The expanded Galerkin's method is applied to the resulting equations of motion (set of coupled PDEs) and the equations are transformed to the time domain ordinary differential equations (time domain ODEs) in terms of mode participation factors (generalized coordinates variables). In order to verify the analytical model and determine the sufficient number of retained modes in the approximation technique, an FEM model is also developed. The ABAQUS FEM solver package with Euler-Bernoulli beam element chosen to maintain the same conditions as the mathematical model is used to develop the FEM model. Modal mass participation factor, which represents how strongly a specific mode contributes to the motion in a certain direction, is extracted from the FEM model to determine the appropriate number of modes to retain in the analytical equations. The simulation results from both models are used to derive natural frequencies of the BHA in presence of the torque and spatially varying axial load. From a practical drilling standpoint, the rotational speed should be adjusted so that it does not correspond to one of the eigenfrequencies. Moreover, the effect of torque and WOB on the natural frequencies in two orthogonal lateral directions is investigated by both models in this step.

In the developed model of this step, only the BHA section was modeled and the mud damping effect in the lateral mode was not considered, which plays a significant role in the drillstring lateral instabilities. Moreover, the contact behavior was not studied in this model and the BHA section was modeled as having a single-span, as opposed to a BHA with multiple spans due to additional stabilizers between the endpoints. Also, the downhole vibration generator tool was not considered in this model. In the next step, the above interactions and assumptions are considered, along with lateral coupling with the axial mode.

3. Analysis of multi-mode nonlinear coupled axial-transverse drillstring vibration in vibration assisted rotary drilling

In this step, the coupled axial-transverse vibration behavior of the entire drillstring (pipes and collars) in presence of the downhole vibration generator tool is studied. The BHA is assumed as a three-span beam with multiple stabilizers. The multi-span BHA model enables multi-mode contact analysis of the drillstring and wellbore. The governing equations are obtained using the “Bypassing PDEs” method with the expanded Galerkin's method, which enables finding the symbolic solution of the governing equations. The model developed in this study enables the axial and bilateral multi-mode time response analysis of any desired point on the entire drillstring, including multiple contact points on the BHA. The multi-mode approximation enables to find more accurate results for the resonance rotary speeds, compared to the single-mode treatment. The effects of mud damping, driving torque, multi-span contact and spatially varying axial load are included; along with nonlinearities due to geometry, axial stiffening, strain energy and Hertzian

contact forces. Simulation results are used to reveal resonant frequencies and to conduct a qualitative contact analysis through the phase planes at the contact point, showing the severity of the contact in each span of the BHA.

The above model includes almost all major interactions which contribute to the axial and lateral motion of the drillstring inside the wellbore. For the verification of the developed analytical model, another model with the same characteristics, dimensions and interactions, but with a different modeling method is required. In the next step, an FEM model is developed to validate the analytical model.

4. Vibration analysis of a drillstring in vibration-assisted rotary drilling – finite element modeling

A dynamic finite element model (FEM) of the vertical drillstring assuming a multi-span BHA is generated and validated with a coupled nonlinear axial-transverse elastodynamic mathematical model, developed in the previous step. The ABAQUS FEM *Explicit* solver package is used to develop the dynamic FEM model. The effects of mud damping, driving torque, multi-span contact and spatially varying axial load are included. The rotary gyroscopic effect is neglected. Geometry, axial stiffening and lateral contact forces are sources of nonlinearity in the model. A mesh sensitivity analysis is conducted to reduce computational time. The accuracy of the retained modes in the analytical equations, developed in the previous step, is verified by extracting the total effective mass in the FEM model. Coupled-transverse and axial velocities, displacements, resonant

frequencies and contact locations and behavior are extracted in this step and the results are compared with the results of the analytical model developed in step 4.

The need to develop a vibration isolation tool and decouple the induced vibration above the bit from the rest of the drillstring over an extended range of rotary speeds of the drillstring needs to be addressed in this research. In the next step, the analytical and FEM models are being enhanced to capture the isolation tool (shock sub) and the rotary speed of the drillstring.

5. Analytical and dynamic finite element analysis of a drillstring with a downhole vibration generator tool: vibration analysis and decoupling study

This step is motivated by the need to understand the role of vibration generators on the complex coupled axial-lateral dynamics of the drillstring inside the wellbore and the developed cutting force at the bit. Designing and tuning a shock sub to decouple the imposed vibration on the bit from the rest of the drillstring is the other goal of this study. The nonlinear coupled axial-lateral vibration of the drillstring inside the wellbore is investigated through a dynamic finite element model (FEM) and an analytical elastodynamic model, capturing the vibration generator tool and a shock sub. The “Bypassing PDEs” method is implemented on the Lagrangian of the system to develop the analytical equations. Multi-mode expanded Galerkin’s approximation, in conjunction with the multi-span BHA assumption, results in multiple points Hertzian contact analysis, and thus more realistic critical rotary speeds. Capturing more realistic axial and lateral boundary conditions, torque, mud damping, spatially varying axial force, geometric

nonlinearity, axial stiffening and shock sub for a drillstring with the vibration generator are enhanced features of the developed and validated models. The concept of mesh sensitivity analysis and sufficient retained modes in the analytical model is also investigated by the FEM model. The vibration suppression ability of the shock sub in an extended range of the drillstring rotary speed, critical rotary speeds, axial and lateral displacements and the contact behavior are investigated through simulation results of both developed models in this step. Moreover, the enhancing effect of the downhole vibration generator tool on the developed cutting force at the bit in presence of a shock sub is investigated.

In order to develop sophisticated models for drillstring vibrations, it is essential to study the mechanics of the drillstring, different modes of drillstring vibration, formulation methods, approximation solution techniques and numerical solution methods. The next chapter is a detailed review of the state-of-the-art of the above subjects.

1.5 References

- [1] Manko, K. I., Pilipenko, V. V., and Zapols'ky, L. G., 2003, "Use Hydrodynamic Cavitation For Increase of Efficiency of Process of Well Drilling," Fifth International Symposium on Cavitation, Osaka, Japan.
- [2] Al Ali, A., Barton, S., and Mohanna, A., 2011, "Unique Axial Oscillation Tool Enhances Performance of Directional Tools in extended Reach Applications," SPE#143216, SPE Brasil Offshore, Macaé, Brazil.

- [3] Burgess, T. M., McDaniel, G. L., and Das, P. K., 1987, "Improving BHA Tool Reliability with Drillstring Vibration Models: Field Experience and Limitations," SPE#16109, SPE/IADC Drilling Conference, New Orleans, Louisiana.
- [4] Chin, W. C., 1994, *Wave Propagation in Petroleum Engineering*, Gulf Publishing Company, Texas, USA.
- [5] Yaveri, M., Damani, K., and Kalbhor, H., 2010, "Solutions to the Downhole Vibrations during drilling," SPE#136956, 34th Annual SPE International Conference and Exhibition, Tinapa, Nigeria.
- [6] Berlioz, A., Der Hagopian, J., Dufour, R., and Draoui, E., 1996, "Dynamic Behavior of a Drillstring: Experimental Investigation of Lateral Instabilities," ASME Journal of Vibration and Acoustics, **118**, pp. 292-298.
- [7] Schlumberger Technical Report, 2010, "Drillstring Vibrations and Vibration Modeling,"
http://www.slb.com/~media/Files/drilling/brochures/drilling_opt/drillstring_vib_br.pdf

2 Technical Background

2.1 Introduction

This chapter is a detailed review of the state-of-the-art methods relevant to drillstring vibration analysis. First, drilling engineering and enhancement techniques will be introduced. Then, fundamental terminologies of a drill rig and the drillstring will be explained. Different modes of drillstring vibrations will be discussed and various methods of vibration suppression techniques for different vibration modes will be explained. Newtonian approach, energy variational technique and the “Bypassing PDEs” method for deriving the equations of motion will be explained and compared. Due to the complexity of the problem, closed form solution of the governing equations is not possible and approximation techniques are required to solve the resulting equations of motion. Approximate solution techniques, their advantages and drawbacks will be also explained. The last section in this chapter is the study of a powerful numerical technique (finite element analysis), which is widely implemented in drillstring vibration modeling.

2.2 Drilling Engineering

Drilling is one of the major methods of exploration and exploitation of oil and gas reservoirs in petroleum engineering and minerals in mining engineering. Drilling engineering is a complex task since different aspects, such as geological formation, different types of reservoir, environmental concerns besides the high cost of drilling equipments are involved. The goal of drilling is to drill wells as safely and economically as possible. The main process of the conventional rotary drilling, which is extensively

used for decades, is the creation of a borehole through the rotation of long pipes (drillstring), and failure of the rock either in tension or shear by the provided cutting force at the cutting tool (bit). The provided power at the rig surface is used to move the rotating drillstring downward and circulate the drilling fluid (mud). The cuttings are transferred to the surface through the drilling mud. Onshore and offshore rotary drill rigs are used for almost any type of rotary mechanical drilling. They include all the equipment required for drilling, such as rotary table and kelly, derrick and swivel (the hoisting system to hold the long drillstring), control units, power generators, blowout preventers and mud pumps. Drilling is a multibillion dollar industry and any enhancement towards a faster drilling can save millions of dollars.

Increasing the rotary speed results in increasing the penetration rate of the drilling, reducing the tripping time, and reducing the drilling cost. However, fast drilling can create other problems, such as bit wear and premature failure of drilling components, especially the drillstring, which results in a huge financial loss.

Development of a more efficient and cost-effective drilling technology will significantly increase oil and gas production by allowing economic exploitation of difficult formations, such as deep, hard rock reservoirs. In 1961, Smith *et al.* [1] estimated that potential savings of \$200 to \$600 million are possible if the penetration rate in hard rock can be doubled while maintaining the bit life. Therefore, drilling techniques have rapidly evolved to increase production rates while decreasing the cost. Simple rotary drilling

techniques have been replaced with advanced percussion or vibration-assisted rotary drilling to achieve higher efficiencies.

There is evidence that the combination of rotary drilling techniques with a downhole vibration generator tool, which generates percussion or vibration, can potentially provide significant improvement in drilling hard rock formations. Percussion drilling was first implemented in 1859 and has evolved over the years into "Down-the-Hole" (DTH) hammer drilling, which has significantly improved the Rate of Penetration (ROP) in hard rock environments. In addition to the faster penetration, other benefits include the ability to use lower cutting force, less contact time with rock and therefore less abrasion, longer bit life and improved hole deviation control [2]. However, in soft rock formations, where most of oil and gas drilling is done, instead of percussion drilling, vibration-assisted rotary drilling technique is applied for more efficient drilling. Vibration-assisted rotary drilling is a new enhancement to the rotary drilling method and has shown an incredible increase in the drilling efficiency and cost reduction. The following section is a literature review of percussion drilling, followed by vibration-assisted rotary drilling.

2.3 Drilling Enhancement Techniques: Percussion Drilling

In rotary percussive drilling, the rock is broken by repeated impacts and the rotation imposes a new point of impact every time. The rock is thereby broken, crushed and flushed out from the hole [3]. One advantage of this technique is that the rock fails due to dynamic loading rather than crushing the rock through static loading as in conventional rotary drilling [4]. More than 2000 cyclic loadings per minute can be applied to the bit,

which generate high stress in a short time interval. This causes the penetration in hard formations to be more efficient than rotary drilling with its lower stresses and long time of static load application [5]. Therefore, percussion drilling transmits power to the bit more efficiently than rotary drilling.

Colonel F. L. Drake was the first one who used a cable tool percussion type machine for oil well production in 1859 [6]. The first technical report of this technique was submitted in 1949 by Harpst and Davis [6]. This report resulted in the creation of several different terms, all of which are used to describe this type of drilling. Examples include percussion hammer, downhole hammer, percussive drill and percussive rotary drilling.

Between 1950 and 1960, there were substantial research breakthroughs on this subject [7]. Most of this research was conducted on laboratory scale rigs. In 1981, Pratt reported the results of the application of percussion drilling with an average time for "Total Vertical Depth" (TVD) of 80 days [8]. This was a definite improvement over the conventional mechanical drilling methods, which took 103 days to drill the same well. Also, a cost per foot reduction of 49% was achieved with hammer percussion tools. In another survey, it was reported that percussive rotary drilling could be 7.3 times faster than the conventional rotary method [9].

The hammers can be categorized into top hammers and down the-hole-hammers. Gas and air, hydraulic, fluid and jet assisted rotary percussion hammers are common means of providing percussion force to the bit [10]. Fluid hammers appeared first in 1990 [2]. After the first appearance of the fluid hammer, the research was mainly on improving hammer

design and performance. Hydraulic hammers have been used to conduct drilling in hard rock formations, as air hammers are limited by penetration depth [11].

Higher and more consistent penetration rates than rotary drilling (by a factor of 5 or more), relatively small, light, and mobile drill rigs and low drilling costs are the main advantages of the percussive drilling, while the high rate of vibration, which is transmitted to the drill rig via the drillstring, is a disadvantage [12]. Old percussive drilling (cable tool) technique is not a commonly accepted method anymore, due to frequent mechanical failures, poor understanding of the method, economical uncertainties and inability to control the drillstring downhole vibrations parameters [4]. The research for more efficient enhancement methods led the drilling companies to vibration-assisted rotary drilling, which is a more industry applicable and controllable technique.

2.4 Drilling Enhancement Techniques: Vibration-Assisted Rotary Drilling

The oil and gas industry is actively searching for technologies to improve drilling technology and efficiency. The interest for implementing high-frequency axial oscillation generator tools in conventional rotary drilling has been increased since the last decade. "Vibration-assisted rotary drilling" can be defined as the intentional introduction of controlled vibration into the drillstring to increase drilling performance. Vibration drilling transmits power to the bit more efficiently than rotary drilling. The tool converts the hydraulic energy of the mud into an axial motion through the pressure acting on the pump-open area. The axial excitation is produced by different mechanisms, but the final outcome is an alternating high-frequency force which excites the lower side of the

drillstring close to the bit. Several classes of recent drilling tools, such as “agitators” are currently used by industry to apply axial vibration intentionally to the drillstring, especially in horizontal or deviated wells.

This imposed vibration significantly reduces drillstring-wellbore friction [13,14], and thus leads to less required "weight-on-bit (WOB), and speeds up the cuttings flushing process. Improved weight transfer, increased power at the bit and consequently a higher "rate of penetration" (ROP) compared to the conventional rotary drilling [14,15] are potential advantages of vibration-assisted rotary drilling. Reducing the probability of stick-slip, controlled reaction torque, improved steering, more efficient cutting removal and improved load buckling capacity compared to conventional rotary drilling are other potential enhancements of these tools.

Several laboratory and field experiments as well as analytical studies have been conducted for the verification and application of this method to oil well rotary drilling. Manko *et al.* [15] introduced a new hydrovibrator tool which superimposes axial vibrations to a drillstring by transforming a stationary mud flow to a high frequency pulsating flow, resulting in a hydrodynamic cavitation impact on the drillstring, and thus axial excitation of the drillstring. Newman *et al.* [16] presented a theoretical torque-drag model to verify the experimental results of the friction reduction through the use of a commercial vibration generator tool (National Oilwell CT AG-imatorTM). Consequently, they approved that the use of this tool increased the depth of penetration by approximately 1000 feet and the developed model and field test results were in

agreement. Al Ali *et al.* [17], meanwhile, investigated axial oscillation generator (AGT) tools which are compatible with most practical "bottom-hole assemblies" (BHAs). The tool was implemented in several vertical drilling field tests in conventional rotary and rotary steerable system (RSS) drilling. 60% increase in ROP, with 63% less required WOB, extended bit life and less stick-slip were reported. However, increase in vibration levels of the drillstring was reported in all field trials. The increase in ROP was also reported by Li *et al.* [18] for a laboratory scale test rig under different input vibration amplitudes with the coring bit, but with a constant input frequency, and the results showed an increase in ROP. Babatunde *et al.* [14], alternatively, investigated the effect of introducing various levels of vibration in diamond drag bits, and concluded that at controlled frequencies the imposed vibration has a significant effect on ROP: a 100% increase in ROP was reported in their experimental test rig for a high-input vibration power, along with an established optimum value for the input frequency for their vibration generator tool. In a recent study, Khorshidian *et al.* [19] investigated the effect of introducing vibration force in a single cutter "Polycrystalline Diamond Compact" (PDC) bit, using the "Distinct Element Modeling" (DEM) methodology. They verified that imposing energized impact on the rock-cutter surface improves the value of the drilling "Mechanical Specific Energy" (MSE), and this factor was then implemented to investigate an optimum level of the cutter vertical vibrations for a faster ROP.

Contrary to the improving rate of penetration and efficiency, downhole vibration generator tools can increase the risk of hole deviation, wellbore washout, and premature failure of the BHA and its components, including "measurement-while-drilling" (MWD)

tools. The drillstring can undergo undesirable vibrations excited by the tool. Also, if the imposed vibration by the vibration generator is not isolated from propagating up the drillstring toward the rig surface, there is a possibility of fatigue failure in the rig and surface components as well. In addition to the above negative consequences, a great portion of the energy that was supposed to be delivered at the bit can be lost if the operating parameters of the vibration generator is not compatible with the overall drillstring configuration and formation properties. Enhanced dynamic modeling of the drillstring, capturing the excitation sources, is the first step towards adjusting and implementing these sophisticated tools to avoid these negative consequences, and designing vibration isolation mechanisms such as shock subs and generating drilling guidelines.

2.5 Fundamentals of Oilwell Drilling and Drilling Tools

The drill rig for conventional rotary drilling is a large structure housing the entire drilling system. A schematic of a typical rotary drilling rig is shown in Figure 2.1. The derrick provides vertical height to raise or lower down the pipes in and out of the wellbore and control units and power generators are installed on the derrick. It is usually placed above the ground using a substructure. The top part is a hoisting system, which consists of the crown block, traveling block and swivel. The block assembly (crown block, traveling block and cables) provides a mechanical advantage for easier handling of the heavy pipes and the BHA. The crown block is a stationary section with a set of sheaves, where the cables are reeved about that. The traveling block is the moving part of the hoisting system which has a set of pulleys. The draw-works provide the hoisting and braking power and is

used to reel in and out the pipes and raising and lowering the traveling block along the length of the derrick. The swivel, kelly, rotary drive and rotary table are major parts of the rotary system. The swivel supports the weight of the drillstring and allows for rotation and its top part is attached to the traveling block. The rotary table generates the rotary motion of the drillstring assembly through the kelly. The kelly is the first section of the pipe below the swivel at the rig floor with an square or hexagonal outside cross section to be gripped easily for rotation of the drillstring. Rotary drive provides the required torque for driving the rotary table (the top end of the drillstring) and consists of an electric motor and a gearbox unit. Drilling fluid (mud) circulating system consists of the mud pit, mud pump and stand pipe. The mud pit is a reserve store for the mud and pumps are used to circulate mud through the system. The stand pipe is used to conduct the mud from the mud pumps to the kelly hose. Drilling mud (water-based or oil-based) circulates up and down the wellbore and fills out the annulus between the drillstring and wellbore. It is used to cool down the bit, transport cuttings to the surface, prevent blowout caused by formation pressure, provide hydraulic power for downhole vibration generators and clean the bottom of the hole. Moreover, the mud plays an important role in stabilizing the lateral vibrations of the BHA as a nonlinear damping media. A shale shaker is used to separate rock cuttings from the mud before it pumps again down the hole. The blowout preventer is a valve which seals and controls formation kick and can withstand extreme pressures.

The drillstring is a large slender structure which transfers energy from the electric motor on the top to the drill bit at the bottom hole. The drillstring is composed of two major

sections: drill pipes and drill collars. Drill pipes are light hollow cylindrical pipes which could be up to kilometres in length. The heavier part is the drill collar (normally with an outer diameter of 120-240 mm and thickness of 30-80 mm), which provides WOB for the drilling process. WOB is the responsible load for penetration at the bit-rock interface.

Drilling performance is very sensitive to WOB, and it is one of the main parameters adjusted during drilling to improve penetration speed. ROP is the conventional index for measuring the efficiency of the drilling process. The bit is attached to the bottom of the collars. The most popular types of bit are roller cone and polycrystalline diamond compact (PDC) bits. The PDC bits are more expensive than the roller cone bits, but more efficient in rock cutting. The lower part of the drillstring which is composed of drill collars, the bit and stabilizers is called the BHA. The rotary speed of the drillstring is typically between 50 and 200 rpm.

The stabilizers are fins placed outside of the drill collars at multiple locations and above the bit to centralize the drillstring inside the wellbore, increase the load carrying capacity of the BHA and are means to control well trajectories in deviated wells. They also provide additional stiffness to the BHA and facilitate the control of the dynamic behavior of the drillstring and the drilling direction [21]. The distance between stabilizers along the collar section varies between 5 to 50 meters and they fit loosely in the borehole. The radial clearance between the BHA and the wellbore is up to 10 cm. Different types of stabilizer (spiral blade, straight blade and inclined blade) are shown in Figure 2.2.

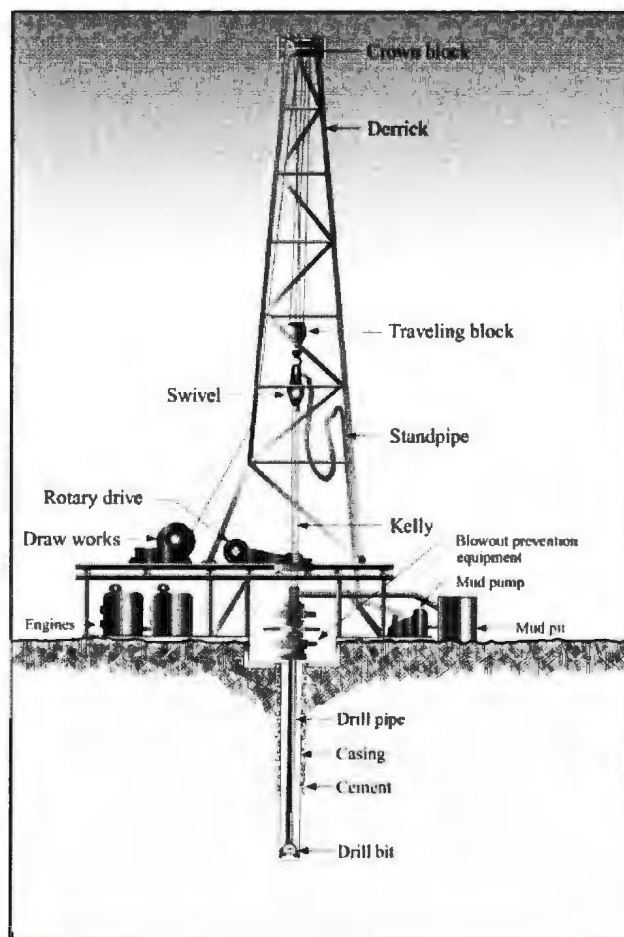


Figure 2.1: Schematic of a typical rotary drill rig [20]

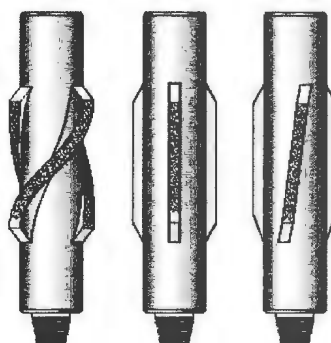


Figure 2.2: Different types of stabilizer [22]

MWD tools are installed on the BHA to record drilling variables such as WOB, torque-on-bit, depth, rotary speed and downhole pressure. The logged data is transmitted to the surface using a mud pulse telemetry system.

The effects of the hook load (a resultant axial force under static equilibrium), WOB, mud hydrostatic force and self weight are presented as spatially varying axial forces along the drillstring. The tendency in drilling engineering is to keep the pipe section under tension, while keeping the stiff BHA under compression. The length and material properties of the BHA, alongside with WOB and mud density, are controllable parameters to keep the BHA under compression [23]. The neutral point in the drillstring is defined as the point above which there is no tendency to buckle. At the neutral point, the axial stress is equal to the average of radial and tangential stresses. Current design practice is to maintain the neutral point below drill pipe during drilling operations. The intersection of the stability analysis plot and the axial compression must be used to find the location of a neutral point [24]. A detailed derivation of the spatially varying axial force and stress distribution along the drillstring is demonstrated in Appendix 1.

2.6 The Vibration Behavior of the Drillstring

Drillstring vibrations have been a challenging issue for drillers in oil fields for a long time. The effects of vibrations on the drilling performance, wellbore stability and joint failures have convinced drilling companies to strengthen components, or try to control and mitigate these effects to attain higher performance [2,25]. In order to control or mitigate the drillstring vibrations, its dynamic behavior and characteristics should be

identified and modeled analytically [26-33], numerically [20,29,34,35,36], experimentally in laboratory scale [37-40], or through field verification [16,41].

The primary modes of drillstring vibrations are axial [42], transverse [43] and torsional [44] as shown in Figure 2.3.

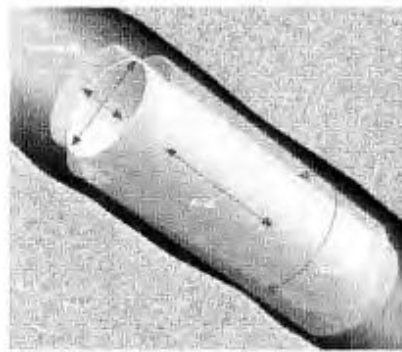


Figure 2.3: The primary modes of the drillstring vibration [45]

The vibration behavior of the drillstring is quite complicated, since these three modes are present in a rotating drillstring simultaneously, have nonlinear behavior, and moreover, are coupled together. These modes are coupled together via terms (in equations of motion) containing variables like torque and strain energy [46]. Coupled torsional-bending [20,47,48,49], coupled axial-bending [50] and coupled axial-torsional [51,52] are three common combinations of coupled modes. Stick-slip oscillations [22,53] are examples of torsional vibration, and whirling and bit bounce [54,55] are examples of lateral and axial vibrations, respectively. Drillstring vibration could be fully transient or dynamically steady. Furthermore, energy transfers between single harmonics of axial, transverse and torsional modes and between any subsets of these modes is possible. Therefore, numerous degrees of freedom exist in its motion.

The majority of drillstring failures occur at the BHA section. Due to the higher stiffness and higher mass of the BHA with compared to the pipe section, the vibration behavior of the drillstring is mostly influenced by the BHA vibration behavior [56]. This dominant role of the BHA vibrations on the total drillstring vibration was verified by Dareing [57], who showed that the collars are easily excited in the lower modes. The pipes act as if they are rigid and do not vibrate laterally during such excitation [58].

Unwanted vibrations of the drillstring dissipate some part of the provided energy, which is supposed to be delivered to the bit. The unwanted vibrations also result in hole deviation, lower penetration rate, premature failure and lower efficiency of the drilling process. Therefore, a thorough understanding and the ability to isolate the unwanted vibrations are essential to the design of the drillstring. It should be mentioned that the vibrations could not be damped by 100%. Dynamic modeling of different modes of the drillstring is the first step towards designing an isolation plan, or generating remedial guidelines for real time field drilling. In the following sections, different modes of drillstring vibration as well as coupled modes and the isolation methods for drillstring vibrations will be further explained.

2.6.1 Axial vibration of the drillstring

The vibration of the drillstring along its longitudinal axis is called axial vibration. Axial vibration has a deleterious effect on the bit and bottomhole assembly. Bit bouncing is the most severe state of the axial vibrations. When the bit loses contact with the hole bottom, it bounces up and down as a result of resonance in the axial direction (Figure 2.4). Axial

vibration is most common in vertical wells while drilling hard formations. It can be detected at the surface measurement tools. Accelerated bearing and tool wear, seal failure, broken tooth cutters, failure of the MWD tools and reduction in the ROP are most common catastrophic outcomes of axial vibration and bit bounce [59].

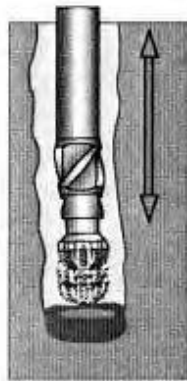


Figure 2.4: Axial vibration of the drillstring and bit bounce [59]

In most cases, pulling off the bottom, changing the rotational speed or changing WOB can reduce the axial vibration [60]. In the drilling situations that the axial vibration is happening in most of the drilling time, installing a shock sub can reduce the vibration in the bottomhole through changing the resonance frequency of the drillstring. This application will be explained in the section detailing isolation methods. Since the drillstring makes the hole parallel to its axis, axial vibration plays an important role in the trajectory deviation as well [61].

Mostly, uncoupled axial vibration is modeled using the linear partial differential equation governing the un-damped longitudinal oscillation of a bar [61]. At the surface, a mass-spring-damper boundary condition was postulated (the mass of swivel, traveling block

and kelly are assumed as a concentrated mass). The surface boundary condition might also be taken as a fixed end and the bottom as a free end [61].

A variety of models have been used to investigate the longitudinal vibration of the drillstring. Continuous models were used in early studies to model this mode [61-64], while more recently, finite element models (FEM) have been applied to axial vibration investigations [65]. Some studies, however, have not used a complete model for drillstrings to extract axial response, but have focused only on natural frequencies, e.g. Dareing [56]. Over the years, a great deal of research has been conducted to investigate the effects of different parts of the drillstring on its axial vibrations. For example Kreisle *et al.* [61] showed the importance of a shock sub in reducing the drillstring axial vibration and Dareing [56] revealed the dominant effect of drill collar length on axial and torsional vibrations of drillstrings. Figure 2.5 shows one of the simple models used in the previous studies to analyze the axial vibration of the drillstring.

Implementation of the damping into models is an important aspect of studies of drillstring axial vibration. Some investigators did not consider any type of damping [62], while some others incorporated the damping ratio into their models [61,63,64,65]. The two most common types of damping used include: simple viscous damping [61,63] and frequency-dependent damping [65].



Figure 2.5: A simple model for the axial vibration of the drillstring [65]

A simple equation for analyzing the axial vibration of a drillstring (Figure 2.6) is as [66]:

$$E \frac{\partial^2 u}{\partial x^2} - \xi \frac{\partial u}{\partial t} - \rho \frac{\partial^2 u}{\partial t^2} - \rho g = F_e(x, t, u) \quad (2.1)$$



Figure 2.6: Geometric configuration of the axial vibration of the drillstring

ρ is the density per unit volume, ξ is the damping factor, E is the Young's Modulus and $u(x, t)$ is the longitudinal displacement of the drillstring. $E \frac{\partial^2 u}{\partial x^2}$ is the result of difference

between the normal stress ($E \frac{\partial u}{\partial x}$ acting on the face of the element mass) and

$E \frac{\partial u}{\partial x} + \partial(E \frac{\partial u}{\partial x})$ acting on the opposite side. $\xi \frac{\partial u}{\partial t}$ refers to the viscous dissipation and ρg

refers to the static weight. $F_e(x, t, u)$ represents the external axial excitation force.

According to the free-fall limit theory, $\frac{\partial u}{\partial t} < 0$ means advance motion toward the hole, or

making the hole, and $\frac{\partial u}{\partial t} > 0$ means the bit bounce [66].

A lot of uncertainties exist regarding the modeling of the boundary conditions (BCs) of the drillstring in the axial mode. Fixed at top-free at the bottom BC [21,50], fixed-fixed BC [64] and free at top-fixed at the bottom BC [62,63] are commonly used BCs for the axial mode of the drillstring vibration. Jogi *et al.* [41] suggested that the free-fixed axial BC does not match well with major axial frequencies observed in the field, and that a free end assumption is closer to the field data. Clayer *et al.* [67] suggested an equivalent mass-spring-damper at the top and verified that this model is sufficiently accurate for rig surface modeling. Arrestad *et al.* [68] also suggested an equivalent mass spring damper for the top boundary condition, but recommended a nonlinear coupled axial model to study the role of this boundary condition on the axial vibration of the drillstring. Later on, bit displacement function was suggested as an accurate lower boundary condition in the axial direction, which depends on the rock formation properties and the bit type. Kreisle

et al. [61] was the first one who applied a sinusoidal bit displacement as the lower BC in the axial motion. The frequency of displacement was assumed to be three times the rotary speed of the drillstring for tricone bits and the same as the rotary speed for the PDC bits [69]. Macpherson *et al.* [70] suggested the same boundary condition proposed by Kreisle *et al.* [61], with a phase shift relative to the drillstring rotary speed. Dareing [64] also suggested a constant amplitude sinusoidal function as the bit displacement. He also indicated that the various types of drill bits (e.g. roller cone and PDC bits) generate different loading conditions to the bottom end of the drillstring. Due to the rolling of the bit, a multi-lobed surface is formed on the formation; the number of lobes formed depends on the number of cones on the bit. This lobed-pattern can be defined by a profile with sinusoidal angular variation elevation [65].

On the other hand, however, in a number of studies the bit in the axial direction was assumed as a free BC, and an excitation force was assumed instead. Elsayed *et al.* [71] proposed a force excitation at the bit which depends on the width of the cut and cutting stiffness of the rock. Yigit *et al.* [49,72,73] and Dunayevsky *et al.* [74] assumed the modulated part of the WOB with the same frequency of the drillstring rotary speed for PDC bits. To decide between these two excitation and boundary condition at the bit, Li *et al.* [42] used a mathematical model of the drillstring and field data and recommended that the bit displacement BC model is supported by the field data and force excitation model is not appropriate for the axial vibration modeling of the drillstring. Skaugen *et al.* [75] also recommended that the bit displacement BC is the most appropriate BC for the shock sub

design. In summary, three sets of boundary condition were assumed in the literature for axial vibration of the drillstring:

- Fixed at top-fixed at the bottom
- Fixed at top- free at the bottom
- Equivalent mass-spring-damper at top and a sinusoidal displacement at the bit location

with the last proposed BC being the most realistic assumption.

2.6.2 Torsional Vibration of the Drillstring

The drillstring is a structure with low torsional stiffness, which is easily excited torsionally. During rotation, the BHA generates torsional oscillations which are transmitted through the drillstring. Torsional vibration often occurs in hard formations [59]. The friction force between the drillstring and the wellbore usually excites this mode [76]. Torsional vibration (Figure 2.7) causes irregular downhole rotation, which causes fatigue failure to the drill collar connections, damage to the bit and slows down the drilling process [71,77].

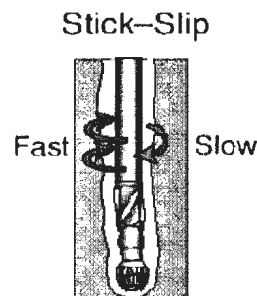


Figure 2.7: Torsional vibration of the drillstring [59]

Stick-slip is a severe form of torsional vibration of the drillstring. It involves periodic fluctuation in the bit rotational speed varying almost from zero velocity to a stage of high rotational speed, often more than twice the surface rotary speed [78]. Stick-slip manifests itself as low frequency torque fluctuations during drilling. In this mode, torque builds up and is then released, resulting in a rotational motion. The BHA and bit alternately rotate faster and slower than the string at the surface (Figure 2.8). In this state, the BHA can over rotate and builds up reverse torque, causing the BHA and the bit to rotate backwards. Stick-slip can also cause the bit to spin backward and destroy the bit.

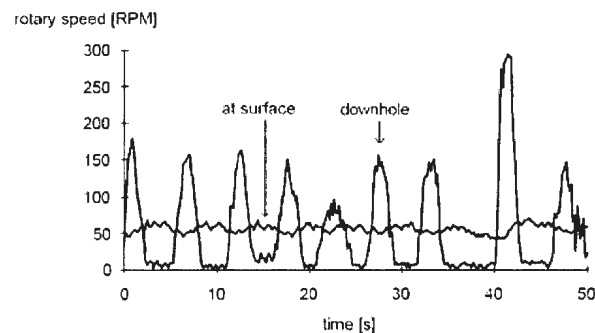


Figure 2.8: Varying downhole rotary speed vs. the input rotary speed at the surface (stick-slip state) [79]

At the start of drilling, an unstressed drillstring will not rotate until some threshold torque-up level that overcomes static friction at the face of the formation is surpassed. The exact threshold depends on the bit type, the bit-rock friction coefficient and the WOB. Once rotating, dynamic rock-bit interaction torque will excite the drillstring with torsional waves that propagate to the surface. Once the BHA starts to rotate it does not have a steady state motion trend due to lateral contacts and axial excitations at the bit. If

the static friction exceeds the dynamic friction acting at the bit, the previously stored energy may be transferred into kinetic energy and convert the steady state motion to a non steady rotational motion. Low dynamic WOB or axial bit bouncing will lead to a free torsional boundary condition at the lower end [80].

In general, torsional vibrations can be detected at the surface by fluctuations in the power needed to maintain a constant rate of rotation [59]. MWD devices have assisted researchers in obtaining a better understanding of this type of drillstring vibration and its effects on downhole tools and drilling performance. Stick-slip behavior is usually seen as cyclical signatures in the surface measured torque.

A variety of models have been used to study the torsional vibration of drillstrings. The most important model, which has been widely used for many years, implements a torsional pendulum (Figure 2.9). In this torsional pendulum model, drill pipes are considered as an inertia-less spring connected to a mass which represents the BHA [81]. Modifications have been made to adopt this model for further investigations; for example, the rotary table has been considered as an added mass [80,82,83], and coupling with other modes of vibration has also been considered, e.g., axial vibrations [82,84] or lateral vibrations [22,83]. In most of the mentioned studies, viscous damping has been applied as a damping effect between the masses and the borehole wall [80,81].

Selecting appropriate boundary conditions is another important step in the modeling of torsional vibrations of drillstrings. The upper boundary represents the rotary table and a constant rotary speed has been considered in most studies at this location, while the free end boundary condition assumed at the bit [22,80,84]. In some studies, a control relationship between the rotary table torque and the rotary speed has been considered to maintain a desired rotary speed [77].

2.6.3 Transverse Vibration of the Drillstring

Among the primary modes of drillstring vibration, the transverse mode (Figure 2.10) is said to be responsible for 75% of drillstring failures [79,85,86]. Bending waves are not propagated up to the surface via the drillstring as are torsional and longitudinal waves (this is due to the difference in the wave speed for different type of modes). As a result, damaging lateral vibration near the bit can go undetected. The propagation speed in steel for axial waves is 17000 ft/sec, for torsional waves is 10000 ft/s, and for the lateral mode is about 550 ft/s [66]. Furthermore, transverse vibration has a larger damping value with respect to the other modes, which is the result of mud damping effect and the drillstring-wellbore contact [66]. Therefore, there could be severe bending vibrations deep in the hole which the surface measuring tools do not indicate. The possible outcomes of transverse vibration include catastrophic failure of the BHA joints due to fatigue, borehole washout, bit failure and wear of stabilizers. Therefore, modeling this mode of vibration, extracting the natural frequencies and analyzing the dynamic behavior of the BHA will help drilling companies avoid these failures.

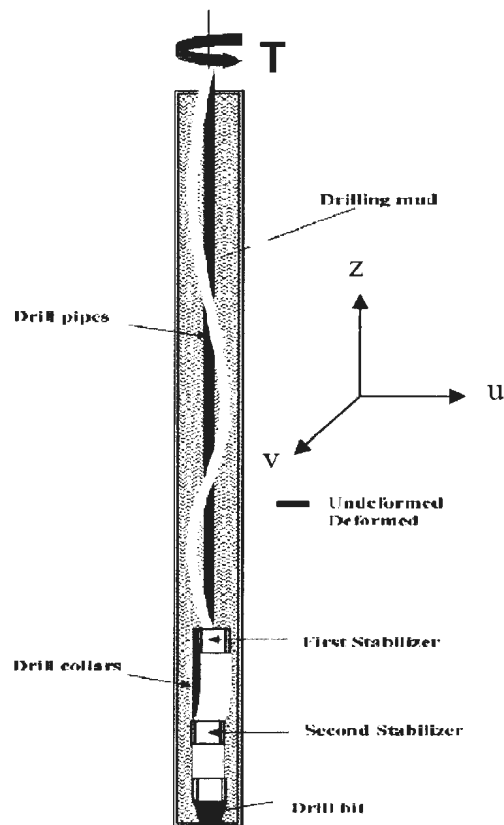


Figure 2.10: Drillstring in the transverse vibration state [87]

The heavier section of the drillstring, the collar section, is easily excited by contact with the wellbore in the lower modes. In the lower frequencies, the collars are vibrating transversely, while the pipes do not vibrate and remain approximately motionless. This is due to the axial load distribution along the drillstring, the collars of which are mainly under compression while the pipes are under tension. As a result of the tension, the natural frequencies of the pipe section increase, while the natural frequencies of the collar section are reduced [88]. Two types of frequency induced whirling are possible to occur at the BHA, namely forward whirl and backward whirl. Forward whirl is the rotation of

the deflected drill collars around the borehole axis in the same direction as it rotates around its axis [22]. The backward whirl is a rolling motion of the drill collars over the borehole wall in the opposite direction as it rotates. Whirling modes are excited due to the wellbore contact with the drillstring in low strength formations and as a result, an over gauge hole can be drilled [22].

Due to the dominant characteristics of the transverse mode, several studies have been undertaken to analyze the dynamic behavior of the drillstring in this mode. Mathematical models have an important role in the investigation of lateral vibrations of drillstrings; both analytical and finite element models have been developed to study this catastrophic mode of vibration. Jansen [89] studied the lateral motion between the drillstring and the wellbore at the contact point, using a lumped segment to model the contact point. Chen *et al.* [90] studied the lateral vibration of a rotating BHA in the presence of a constant WOB with the transfer matrix technique. Berloiz *et al.* [86] performed a laboratory test to study the lateral vibration of the drillstring and investigated that the influence of axial force is greater than that of the torque on the natural frequencies of the drillstring. Christoforou *et al.* [69] used the Lagrangian method to derive the equations of motion and study the drillstring trajectory inside the wellbore in the lateral mode at the contact point. WOB was assumed as a sinusoidal force with the same rotary speed as of the drillstring in their study. Stability of the drillstring in the lateral mode was studied by Gulyaev *et al.* [91]. The buckling mode of the drillstring as a function of its length was studied and the results verified that buckling would occur at the section with compressive axial force (collar section). In another study, they also studied the effect of the length and critical speed on

the stability of the drillstring in the lateral mode [92]. In another work by Dareing [57], the sensitivity of the drill collar lateral vibration to the length was studied. Khulief *et al.* [20] used the finite element method to derive the frequency and modal response of a rotating drillstring while neglecting torque. The results for the full order model and the developed reduced order model were in agreement. A mesh sensitivity analysis was conducted to find optimum number of elements and reduce the computational time. It was proved that further increase of elements does not have a significant effect on the natural frequencies.

The drillstring-borehole interaction is also an interesting subject in the lateral mode analysis and several studies have been carried out on this subject [32,87,93,94].

Catastrophic collisions of the BHA with the wellbore lead to wear of the drillstring and MWD tools can also be catastrophically damaged by the successive side contacts [36]. The lateral contact force was considered as a Hertzian contact force in most studies [32,33,36,50,69,73,95]. An energy variational approach, the “Bypassing PDEs” method, and bond graph models were implemented to model the contact behavior with a Hertzian contact force by Christoforou *et al.* [69] and Ghasemloonia *et al.* [32,33,36]. Yigit *et al.* [48] and Jansen [89] applied the momentum balance method for the lumped representation of the drillstring element at the contact point to study the drillstring trajectory at the contact point. A detailed literature review about different drillstring-wellbore contact models can be found in chapter 5 for analytical models and in chapter 6 for FEM models.

The drillstring-mud interaction effects on the drillstring lateral dynamic behavior are important. Damping has been treated in different ways to model the lateral vibration of the drillstring. Paslay *et al.* [96] used an undamped model in their analyses, while Christoforou *et al.* [69], Jansen [89] and Ghasemloonia *et al.* [36] modeled the mud damping as a hydrodynamic drag force (velocity-squared proportional force). Spanos *et al.* [29] investigated an equation for damping as a function of the working frequency and the mud density in a developed FEM model. He divided the damping matrix into two dissipative and non-dissipative matrices to account for both Rayleigh damping and gyroscopic effects. The internal and external flow of the mud on the drillstring dynamic behavior (load carrying capacity and natural frequencies) was studied by Paidoussis *et al.* [97], Zhang *et al.* [98] and Ritto *et al.* [99]. Ritto *et al.* [99] reported that the role of mud damping on the axial and torsional natural frequencies is negligible, but should be considered in lateral vibration analysis of the drillstring. They also concluded that the effect of mud flow does not have a considerable effect on the lateral time response of the drillstring. In the FEM models, the mud viscous damping behavior in the lateral mode was mostly considered as Rayleigh damping, which is proportional to the mass and stiffness of each mode [51]. In the absence of a major source of dissipation, Rayleigh damping provides a convenient abstraction for damping low-frequency range behavior (mass dependent) and higher-frequency range behavior (stiffness dependent). A detailed literature review of applied damping models in the lateral mode can be found in chapter 6.

For the boundary value problem of the transverse motion of the drillstring, a beam element is often used to derive the mathematical equations. Drillstrings are assumed to be

beamlike structures. Due to the high slenderness ratio of the drillstring and low rotational speed, among the conventional models of the beam theory (Timoshenko, Rayleigh and Euler-Bernoulli), the Euler-Bernoulli beam theory is mostly used to model the lateral vibration of drillstrings [100]. The use of Euler-Bernoulli beam theory to model flexure-dominated (long) beams and the Timoshenko theory for shear-dominated (short) beams was also recommended by Beck *et al.* [101]. Simply-supported BCs for lateral vibrations at the stabilizer locations were suggested by Khulief *et al.* [37], Dareing [57], Heisig *et al.* [43] and Yigit *et al.* [48,50]. Field investigation by Jogi *et al.* [41] supported the assumption of simply supported BCs at the location of stabilizers. The top BC in the lateral direction is suggested to be fixed at the location of the rotary table [26,47,91,92]. Using the above conditions, one can find solution to the boundary value problem of the transverse vibration of the drillstring, extract lateral resonance frequencies, as well as lateral or radial trajectories of the drillstring inside the wellbore, including the contact points.

2.6.4 Coupled Modes of the Drillstring Vibration

As discussed earlier, the primary modes of the drillstring vibrations are axial, transverse and torsional. The change of axial force from tension to compression along the drillstring, the coupling nature of bit-rock interaction, high static driving torque and the curvature of the drillstring are major causes of coupled vibrations of the drillstring. While each certain mode of drillstring vibration is of great academic interest, coupled vibration study is very important in practical drilling engineering for a better understanding of the dynamic behavior of the drillstring. Coupled torsional-bending [20,47,49,73], coupled axial-

bending [36,50] and coupled axial-torsional [51,52] are three common coupled modes which are extensively studied by the researchers. It should be clarified that mode coupling does not imply nonlinearity, when simple classical boundary conditions are used as auxiliary equations in approximate solutions. Sampaio *et al.* [51] analyzed the axial-torsional vibration coupling of the drillstring. They analyzed the geometrical stiffening by the nonlinear finite element analysis, considering nonlinear strain displacement. Energy variational method was used to generate the equations. Both linear and nonlinear strain energy were assumed in their model. The coupled torsional-bending vibration of the drillstring was studied by Yigit *et al.* [73]. Due to the assumption of the bit-rock interaction, a highly nonlinear set of equations was derived. For the governing equations, they implemented Newton's method in polar coordinates for the lumped mass of the drillstring at the contact point with the wellbore. The stick-slip phenomenon for this coupled mode was also investigated in their research. Al-Hiddabi *et al.* [47] applied Newton's method in polar coordinates to derive the equations for coupled torsional-bending vibrations of the drillstring. According to their mathematical model, a nonlinear control method to suppress this coupled mode was suggested.

As a case study to show the coupled vibrations in the drillstring, a simple case of axial-lateral coupling is demonstrated here. A detailed explanation on deriving the coupled equations can be found in Chapters 4, 5, 6 and 7. Yigit *et al.* [50] derived the coupled axial-transverse vibration of a non rotating drillstring. Using the kinetic and strain energy of the beam and Lagrange's equations, the equations were developed. They assumed one Cartesian coordinate direction for lateral motion, instead of two orthogonal transverse

motions. Then, appropriate admissible functions according to the boundary conditions were substituted in the energy equations and after integration over the drillstring length domain, the coupled time domain differential equations were developed. A constant compressive force along the BHA was assumed and the mud damping, the buoyancy effect and gyroscopic terms were neglected. The following set of equations was derived at the last step after rearranging:

$$\begin{aligned} \ddot{q}_r + \left(\int_0^L EA(\phi_r')^2 dx \right) q_r + \frac{1}{2} \sum_{j=1}^N \sum_{k=1}^N \eta_j \eta_k \left(\int_0^L EA\phi_j' \phi_k' dx \right) &= 0 \\ \ddot{\eta}_n + \left\{ \left(\int_0^L EI(\phi_n'')^2 dx \right) - \sum_{i=1}^N \left[\int_0^L P\phi_i' \phi_n' dx \right] \right\} \eta_n + \sum_{i=1}^R \sum_{j=1}^N q_i \eta_j \left(\int_0^L EA\phi_j' \phi_i' dx \right) &= Q_n \end{aligned} \quad (2.5)$$

The third term in the second equation is the result of coupling for two generalized coordinates, i.e. q_r and η_j . The ϕ_r and ϕ_n are two admissible functions which are assumed for simply supported boundary conditions at both ends for transverse motion. The authors noted that assuming more realistic boundary conditions will result in slightly different results. R and N in the above set of equations are number of modes, which should be retained in the calculations. In their study only one mode was assumed for the sake of simplicity. Retaining higher number of modes will result in more realistic results, although it adds complexity to the model and numerical solutions. Although the torsional mode was neglected in their study, their model accurately predicted the axial and lateral drillstring downhole trend. A detailed discussion on the retained modes in analytical studies can be found in chapters 4 and 6.

2.7 Vibration Isolation Methods for the Drillstring

Unwanted vibrations of the drillstring can diminish the life of the collars and pipes. As a result of the drillstring vibrations, the rate of penetration and bit longevity will be reduced. The vibration isolation methods for drillstring axial and lateral vibrations are based primarily on two strategies: proper design of drillstring configuration (BHA length and stabilizer locations) to stay far away from the resonance state [21], passive isolators such as shock subs [103]. One of the best options for drillstring vibration isolation is to monitor the controllable parameters during the drilling process through the MWD tools. In the state of high vibrations level, the driller may adjust these parameters to reduce the vibration based on the provided remedial guidelines [102].

Vibration analysis at the design step of the BHA was proposed by Dareing [57] to avoid resonance state in drillstring through the adjustment of the BHA length. From a practical drilling standpoint, the rotational speed should be adjusted so that it does not correspond to one of the natural frequencies [92]. Certain combination of the WOB and rotary speed can be used to avoid or reduce vibrations for any configuration of the BHA. In another study, Gulyaev *et al.* [91,92] derived a mathematical model to describe the critical quasi static equilibrium of the rotating drillstring. They assumed gyroscopic interaction of linear and rotary motion. Then, the boundary value equations of the coupled orthogonal transverse mode with the simply supported boundary conditions were derived. The critical frequencies of this coupled mode were extracted and it was stated that the rotating speed of the drillstring should not be located in the resonance range.

Passive control through the use of shock subs is an efficient method in decoupling the source of vibration from the rest of the drillstring. Shock subs are mainly used to control the axial vibration of the drillstring. Shock subs are composed of a spring-damper system which is installed between the bit and the drill collars. Kreisle *et al.* [61] used a simple axial vibration model to study the effect of shock sub on the drillstring vibration reduction (Figure 2.11). A harmonic displacement BC at the bit was assumed and the boundary value problem of the drillstring axial vibration was numerically solved, using the Laplace method. Based on the numerical results, it was reported that the shock sub reduces the vibrations transmitted to the drillstring and the rig floor through a phase shift between the force and displacement at the bit. This is on the contrary to the common belief that the change in the resonance frequency due to the shock sub is the main cause of reducing the drillstring vibrations.

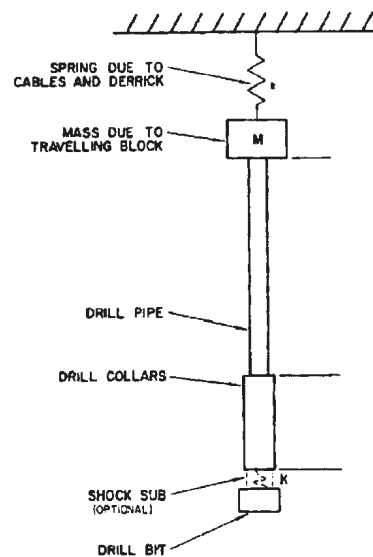


Figure 2.11: Schematic of the drillstring with shock sub [61]

Elsayed *et al.* [103] also suggested using a shock sub to isolate the source of vibration (bit-rock interaction) from the rest of the drillstring. They modeled the shock sub as a damped spring-mass system and used Matlab Simulink[®] to numerically solve the problem. The analysis was in the time domain and the results were presented for different damping ratios as well as different natural frequencies of the shock sub. Optimum values for shock sub parameters were suggested based on the RMS values of the acquired vibration signal for different combinations of the shock absorber parameters. They reported that springs which are too weak or too stiff are not effective in vibration reduction. Magneto-rheological dampers to achieve desired damping ratios was suggested in their study. The effect of axial lateral coupling on the efficacy of the shock sub was investigated by Warren *et al.* [104] and it was recommended to account for axial-lateral coupling in the shock sub performance studies. They investigated the role of shock sub on the reduction of axial vibrations and a reduction in lateral vibration levels with the use of shock subs was also reported. A detailed review of the state-of-the art methods of shock sub implementation in drillstring vibration isolation can be found in chapter 7.

2.8 Formulation of Equations of Motion: Newtonian and Energy Variational Approaches

In order to investigate the dynamic behavior of the drillstring, either in the frequency domain or the time domain, it is essential to derive the equations of motion of the drillstring for any desired state of motion (axial, transverse, torsional, or coupled modes) under prescribed loading condition (torque, load of downhole vibration generator, axial load, contact load). In the following section, two generalized methods for deriving the

equations of motion, namely the Newtonian approach and energy variational method (Lagrange's equation) will be discussed and some case studies of deriving the drillstring equations of motion based on these methods will be demonstrated. Also, the integral formulation approach can be implemented to derive the equations of motion of continuous systems. The reader is referred to [100] for further explanation of this method.

The Newtonian approach is based on the Newton's second law and is more suitable for concentrated systems (lumped modeling) or systems having one degree of freedom. This law states that "the rate of a change of the linear momentum of a system is equal to the net force acting on the system". This approach can be expressed mathematically as a differential equation [100]:

$$f(t) = \frac{d}{dt} \left(m \frac{dr}{dt} \right) = \frac{d}{dt} (m\bar{v}) = m\bar{a} \quad (2.6)$$

where $f(t)$ is the applied force vector, r is the position vector of the mass m , \bar{v} is the linear velocity and \bar{a} is the linear acceleration. The force $f(t)$ may be considered to include many types of force acting on the mass, such as elastic constraints which oppose displacements, viscous forces which resist velocities and independently defined external loads. For most problems in structural dynamics, it may be assumed that the mass is not varying with time.

The above equation can be rearranged as [100]:

$$f(t) - m \frac{d^2 r}{dt^2} = f(t) - m\bar{a} = 0 \quad (2.7)$$

which is the d'Alembert's principle. The second term, $m \frac{d^2 r}{dt^2}$, is called the inertia force or d'Alembert's force and resists the acceleration of the mass. This principle is just a restatement of the Newton's second law and states that "the sum of all external forces, including the inertia force, keeps the body in the state of dynamic equilibrium".

The Newtonian approach can be extended to the angular motion with the following definition: "the rate of change of angular momentum is equal to the net moment acting about the centroidal axis of the body":

$$M(t) = \frac{d}{dt}(I\omega) = I\dot{\omega} = I\alpha \quad (2.8)$$

$I\omega$ is the angular momentum about the center of mass, I is the constant mass moment of inertia of the body about the centroidal axis perpendicular to the plane of motion, ω is the angular velocity and α is the angular acceleration of the body. $M(t)$ is the net moment acting about the centroidal axis of the body.

Ghasemloonia *et al.* [32,33], Yigit *et al.* [48,49], Gulyaev *et al.* [91], Hakimi *et al.* [58] and Jansen [89] implemented the force-balance equation (Newtonian modeling) and derived the equations of motion of the drillstring. In all these studies a beam element was assumed and Newton's second law was expanded for all of the forces acting on the assumed beam element for a lumped parameter model. Vectorial notation was applied, while writing down the equations. Two case studies for deriving the equations of motion of the drillstring with the Newtonian approach will be discussed in details in chapters 3 and 4. This formulation is appropriate for formulation of certain points of the drillstring,

such as the drillstring-wellbore contact location and sensitivity studies of the dynamic behavior in that specific point.

The energy variational approach is preferred to the Newtonian approach for complicated systems having multiple degrees of freedom, systems having complex coordinate systems and systems having coupled motion in certain directions. This fact is due to the scalar measuring of energy variables compared to the vector form of the forces in the Newtonian approach. For problems with a rotary coordinate system or for nonlinear systems the energy method is also preferred. This approach is based on the concepts of Hamilton's principle and the principle of virtual work and will result in a set of equations called Lagrange's equations. A detailed discussion on the fundamental concepts of Hamilton's principle, the principle of virtual work and the mathematical derivation of the Lagrange's equation can be found in Appendix 2.

The Lagrange's equations based on the variational approach and energy conservation concept is a more fundamental method to derive the equations of motion of continuous structures, although more mathematical computations are involved in this method compared to the Newton's second law. Finally, it should be noted that two approaches are compatible. Recently, a new method for setting up the equations of motion through the conservation of energy is extensively applied to nonlinear coupled problems. This method is called the "Bypassing PDEs" and is implemented in chapters 5, 6 and 7 to derive the equations of motion in the coupled states of the drillstring vibration and will be discussed in the last part of this section.

The energy variational approach with Hamilton's principle was applied to the problem of drillstring vibration modeling by Mahyari *et al.* [21], Melakhessou *et al.* [30], Sahebkar *et al.* [105], Sampaio *et al.* [51], Heisig *et al.* [43], Christopherrou *et al.* [69] and Khulief *et al.* [37]. It starts with deriving the potential (strain) and kinetic energy equations of the drillstring as an integral over the drillstring length. Then, the equations for virtual work done by all the external forces (e.g. contact force, bit-rock interaction force, axial loads along the drillstring) are derived. In the next step, approximation methods such as assumed modes method are applied and integration is conducted over the length domain. The last step is deriving the time domain ODEs, using Lagrange's equations for generalized coordinates. Having the above set of ODE equations, one can proceed to the analysis of motion in the time or the frequency domain. A discussion of the solution methods of the resulting equations will follow in section 2-8.

2.9 The “Bypassing PDEs” Method

This enhanced method is developed to bypass the partial differential equations and set up the ordinary time differential equations from the Lagrangian equation of continuous systems. This method, which has been proven accurate for nonlinear problems [88], is based on combining the expanded Galerkin's technique with the Lagrange's equation for continuous structures, instead of the conventional Hamiltonian approach. In the expanded Galerkin technique, test functions, admissible functions and eigenfunctions (mode shapes) could be implemented, depending on the geometric configuration of the problem and the expected accuracy of results. A great advantage of the “Bypassing PDEs” is the use of conventional energy terms, rather than the variational form of the energy

equations, which further simplifies numerical solution of the developed equations at the final step. Therefore, conventional energy terms are derived instead of the variational form. The resulting time domain ODEs by this method are identical to the ones which are derived using the Hamilton's principle and assumed modes method. For further demonstration of this method, the lateral vibration of a continuous beam with a point mass and a concentrated load is analyzed in Appendix 3, using both conventional Hamiltonian method and the "Bypassing PDEs" method, which result in identical time domain ODEs in both methods. Ghasemlooia *et al.* [36] implemented this method to derive multi-mode analytical equations of the coupled axial-lateral vibrations of the drillstring in the presence of the downhole vibration generator tool and verified this method with a FEM model.

2.10 Solution Methods of Drillstring Analytical Models

Using either Newtonian or energy approaches, one will arrive at an "analytical" formulation of the boundary value problem. Applying a proper solution method is the next step to extract the dynamic time response of the drillstring vibration. Due to the coupling effect and nonlinearity of the drillstring vibration problem, closed form solution of the resulting PDEs is not feasible. Approximate methods must be applied to the set of resulting PDE's to convert them into a set of ODEs. One possible method is to implement approximate space domain functions in the resulting PDEs and integrate over the drillstring length to come up with low order set of time domain ODEs. The Rayleigh-Ritz method, assumed modes method and Galerkin's method are three common approximation methods which are extensively used to solve the resulting drillstring vibration PDE

equations [100]. These three methods are based on the assumption of a space domain function (trial function) according to the boundary conditions of the problem. Assume $u(x,t)$ is a displacement function in a certain direction for the drillstring [88]:

$$u(x,t) = \sum_{i=1}^n \phi_i(x) \eta_i(t) \quad (2.9)$$

Where $\phi_i(x)$ is a trial functions depending on the boundary conditions and the eigenvalue problem of free vibration and $\eta_i(t)$ is an unknown function of time (also called generalized coordinates).

Two categories of boundary conditions could be assumed for the vibration of continuous systems: essential and suppressible [88]. The geometric boundary conditions of the drillstring are categorized in the first class, while the static boundary conditions are in the second class. For example, for a clamped-clamped beam, all boundary conditions are essential, while for the clamped-free beam, the boundary conditions at the clamped end are essential, while the zero moment and zero shear force at the free end are suppressible boundary conditions. Based on these two classes of boundary condition, three types of trial functions can be defined and implemented with the above mentioned approximation methods: eigenfunction, test function (also called comparison function) and admissible function. Eigenfunction is the exact solution of the eigenvalue problem, which satisfies the differential equation and both types of boundary conditions. The test function is an approximate function which satisfies all the boundary conditions of the eigenvalue problem, but not necessarily the eigenvalue problem itself. The admissible function is the function which just satisfies the geometric or essential boundary condition of the

eigenvalue problem. Now, depending on the selection of the trial functions, one can decide about the type of approximate methods. If an admissible function is used for $\phi_i(x)$, it is called the Rayleigh-Ritz or assumed modes method and if a comparison function is used, it is called the Galerkin's approximation. The difference between the Rayleigh-Ritz and the assumed modes method is that the first one is used to solve the free vibration or the eigenvalue problem of a continuous system, while the later one is implemented to approximate forced vibration of a continuous system [100].

The above mentioned approximation methods are widely used for the nonlinear coupled vibration analysis of the drillstring. Assumed modes method is implemented by Yigit *et al.* [50], Christoforou *et al.* [69] and Mahyari *et al.* [21]. The Galerkin method is applied by Ghasemlooni *et al.* [33,36] and Vaz *et al.* [106]. Other techniques, such as Laplace transform [61], differential quadrature method [58] and transfer matrix method [90] were also applied as approximate solution techniques in the vibration analysis of the drillstring.

The number of modes (i value in equation 3-17) which should be retained in the approximation methods depends on the upper bound for the frequency of interest and the expected accuracy of the results. Most of the studies in the drillstring vibration assumed a single mode approximation [50], while some others conducted a multi-mode analysis of the problem by considering higher number of retained modes in the approximation methods [33,36]. The mass participation factor, the effective mass and the total modal effective mass are three factors, which can be extracted from finite element models, and are indicators of modes which are contributing more to the motion in a specific direction.

The participation factor indicates the predominant degree of freedom in which each mode acts in the model. In other words, this parameter indicates the strength of the motion in the eigenvector of that mode. The effective mass indicates the value of active mass in each degree of freedom at a specific mode. The total modal mass of the model is the sum of effective masses of all modes in any particular direction. The modes that are contributing a high mass compared to the mass of the model are kept in the analysis. This subject is discussed in detail in chapter 6 for the coupled-axial transverse vibration of the drillstring and the role of each parameter in retaining sufficient number of modes is discussed.

Once one of the above approximation methods is implemented to the coupled nonlinear PDE's of the drillstring vibration, and after integration over the drillstring length, using the mode orthogonality characteristic, the result is a set of coupled ordinary time differential equations. The initial conditions are then required to excite the system of ODEs. Any compatible set of initial conditions will suffice, as natural frequencies and steady state responses are not initial condition dependent. Several solution methods, such as Fehlberg fourth-fifth order adaptive Runge-Kutta method [33], Runge-Kutta method [36] and finite difference method [66] are applied to solve these algebraic equations. The great advantage of the adaptive solver is the dynamic time step reduction strategy compared to the fixed-step solvers. For the stiff ODEs, it is suggested to implement fixed step solvers with very small time increments to avoid jump discontinuities.

The result of the above solution procedure is a numerical matrix for the generalized coordinates. The results are then substituted back in the approximate methods to derive the time response of any point of interest along the drillstring. The equations can also be used to extract the drillstring or BHA natural frequencies [56,58,89,107,108].

Determining natural frequencies is important, because from an operational standpoint, vibration severity can be reduced if rotary speeds are kept far away from these frequencies.

In addition to natural frequencies, the axial, lateral and torsional time responses of the desired locations on the drillstring or BHA could be extracted from these analytical models. Yigit *et al.* [50], Spanos *et al.* [29], Li *et al.* [42] and Ghasemloonia *et al.* [32,33] used the analytical modeling to derive time response of the desired points on the BHA and the pipe section. A complete review of the outcomes and deliverables of analytical models can be found in chapter 5.

Solving the drillstring vibration problems with analytical methods is not always feasible. Difficulties in setting up the equations (specially in the coupled modes), difficulties in finding the approximate functions for realistic boundary conditions and complicated drillstring geometries, complexities in numerical solutions of the resulting system of ODEs due to the coupling and nonlinearity nature of the problem, as well as multi-mode analysis (retaining sufficient modes) are challenges involved in the analytical modeling of the drillstring vibration problems. It is also very difficult to reconfigure analytical models for new interactions and boundary conditions. These facts led researchers in the field to

the use of powerful numerical methods such as finite element analysis (FEA) and finite difference method (FDM). The FEA has been extensively implemented in the drillstring vibration modeling and the next section is a brief review of this technique and associated challenges.

2.11 Dynamic Finite Element Analysis (FEA) of the Drillstring

The difficulties and limitations of analytical modeling, coupled with the development of fast processing computers, have attracted investigators to the use of recognized powerful numerical methods, such as finite element analysis (FEA). FEA is an alternative method to derive and solve the equations of motion of the drillstring, investigate its vibration behavior, extract stress values and study the developed forces at different locations (nodes). It can also be a verification and tuning tool for the analytical models.

This technique is based on discretization of the continuous drillstring, setting up equilibrium compatibility equations, and their numerical solutions. This procedure is coded in off-the-shelf software such as ABAQUS. An extensive library of beam elements, dashpot elements, time varying forces, different contact algorithms, sophisticated hydrostatic damping models, efficient solvers, the ability to record nodal time histories and accounting for higher modes in modal analysis are the advantages of this software.

The first application of FEA to the problem of drillstring vibration was by Millheim *et al.* [34]. They modeled the non-rotating BHA using beam elements, and gap elements were used between drill collars and the wellbore. Stress and deflection modes at different parts of the BHA were investigated. Forced frequency response of the BHA was studied by

Apostal *et al.* [35], using the FEA method. They modeled the BHA as a non-rotating lumped mass. Flexural and torsional modes of the drillstring were studied by Axisa *et al.* [109] as two uncoupled modes. Gyroscopic and gravitational effects were not considered in their model. Dunayevsky *et al.* [74] used the FEA method to study the parametric instability of the drillstring, which was simply modeled as a uniform pinned-pinned beam. Berlioz *et al.* [86] used rotor dynamics FEA to derive a dynamic model of the drillstring. A shaft element with 6 degrees of freedom was assumed for modeling. They did not account for the change of the axial force in the drillstring from tension to compression at the neutral point. Melakhessou *et al.* [30] used FEA to study the contact behavior of the drillstring and the wellbore, just at the contact point. The drillstring was assumed as an unbalanced rotor supported by two bearings. They derived nonlinear equations of motion using Lagrange's equation. In a recent study, Khulief *et al.* [20] used the FEA method to study the rotating drillstring. Both drill collars and drill pipes sections were modeled and Lagrange's equations were applied to generate the equations of motion in the torsional-transverse mode. The drillstring with circular cross section was discretized into a number of finite shaft elements with 12 degrees of freedom. The gyroscopic effect, torsional-bending coupling and the gravity were considered in their model. The modal transformation technique was applied to develop a reduced order model form of the dynamic equations. Their model deliverables were the explicit expression of the lateral mode motion, modal characteristics (resonance frequency for the lateral mode in the first few modes) and time response of the drillstring (response of a specific node along the drillstring).

Approaches to model drillstring-wellbore contact in FEA are based on two major algorithms [110]. The first algorithm is based on the smooth impulsive force distribution during the impact interval, where the contact location could be modeled by an interface spring. In this approach the impact force is presented by the force-displacement law. Khulief *et al.* [87] implemented the continuous force-displacement law to model impulsive contact force in their FEM model. The material stiffness and damping coefficients were determined at the contact zone according to the energy balance relation. The second algorithm which is numerically more efficient [111] is based on an impulse-momentum balance equation or the conservation of momentum rule, since the impulsive forces cause an abrupt change in system velocities or momentum [36]. Yigit *et al.* [48] modeled the contact behavior in coupled torsional-bending motion, using the momentum balance method. Their impulse friction model included a compression phase and restitution phase, with assumed friction and restitution coefficients. A detailed literature review on the studies of drillstring-wellbore contact in both analytical and finite element modeling schemes can be found in chapter 6.

Two types of mud damping have been applied in FEA studies of the drillstring: Rayleigh damping and viscous damping (fluidelastic effects). Rayleigh damping relates the damping in the drillstring to the stiffness matrix and mass matrix developed in FEA models [51]. α_r (mass proportional damping) and β_r (stiffness proportional damping) are defined as:

$$C_i = \alpha_i m_i + \beta_i k_i \quad (2.10)$$

Rayleigh damping can be related to the other type of damping (critical damping) through the following equation [35]:

$$\xi_i = \frac{\alpha_r}{2\omega_i} + \frac{\beta_r\omega_i}{2} \quad (2.11)$$

where ω_i is the natural frequency of mode i . Spanos *et al.* [28] developed another equation for finding the damping ratios based on the frequency of each mode and the density of the mud and verified the equation with field test results. The mass proportional damping causes damping at each node in the FEA models which is related to the absolute velocity of that node. This is in agreement with the hydrodynamic drag damping model which is used in analytical studies of the drillstring vibrations, since both of them are velocity proportional damping models. Another advantage of the mass proportional damping is that the stability limit in the final numerical solution step is not sensitive to this factor, while the stiffness proportional damping reduces the stability limit of the numerical solution.

Khulief *et al.* [37] modeled the fluidelastic effects of the mud on the drillstring, using the semi-analytical approach introduced by Fritz [112] and Antunes *et al.* [113]. The early model was modified, since it was valid for annulus gap ratios less than 0.1 (the annulus gap ratio is greater than 0.1 in drilling applications). They developed the fluidelastic force equations in two directions (normal and tangential) for each element of the drillstring. The force equations were based on the density of mud, radial clearance, deflection of the string element and the rotary speed. The developed equations were then implemented in an FEA model and the model was tuned based on a laboratory test rig results.

One of the major problems of numerical modeling methods, such as the finite element analysis, is the heavy burden of computations. Determining a sufficient number of retained modes and element length is a critical task for numerical modeling to simplify the problem, while maintaining the accuracy of the results [33,36]. Mesh sensitivity analysis and effective mode determination techniques can be implemented to achieve low order, but accurate models. A detailed definition of the mesh sensitivity analysis and modal order determination can be found in chapter 6.

The FEA method in the present research is used as a verification tool for the analytical modeling. The natural frequencies as well as time responses of two implemented methods are compared. Also, the FEA technique is implemented to determine the predominant modes required for multi-mode analysis in the developed analytical models. As a case study of applying the FEA technique to drillstring vibration, a finite element model for lateral vibrations of the drillstring is explained in Appendix 4.

The following five chapters are the manuscripts based on the research plan defined in chapter one, section 1.4. Each chapter is a manuscript which is published or currently under review. At the start of each of the following chapters a brief review of the paper, where it has been published and its current status will be discussed. The last chapter (chapter 8) is a general concluding remark and recommendations for the future work.

2.12 References

[1] Smith, F. W., Kopczynski, W., 1961, "Oilfield Percussion Drilling," SPE#222, SPE California Regional Meeting, Bakersfield, California.

- [2] Han, G., Bruno, M., 2006, "Percussion Drilling: From Laboratory Tests to Dynamic Modeling," SPE#104178, SPE International Oil and Gas Conference, Beijing, China.
- [3] Sneddon, M. V., Megadiamond, S., and Hall, D. R., 1987, "Recent Advances in Polycrystalline Diamond (PDC) Technology Open New Frontiers in Drilling," SPE#17007, SPE Annual Technical Conference and Exhibition, Dallas, Texas.
- [4] Han, G., Bruno, M., and Dusseault, M. B., 2005, "Dynamically Modeling Rock Failure in Percussion Drilling," ARMA#05819, The 40th U.S. Symposium on Rock Mechanics (USRMS), Anchorage, Alaska.
- [5] Howard, G. C., Vincent, R. P., and Wilder, L. B., 1960, "Development and Field Use of a High Frequency Gas Operated Rotary Percussion Drilling Tool," *Journal of Petroleum Technology*, **12**(5), pp. 20-26.
- [6] Samuel, G. R., 1996, "Percussion Drilling ... Is It a Lost Technique? A Review," SPE#35240, Permian basin Oil and Gas Recovery Conference, Midland, Texas.
- [7] Han, G., Bruno, M., 1999, "Technology Assessment for Fundamental Research on Percussion Drilling: Improved Rock Mechanics Analysis, Advanced Simulation Technology and Full Scale Laboratory Investigation," Report submitted to U.S. Department of Energy, Contract No. DE-FC26-03NT4.
- [8] Han, G., Bruno, M., and Lao, K., 2005, "Percussion Drilling in Oil Industry: Review and Rock Failure Modeling," American Association of Drilling Engineers (AADE) National Technical Conference and Exhibition, Houston, Texas.
- [9] Bates, R. E., 1965, "Field Results of Percussion Air Drilling," *Journal of Petroleum Technology*, **17**(3), pp. 257-262.

- [10] Pixton, D. S., Hall, D R., and Summers, D., 1999, "Development and Testing of a Jet Assisted Polycrystalline Diamond Drilling Bit," Federal Geothermal Research Program Update, pp. 9-20.
- [11] Melamed, Y., Kiselev, A., Gelfgat, M., Dreesen, D., and Blacic, J., 2000, "Hydraulic Hammer Drilling Technology: Developments and Capabilities," ASME Journal of Energy Resources Technology, **122**(1), pp. 1-7.
- [12] Kutzner, C., 1996, *Grouting of Rock and Soil*, A. A. Balkema, Rotterdam, Netherlands.
- [13] Barton, S., Baez, F., and Al Ali, A., 2011, "Drilling Performance Improvement in Gas Shale Plays Using a Novel Drilling Agitator Device," SPE#144416, SPE North American Unconventional Gas Conference and Exhibition, The Woodlands, Texas.
- [14] Babatunde, Y., Butt, S. D., Molgard, J., and Arvani, F., 2011, "Investigation of the Effects of Vibration Frequency on Rotary Drilling Penetration Rate Using Diamond Drag Bit," ARMA#11-527, 45th US Rock Mechanics/Geomechanics Symposium (ARMA), San Francisco, California.
- [15] Manko, K. I., Pilipenko, V. V., and Zapols'ky, L. G., 2003, "Use Hydrodynamic Cavitation For Increase of Efficiency of Process of Well Drilling," Fifth International Symposium on Cavitation, Osaka, Japan.
- [16] Newman, K., Burnett, T., Pursell, J., and Ouahab Gouasmia, S., 2009, "Modeling the Affect of a Downhole Vibrator," SPE#121752, SPE/ICO TA Coiled Tubing and Well Intervention Conference, Houston, Texas.

- [17] Al Ali, A., Barton, S., and Mohanna, A., 2011, "Unique Axial Oscillation Tool Enhances Performance of Directional Tools in extended Reach Applications," SPE#143216, SPE Brasil Offshore, Macaé, Brazil.
- [18] Li, H., Butt, S. D., Munaswamy, K., and Arvani, F., 2010, "Experimental Investigation of Bit Vibration on Rotary Drilling Penetration Rate," ARMA# 10-426, 44th US Rock mechanics symposium (ARMA), Salt Lake City, Utah.
- [19] Khorshidian, H., Mozaffari, M., and Butt, S. D., 2012, "The Role of Natural Vibrations in Penetration Mechanism of a Single PDC Cutter," ARMA# 12-9, 46th U.S. Rock Mechanics/ Geomechanics Symposium (ARMA), Chicago, Illinois.
- [20] Khulief, Y. A., and Al-Naser, H., 2005, "Finite Element Dynamic Analysis of Drillstrings," *Finite Element in Analysis and Design*, **41**(13), pp. 1270-1288.
- [21] Mahyari, M. F., Behzad, M., and Rashed, G. R., 2009, "Drillstring Instability Reduction by Optimum Positioning of Stabilizers," *International Journal of Mechanical Engineering science, IMechE (Part C)*, **224**, pp. 647-653.
- [22] Leine, R. I., Van Campen, D. H., and Keultjes, W. J. G., 2002, "Stick-Slip Whirl Interaction in Drillstring Dynamics," *ASME Journal of Vibration and Acoustics*, **124**(2), pp. 209-220.
- [23] Mitchell, R. F., and Miska, S. Z., 2011, *Fundamentals of Drilling Engineering*, SPE textbook series, Texas, USA.
- [24] Aadnoy, B. S., and Kaarstad, E., 2006, "Theory and Application of Buoyancy in Wells," IADC/SPE#101795, IADC/SPE Asia Pacific Drilling Technology Conference and Exhibition, Bangkok, Thailand.

- [25] Wiercigroch, M., Krivtsov, A. M., and Wojewoda, J., 2008, "Vibrational Energy Transfer via Modulated Impacts for Percussive Drilling," *Journal of Theoretical and Applied Mechanics*, **46**(3), 715-726.
- [26] Bailey, J. R., et al., 2008, "Development and Application of a BHA Vibrations model," IPTC#12737, International Petroleum Technology Conference (IPTC), Kuala Lumpur, Malaysia.
- [27] Elsayed, M. A., Phung, C. C., 2005, "Modeling of Drillstrings," 24th ASME International Conference on Offshore Mechanics and Arctic Engineering (OMAE), Halkidiki, Greece.
- [28] Spanos, P. D., and Payne, M. L., 1992, "Advances in Dynamic Bottomhole Assembly Modeling and Dynamic Response Determination," SPE/IADC# 23905, SPE/IADC Drilling Conference, New Orleans, Louisiana.
- [29] Spanos, P. D., Payne, M. L., and Secora, C. K., 1997, "Bottom-Hole Assembly Modeling and Dynamic Response Determination," *ASME Journal of Energy Resources Technology*, **119**(3), pp. 153-158.
- [30] Melakhessou, H., Berlioz, A., and Ferraris, G., 2003, "A Nonlinear Well-Drillstring Interaction Model," *ASME Journal of Vibration and Acoustics*, **125**, pp. 46-52.
- [31] Navarro-Lopez, E. M., Cortes, D., 2007, "Avoiding Harmful Oscillations in a Drillstring Through Dynamical Analysis," *Journal of Sound and Vibration*, **307**, pp. 152-171.

- [32] Ghasemloonia, A., Rideout, D. G., and Butt, S. D., 2010, "The Effect of Weight-On-Bit on the Contact Behavior of Drillstring and Wellbore," 9th International Conference on Bond Graph Modeling (ICBGM2010), Orlando, Florida.
- [33] Ghasemloonia, A., Rideout, D. G., and Butt, S. D., 2012, "Coupled Transverse Vibration Modeling of Drillstrings Subjected to Torque and Spatially Varying Axial Load," *Journal of Mechanical Engineering Science (IMechE, part C)*, **227**(5), pp. 946-960.
- [34] Millheim, K., Jordan, S., and Ritter, C. J., 1978, "Bottom Hole Assembly Analysis Using the Finite Element Method," *Journal of Petroleum Technology*, **30**(2), pp. 265-274.
- [35] Apostal, M. C., Haduch, G. A., and Williams, J. B., 1990, "A Study to Determine the Effect of Damping on Finite Element Based Forced Frequency Response Models for Bottomhole Assembly Vibration Analysis," SPE#20458, SPE Annual Technical Conference and Exhibition, New Orleans, Louisiana.
- [36] Ghasemloonia, A., Rideout D. G. and Butt, S. D., 2013, "Vibration Analysis of a Drillstring in Vibration-Assisted Rotary Drilling: Finite Element Modeling With Analytical Validation," *ASME Journal of Energy Resources Technology*, **135**(3), pp. 032902-1-032902-18.
- [37] Khulief, Y. A., Al-Sulaiman, F. A., 2009, "Laboratory Investigation of Drillstring Vibrations," *Journal of Mechanical Engineering Science (IMechE Part C)*, **223**(10), pp. 2249-2262.

- [38] Khulief, Y. A., Al-Sulaiman, F. A., 2007, "Experimentally-Tuned Mathematical Model for Drillstring Vibrations," DETC# 2007-350357, ASME International Design Engineering Technical Conference (IDETC/CIE), Las Vegas, Nevada.
- [39] Raymond, D. W., Elsayed, M. A., Polsky, Y., and Kuszmaul, S. S., 2007, "Laboratory Simulation of Drill Bit Dynamics Using a Model-Based Servohydraulic Controller," ASME Journal of Energy resources technology, **130**(4), 1-12.
- [40] Franca, L. F. P., Weber, H. I., 2003, "Experimental and Numerical Study of a New Percussive Drilling Model with a Drift," 19th ASME Biennial Conference on Mechanical Vibration and Noise, Chicago, Illinois.
- [41] Jogi, P. N., Macpherson, J. D., and Neubert, M., 2002, "Field Verification of Model-Derived Natural Frequencies of a Drillstring," ASME Journal of Energy Resources technology, **124**(3), pp. 154-162.
- [42] Li, Z., Yanshan, U., and Guo, B., 2007, "Analysis of Longitudinal Vibration of Drillstring in Air and Gas Drilling," SPE#107697, SPE Rocky Mountain Oil and Gas Technology Symposium, Denver, Colorado.
- [43] Heisig, G., Neubert, M., 2000, "Lateral Drillstring Vibrations in Extended-Reach Wells," IADC/SPE# 59235, IADC/SPE Drilling Conference, New Orleans, Louisiana.
- [44] Aminfar, O., Khajepour, A., 2008, "Torsional Vibration Analysis of Drillstring in Blasthole Drilling," ASME International Mechanical Engineering Congress (IMECE), Boston, Massachusetts.
- [45] Jardine, S., Malone, D., and Sheppard, M., 1994, "Putting a Damper on Drillings Bad Vibrations," Oilfield Review, 6(1), pp. 15-20.

- [46] Christoforou, A. P., Yigit, A. S., 2001, "Active Control of Stick-Slip Vibrations: The Role of Fully Coupled Dynamics," SPE#68093, SPE Middle East Oil Show, Bahrain.
- [47] Al-Hiddabi, S. A., Samanta, B., and Seibi, A., 2003, "Nonlinear Control of Torsional and Bending Vibrations of Oil Well Drillstrings," *Journal of Sound and Vibration*, **265**(2), pp. 401-415.
- [48] Yigit, A. S., Christoforou, A. P., 1998, "Coupled Torsional and Bending Vibrations of Drillstrings Subject to Impact With Friction," *Journal of Sound and Vibration*, **215**(1), pp. 167-181.
- [49] Yigit, A. S., Christoforou, A. P., 2000, "Coupled Torsional and Bending Vibrations of Actively Controlled Drillstrings," *Journal of Sound and Vibration*, **234** (1), 67-83.
- [50] Yigit, A. S., and Christoforou, A. P., 1996, "Coupled Axial and Transverse Vibrations of Oilwell Drillstrings," *Journal of Sound and Vibration*, **195**(4), pp. 617-627.
- [51] Sampaio, R., Piovan, M. T., and Lozano, G. V., 2007, "Coupled Axial Torsional Vibrations of Drillstring by Means of Nonlinear Model," *Journal of Mechanics Research Communications*, **34**, pp. 497-502.
- [52] Elsayed, M. A., Raymond, D. W., 2002, "Analysis of Coupling Between Axial and Torsional Vibration in a Compliant Model of a Drillstring Equipped with a PDC Bit," ASME 2002 Engineering Technology Conference on Energy (ETCE), Houston, Texas.
- [53] Challamel, N., Sellami, H., Chenevez, E., and Gossuin, L., 2000, "A Stick-Slip Analysis Based on Rock-Bit Interaction: Theoretical and Experimental Contribution," IADC/SPE#59230, IADC/SPE Drilling Conference, New Orleans, Louisiana.

- [54] Baumgart, A., 2000, "Stick-Slip and Bit-Bounce of Deep-Hole Drillstrings," ASME Journal of Energy Resources Technology, **122**(2), pp. 78-82.
- [55] Yigit, A. S., Christoforou, A. P., 2006, "Stick-Slip and Bit-Bounce Interaction in Oil-Well Drillstrings, ASME Journal of Energy Resources Technology, **128**(4), 268-274.
- [56] Dareing, D. W., 1984, "Guidelines for Controlling Drillstring Vibrations," ASME Journal of Energy Resources Technology, **106**(2), pp. 272-277.
- [57] Dareing, D. W., 1984, "Drill Collar Length Is a Major Factor in Vibration Control," Journal of Petroleum Technology, **36**(4), pp. 637-644.
- [58] Hakimi, H., Moradi, S., 2009, "Drillstring Vibration Analysis Using Differential Quadrature Method," Journal of Petroleum Science and Engineering, **70**(3-4), pp. 235-242.
- [59] Ashley, D. K., McNary, X. M., and Tomlinson, J.C., 2001, "Extending BHA Life With Multi-Axis Vibration Measurements," SPE/IADC# 67696, IADC/SPE Drilling Conference, Amsterdam, Netherlands.
- [60] Shuttleworth, N. E., Kerkoerle, E. J., Folmer, D. R., and Foekema, N., 1998, "Revised Drilling Practices, VSS-MWD Tool Successfully Addresses Catastrophic Bit/Drillstring Vibrations," IADC/SPE#39314, IADC/SPE Drilling Conference, Dallas, Texas.
- [61] Kreisle, L. F., and Vance, J. M., 1970, "Mathematical Analysis of the Effect of Shock Sub on the Longitudinal Vibrations of an Oilwell Drillstring," SPE Journal, **10**(4), pp. 349-356.

- [62] Bailey, J. J., and Finnie, I., 1960, "An Analytical Study of Drillstring Vibration," ASME Journal of Engineering Industry," **82**(2), pp. 122 – 128.
- [63] Paslay, P., Bogy, D. B., 1963, "Drill String Vibrations Due to Intermittent Contact of Bit Teeth," ASME Journal of Manufacturing Science and Engineering, **85**(2), pp. 1-8.
- [64] Dareing, D. W., Livesay, B. J., 1968, "Longitudinal and Angular Drillstring Vibrations With Damping," ASME Journal of Manufacturing Science and Engineering, **90**(4), pp. 1-9.
- [65] Spanos, P. D., Sengupta, R. A., and Pasley, P. R., 1995, "Modeling of Roller Cone Bit Lift-Off Dynamics in Rotary Drilling," ASME Journal of Energy Resources Technology, **117**(3), 115-124.
- [66] Chin, W. C., 1994, *Wave Propagation in Petroleum Engineering*, Gulf Publishing Company, Texas, USA.
- [67] Clayer, F., Vandiver, J. K., and Lee, H. Y., 1990, "The Effect of Surface and Downhole Boundary Conditions on the Vibration of Drillstrings," SPE#20447, SPE Annual Technical Conference, New Orleans, Louisiana.
- [68] Aarrestad, T. V., and Kyllingstad, A., 1993, "Rig Suspension Measurements and Theoretical Models and the Effect on Drillstring Vibrations," SPE Drilling and Completion, **8**(3), pp. 201-206.
- [69] Christoforou, A. P., and Yigit, A. S., 1997, "Dynamic Modeling of Rotating Drillstrings With Borehole Interactions," Journal of Sound and Vibration, **206** (2), pp. 243-260.

- [70] Macpherson, J. D., Jogi, P. N., and Kingman, J. E. E., 2001, "Application and Analysis of Simultaneous Near Bit and Surface Dynamics Measurements," *SPE Drilling and Completion*, **16**(4), pp. 230-238.
- [71] Elsayed, M. A., Dareing, D. W., and Vonderheide, M. A., 1997, "Effect of Torsion on Stability, Dynamic Forces and Vibration Characteristics in Drillstrings," *ASME Journal of Energy Resources Technology*, **119**(1), pp. 11-19.
- [72] Yigit, A. S., Al-Ansary, M.D., and Khalid, M., 1997, "Active Control of Drillstring Vibrations by Mode Localization," *Journal of Structural Control*, **4**(1), pp. 47-63.
- [73] Yigit, A. S., and Christoforou, A. P., 1998, "Coupled Torsional and Bending Vibrations of Drillstrings Subject to Impact With Friction," *Journal of Sound and Vibration*, **215**(1), pp. 167-181.
- [74] Dunyaevsky, V. A., Abbassian, F., and Judzls, A., 1993, "Dynamic Stability of Drillstrings Under Fluctuating Weight on Bit," *SPE Drilling and Completion*, **8**(2), pp. 84-92.
- [75] Skaugen, E., Kyllingstad, A., Aarrestad, T. V., and Tonnesen, H. A., 1987, "Experimental and Theoretical Studies of Vibrations in Drillstrings Incorporating Shock Absorbers," 12th World Petroleum Congress, Houston, Texas.
- [76] Sananikone, P., Kamoshima, O., and White, D. B., 1992, "A Field Method for Controlling Drillstring Torsional Vibrations," IADC/SPE#23891, SPE/IADC Drilling Conference, New Orleans, Louisiana.
- [77] Brett, J. F., 1992, "The Genesis of Torsional Drillstring Vibrations," *SPE Drilling Engineering*, **7**(3), pp. 168-174

- [78] Chen, S. L., Blackwood, K., and Lamine, E., 2002, "Field Investigation of the Effects of Stick-Slip, Lateral and Whirl Vibration on Roller Cone Bit Performance, SPE Drilling & Completion," **17**(1), pp. 15-20.
- [79] Kriesels, P. C. et al., 1999, "Cost Saving Through an Integrated Approach to Drillstring Vibration Control," SPE/IADC#57555, SPE/IADC Middle East drilling technology conference, Abu Dhabi, UAE.
- [80] Jansen, J. D., Steen, L. V. D., 1995, "Active Damping of Self Excited Torsional Vibrations in Oil Well Drillstrings," *Journal of Sound and Vibration*, **179**(4), 647-668.
- [81] Lin, Y. Q., Wang, Y. H., 1991, "Stick-Slip Vibration of Drillstrings," *ASME Journal of Engineering for Industry*, **113**, pp. 38-43.
- [82] Zamanian, M., Khadem, S. E., and Ghazavi, M. R., 2007, "Stick-Slip Oscillations of Drag Bits by Considering Damping of Drilling Mud and Active Damping System," *Journal of Petroleum Science and Engineering*, **59**(3-4), pp. 289-299.
- [83] Dunayevsky, V. A., Abbasian, F., 1998, "Application of Stability Approach to Bit Dynamics," *SPE Drilling and Completion*, **13**(2), pp. 99-107.
- [84] Richard, T., Gernay, C., and Detournay, E., 2007, "A Simplified Model to Explore the Root Cause of Stick-Slip Vibrations in Drilling Systems With Drag Bits," *Journal of Sound and Vibration*, **305**(3), pp. 432-456.
- [85] Sotomayor, G. P. G., Placido, J. C., and Cunha, J. C., 1997, "Drillstring Vibration: How to Identify and Suppress," SPE#39002, Latin American and Caribbean Petroleum Engineering Conference, Rio de Janeiro, Brazil.

- [86] Berlioz, A., Der Hagopian, J., Dufour, R., and Draoui, E., 1996, "Dynamic Behavior of a Drillstring: Experimental Investigation of Lateral Instabilities," *ASME Journal of Vibration and Acoustics*, **118**(3), pp. 292-298.
- [87] Khulief, Y. A., Al-Sulaiman, F. A., and Bashmal, S., 2008, "Vibration Analysis of Drillstrings With String-Borehole Interaction," *International Journal of Mechanical Engineering Science, (IMEchE Part C)*, **222**(11), pp. 2099-2110.
- [88] Thomsen, J. J., 2003, *Vibrations and Stability*, 2nd ed., Springer, Berlin, Germany.
- [89] Jansen, J. D., 1991, "Nonlinear Rotor Dynamics as Applied to Oil Well Drillstring Vibrations," *Journal of Sound and Vibration*, **147** (1), 115-135.
- [90] Chen, S. L., Geradin, M., 1995, "An Improved Transfer Matrix Technique as Applied to BHA Lateral Vibration Analysis," *Journal of Sound and Vibration*, **185**(1), pp. 93-106.
- [91] Gulyaev, V. I., Lugovoi, P. Z., Belova, M. A., and Solov'ev, I. L., 2006, "Stability of the Equilibrium for Rotating Drillstrings," *International Applied Mechanics*, **42**(6), pp. 692-698.
- [92] Gulyaev, V. I., Lugovoi, P. Z., Gaidaichuk, V. V., and Solov'ev, I. L., 2007, "Effect of the Length of a Rotating Drillstring on the Stability of Its Quasistatic Equilibrium," *International Applied Mechanics*, **43** (9), pp. 1017-1023.
- [93] Zhao, G. H., Lian, Z., 2008, "Analysis of Collision Between Drillstring and Well Sidewall," *International Journal of Modern Physics B*, **22**(31-32), pp. 5459-5464.

- [94] Placido, J. C. R., Santos, H. M. R., and Galeano, Y. D., 2002, "Drillstring Vibration and Wellbore Instability," *AME Journal of Energy Resources Technology*, **124**(4), pp. 217-222.
- [95] Hsu, F., Wilhoit, J., and James, C., 1965, "Lateral Vibration of Drill Pipe Including Wall Reaction," SPE#1046, Conference on Drilling and Rock Mechanics, Austin, Texas.
- [96] Paslay, P. R., Yih-Min, J., Kingman, J. E. E., and Macpherson, J. D., 1992, "Detection of BHA Lateral Resonances While Drilling With Surface Longitudinal and Torsional Sensors," SPE#24583, SPE Annual Technical Conference and Exhibition, Washington, D.C.
- [97] Paidoussis, M. P., Luu, T. P. and Prabhakar, S., 2008, "Dynamics of a Long Tubular Cantilever Conveying Fluid Downwards, Which Then Flows Upwards Around the Cantilever as a Confined Annular Flow," *Journal of Fluids and Structures*, **24**, pp. 111-128.
- [98] Zhang, Q. and Miska, S., 2005, "Effects of Flow-Pipe Interaction on Drill Pipe Buckling and Dynamics," *ASME Journal of Pressure Vessels*, **127**, pp. 129-136.
- [99] Ritto, T. G., Sampaio, R. and Soize, C., 2009, "Drill-String Nonlinear Dynamics Accounting for Drilling Fluid," 30^o CILAMCE-Iberian-Latin-American Congress on Computational Methods in Engineering, Armação dos Búzios, Rio de Janeiro.
- [100] Rao, S. S., 2007, *Vibration of Continuous Systems*, JOHN WILEY & SONS, Inc, New Jersey, USA.
- [101] Beck, A. T., da Silva Jr., C.R.A., 2010, "Timoshenko Versus Euler Beam Theory: Pitfalls of a Deterministic Approach," *Structural Safety*, **33**(1), pp. 19-25.

- [102] Nicholson, J. W., 1994, "An Integrated Approach to Drilling Dynamics Planning, Identification and Control," IADC/SPE#27537, SPE/IADC Drilling Conference, Dallas, Texas.
- [103] Elsayed, M. A., Aissi, C., 2006, "Analysis of Shock Absorber Characteristics for Drillstrings," 8th Biennial ASME Conference on Engineering System Design and Analysis, Torino, Italy.
- [104] Warren, T. M., Oster, J. H., Hughes, C., and Chen, D. C. K., 1998, "Shock Sub Performance Tests," IADC/SPE# 39323, IADC/SPE Drilling Conference, Dallas, Texas.
- [105] Sahebkar, S. M., Ghazavi, M. R., Khadem, S. E., Ghayesh, M. H., 2011, "Nonlinear Vibration Analysis of an Axially Moving Drillstring System With Time Dependent Axial Load and Axial Velocity in Inclined Well," *Journal of Mechanisms and Machine Theory*, **46**(5), pp. 743-760.
- [106] Vaz, M. A., and Patel, M. H., 1995, "Analysis of Drillstrings in Vertical and Deviated Holes Using the Galerkin Technique," *Engineering Structures*, **17**(6), pp. 437-442.
- [107] Gulyayev, V. I., Borshch, O. I., 2011, "Free Vibrations of Drillstrings in Hyper Deep Bore-Wells," *Journal of Petroleum Science and Engineering*, **78**(3-4), pp. 759-764.
- [108] Gulyayev, V. I., Gaidaichuk, V. V., Solovjov, I. L., and Gorbunovich, I. V., 2009, "The Buckling of Elongated Rotating Drillstrings," *Journal of Petroleum Science and Engineering*, **67**(3-4), pp. 140-148.
- [109] Axisa, F., Antunes, J., 1992, "Flexural Vibration of Rotors Immersed in Dense Fluids: Part I- Theory," *Journal of Fluids and Structures*, **6**(1), pp. 3-21.

- [110] Khulief, Y. A., 2000, "Spatial Formulation of Elastic Multibody Systems with Impulsive Constraints," *Multibody System Dynamics*, **4**(4), pp. 383-406.
- [111] Wong, S. V., Hamuda, A. M. S., and Hasmi, M. S. J., 2001, "Kinematic Contact-Impact Algorithm with Friction," *International Journal of Crashworthiness*, **6**(1), pp. 65-82.
- [112] Fritz, R. J., 1970, "The Effect of an Annular Fluid on the Vibrations of a Long Rotor: Part 1-Theory, *Journal of Basic Engineering*," **92**, pp. 923-929.
- [113] Antunes, j., Axisa, f., and Hareux, F., 1990, "Flexural Vibrations of Rotors Immersed in Dense Fluids, Part 2-Experiments," *Third International Symposium on Transport Phenomena and Dynamics Rotating Machinery*, Honolulu, Hawaii.

3 The Effect of Weight on Bit on the Contact Behavior of Drillstring and Wellbore

Ahmad Ghasemloonia, Graduate Student

D. Geoff Rideout, Assistant Professor

Stephen D. Butt, Professor

Faculty of Engineering and Applied Science, Memorial University of Newfoundland,
St. John's, NL, Canada A1B 3X5

This chapter is based on the modeling step 1 defined in section 1.4 of this thesis and was presented as a research paper to the 9th International Conference on Bond Graph Modeling (ICBGM2010) in Orlando, Florida.

3.1 Abstract

The contact behavior of drillstring and wellbore is of great concern to drilling companies in the oil and mineral exploration industries. Due to the nonlinear, random motion of the drillstring in contact with the wellbore, it is difficult to predict the response of the drillstring. Successive contacts of wellbore and drillstring will result in fatigue failure and inhibit vibration-assisted rotary drilling mechanisms. Transverse vibration of a drillstring under a range of axial loads is studied in this paper. The impact of drill collars with the wellbore is modeled using Hertzian contact theory. The drillstring is treated as a simply

supported Euler-Bernoulli beam under axial load, or “weight-on-bit” (WOB). Natural frequencies were generated analytically using the assumed modes method and a bond graph model was generated. Extracting the motion of the contact point on the drill collar, which is at a known axial location, is easily done with modal bond graphs. The effect of WOB on the behavior of drill collar motion near the wellbore is studied, and the expected random, nonlinear behavior of the drillstring at the contact point is demonstrated and discussed. This work illustrates the advantages of the bond graph method to the drilling community, in which bond graphs are currently an underutilized technique.

Keywords: Drillstring, Vibration, Wellbore Contact, Weight-on-Bit

3.2 Introduction

The effect of different weight on bit (WOB) on the vibration behavior of a drillstring is studied in this paper. Weight on bit is an essential factor in the drilling process, which can affect the rate of penetration as well as natural frequencies of the drillstring in the bending mode of vibration. The WOB can also be related to the load carrying capacity of the drillstring (buckling load). In most cases of bending vibration, in the interest of simplicity or due to small values of loads, the effect of axial load on the vibration behavior is neglected. It is obvious that in the presence of large amount of axial force, natural frequencies decrease in compression and increase in tension [1]. In the extreme, as the WOB nears the buckling load, the first natural frequency approaches zero.

Yigit *et al.* [2] numerically solved the coupled transverse and axial vibration equations of motions of the drillstring using Lagrange’s equation. They found a nonlinear time-

dependent coupling term which affects the stability criteria of vibration behavior. In some papers, the Euler-Bernoulli beam model was assumed for drillstrings [2]. In another paper Christoforou [3] modeled the axial and transverse vibration of a rotating drillstring and found that it shows a nonlinear chaotic behavior in its contact with wellbore. Yigit *et al.* [4,5] also studied the torsional and bending motion of a rotating drillstring. It was found that these two modes of motion are also coupled to each other and have the potential for self-excited behavior.

In most previous works, only two kinds of motion, such as axial and transverse, axial and torsional, etc. have been studied [2,3,4,5]. In the case of a rotating drillstring, rotary inertia effects were neglected in [6] and the drillstring was modeled as a Rayleigh beam. In this inherently complex problem there are yet other forces such as bit-formation interaction force and borehole contact force at stabilizer locations, which could be inserted into equations of motion.

Bond graph modeling of drillstrings is advantageous given that when new forces or interactions are added to the model, it is not essential to reconstruct the system model from a primary level again. Simulation models can be regenerated automatically to incorporate new forces [7]. This characteristic helps in creating basic drillstring models which can be augmented with phenomena such as mud damping effects and bit-rock interaction forces.

In this paper, the vibration behavior of a drillstring at the stabilizer point of contact is studied. This model is, to the authors' knowledge, the first application of the bond graph

modeling method to simulate drillstring behavior with wellbore contact. This problem is important due to the fact that vibration behavior of the drillstring affects bottomhole assembly (BHA) vibration, which has a significant effect on the drilling efficiency. In emerging drilling technologies such as vibration-assisted rotary drilling (VARD), it is essential to study and control the vibration of the drillstring, since any kind of vibration could impact penetration rate and bit wear.

3.3 Analytical Overview of the Problem

A drillstring can be considered to be a slender beam that consists of two main parts. The thin lightweight upper part is called the drill pipe and the thicker heavier section at the bottom is comprised of drill collars. The weight of the latter provides enough axial loads to maintain a certain amount of WOB. The bottomhole assembly components are attached to the end of the drill collars. A drillstring is under tension in the upper part and under compression in the collar section. It is desired that the drill pipe never undergoes compression and mostly drill collars are under compression [8]. This phenomenon is controlled through mud hydrostatic effects in the drilling process. In this paper, the vibration behavior of drill collars at the point of contact with wellbore is modeled. Therefore, the assumed model for this part is a beam, which is under compression as stated above. The gap between drill collars and the borehole wall is reduced with stabilizers, which help to keep drill collars centralized. A schematic view of drill string sections along with drill collars is shown in Figure 3.1.

An Euler-Bernoulli beam under axial compression load is assumed in this paper. The boundary condition in the lower point of the drillstring, *i.e.* bit, is assumed as simply supported for transverse motion, since it has the ability to move downward and is ideally restricted from moving laterally. The upper part of the beam (top of collars) is also considered as a simply supported constraint, due to the fact that the drill pipe restricts lateral motion. A schematic view of the Euler-Bernoulli beam under compression load is shown in Figure 3.2.

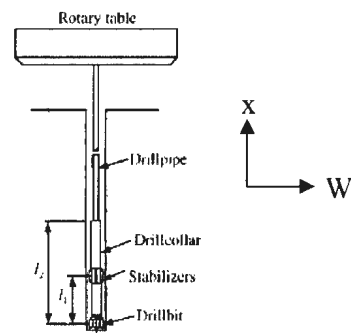


Figure 3.1: Schematic view of drillstring and stabilizer [5]

In order to derive the characteristic equation of the beam, Newton's law is applied on an element of the beam as follows:

$$-(V + dV) + V - (P + dP)\sin(\theta + d\theta) + P\sin\theta = \rho A dx \frac{\partial^2 W}{\partial t^2} \quad (3.1)$$

$$(M + dM) - (V + dV)dx - M = 0 \quad (3.2)$$

Having $\frac{\partial M}{\partial x} = V$, $EI \frac{\partial^2 W}{\partial x^2} = M(x)$ and assuming the following equation for small θ :

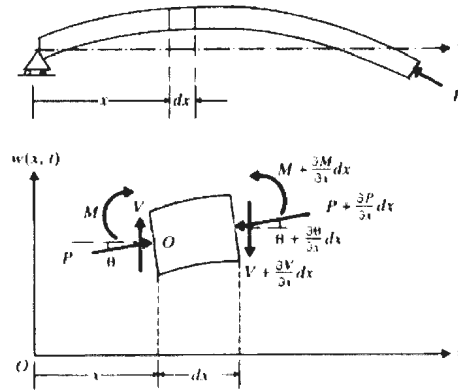


Figure 3.2: Schematic of drillstring under weight on bit and corresponding element [9]

$$\sin(\theta + d\theta) \cong \theta + d\theta \approx \theta + \frac{\partial \theta}{\partial x} dx = \frac{\partial W}{\partial x} + \frac{\partial^2 W}{\partial x^2} dx \quad (3.3)$$

Substituting the above assumptions in Equation 3.1:

$$EI \frac{\partial^4 W}{\partial x^4} + \rho A \frac{\partial^2 W}{\partial t^2} + P \frac{\partial^2 W}{\partial x^2} = 0 \quad (3.4)$$

Using the method of separation of variables and assuming that $W(x,t) = Y(x) \cdot f(t)$, the

following equation will be generated:

$$EI \frac{d^4 Y}{dx^4} + P \frac{d^2 Y}{dx^2} - \rho A \omega^2 Y = 0 \quad (3.5)$$

The general solution for the above equation is in the following form:

$$Y(x) = C_1 \left\{ \cosh \left(\frac{P}{2EI} + \left(\frac{P^2}{4E^2 I^2} + \frac{\rho A \omega^2}{EI} \right)^{1/2} x \right) \right\} + C_2 \left\{ \sinh \left(\frac{P}{2EI} + \left(\frac{P^2}{4E^2 I^2} + \frac{\rho A \omega^2}{EI} \right)^{1/2} x \right) \right\} \\ + C_3 \left\{ \cos \left(\frac{P}{2EI} - \left(\frac{P^2}{4E^2 I^2} + \frac{\rho A \omega^2}{EI} \right)^{1/2} x \right) \right\} + C_4 \left\{ \sin \left(\frac{P}{2EI} - \left(\frac{P^2}{4E^2 I^2} + \frac{\rho A \omega^2}{EI} \right)^{1/2} x \right) \right\} \quad (3.6)$$

Since the boundary conditions are assumed as simply supported, the coefficients of C_1 up

to C_4 are determined by substituting the following equations in Equation 3.6:

$$Y(0) = 0 \quad Y(l) = 0 \quad (3.7)$$

$$\frac{d^2Y}{dx^2}(0) = 0 \quad \frac{d^2Y}{dx^2}(l) = 0$$

Substituting the above boundary conditions in Equation 3.6, the equation of motion and frequency characteristic equation for the drillstring as a function of weight on bit, geometry and material properties of drillstring are:

$$Y(x) = C_4 \sin\left(\frac{n\pi}{l}x\right) \quad (3.8)$$

$$\omega_n = \frac{\pi^2}{l^2} \left\{ \frac{EI}{\rho A} \left(n^4 - \frac{n^2 Pl^2}{\pi^2 EI} \right) \right\}^{1/2}$$

Since for the Euler-Bernoulli beam, the critical buckling load is $P_{cr} = \frac{\pi^2 EI}{l^2}$, Equation 3.8

can be restated in the following form:

$$\omega_n = \frac{\pi^2}{l^2} \left\{ \frac{EI}{\rho A} \left(n^4 - n^2 \frac{P}{P_{cr}} \right) \right\}^{1/2} \quad (3.9)$$

It is obvious that the natural frequency of the first mode will tend to zero as the weight on bit reaches to the buckling load limit [9, 1].

3.4 Bond Graph Modeling of the Drillstring

Due to the accuracy limitation of lumped segment models, the modal expansion method of bond graph modeling is used in this paper [7]. The exact response is an infinite sum of a linear combination of individual mode shapes. In this paper, the first five modes have been retained.

Applying the modal expansion equations, the modal mass of the model is, using Equation 3.8:

$$m_n = \int_0^l \rho A Y_n^2 dx = \int_0^l \rho A \sin^2\left(\frac{n\pi}{l} x\right) dx = \frac{\rho A l}{2} \quad n = 1, 2, 3, \dots \quad (3.10)$$

The modal stiffness would be in the following form:

$$k_n = m_n \omega_n^2 \quad \text{for } n=1, 2, 3, \dots \quad (3.11)$$

Substituting the natural frequency for each mode from Equation 3.8 and modal mass from Equation 3.10, which is a constant value in this case, the modal stiffness value for each mode is calculated.

The designed bond graph model for this paper is shown in Figure 3.3. The modal mass constant box provides the mass signal for each mode. There is a corresponding C element for each mode, which accounts for related modal stiffness. Since it is of interest to study the behavior of the drillstring at the point of contact with wellbore via a stabilizer, the transformers are the values of the mode shapes at the stabilizer axial location.

At the point of contact between the stabilizer and the wellbore, Hertzian contact theory is used to model the impact force on the drillstring. In the simplest form, the Hertzian contact force is estimated by the following nonlinear equation:

$$F = k_s \delta^{3/2} \quad (3.12)$$

where k_s is related to the material properties (Young modulus) of the colliding objects and their geometry as well as their shapes [10]. In the case of a drillstring at the point of contact with wellbore, there is a small gap, which should be taken into account in

determining Hertzian contact force. Since there is a back and forth displacement of the center of the drill collars with respect to the central axis of wellbore, the direction of the applied force should be tuned to the direction of movement via a sign function in the output of the contact force block. The contact force equation thus takes the following form:

$$F = k_s(Y - b_{cl})^{3/2} \text{sign}(Y) \quad (3.13)$$

where b_{cl} is the small gap between borehole and drill collars and Y is the transverse displacement of the drill collars.

The transverse displacement “ Y ”, obtained through an integration block, is an input signal to the contact force block. The output of the contact force block modulates the source of effort (Mse) which is applied to the contact point as shown in Figure 3.3. In order to excite the system, initial values are assigned to the parameters. To generate a consistent set of initial displacement conditions, a step force input is applied to the stabilizer and the steady state variable values are used as initial conditions for subsequent simulation.

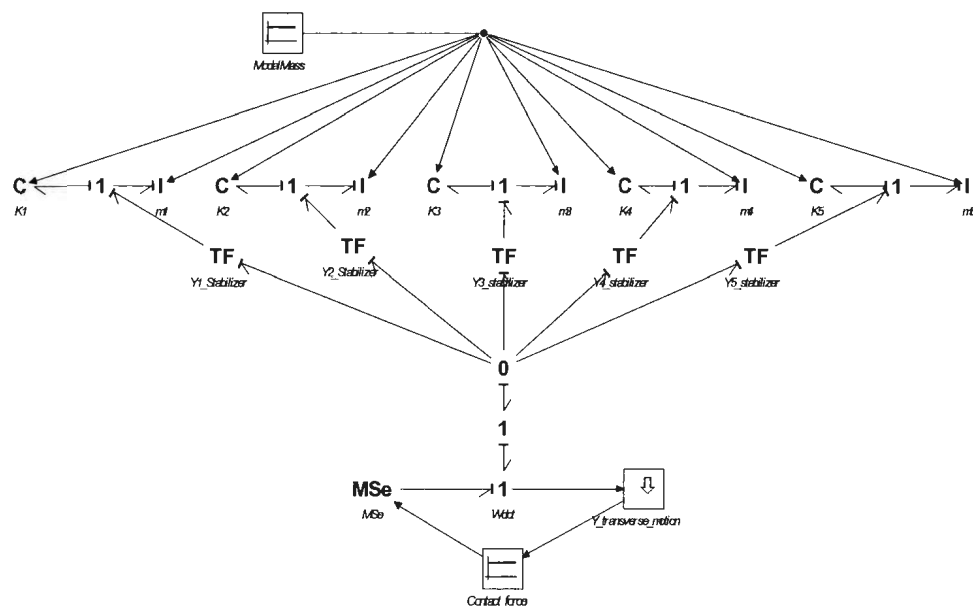


Figure 3.3: Bond graph model of drillstring with wellbore contact point at stabilizer

3.5 Modeling Results

The object of this paper is to study the effect of weight on bit on the vibration behavior of a drillstring as it contacts the wellbore. According to the drillstring length, geometry and material characteristics, the buckling load is about 400 kN. A complete table of parameters and their numerical values is given in Appendix 3.1. Two values of weight on bit are used: 150 kN and 350 kN. The latter value is close to the buckling load. 20Sim software was used for bond graph modeling. The Vode Adams integration method was selected with absolute and relative integration tolerances of $1e^{-6}$. The maximum step size was 0.0001. The simulation results for the 150 kN force are shown in Figure 3.4.

As shown in Figure 3.4, for a low value of weight on bit, the drillstring bounces to the other side of the wellbore with each contact. As expected, when the contact load is

applied to the drillstring, the velocity decreases to zero and changes direction. Figure 3.5 is a zoomed view of Figure 3.4 at one contact point, showing appropriate behavior of the elastic contact model. Figure 3.6 shows the phase plane of the drillstring response for the 150 kN weight on bit. As shown in this Figure, the drillstring shows a chaotic behavior, moving all around the gap between wellbore and drillstring.

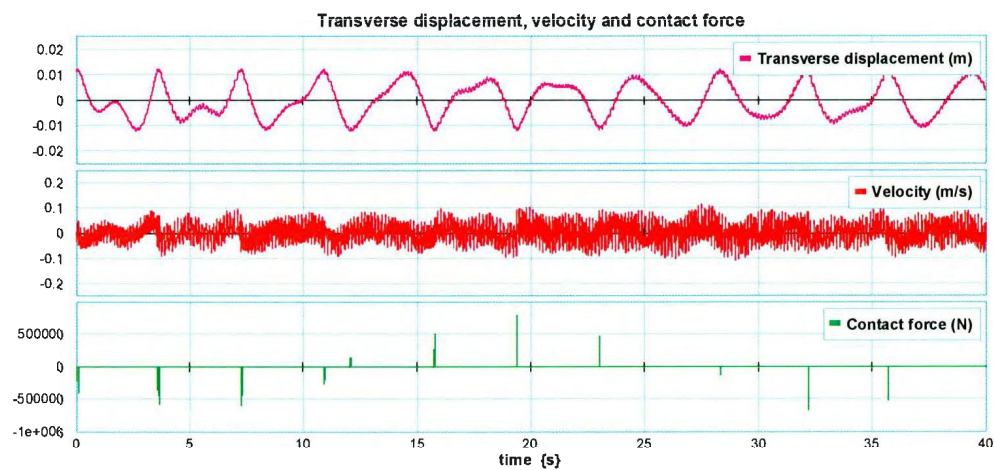


Figure 3.4: Transverse displacement (w), velocity and contact force at the point of contact between drillstring and wellbore for 150 kN weight on bit

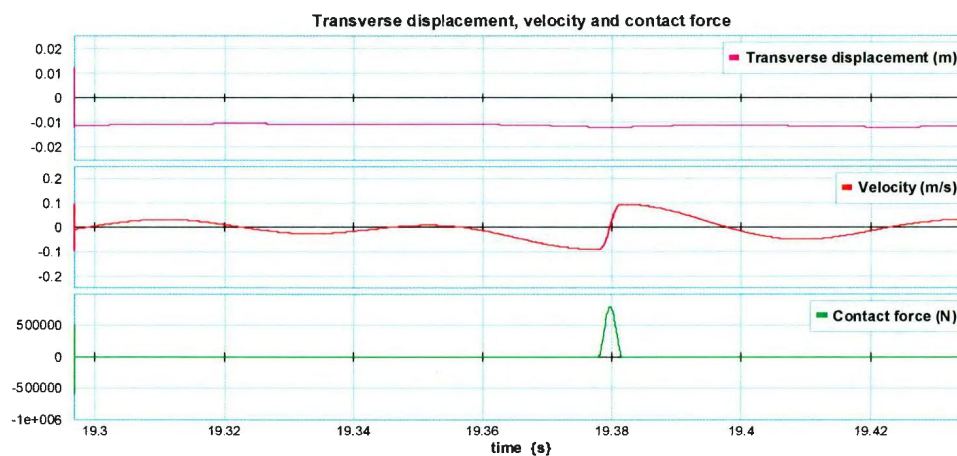


Figure 3.5: Behavior of Hertzian contact element

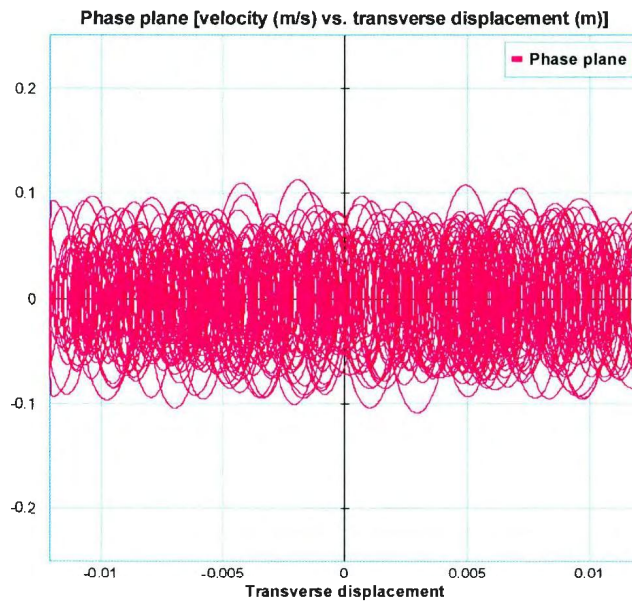


Figure 3.6: Phase plane for WOB = 150 kN

The contact force versus position of the drillstring is shown in Figure 3.7. The contact force is only applied to the drillstring when the position of the drillstring exceeds the gap between the wellbore and drillstring.

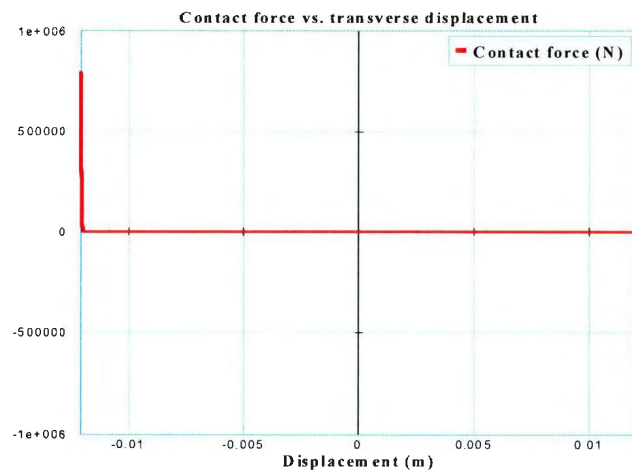


Figure 3.7: Contact force versus position of drillstring

The results of modeling the drillstring with 350 kN of WOB are shown in Figures 3.8, 3.9 and 3.10. In contrast to the 150 kN case, the drillstring contacts one side of the wellbore repeatedly before moving to the other side. The transition from one side to the other is non-periodic.

Comparing the contact force diagram (part 3 of each Figure) of Figures 3.4 and 3.10, it is clear that in the case of higher weight on bit, the majority of drillstring motion should be around the wellbore walls. This fact is verified again in the phase diagram of Figure 3.8.

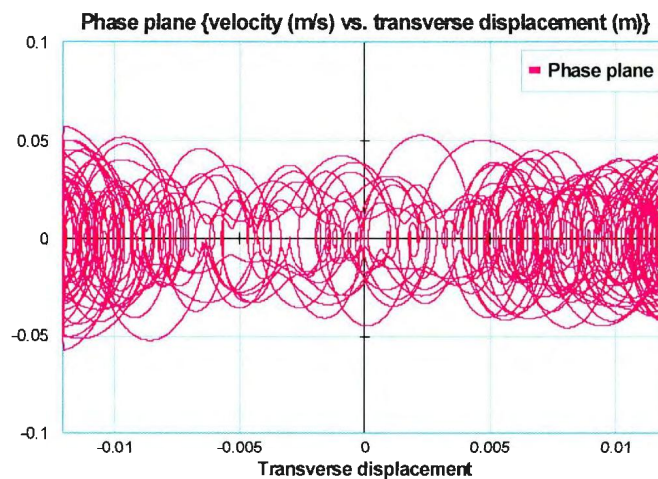


Figure 3.8: Phase plane for WOB = 350 kN

The diagram is much denser near the walls of the wellbore than at the center of the well. For 150 kN WOB there is no concentration in a specific location. The contact force diagram with respect to the location of the drillstring for the higher loading is shown in Figure 3.9.

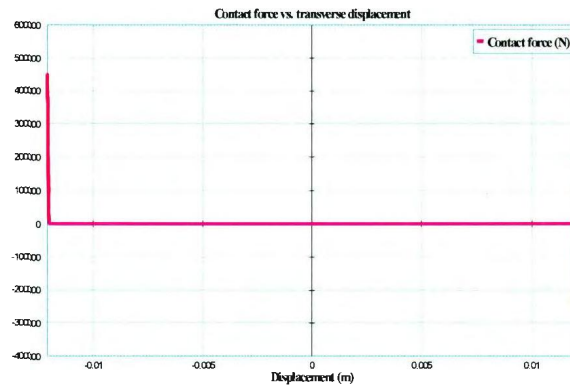


Figure 3.9: Contact force versus position of drillstring

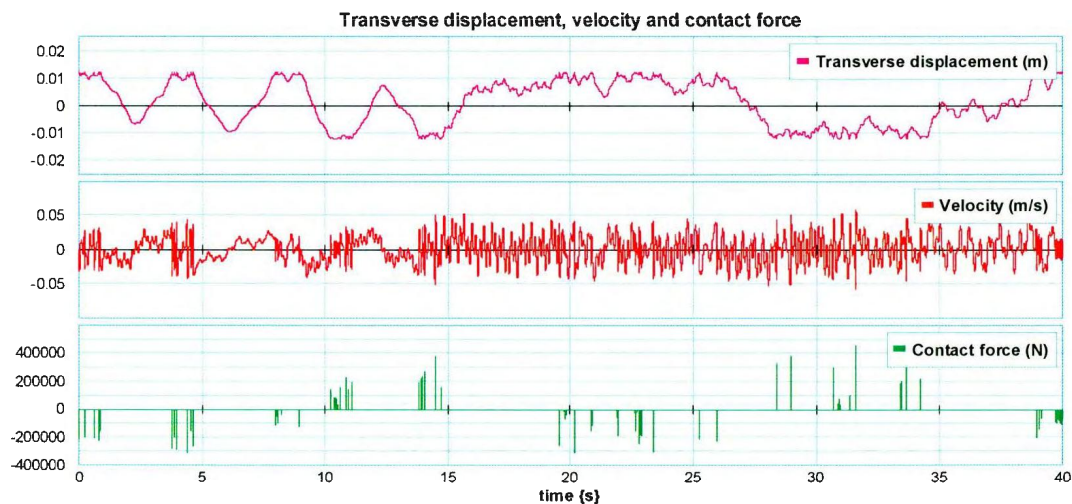


Figure 3.10: Transverse displacement (w), velocity and contact force at the point of contact between drillstring and wellbore for 350 kN weight on bit

3.6 Conclusions

Transverse vibration behavior of a drillstring under different weight on bit (WOB) at the contact point with a wellbore was studied. Both low weight on bit and high weight on bit (close to buckling load limit) loadings show nonlinear chaotic behavior. Motion of the drillstring under low WOB showed that after each contact with the wellbore, the

drillstring moves to the other side of the wellbore. In the case of higher WOB, which is close to the buckling limit of the Euler-Bernoulli beam, multiple impacts with the same side of the wellbore occur. Mostly, drilling companies work under low WOB, which is not close to buckling limit. It is recommended as future work to consider the frequency of a rotating beam under axial load, take into account the mud damping effect at the point of contact, and study the vibration behavior in two states - drill bit in contact with formations and drill bit not in contact with formations. Research is ongoing to study the effect of introducing vibration to the drillstring to improve penetration rate and drilling efficiency. Therefore, studying the vibration behavior in contact with wellbore under all engaging loads, using the approach of this paper, will be useful for the design of control methods to improve efficiency and penetration rate.

3.7 References

- [1] Meirovitch, L., 1967, *Analytical Methods in Vibration*. The Macmillan Company, London.
- [2] Yigit, A. S., Christoferou, P., 1996, "Coupled Axial and Transverse Vibrations of Oilwell Drillstring," *Journal of Sound and Vibration*, **195**(4), pp. 617-627.
- [3] Christoferou, A. P., and Yigit, A. S., 1997, "Dynamic Modeling of Rotating Drillstrings With Borehole Interactions," *Journal of Sound and Vibration*, **206** (2), pp. 243-260.
- [4] Yigit, A. S., Christoferou, A. P., 1998, "Coupled Torsional and Bending Vibrations of Drillstrings Subject to Impact With Friction," *Journal of Sound and Vibration*, **215**(1), pp. 167-181.

- [5] Yigit, A. S., Christoforou, A. P., 2000, "Coupled Torsional and Bending Vibrations of Actively Controlled Drillstrings," *Journal of Sound and Vibration*, **234** (1), 67-83.
- [6] Sheu, G. J., Yang, S. M., 2005, "Dynamic Analysis of a Spinning Rayleigh Beam," *International Journal of Mechanical Science*, **47**(2), pp. 157-169.
- [7] Karnopp, D. C., Margolis, D. L., and Rosenberg, R. C., 2006, *System Dynamics: Modeling and Simulation of Mechatronic Systems*, 4th edition, John Wiley&Sons, Inc., New Jersey, USA.
- [8] Bourgoyne, A. T., Chenevert, M. E., Millheim, K. K., and Young, F. S., 1986, *Applied Drilling Engineering*, SPE Text Book Series, Society of Petroleum Engineers, Texas, USA.
- [9] Rao, S. S., 1995, *Mechanical Vibrations*, 3rd edition, Addison-Wesley Publishing Company, New York, USA.
- [10] Stronge, W. J., 2000, *Impact mechanics*, Cambridge University Press, Cambridge, UK.

3.8 Biography

Ahmad Ghasemloonia received his B.Eng. (Mechanical) from the University of Tabriz, Iran in 2003. He worked in Quality Control at the SAPCO Company while pursuing his M.Sc. in Applied Mechanics at Tarbiat Modares University. His research areas during Master's study were engine condition monitoring and gearbox fault diagnosis. He worked for MAPNA Group after graduation as a Q.C. engineer. He is currently a Ph.D. student in Mechanical Engineering at Memorial University, Canada. His main research areas are

assessment of vibration modes, coupled vibration simulation of drillstrings in offshore oil drilling and rotary percussive dynamics.

Geoff Rideout received his B.Eng. (Mechanical) from Memorial University of Newfoundland in 1993. After working in the telecommunications equipment manufacturing and building systems consulting industries, he earned his M.A.Sc. in Mechanical Engineering from Queen's University in Kingston, Ontario and his Ph.D. in Mechanical Engineering from the University of Michigan. He has lectured at the University of Michigan and at the Humber Institute for Advanced Technology and Applied Learning in Toronto. He is currently an Assistant Professor at Memorial University, teaching mechanics and design. His research areas are automated modeling, vehicle dynamics and control, vibration-assisted drilling, and nondestructive testing of power transmission line poles.

Stephen D. Butt has B.Eng. and M.Sc. degrees from Memorial University of Newfoundland, a Ph.D. from Queen's University in Kingston, Canada, and is a registered Professional Engineer. In 1996, he joined the Department of Mining and Metallurgical Engineering at Technical University of Nova Scotia in Halifax, Canada (which later merged with Dalhousie University) where he held several academic appointments including Professor and Mining Program Chair. In 2006, he joined the Faculty of Engineering and Applied Science at Memorial University of Newfoundland where he is currently Professor and Associate Dean. His research activities are in the area of geomechanics and the development of geophysical imaging technology for various

applications in petroleum, mining and civil engineering, such as innovative drilling technology, reservoir characterization, geotechnical subsurface investigations, structural health monitoring of concrete structures, and sub-sea moorings. He holds current or recent research funding from the Natural Sciences and Engineering Research Council, Atlantic Innovation Fund, Petroleum Research Atlantic Canada, Husky Energy, Suncor Energy, and Conestoga Rover Associates, along with in-kind contributions from several mining, petroleum and technology development companies. He has supervised numerous Highly Qualified Personnel and has published in a variety of scholarly journals, industry publications and conference proceedings.

3.9 Appendix 3.1

Table 3.1: Drillstring Properties

Characteristic	Value
Modulus of Elasticity	200 GPa
Density	7860 kg/m ³
L1	20 m
L2	200 m
Collar Diameter	0.2 m
Hertzian Coefficient	$6.78 \times 10^{11} \text{ N.m}^{3/2}$
Borehole Gap	0.1 m

Table 3.2: Bond Graph Model Properties

Characteristic	Value
Modal mass (kg)	24680.4
First mode transformer modulus	0.3
Second mode transformer modulus	0.58
Third mode transformer modulus	0.8
Fourth mode transformer modulus	0.95
Fifth mode transformer modulus	1.0

4 Coupled Transverse Vibration Modeling of Drillstrings Subjected to Torque and Spatially Varying Axial Load

Ahmad Ghasemloonia, Ph.D. Candidate

D. Geoff Rideout, Associate Professor

Stephen. D. Butt, Professor

Advanced Drilling Group, Faculty of Engineering and Applied Science, Memorial
University, St. John's, NL, Canada

This chapter is based on the modeling step 2 defined in section 1.4 of this thesis and is published as a full research paper in the International Journal of Mechanical Engineering Science (IMechE, Part C), vol. 227(5), pp. 946-960.

4.1 Abstract

Predicting and mitigating unwanted vibration of drillstrings is an important subject for oil drilling companies. Uncontrolled vibrations cause premature failure of the drillstring and associated components. The drillstring is a long slender structure that vibrates in three primary coupled modes: torsional, axial and transverse. Among these coupled modes, the transverse mode is the major cause of drillstring failures and wellbore washout. Modal analysis of drillstrings reveals critical frequencies and helps drillers to avoid running the bit near critical modes. In this paper, the coupled orthogonal modes of transverse

vibration of a drillstring in the presence of torque and spatially varying axial force (due to mud hydrostatic effect, self weight and hook load) are derived and the mode shapes and natural frequencies are determined through the expanded Galerkin method. The results are verified by the nonlinear finite element method. Modal mass participation factor, which represents how strongly a specific mode contributes to the motion in a certain direction, is used to determine the appropriate number of modes to retain so that computational efficiency can be maximized.

Keywords: Drillstring, transverse vibration, coupled modes, Galerkin's method, mode participation factor, finite element method, modal mass participation factor

4.2 Introduction

The subject of drillstring vibration is an ongoing challenging for drillers in oil fields. The effects of vibration on drilling performance, wellbore stability, joint failures, fatigue, etc. have led drilling companies to strengthen components or try to control and mitigate these effects to attain higher performance. In order to control or mitigate the vibration, its behavior and characteristics should be revealed and modeled analytically [1, 2], experimentally in laboratory scale [3], or through field verification [4].

A drillstring is a slender structure which consists of drill pipes at the upper sections and drill collars and stabilizers at the bottom sections. The drill pipes are hollow pipes (assumed 120 mm outer diameter, 10 mm thickness in this paper) that are lighter than the collars (normally with an outer diameter of 120-240 mm and thickness of 30-80 mm). The bit is attached to the bottom of the collars. The lower section is called the "bottom

hole assembly” or BHA. The lower, heavier BHA is more easily excited to vibrate than the pipe section. This is due to the presence of an axial load, which is varying spatially along the drillstring length. This linearly varying axial load is a result of three interacting axial forces: hook load, self weight of the drillstring and mud hydrostatic force. Drilling performance is very sensitive to the axial force at the bit, i.e., weight on bit (WOB), and WOB is one of the main parameters adjusted during drilling to improve penetration rate. Rate of penetration, or ROP, is the conventional index for measuring the efficiency of the drilling process.

The dominant role of BHA vibrations on the total drillstring vibration was verified by Dareing [5], who showed that the collars are easily excited in the lower modes. The pipes, in tension, vibrate at higher excitation frequencies [6], as will be shown in the later section on finite element modeling. In most cases, the rotational speed at the normal operational conditions is not high enough to excite the higher modes. The other reason for analyzing the BHA is that measurement-while-drilling (MDW) tools are mostly located near the bit in the BHA and any type of BHA vibrations interfere with the interpretation of down-the-hole (DTH) status at the surface. Finally, the BHA is composed of collars which are heavy and stiff and any type of unwanted vibration dissipates a portion of energy which is supposed to be delivered to the bit. Therefore, an increased understanding of the BHA vibrations will give valuable insight into potential vibration, and ways to avoid it, under normal operating conditions.

The primary modes of drillstring vibrations are axial, transverse and torsional [7, 8, 9]. These modes are coupled together via terms containing variables like torque [10]. Coupled torsional-bending [11], coupled axial-bending [12] and coupled axial-torsional [13] are three common combinations of coupled modes. Stick-slip oscillations [14] are torsional, while whirling and bit bounce [15] are examples of lateral and axial vibrations respectively. These vibrations can be transient or steady, depending on the drilling parameters such as WOB, torque, rotational speed and many other drilling conditions.

Among these primary modes, the transverse mode is said to be responsible for 75% of failures [16]. Bending waves are not propagated to the surface via the drillstring as are torsional and longitudinal waves, due to the difference in the wave speed for different types of modes. The propagation speed for axial and torsional motions is quite high compared to the lateral motion. Therefore, for any given length of the drillstring, axial and torsional waves travel a few wavelengths to reach to the surface, while in contrast, the lateral wave travels many wavelengths to be felt at the surface. Furthermore, transverse vibration is more highly damped than the other modes due to mud effects and wellbore contact [16]. Therefore, there could be severe bending vibrations deep in the hole, which the surface measuring tools do not indicate. As later finite element method (FEM) modeling will show, in the lower frequencies the collars are vibrating transversely, while the pipes do not vibrate and remain approximately undeflected. This is due to the axial load distribution along the drillstring, the collars of which are mainly under compression while the pipes are under tension. As a result of the tension, the natural

frequencies of the pipe section increase, while the natural frequencies of the collar section are reduced.

4.3 Literature Review

Due to the importance of the transverse mode, several studies have been done to understand the behavior of the drillstring in this mode. Jansen [17] studied the contact behavior between the stabilizer and the wellbore at the point of contact, using a lumped segment approach. He noticed that gravity and lateral coupling should be taken into account for more quantitative analysis. Chen *et al.* [18] studied the lateral vibration of a BHA in the presence of constant weight on bit, but neglecting the torque. Berlioz *et al.* [19] performed a laboratory test to study lateral vibration of the drillstring and showed that the influence of axial force is greater than that of the torque on the natural frequencies of the drillstring. However, they did not consider spatially varying axial load and coupled orthogonal lateral modes. Christoforou *et al.* [20] used the Lagrangian method to derive the equations of motion and study the drillstring trajectory in the lateral mode at the contact point. They used a sine wave as the dynamic WOB, without considering the torque as the coupling term for the lateral modes. Stability of the drillstring in the lateral mode was studied by Gulyaev *et al.* [21]. They investigated the buckling mode of the drillstring as a function of its length for special cases which have analytical solution. They showed that the buckling mode will occur at the section with the compressive axial force (collar section). In another work by Dareing [22], the sensitivity of drill collar vibration to the length was studied using simple beam equations without torque and axial load. Khulief *et al.* [23] used the finite element method to derive the

frequency and modal response of a rotating drillstring without torque. They compared the results for the full order model and developed a reduced order model for the total drillstring. The string borehole interaction was also an interesting subject in the lateral mode analysis and several studies have been carried out on this subject [24, 25].

Laboratory test rigs, field data and FEM models have been used extensively for verification of derived natural frequencies or time response of the BHA [4, 19, 23].

Coupled orthogonal transverse vibration of the drillstring in presence of torque and linearly varying axial force has not been previously addressed. The goals of this paper are analytical and numerical modeling of bending vibration of drill collars and accurate prediction of natural frequencies. Knowledge of such frequencies and understanding of the underlying physics will help drilling companies avoid resonance and reduce drillstring failures. In contrast to previous studies, this work includes the effects of steady torque and spatially-varying axial load, thereby revealing coupling between the orthogonal components of lateral vibration. The finite element method is used to validate analytical model predictions. This paper also uses the concept of modal mass participation factor to determine the required number of modes to retain. Retaining unnecessary modes can increase computation burden without significantly increasing model fidelity. The natural frequencies and mode shapes calculated using the methods of this paper can be exported for use in low-order modal expansion models [26]. While not matching the fidelity of high-order FEM models, low-order models can be more computationally efficient, more easily interfaced to other subsystem models, and still useful for top-level design studies.

In the following section, analytical equations of the drillstring lateral vibration, which are coupled via torque under linearly varying axial load, will be derived. The next section derives the governing equations and applied the expanded Galerkin method to solve them. Section 3 describes the FEM application and results. Section 4 discusses proper model order, and Section 5 states conclusions and future work.

4.4 Derivation of Governing Equations

Drillstrings are assumed to be beamlike structures. Due to the high slenderness ratio of the drillstring and low rotational speed, among the conventional models of beam theory (Euler-Bernoulli, Timoshenko and Rayleigh), the Euler-Bernoulli beam theory is used to model the lateral vibration of drillstrings. Since the aspect ratio is greater than 10 for the drillstring, the use of classical thin beam element (Euler-Bernoulli) is valid. Several studies have been carried out to model different types of vertical beams, e.g. Hijmissen *et al.* [27] which modeled the vertical beam under the effect of gravity.

In this paper, the direct Newtonian approach is used to derive the mathematical model. The rotation of the drillstring (Figure 4.1) and gyroscopic effect are neglected, since the string could be assumed as a low speed rotor [6, 9, 12, 18].

An element of the beam, which is under torque and linearly varying axial load, is considered. This element is located on a portion of the drillstring (beam), which is between two stabilizers (Figure 4.2). Two lateral directions, namely u and v , are considered for extracting the equations of motion. The elements in the uz plane and for vz

plane are shown in Figure 4.2. The following derivation refers to Equations 4.15-4.21 which can be found in Appendix 4.2.

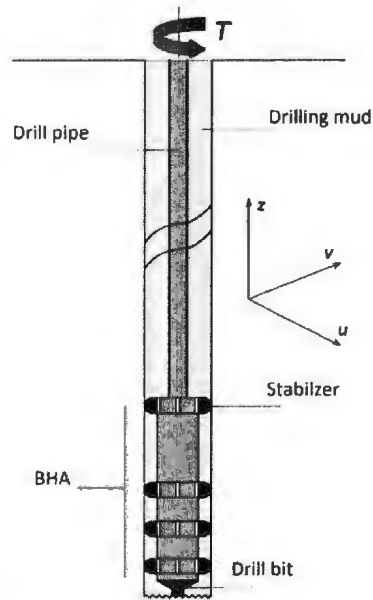


Figure 4.1: Schematic diagram of the drillstring in the wellbore

The torque \vec{T} is resolved along the selected element as two separate bending moments in the u and v directions as a result of bending curvature of the drillstring (Figure 4.3):

$$\vec{T} = \vec{T}_t + \vec{T}_n \quad (4.1)$$

The \vec{T} vector in the normal direction will be:

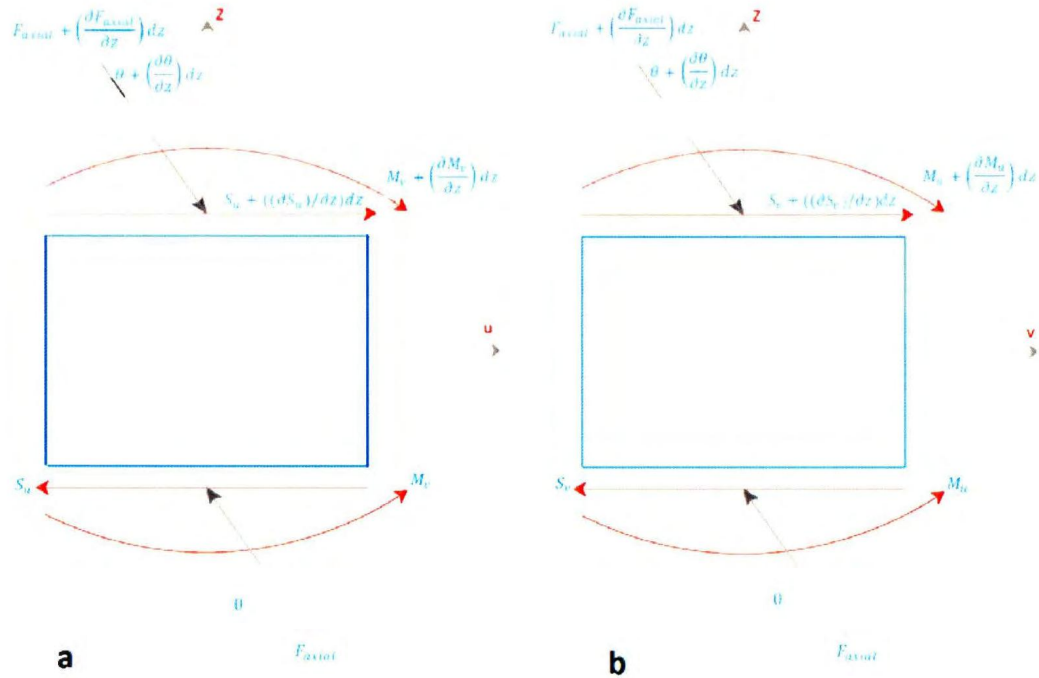


Figure 4.2: Drillstring elements between two stabilizers

a) The uz plane b) the vz plane

$$\begin{aligned}
 |\vec{T}_n| &= \vec{T} \cdot \vec{n} = (0, 0, T) \cdot \frac{1}{\sqrt{\left(\frac{du}{dz}\right)^2 + \left(\frac{dv}{dz}\right)^2 + 1}} \left(\frac{du}{dz}, \frac{dv}{dz}, 1\right) = \frac{T}{\sqrt{\left(\frac{du}{dz}\right)^2 + \left(\frac{dv}{dz}\right)^2 + 1}} \\
 \vec{T}_n &= |\vec{T}_n| \vec{n} = \frac{T}{\sqrt{\left(\frac{du}{dz}\right)^2 + \left(\frac{dv}{dz}\right)^2 + 1}} \cdot \frac{1}{\sqrt{\left(\frac{du}{dz}\right)^2 + \left(\frac{dv}{dz}\right)^2 + 1}} \left(\frac{du}{dz}, \frac{dv}{dz}, 1\right) \\
 &= \frac{T}{\left(\frac{du}{dz}\right)^2 + \left(\frac{dv}{dz}\right)^2 + 1} \left(\frac{du}{dz}, \frac{dv}{dz}, 1\right)
 \end{aligned} \tag{4.2}$$

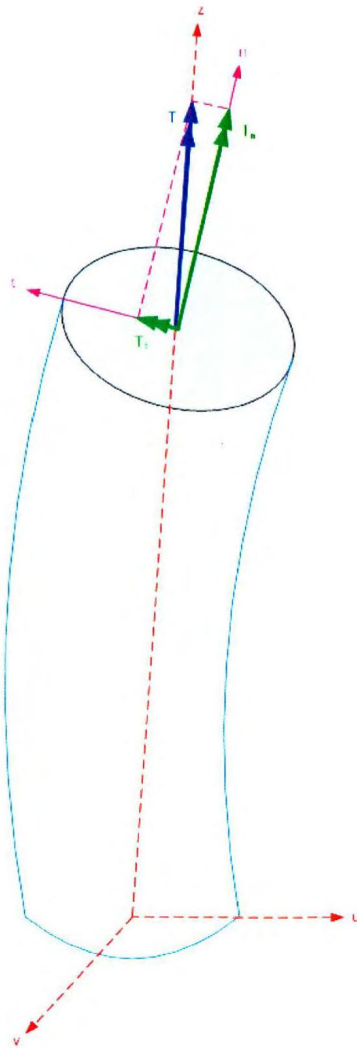


Figure 4.3: Torque in the z direction decomposed to tangential and normal components

Hence, the tangential component of the torque will be:

$$\begin{aligned}
 \vec{T}_t &= \vec{T} - \vec{T}_n = (0, 0, T) - \frac{T}{\left(\frac{du}{dz}\right)^2 + \left(\frac{dv}{dz}\right)^2 + 1} \left(\frac{du}{dz}, \frac{dv}{dz}, 1\right) \\
 &= \frac{T}{\left(\frac{du}{dz}\right)^2 + \left(\frac{dv}{dz}\right)^2 + 1} \left(-\frac{du}{dz}, -\frac{dv}{dz}, \left(\left(\frac{du}{dz}\right)^2 + \left(\frac{dv}{dz}\right)^2\right)\right)
 \end{aligned} \tag{4.3}$$

\bar{T}_i acts as a bending moment in the u and v directions. The corresponding coupled term in the equation of motion will be third order. The corresponding component of T_i as a

bending moment in the u direction is $\frac{-T \frac{dv}{dz}}{\left(\frac{du}{dz}\right)^2 + \left(\frac{dv}{dz}\right)^2 + 1}$. According to Equation 4.16 and

substituting for M_v (neglecting the second order differential terms):

$$\frac{\partial}{\partial z} \left(-T \frac{dv}{dz} \right) = S_u \quad (4.4)$$

As it is clear from Equations 4.18 and 4.19, the terms related to S_u will appear in the final equation of motion as $-\frac{\partial S_u}{\partial z}$. Therefore, Equation 4.20 is modified by substituting $-\frac{\partial S_u}{\partial z}$

and assuming the torque is constant:

$$-\frac{\partial S_u}{\partial z} = -\frac{\partial}{\partial z} \left(\frac{\partial}{\partial z} \left(-T \frac{dv}{dz} \right) \right) = T \frac{\partial^3 v(z,t)}{\partial z^3} \quad (4.5)$$

Therefore, the T term will be added to the equation of motion in the u direction as a third order derivative of v . The above procedure can be repeated in the v direction with the similar results, except a negative sign due to the opposite direction.

Adding these two coupling effects to Equations 4.20 and 4.21, and assuming the spatially varying axial force as $F_{axial} = F_0 - \rho Agz$ (Figure 4.4), the final form of the equations of motion for the two lateral directions is:

$$\begin{aligned} E.I_v \frac{\partial^4 u(z,t)}{\partial z^4} - \rho Ag \frac{\partial u(z,t)}{\partial z} + (F_0 - \rho Agz) \cdot \frac{\partial^2 u(z,t)}{\partial z^2} + T \frac{\partial^3 v(z,t)}{\partial z^3} + \rho A \frac{\partial^2 u(z,t)}{\partial t^2} &= 0 \\ E.I_v \frac{\partial^4 v(z,t)}{\partial z^4} - \rho Ag \frac{\partial v(z,t)}{\partial z} + (F_0 - \rho Agz) \cdot \frac{\partial^2 v(z,t)}{\partial z^2} - T \frac{\partial^3 u(z,t)}{\partial z^3} + \rho A \frac{\partial^2 v(z,t)}{\partial t^2} &= 0 \end{aligned} \quad (4.6)$$

where F_0 is the amount of compressive axial force at the top point of the collar section. The concentrated load at this point is due to mismatch of projected areas and the resulting resolved hydrostatic axial forces [28]. The derivation of the spatially varying axial force along the collar section can be found in Appendix 4.3.

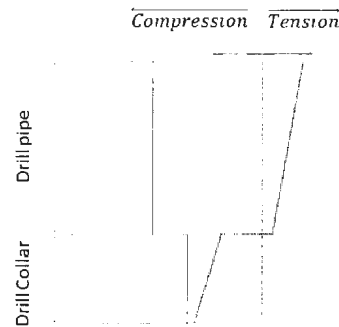


Figure 4.4: The profile of axial load along drillstring

The above set of equations is coupled by order of 3 through the torque. Although it is a set of linear equations, the varying axial load means there is not a closed form solution. In the following section, the above equations will be solved to find the natural frequencies of the drillstring as well as mode participation factors (Equation 4.7) for the first five modes of lateral vibration

4.5 Analytical Solution of the Equations

In this section the expanded Galerkin method is used to derive the characteristics of the lateral vibration of the drillstring. Transforming the set of coupled PDEs to a set of linear differential ODEs is the major benefit of this method. Due to the discretized mode shape functions in this method, the results can be analyzed separately in each mode and the

predominance of the modes for different sets of initial conditions can be verified. To apply this method to the above problem, $u(z, t)$ and $v(z, t)$ should be assumed as:

$$\begin{aligned} u(z, t) &= \sum_{i=1}^n \phi_i(z) \cdot p_i(t) \\ v(z, t) &= \sum_{j=1}^m \psi_j(z) \cdot q_j(t) \end{aligned} \quad (4.7)$$

where $\phi_i(x)$ and $\psi_j(x)$ are comparison functions, and $q_i(t)$ and $p_j(t)$ are mode participation factors [29]. The i and j subscripts depend on the desired mode shapes according to the frequency range of interest. For this problem five modes will be retained. Further discussion on the number of mode shapes that should be retained can be found in Section 4. The comparison functions based on assumption of simply supported B.C.s [3, 5, 9, 11, 12] are:

$$\begin{aligned} \phi_i(z) &= \text{Sin}\left(\frac{i\pi \cdot z}{l}\right) \\ \psi_j(z) &= \text{Sin}\left(\frac{j\pi \cdot z}{l}\right) \end{aligned} \quad (4.8)$$

If the above assumptions are substituted in Equation 4.7 and finally in Equation 4.6, the result is:

$$\begin{aligned}
& \rho A \left\{ \sin\left(\frac{\pi z}{l}\right) \ddot{p}_1(t) + \sin\left(\frac{2\pi z}{l}\right) \ddot{p}_2(t) + \sin\left(\frac{3\pi z}{l}\right) \ddot{p}_3(t) + \sin\left(\frac{4\pi z}{l}\right) \ddot{p}_4(t) + \sin\left(\frac{5\pi z}{l}\right) \ddot{p}_5(t) \right\} + EI_v \left\{ \frac{\pi^4 \sin\left(\frac{\pi z}{l}\right)}{l^4} p_1(t) \right. \\
& + \frac{16\pi^4 \sin\left(\frac{2\pi z}{l}\right)}{l^4} p_2(t) + \frac{81\pi^4 \sin\left(\frac{3\pi z}{l}\right)}{l^4} p_3(t) + \frac{256\pi^4 \sin\left(\frac{4\pi z}{l}\right)}{l^4} p_4(t) + \frac{625\pi^4 \sin\left(\frac{5\pi z}{l}\right)}{l^4} p_5(t) \left. \right\} + T \left\{ -\frac{\pi^3 \cos\left(\frac{\pi z}{l}\right)}{l^3} q_1(t) \right. \\
& - \frac{8\pi^3 \cos\left(\frac{2\pi z}{l}\right)}{l^3} q_2(t) - \frac{27\pi^3 \cos\left(\frac{3\pi z}{l}\right)}{l^3} q_3(t) - \frac{64\pi^3 \cos\left(\frac{4\pi z}{l}\right)}{l^3} q_4(t) - \frac{125\pi^3 \cos\left(\frac{5\pi z}{l}\right)}{l^3} q_5(t) \left. \right\} - \rho A g \left\{ -\frac{\pi \cos\left(\frac{\pi z}{l}\right)}{l} p_1(t) \right. \\
& + \frac{2\pi \cos\left(\frac{\pi z}{l}\right)}{l} p_2(t) + \frac{3\pi \cos\left(\frac{\pi z}{l}\right)}{l} p_3(t) + \frac{4\pi \cos\left(\frac{\pi z}{l}\right)}{l} p_4(t) + \frac{5\pi \cos\left(\frac{\pi z}{l}\right)}{l} p_5(t) \left. \right\} + (F_0 - \rho A g z) \left\{ -\frac{\pi^2 \sin\left(\frac{\pi z}{l}\right)}{l^2} p_1(t) \right. \\
& - \frac{4\pi^2 \sin\left(\frac{\pi z}{l}\right)}{l^2} p_2(t) - \frac{9\pi^2 \sin\left(\frac{\pi z}{l}\right)}{l^2} p_3(t) - \frac{16\pi^2 \sin\left(\frac{\pi z}{l}\right)}{l^2} p_4(t) - \frac{25\pi^2 \sin\left(\frac{\pi z}{l}\right)}{l^2} p_5(t) \left. \right\} = 0
\end{aligned} \tag{4.9}$$

For the v direction the result is as follows:

$$\begin{aligned}
& \rho A \left\{ \sin\left(\frac{\pi z}{l}\right) \ddot{q}_1(t) + \sin\left(\frac{2\pi z}{l}\right) \ddot{q}_2(t) + \sin\left(\frac{3\pi z}{l}\right) \ddot{q}_3(t) + \sin\left(\frac{4\pi z}{l}\right) \ddot{q}_4(t) + \sin\left(\frac{5\pi z}{l}\right) \ddot{q}_5(t) \right\} + EI_v \left\{ \frac{\pi^4 \sin\left(\frac{\pi z}{l}\right)}{l^4} q_1(t) \right. \\
& + \frac{16\pi^4 \sin\left(\frac{2\pi z}{l}\right)}{l^4} q_2(t) + \frac{81\pi^4 \sin\left(\frac{3\pi z}{l}\right)}{l^4} q_3(t) + \frac{256\pi^4 \sin\left(\frac{4\pi z}{l}\right)}{l^4} q_4(t) + \frac{625\pi^4 \sin\left(\frac{5\pi z}{l}\right)}{l^4} q_5(t) \left. \right\} - T \left\{ -\frac{\pi^3 \cos\left(\frac{\pi z}{l}\right)}{l^3} p_1(t) \right. \\
& - \frac{8\pi^3 \cos\left(\frac{2\pi z}{l}\right)}{l^3} p_2(t) - \frac{27\pi^3 \cos\left(\frac{3\pi z}{l}\right)}{l^3} p_3(t) - \frac{64\pi^3 \cos\left(\frac{4\pi z}{l}\right)}{l^3} p_4(t) - \frac{125\pi^3 \cos\left(\frac{5\pi z}{l}\right)}{l^3} p_5(t) \left. \right\} - \rho A g \left\{ \frac{\pi \cos\left(\frac{\pi z}{l}\right)}{l} q_1(t) \right. \\
& + \frac{2\pi \cos\left(\frac{\pi z}{l}\right)}{l} q_2(t) + \frac{3\pi \cos\left(\frac{\pi z}{l}\right)}{l} q_3(t) + \frac{4\pi \cos\left(\frac{\pi z}{l}\right)}{l} q_4(t) + \frac{5\pi \cos\left(\frac{\pi z}{l}\right)}{l} q_5(t) \left. \right\} + (F_0 - \rho A g z) \left\{ -\frac{\pi^2 \sin\left(\frac{\pi z}{l}\right)}{l^2} q_1(t) \right. \\
& - \frac{4\pi^2 \sin\left(\frac{\pi z}{l}\right)}{l^2} q_2(t) - \frac{9\pi^2 \sin\left(\frac{\pi z}{l}\right)}{l^2} q_3(t) - \frac{16\pi^2 \sin\left(\frac{\pi z}{l}\right)}{l^2} q_4(t) - \frac{25\pi^2 \sin\left(\frac{\pi z}{l}\right)}{l^2} q_5(t) \left. \right\} = 0
\end{aligned} \tag{4.10}$$

The above equations are simplified according to the fact that the expanded Galerkin method is based on the orthogonality of modes; i.e.

$$\begin{aligned}
& \int_0^l \varphi_i(z) \varphi_j(z) dz = \frac{l}{2} \delta_{ij} \\
& \int_0^l \psi_i(z) \psi_j(z) dz = \frac{l}{2} \delta_{ij}
\end{aligned} \tag{4.11}$$

Since the comparison functions are assumed to be $\varphi_i(z) = \sin\left(\frac{i\pi z}{l}\right)$ and $\varphi_j(z) = \sin\left(\frac{j\pi z}{l}\right)$, applying integration by parts to Equation 4.11 results in:

$$\begin{aligned} \int_0^l \varphi_i''(z) \varphi_j''(z) dz &= \frac{l}{2} \left(\frac{j\pi}{l} \right)^4 \delta_{ij} \\ \int_0^l \psi_i''(z) \psi_j''(z) dz &= \frac{l}{2} \left(\frac{j\pi}{l} \right)^4 \delta_{ij} \end{aligned} \quad (4.12)$$

Using the above comparison functions, Equation 4.9 is multiplied by $\varphi_i(z) = \sin\left(\frac{i\pi z}{l}\right)$ for $i = 1, 2, \dots, 5$ and then is integrated term by term over $z \in [0, l]$, resulting in five coupled time dependent equations (in the case of uncoupled equations, this method will result in five ordinary uncoupled time-varying differential equations). Equation set 4.10 is multiplied by $\varphi_j(z) = \sin\left(\frac{j\pi z}{l}\right)$ for $j = 1, 2, \dots, 5$ and the results are integrated term by term over the same domain. The result is another set of five ordinary coupled time-varying differential equations. The resulting set of ten equations after simplification of integrations is shown in Appendix 4.2.

The ten equations make a system of coupled second order time-varying differential equations. This system was numerically solved using a Fehlberg fourth-fifth order Runge-Kutta method with degree four interpolant, which is an adaptive numeric procedure for solving the initial value problems combining fourth-order and fifth-order Runge-Kutta techniques. The great advantage of this method is the dynamic step reduction strategy compared to the fixed-step fourth-order Runge-Kutta method. The initial conditions were derived from the FEM solver as discussed later in the next section, to ensure geometric compatibility. Any compatible set of initial conditions will suffice, as natural frequencies are not initial condition dependent. Parameter values are shown in Table 4.1.

Table 4.1: Dimensions and characteristics of the drillstring and collar section

Drillstring length	1000 m	Collar density	$\rho = 7860 \frac{kg}{m^3}$
Drill collar length	200 m	Collar modulus of elasticity	$E = 210GPa$
Length between 2 adjacent stabilizers	30 m	Gravity acceleration	$g = 9.81 \frac{m}{s^2}$
Outside diameter of the collar section	$d_o = 0.22m$	Rotational torque	$T = 5kN.m$
Inside diameter of the collar section	$d_i = 0.08m$	Axial load at the top pint of the collar section	$F_0 = -30 kN$
Area moment of inertia of the collars in the u direction	$I_u = 1.129 * 10^{-4} m^4$	Area moment of inertia of the collars in the v direction	$I_v = 1.129 * 10^{-4} m^4$

The results for $p_1(t)$ up to $p_5(t)$ are shown in Figure 4.5 and for $q_1(t)$ up to $q_5(t)$ in

Figure 4.6.

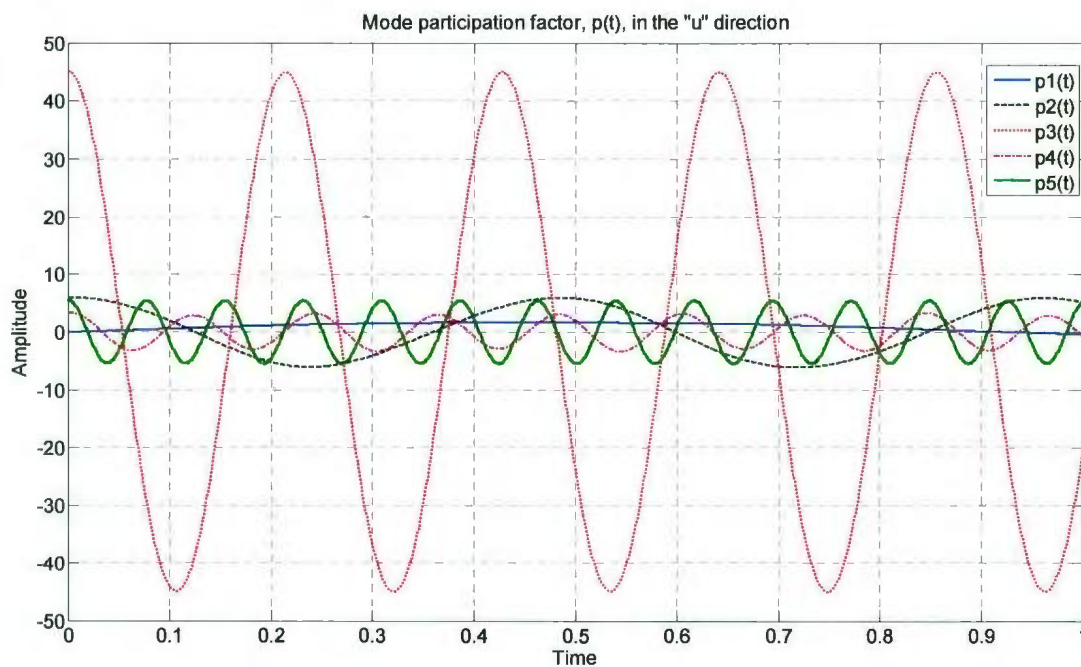


Figure 4.5: The function $p(t)$ for the first five modes (the u direction)

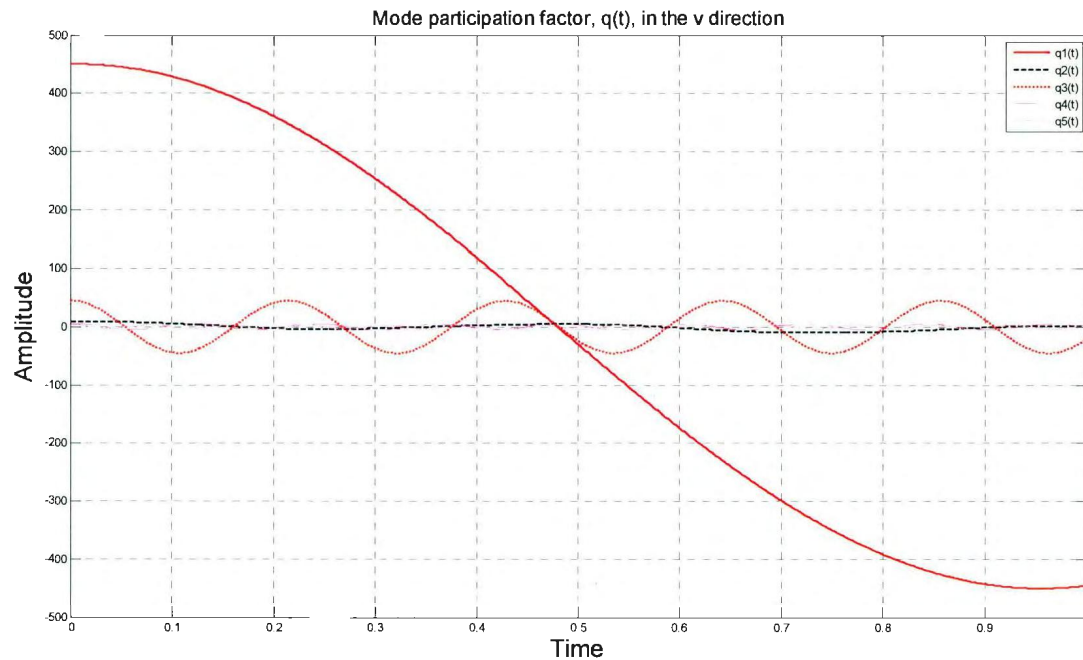


Figure 4.6: The function $q(t)$ for the first five modes (the v direction)

Figure 4.7 is an expanded view of Figure 4.6 without $q_1(t)$. Using the imposed set of initial conditions, the third mode as shown in Figure 4.5 and the first mode as shown in Figure 4.6 are the dominant modes.

If a specific location is selected along the beam, in the vicinity of an anti-node, then the product of $\varphi_i(z) \cdot p_i(t)$ and $\psi_j(z) \cdot q_j(t)$ determines the transverse motion of that location over the time period. The final transverse motion is the summation of these transverse motions in each mode.

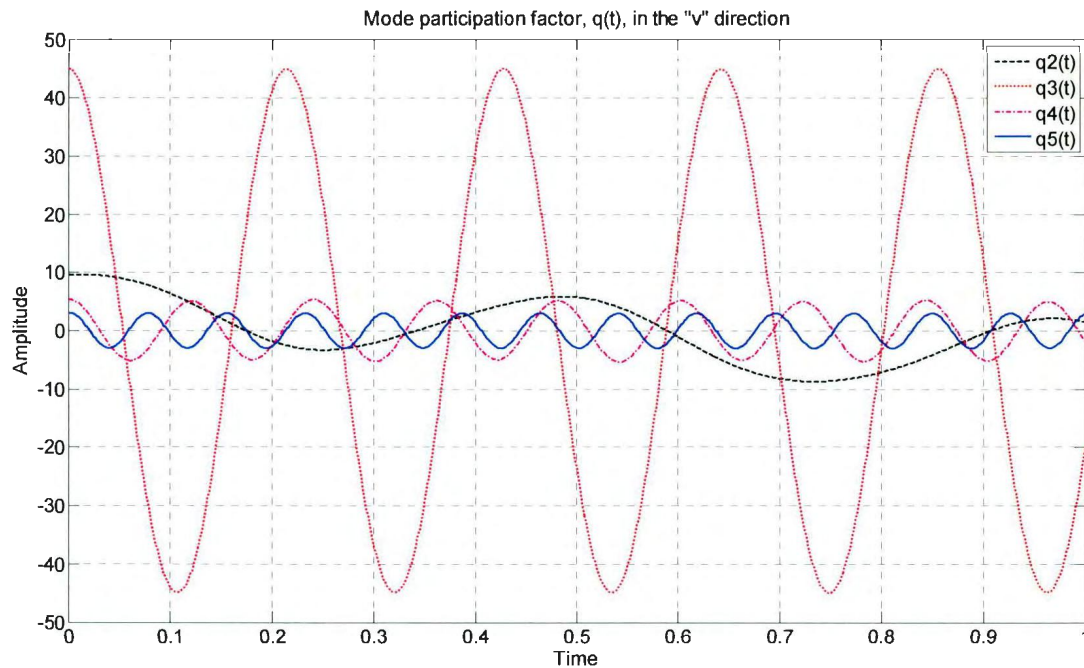


Figure 4.7: The function $q(t)$ for the second mode to the fifth mode

In order to derive the eigenfrequencies of each mode in both directions the values of $p(t)$ and $q(t)$ are stored for the first five modes. If the FFT of each $p(t)$ and $q(t)$ is determined separately, the natural frequency will be revealed. The sampling rate was 1000, and 512 points were selected for FFT computations. The natural frequencies are compared for both directions in Figure 4.8. There is a small variation between resonance frequencies in the u and v directions as a result of the numerical solution. The maximum difference is 0.03 Hz.

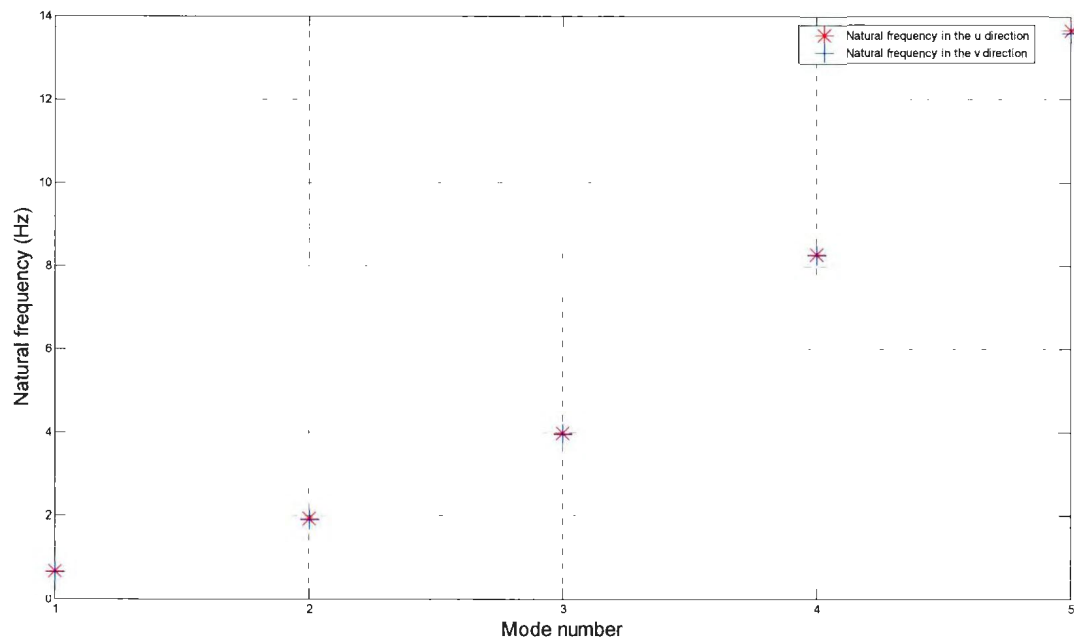


Figure 4.8: The natural frequency in the u and v directions for the first five modes by the analytical model

From a practical drilling standpoint, the rotational speed should be adjusted so that it does not correspond to one of the eigenfrequencies. Effect of torque and WOB on the natural frequencies in the u and v directions has been studied as well. The torque was varied from 1-10 kN.m and the WOB from 30-150 kN. The sensitivity of natural frequency to changes in WOB (Figure 4.9) is higher than the sensitivity to changes in torque (Figure 4.10).

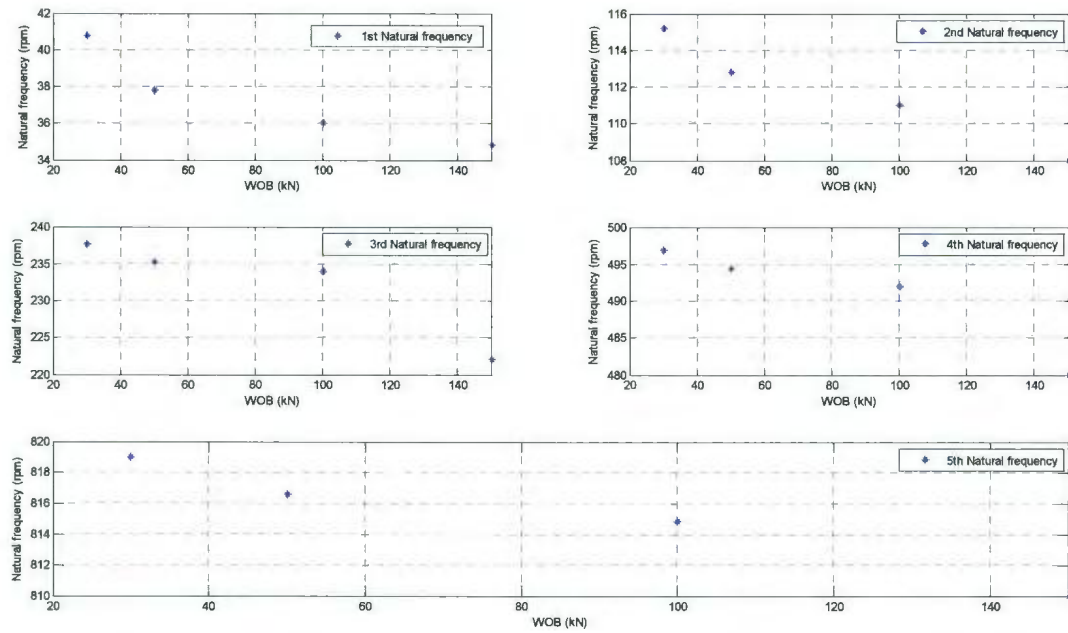


Figure 4.9: The effect of WOB on the natural frequency in the u direction

For the change in WOB the maximum change in the natural frequency is around 17 rpm, while for the torque the maximum change is around 4 rpm. Due to the similarity of the u and v frequencies, the sensitivity analysis in Figures 4.9 and 4.10 are just for the u direction.

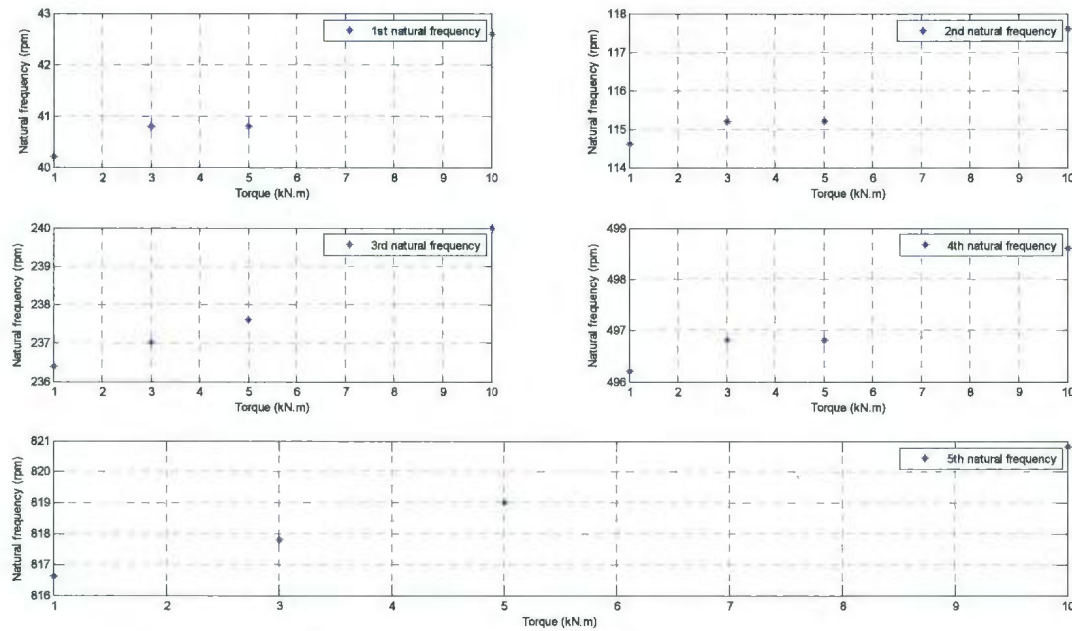


Figure 4.10: The effect of torque on the natural frequency in the u direction

The following section applies the FEM method to the current problem and verifies the results derived by the expanded Galerkin method. Linear and nonlinear FEM has also been used to verify linear analytical results by Heisig *et al.* [9].

4.6 Application of the FEM Method to the Transverse Vibration of the Drillstring

The ABAQUS FEM solver package (SIMULIA Inc., version 6.7.1) was used, with Euler-Bernoulli beam elements chosen to maintain the same conditions as the mathematical model. The material specifications, given in Table 4.1, are the same as for the analytical model. The beam is modeled by a planar wire shape with a pipe profile to build the hollow drill collar pipe. Solution follows a three-step process with initial, general static and perturbation steps. The boundary conditions are applied at the initial step to constrain the model. The general static step is defined by the fixed time increments with the direct

full-Newtonian equation solver method to apply the static loads (body and hydrostatic forces). The resulting deformations of this step are propagated to the next step. In the last step (perturbation step) the “Lanczos” eigensolver was used to extract the eigenfrequencies. This method is in contrast to the “subspace iteration method” and falls into the class of transformation methods (transformation of the normalized eigenvectors through the displacement). It is widely used when the higher modes are of interest [30]. Simply supported boundary conditions are used in the lowest node and all the DOFs except two (rotation along the beam axis and the downward motion) are constrained. The “cubic element” is used, in which the shear flexibility is not considered, and this is in agreement with the Euler-Bernoulli beam theory assumption in the analytical model. Eighty elements were assumed, giving a total collar length of 200 m, and using the convergence analysis [24], the results did not change significantly when more elements were added.

As discussed in the introduction section, this fact that the collar section is more easily excited than the pipe section and vibrates in lower modes, while the pipes do not vibrate significantly, is verified by the FEM model as shown in Figures 4.11(a-f). Figures 4.11-a and 4.11-b are the second and the fifth modes of the drillstring, respectively, with the pipe section remaining steady. Figures 4.11-c, 4.11-d and 4.11-e are the modes 10, 25 and 50 respectively, with the vibration propagating up to the pipe section and the amplitude becoming larger in the pipe section. Figure 4.11-f is the axial mode of the drillstring, which is a higher frequency mode, than the transverse vibration and the effective mass for the axial direction is a large value as associated with higher modes. The mode shapes

magnitudes derived by the FEM are not absolute values, and are intended only to represent the correct shape distribution. They are shown exaggerated for clarity.

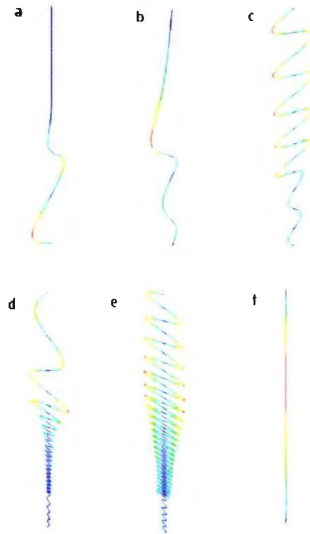


Figure 4.11: The deformed shape of the drillstring in different modes

The values of frequencies for the u and v directions extracted by the FEM are shown in Figure 4.12 and compared with the results derived by the expanded Galerkin method. These values are in agreement with the results of the last section with slightly lower values. This is due to selection of a comparison function in the last section that is not exactly the same as the real displacement function (eigenfunction).

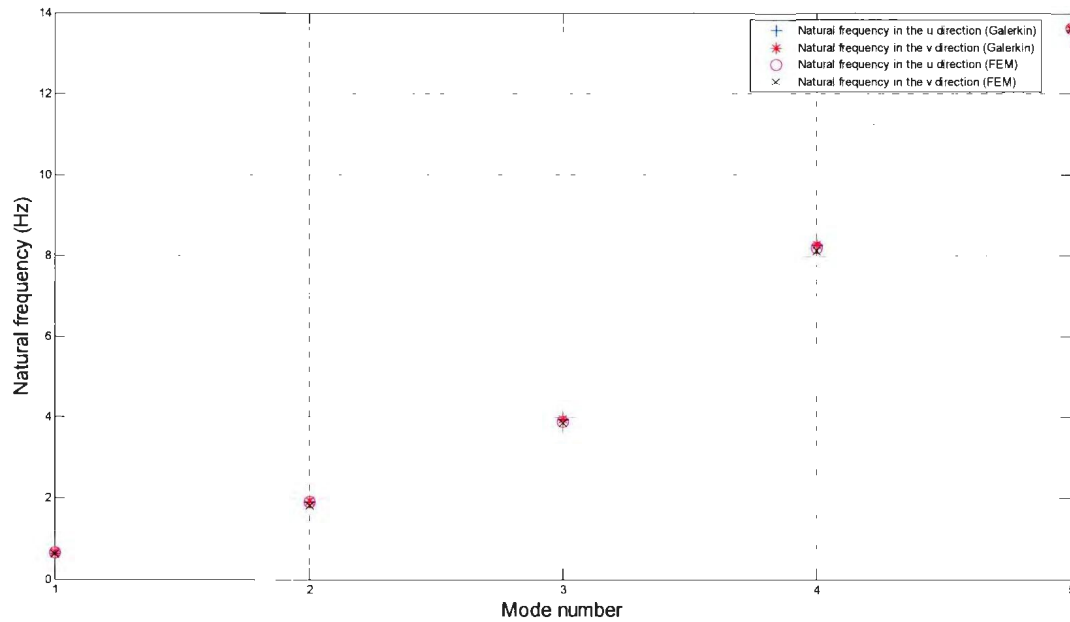


Figure 4.12: Comparison of the natural frequencies in the u and v directions for the FEM and the expanded Galerkin method

4.7 Determination of Appropriate Model Order

Another interesting result of the last section is the effective mass of each mode in any direction. The generalized mass, m_α , associated with the mode α is defined as:

$$m_\alpha = \chi_\alpha^N M^{NM} \chi_\alpha^M \quad (4.13)$$

where M^{NM} is the structural matrix and χ_α^N is the eigen vector for mode α . “ M ” and “ N ” are degrees of freedom of the FEM model. In the case of eigen vector normalization, m_α is defined as unity. After finding the m_α , the modal mass participation factor, $\Gamma_{\alpha i}$, is defined as:

$$\Gamma_{\alpha i} = \frac{1}{m_{\alpha}} \chi_{\alpha}^N M^{NM} Y_i^M \quad (4.14)$$

The modal mass participation factor indicates the participation factor of a certain motion (global translation or rotation) in the eigenvector of the mode α in the i direction. Y_i^M defines the magnitude of the rigid body response of the degree of freedom M in the model [31]. Effective masses are plotted in Figures 4.13 and 4.14.

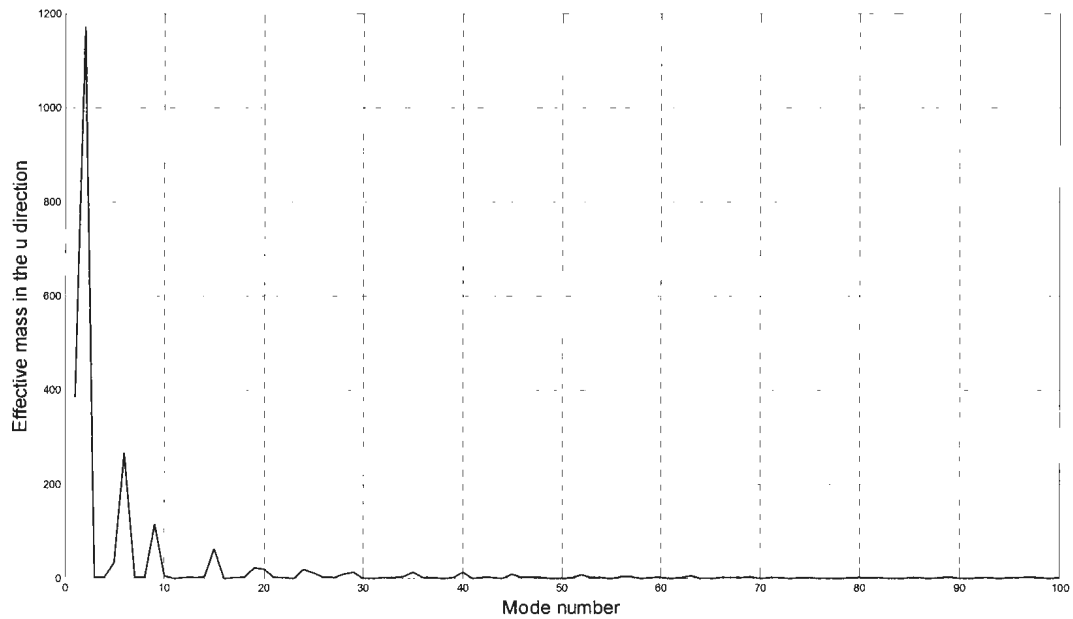


Figure 4.13: Effective mass in the “ u ” direction

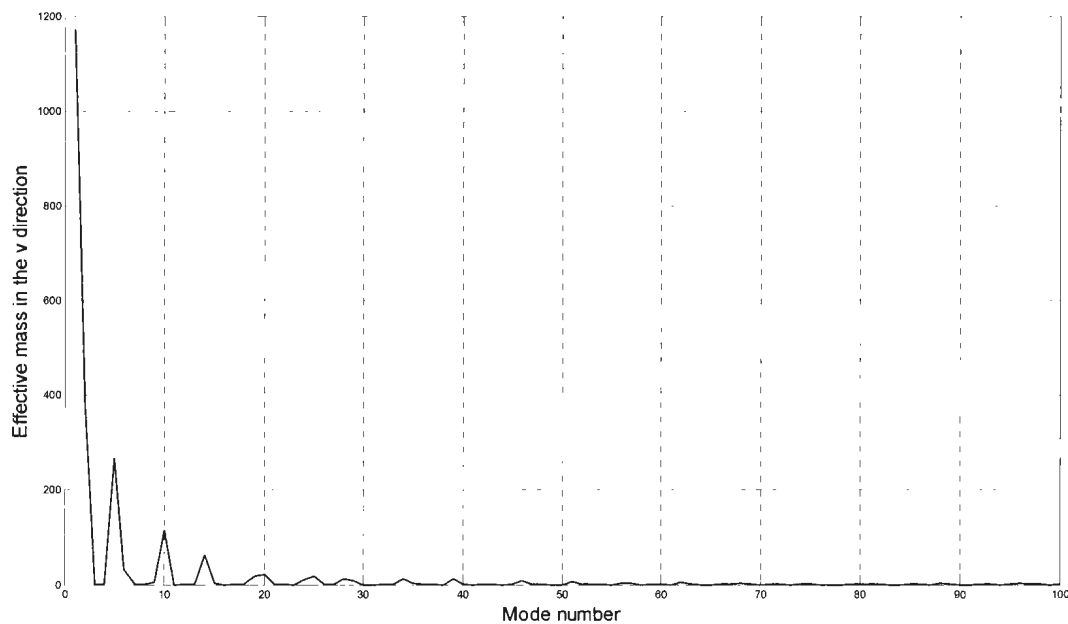


Figure 4.14: Effective mass in the “ v ” direction

As can be seen, for the u direction, modes up to the fifth mode account almost entirely for the motion in this direction. This fact validates the truncation of modes after the fifth mode in the expanded Galerkin method. Another result is that the third mode is the dominant mode in the u direction with higher effective mass and the first mode is the dominant mode in the v direction, which is in agreement with the results of the analytical solutions. The same initial conditions were used in both methods. The effective mass in the axial direction happens at higher modes, compared to lateral modes, which is in agreement with beam theory, since the first natural frequency of the beam in the longitudinal direction is much higher than in the transverse direction. The modal mass participation factor in the v direction is very similar to the u direction. The difference is due to the different coupling terms in Equation 4.6. However the mass participation

factors after the fifth mode decreases drastically in both directions. The numerical value of the modal participation factor is much higher in the axial direction with respect to the lateral motion. The approach of this section, and the ability to truncate unnecessary modes, helps to avoid excessive numerical computational costs.

4.8 Conclusions

Coupled lateral vibration of a drillstring was studied in two orthogonal transverse directions, under the action of a steady torque and varying axial load. The axial force arises from the interaction of the mud hydrostatic force, the drillstring self weight and hook weight. As a result, a linear force profile was assumed along the drillstring. The torque along the drillstring was resolved into tangential and normal components, with the tangential component acting as the bending moment for the lateral modes. The coupled equations were derived using the direct Newtonian approach. The expanded Galerkin method was used to solve the coupled equations and reveal the natural frequencies as well as the mode participation factors. Then, the nonlinear finite element method was applied to the problem with the same conditions to verify the results. The modal mass participation factor was derived for each direction and the effective number of modes for each direction was selected according to this criterion. Transverse coupled natural frequencies are more sensitive to changes in the WOB than torque. The rotary speed of the drillstring should be kept far enough from the natural frequencies to avoid excessive deflections and contact with the wellbore, both of which can cause premature failure of bottom-hole assembly components.

4.9 Funding Acknowledgment

The authors would like to acknowledge Husky Energy, Suncor Energy, the Atlantic Innovation Fund and Industrial Research & Innovation Fund for funding this research. The authors would like to thank Dr. Hajnayeb at Chamran University of Ahvaz for his valuable suggestions on the analytical code.

4.10 References

- [1] Elsayed, M. A., Phung, C. C., 2005, "Modeling of Drillstrings," 24th ASME International Conference on Offshore Mechanics and Arctic Engineering (OMAE), Halkidiki, Greece.
- [2] Spanos, P. D., Payne, M. L., and Secora, C. K., 1997, "Bottom-Hole Assembly Modeling and Dynamic Response Determination," ASME Journal of Energy Resources Technology, **119**(3), pp. 153-158.
- [3] Khulief, Y. A., Al-Sulaiman, F. A., 2009, "Laboratory Investigation of Drillstring Vibrations," Journal of Mechanical Engineering Science (IMEchE Part C), **223**(10), pp. 2249-2262.
- [4] Jogi, P. N., Macpherson, J. D., and Neubert, M., 2002, "Field Verification of Model-Derived Natural Frequencies of a Drillstring," ASME Journal of Energy Resources technology, **124**(3), pp. 154-162.
- [5] Dareing, D. W., 1984, "Guidelines for Controlling Drillstring Vibrations," ASME Journal of Energy Resources Technology, **106**(2), pp. 272-277.

- [6] Hakimi, H., Moradi, S., 2009, "Drillstring Vibration Analysis Using Differential Quadrature Method," *Journal of Petroleum Science and Engineering*, **70**(3-4), pp. 235-242.
- [7] Li, Z., Yanshan, U., and Guo, B., 2007, "Analysis of Longitudinal Vibration of Drillstring in Air and Gas Drilling," SPE#107697, SPE Rocky Mountain Oil and Gas Technology Symposium, Denver, Colorado.
- [8] Aminfar, O., Khajepour, A., 2008, "Torsional Vibration Analysis of Drillstring in Blasthole Drilling," ASME International Mechanical Engineering Congress (IMECE), Boston, Massachusetts.
- [9] Heisig, G., Neubert, M., 2000, "Lateral Drillstring Vibrations in Extended-Reach Wells," IADC/SPE# 59235, IADC/SPE Drilling Conference, New Orleans, Louisiana.
- [10] Christoforou, A. P., Yigit, A. S., 2001, "Active Control of Stick-Slip Vibrations: The Role of Fully Coupled Dynamics," SPE#68093, SPE Middle East Oil Show, Bahrain.
- [11] Yigit, A. S., Christoforou, A. P., 1998, "Coupled Torsional and Bending Vibrations of Drillstrings Subject to Impact With Friction," *Journal of Sound and Vibration*, **215**(1), pp. 167-181.
- [12] Yigit, A. S., and Christoforou, A. P., 1996, "Coupled Axial and Transverse Vibrations of Oilwell Drillstrings," *Journal of Sound and Vibration*, **195**(4), pp. 617-627.
- [13] Sampaio, R., Piovan, M. T., and Lozano, G. V., 2007, "Coupled Axial Torsional Vibrations of Drillstring by Means of Nonlinear Model," *Journal of Mechanics Research Communications*, **34**, pp. 497-502.

- [14] Leine, R. I., Van Campen, D. H., and Keultjes, W. J. G., 2002, "Stick-Slip Whirl Interaction in Drillstring Dynamics," *ASME Journal of Vibration and Acoustics*, **124**(2), pp. 209-220.
- [15] Yigit, A. S., Christoforou, A. P., 2006, "Stick-Slip and Bit-Bounce Interaction in Oil-Well Drillstrings," *ASME Journal of Energy Resources Technology*, **128**(4), 268-274.
- [16] Chin, W. C., 1994, *Wave Propagation in Petroleum Engineering*, Gulf Publishing Company, Texas, USA.
- [17] Jansen, J. D., 1991, "Nonlinear Rotor Dynamics as Applied to Oil Well Drillstring Vibrations," *Journal of Sound and Vibration*, **147** (1), 115-135.
- [18] Chen, S. L., Geradin, M., 1995, "An Improved Transfer Matrix Technique as Applied to BHA Lateral Vibration Analysis," *Journal of Sound and Vibration*, **185**(1), pp. 93-106.
- [19] Berlioz, A., Der Hagopian, J., Dufour, R., and Draoui, E., 1996, "Dynamic Behavior of a Drillstring: Experimental Investigation of Lateral Instabilities," *ASME Journal of Vibration and Acoustics*, **118**(3), pp. 292-298.
- [20] Christoforou, A. P., and Yigit, A. S., 1997, "Dynamic Modeling of Rotating Drillstrings With Borehole Interactions," *Journal of Sound and Vibration*, **206** (2), pp. 243-260.
- [21] Gulyaev, V. I., Lugovoi, P. Z., Belova, M. A., and Solov'ev, I. L., 2006, "Stability of the Equilibrium for Rotating Drillstrings," *International Applied Mechanics*, **42**(6), pp. 692-698.

- [22] Dareing, D. W., 1984, "Drill Collar Length Is a Major Factor in Vibration Control," *Journal of Petroleum Technology*, **36**(4), pp. 637-644.
- [23] Khulief, Y. A., and Al-Naser, H., 2005, "Finite Element Dynamic Analysis of Drillstrings," *Finite Element in Analysis and Design*, **41**(13), pp. 1270-1288.
- [24] Khulief, Y. A., Al-Sulaiman, F. A., and Bashmal, S., 2008, "Vibration Analysis of Drillstrings With String-Borehole Interaction," *International Journal of Mechanical Engineering Science, (IMechE Part C)*, **222**(11), pp. 2099-2110.
- [25] Ghasemloonia, A., Rideout, D. G., and Butt, S. D., 2010, "The Effect of Weight-On-Bit on the Contact Behavior of Drillstring and Wellbore," 9th International Conference on Bond Graph Modeling (ICBGM2010), Orlando, Florida.
- [26] Karnopp, D. C., Margolis, D. L., and Rosenberg, R. C., 2006, *System Dynamics: Modeling and Simulation of Mechatronic Systems*, 4th edition, John Wiley&Sons, Inc., New Jersey, USA.
- [27] Hijmissen, J. W., Van Horsen, W. T., 2008, "On Transverse Vibrations of a Vertical Timoshenko Beam," *Journal of Sound and Vibration*, **314**(1-2), pp. 161-179.
- [28] Bourgoyne, A. T., Chenevert, M. E., Millheim, K. K., and Young, F. S., 1986, *Applied Drilling Engineering*, SPE Text Book Series, Society of Petroleum Engineers, Texas, USA.
- [29] Thomsen, J. J., 2003, *Vibrations and Stability*, 2nd ed., Springer, Berlin, Germany.
- [30] Craig, R. R., and Kurdila, A. J., 2006, *Fundamentals of Structural Dynamics*, 2nd ed., John Wiley& Sons, Inc., New Jersey, USA.

[31] ABAQUS Theory Manual (version 6.10), 2012, Dassault Systèmes Simulia Corp., RI, USA.

4.11 Appendix 4.1: Nomenclature

A	Cross sectional area of the collar section	\vec{T}_t, \vec{T}_n	Torque components in the tangent and normal planes of the beam element
EI_u, EI_v	Flexural rigidity of the beam in the u and the v directions	$u(z, t)$	Displacement in 1 st lateral direction
F_0	Axial compressive force at the top point of the collar section	$v(z, t)$	Displacement in 2 nd lateral direction
g	Gravity acceleration	WOB	Weight on bit
m_α	Generalized mass associated with the mode α	χ_α^N	Eigen vector of the mode α
M, N	Degrees of freedom of the FEM model	Y_i^M	Magnitude of rigid body response of the degree of freedom M in the i direction
$p_i(t)$	Mode participation factor for the u direction	Γ_α	Modal mass participation factor
$q_j(t)$	Mode participation factor for v direction	ρ	BHA density
S_u, S_v	Shear force in the u and the v directions	$\phi_i(z)$	Comparison function in the u direction
\vec{T}	Torque vector in the z direction	$\psi_j(z)$	Comparison function in the v direction

4.12 Appendix 4.2: Analytical Equations

The element in the uz plane is shown in Figure 4.1 and in the vz plane in Figure 4.2. The equilibrium equations in the “ uz ” plane are:

$$\sum M_v = 0 \Rightarrow M_v + \frac{\partial M_v}{\partial z} dz - M_v + (S_u + \frac{\partial S_u}{\partial z} dz) \cdot \frac{dz}{2} + S_u \cdot \frac{dz}{2} = 0 \quad (4.15)$$

Neglecting the 2nd and higher order terms of dz will result in:

$$\frac{\partial M_v}{\partial z} = S_u \quad (4.16)$$

The force equilibrium in the “uz” plane is:

$$S_u + \frac{\partial S_u}{\partial z} dz - S_u + (F_{axial} + \frac{\partial F_{axial}}{\partial z} dz) \cdot \sin(\theta + \frac{\partial \theta}{\partial z} dz) - F_{axial} \cdot \sin(\theta) + \rho A \frac{\partial^2 u(z,t)}{\partial t^2} = 0 \quad (4.17)$$

Assuming small angle θ , and discarding 2nd or higher order terms of dz , the above equation reduces to:

$$\frac{\partial S_u}{\partial z} dz + F_{axial} \frac{\partial \theta}{\partial z} dz + \frac{\partial F_{axial}}{\partial z} \theta dz + \rho A \frac{\partial^2 u(z,t)}{\partial t^2} = 0 \quad (4.18)$$

Using the result of Equation 4.2 in Equation 4.4, considering that $M_v = E.I_v \frac{\partial^2 u(z,t)}{\partial z^2}$:

$$\begin{aligned} -\frac{\partial}{\partial z} \left(\frac{\partial M_v}{\partial z} \right) &= \frac{\partial}{\partial z} \left(F_{axial} \cdot \frac{\partial u(z,t)}{\partial z} \right) \\ \frac{\partial}{\partial z} \left(\frac{\partial}{\partial z} (E.I_v \frac{\partial^2 u(z,t)}{\partial z^2}) \right) + \frac{\partial}{\partial z} \left(F_{axial} \cdot \frac{\partial u(z,t)}{\partial z} \right) &= -\rho A \frac{\partial^2 u(z,t)}{\partial t^2} \end{aligned} \quad (4.19)$$

Assuming constant $E.I_v$ for the drill string in the collar section and a linearly varying

axial load F_{axial} :

$$E.I_v \frac{\partial^4 u(z,t)}{\partial z^4} + \frac{\partial}{\partial z} \left(F_{axial} \cdot \frac{\partial u(z,t)}{\partial z} \right) + \rho A \frac{\partial^2 u(z,t)}{\partial t^2} = 0 \quad (4.20)$$

The equation of motion in the v direction is obtained in the similar way to the u direction (Figure 4.2). Therefore:

$$E.I_u \frac{\partial^4 v(z,t)}{\partial z^4} + \frac{\partial}{\partial z} \left(F_{axial} \cdot \frac{\partial v(z,t)}{\partial z} \right) + \rho A \frac{\partial^2 v(z,t)}{\partial t^2} = 0 \quad (4.21)$$

Ten coupled ordinary coupled time differential equations in the u and v directions:

$$\begin{aligned} \frac{\pi^4}{2l^3} EIp_1(t) - \frac{20}{9} \rho Agp_2(t) - \frac{136}{225} \rho Agp_4(t) + 0.5 \rho Al\ddot{p}_1(t) + \frac{16\pi^2}{3l^2} Tq_2(t) + \frac{128\pi^2}{15l^2} Tq_4(t) - \frac{\pi^2}{2l} F_0 p_1(t) \\ + \frac{\pi^2}{4} \rho Agp_1(t) = 0 \end{aligned}$$

$$\begin{aligned}
& \frac{\pi^4}{2l^3} EIq_1(t) - \frac{20}{9} \rho Agq_2(t) - \frac{136}{225} \rho Agq_4(t) + 0.5 \rho Al\ddot{q}_1(t) - \frac{16\pi^2}{3l^2} Tp_2(t) - \frac{128\pi^2}{15l^2} Tp_4(t) - \frac{\pi^2}{2l} F_0q_1(t) \\
& + \frac{\pi^2}{4} \rho Agq_1(t) = 0 \\
& 0.5 \rho LA\ddot{p}_2(t) - \frac{20}{9} \rho Agp_1(t) + \pi^2 \rho Agp_2(t) - \frac{156}{25} \rho gAp_3(t) - \frac{580}{441} \rho gAp_5(t) - \frac{4\pi^2}{3l^2} Tq_1(t) + \frac{108\pi^2}{5l^2} Tq_3(t) \\
& + \frac{500\pi^2}{2l^2} Tq_5(t) - \frac{2\pi^2}{l} F_0p_2(t) + \frac{8\pi^4}{l^3} Elp_2(t) = 0 \\
& \frac{8\pi^4}{l^3} Iq_2(t) + 0.5 \rho LA\ddot{q}_2(t) - \frac{580}{441} \rho gAq_3(t) - \frac{156}{25} \rho gAq_5(t) - \frac{500\pi^2}{2l^2} Tp_3(t) - \frac{20}{9} \rho Agq_1(t) + \pi^2 \rho Agq_2(t) \\
& - \frac{108\pi^2}{5l^2} Tp_3(t) + \frac{4\pi^2}{3l^2} Tp_1(t) - \frac{2\pi^2}{l} F_0q_2(t) = 0 \\
& \frac{384\pi^2}{7l^2} Tq_4(t) + \frac{81\pi^4}{2l^3} Elp_3(t) - \frac{156}{25} \rho gAp_2(t) - \frac{48\pi^2}{5l^2} Tq_2(t) - \frac{600}{49} \rho gAp_4(t) + 0.5 \rho LA\ddot{p}_3(t) + \frac{9\pi^2}{4} \rho gAp_5(t) \\
& - \frac{9\pi^2}{2l} F_0p_3(t) = 0 \\
& 0.5 \rho LA\ddot{q}_3(t) - \frac{156}{25} \rho gAq_2(t) - \frac{600}{49} \rho gAq_4(t) + \frac{48\pi^2}{5l^2} Tp_2(t) - \frac{384\pi^2}{7l^2} Tp_4(t) + \frac{9\pi^2}{4} \rho gAq_3(t) + \frac{81\pi^4}{2l^3} EIq_3(t) \\
& - \frac{9\pi^2}{2l} F_0q_3(t) = 0 \\
& 0.5 \rho LA\ddot{p}_4(t) - \frac{136}{225} \rho gAp_1(t) + 4\pi^2 \rho gAp_4(t) + \frac{1000\pi^2}{9l^2} Tq_5(t) - \frac{216\pi^2}{7l^2} Tq_3(t) - \frac{1640}{81} \rho gAp_5(t) + \frac{128\pi^4}{l^3} Elp_4(t) \\
& - \frac{8\pi^2}{15l^2} Tq_1(t) - \frac{600}{49} \rho gAp_3(t) - \frac{8\pi^2}{l} F_0p_4(t) = 0 \\
& 0.5 \rho LA\ddot{q}_4(t) - \frac{136}{225} \rho gAq_1(t) - \frac{1640}{81} \rho gAq_3(t) - \frac{8\pi^2}{l} F_0q_4(t) + 4\pi^2 \rho gAq_4(t) - \frac{600}{49} \rho gAq_5(t) - \frac{1000\pi^2}{9l^2} Tp_3(t) \\
& + \frac{8\pi^2}{15l^2} Tp_1(t) + \frac{216\pi^2}{7l^2} Tp_3(t) + \frac{128\pi^4}{l^3} EIq_4(t) = 0 \\
& - \frac{580}{441} \rho gAp_2(t) - \frac{1640}{81} \rho gAp_4(t) - \frac{25\pi^2}{2l} F_0p_5(t) - \frac{80\pi^2}{2l^2} Tq_2(t) + 0.5 \rho LA\ddot{p}_5(t) + \frac{625\pi^4}{2l^3} Elp_5(t) - \frac{640\pi^2}{9l^2} Tq_4(t) \\
& + \frac{25\pi^2}{4} \rho gAp_5(t) = 0 \\
& - \frac{580}{441} \rho gAq_2(t) - \frac{1640}{81} \rho gAq_4(t) + \frac{80\pi^2}{2l^2} Tp_2(t) + \frac{25\pi^2}{4} \rho gAq_5(t) + \frac{640\pi^2}{9l^2} Tp_4(t) + 0.5 \rho LA\ddot{q}_5(t) + \frac{625\pi^4}{2l^3} EIq_5(t) \\
& - \frac{25\pi^2}{2l} F_0q_5(t) = 0
\end{aligned} \tag{4.22}$$

4.13 Appendix 4.3: Axial Force in the Collar Section

The effects of the hook load, WOB, mud hydrostatic force and self weight are presented as a spatially varying axial force along the drillstring. The buoyant force in the drillstring should not be treated with the Archimedes' rule and the effective tension point of view should be implemented for more precise results [27]. Therefore, at the last point of the collar section, there are two axial upward forces, namely the WOB and the hydrostatic force at the lower cross section. The varying axial force in the collar section is:

$$F_{collar} = \rho_{collar} A_{collar} g z - WOB - F_{hydrostatic} \quad (4.23)$$

Substituting for the hydrostatic force at the bottom of the collar section, the collar force will be:

$$F_{collar} = \rho_{collar} A_{collar} g z - WOB - (\rho_{mud} g l) A_{collar} \quad (4.24)$$

According to dimensions and material properties given in Table 4.1, the varying axial force along the collar section is:

$$F_{collar} = -30 \cdot 10^3 - 2543.49 \cdot z \quad (4.25)$$

The value of the axial force at the top point of the collar section (neutral point) is -30 kN , as shown in Table 4.1 and Figure 4.15.

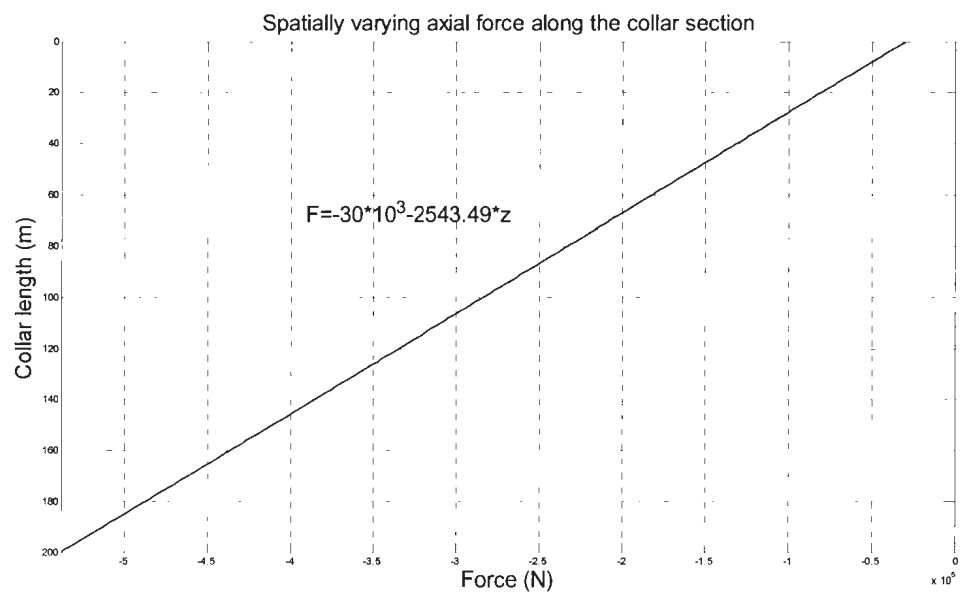


Figure 4.15: Force profile along the collar section

5 Analysis of Multi-Mode Nonlinear Coupled Axial-Transverse Drillstring Vibration in Vibration Assisted Rotary Drilling

Ahmad Ghasemloonia, Graduate Student

D. Geoff Rideout, Associate Professor

Stephen. D. Butt, Professor

Advanced Drilling Group, Faculty of Engineering and Applied Science, Memorial University, St. John's, NL, Canada

This chapter is based on the modeling step 3 defined in section 1.4 of this thesis and is submitted as a full research paper to the Journal of Petroleum Science and Engineering on August 2012 and currently is under review.

5.1 Abstract

Applying a source of axial vibration near the bit has the potential to enhance the efficiency of drilling. Drilling tools are under development to apply axial vibrations to oilwell drillstrings for the purpose of overcoming drillstring-wellbore friction, facilitating cutting removal and improving the rate of penetration (ROP) of the bit. However, introducing controlled vibrations into the drillstring excites many unwanted vibration modes of the drillstring that can result in inefficient drilling, damage to drillstring, bit, BHA components, MWD tools and mud motors. This study is motivated by the need to

understand the complex dynamic behavior of drillstrings, in order to implement control strategies and reduce the potentially destructive effects of unwanted drillstring vibration when using axial vibration generator tools. The coupled axial-transverse mode is assumed as the most detrimental state of drillstring vibration. In this paper, the coupled nonlinear axial-transverse dynamics of the entire drillstring are modeled and lateral instabilities are qualitatively studied. The drillstring includes the pipes and a multi-span bottom-hole assembly (BHA) subjected to a controlled force generator tool down-the-hole. The multi-span BHA model enables multi-mode contact analysis of the drillstring and wellbore. The governing equations are obtained using the “Bypassing PDEs” method with the expanded Galerkin's method, which enables finding the symbolic solution of the governing equations. A multi-mode approximation is used to achieve more precise results than are possible from a single-mode treatment, for determining the resonance rotary speeds. The effects of mud damping, driving torque, multi-span contact and spatially varying axial load are included, along with nonlinearities due to geometry, axial stiffening, strain energy and Hertzian contact forces. Simulations are used to reveal resonant frequencies and to conduct a qualitative contact analysis showing the severity of the contact in each span of the BHA. Fast running time and symbolic solution are the major advantages of the developed analytical model.

Keywords: Drillstring model; Vibration-assisted drilling; Coupled nonlinear axial-transverse vibration; Multi-span BHA; Bypassing PDEs; Expanded Galerkin's method; Wellbore contact; Multi-mode analysis

5.2 Introduction

Drilling is one of the most costly and risky activities in oil and gas exploration and field development. The oil and gas industry is actively researching technologies to improve drilling technology and efficiency. Several recent classes of drilling tools apply axial vibration to the drillstring for the purpose of reducing drillstring-wellbore friction [1], enhancing penetration mechanism [2,3] and facilitating cutting removal. Vibration drilling may transmit power to the bit more efficiently than rotary drilling. Vibration tools improve drilling performance by various means, and collectively for the purpose of this investigation their use is called “vibration assisted rotary drilling” (VARD).

Implementation of vibration in rotary drilling raises questions about the effects of the imposed vibration on drill rigs and in particular on the drillstring. The drillstring is one of the major components of any drill rig and many important drilling parameters are controlled through the drillstring.

Contrary to the improving effect on the rate of penetration (ROP) and efficiency, the implementation of a vibration force (VARD force) above the bit excites the drillstring axially, and as a result of the coupling effect, the lateral mode will also be excited. The excited vibration wave propagates along the drillstring. The propagation of unwanted vibration to the drillstring and drill rig is a potential disadvantage of VARD. Therefore, the vibration behavior of the drillstring under the effect of axial force generators such as jars, agitators, and higher-frequency tools for ROP enhancement in rotary drilling is of significant interest. Several parameters such as weight on bit (WOB), rotary speed, natural frequencies, and quality of the hole are related to the behavior of the drillstring.

The drillstring is a long rotary slender structure which transmits rotary torque from the rotary table at the surface to the bit. It is mainly composed of a thin light upper section (the pipe section) and a heavy larger lower section (collar section) which is attached to the bit. The drillstring is confined in the wellbore, which is filled with the drilling mud, used for bit cooling and flushing out the cuttings. The mud is also assumed to be a damping medium for the drillstring lateral vibrations. Stabilizers are located along the collar section to prevent bending and buckling of the collars and to control directional drilling trajectories and drillstring vibration. The radial clearance between the stabilizers and the wellbore could be up to 100 mm. The assembly of the collar section, bit and stabilizers is called the bottom-hole assembly (BHA). The drillstring is under interaction of the hydrostatic load, the hoisting load of the top cables and the self weight, which result in an internal spatially-varying axial load. As a result, the pipes are under tension and the collars are under compression. A part of the force at the bit is called the weight on bit (WOB), which provides the cutting force and is an important controllable parameter to improve rate of penetration and drilling efficiency. The rotary speed is typically around 50-200 rpm.

Drillstring vibration is assumed as the primary cause of drillstring components' premature failure, deterioration of the well trajectory, successive bit and stabilizer wear, lower penetration rate, deteriorating accuracy of the measurement while drilling (MWD) systems and decreased efficiency. Also, unwanted vibrations of the drillstring dissipate a part of the provided energy, which is supposed to be delivered to the bit. Working guidelines and control strategies are required for VARD drilling to increase the efficiency

and avoid energy dissipation by unwanted drillstring vibration. The only way to design and implement isolation methods (passive or active) to suppress the vibration of the drillstring is to investigate the vibration patterns, either in the frequency domain or the time domain. This study is motivated by the need to develop an enhanced dynamic model which could be implemented to reveal the modal characteristics (frequency domain) and modal dynamic time response of the entire drillstring. To conduct sensitivity studies, the model is required to be solved symbolically to achieve a symbolic set of resulting PDEs. Several methodologies including static modeling, elastodynamic modeling, dynamic numerical modeling (e.g. finite element, finite difference models and dynamic stiffness method) and laboratory scale test rigs have been implemented by others to investigate this phenomenon.

The following section reviews relevant literature about importance of various vibration modes and physical phenomena associated with the drillstring; modeling of wellbore contact, and methods for equation derivation and solution. Section 3 derives governing equations, including eigenfrequencies and eigenfunctions of a multi-span beam which are implemented using a Lagrangian approach. Section 4 provides numerical simulation results, and Section 5 gives conclusions and future research directions.

5.3 Literature Review

Drillstring vibration is not simply independent axial, torsional and lateral vibration. A typical drillstring vibrates in 3 major coupled modes: lateral-axial, lateral-torsional and axial-torsional. Bit bouncing, stick-slip and whirling are extreme examples of coupled

vibration dominated by axial, torsional and lateral motions respectively. Among these coupled modes, the coupled transverse mode is the major cause of drillstring failures [4,5,6,7] and wellbore washout which happens at low frequencies. The deteriorating effect of the orthogonal lateral modes could be explained through the wave speed phenomenon. Bending waves are not propagated to the surface via the drillstring as are torsional and longitudinal waves, due to the difference in the wave speed for different types of modes. The propagation speed for axial and torsional motions is quite high compared to the lateral motion [4]. Therefore, there could be severe bending vibrations deep in the hole, which the surface measuring tools do not detect. BHA-wellbore contact is the main excitation source for lateral vibration. In the case of VARD drilling, axial vibration plays an important role since the high frequency VARD force directly excites the axial modes and lateral instabilities may exist due to axial excitation [8]. Therefore, in order to precisely model the VARD drillstring, two orthogonal coupled transverse modes along with the axial mode will be considered in this study. A symbolic mathematical model will capture the coupled axial-transverse vibrations of the drillstring, including a multi-span BHA and the pipe section, subjected to imposed VARD force and wellbore contact. A multi-span contact analysis of the BHA is done to provide more realistic results for the natural frequencies. Mud damping, driving torque, and spatially varying axial load have been included. The driving torque is an important parameter for the drillstring vibration, related to the top rotary speed. Therefore, natural frequencies in these directions are related to the driving torque [5,9,10,11,12]. Also, since in this study, two orthogonal lateral modes are included in the model, the torque couples these two

modes and must be kept in the equations, although it adds complexity to the equations. Since the rotation speed of the drillstring is small enough (50-150 rpm in practice), the gyroscopic effect may be negligible [13,14,5,15,11]. Current literature reports no studies of the effect of the imposed vibration of the VARD force generator on the nonlinear coupled axial-transverse vibration of the drillstring, either in the frequency or the time domain. The model described herein has the important benefits of providing accurate natural frequencies, generating time domain response, and capturing wellbore contact with greater fidelity than simpler single-span BHA models.

Determining natural frequencies is important because, from an operational standpoint, vibration severity can be reduced if working guidelines keep rotation speed away from these frequencies [16,17]. In the last decades, several studies have been conducted to investigate the lateral natural frequencies of the drillstring or BHA. For example, based on a simple beam vibration model, Dareing [16,18] suggested basic equations in terms of the drillstring length to control unwanted vibrations of a non-rotating drillstring, using a standard neutral point calculation. Hakimi *et al.* [14] applied the differential quadrature method to investigate the single plane lateral-axial natural frequencies of the single span BHA. The method was preferred to FEM for its simplicity and ease of application. Gulyayev *et al.* [19] studied the effect of length of the BHA on its stability, assuming two orthogonal lateral modes and mud internal flow, while neglecting the contact, axial mode and damping effect. Reported lateral natural frequencies based on buckling analysis for different BHA lengths [9], were much lower than values measured in the field [20]. A working guideline which is far away from the resonance state was suggested. Chen *et al.*

[13] used the transfer matrix method to derive the lateral natural frequencies of a single span BHA, proposing an effective drillstring density due to the added fluid mass effect and neglecting contact. A sensitivity analysis of lateral natural frequencies with respect to mud, rotary speed and WOB was accomplished. Increasing the mud damping and WOB decreased the lateral natural frequencies and the length of the BHA had a great effect on the load carrying capacity of the BHA. Neither axial coupling, nor the axial force was assumed in their model. The gyroscopic effect of rotation was also neglected. Khulief *et al.* [21] developed an FEM model of the drillstring to investigate the coupled axial-transverse vibration of a rotating drillstring. They found lateral natural frequencies and their corresponding sensitivity to the rotary speed. It was concluded that the resonance frequencies were not highly sensitive to rotary speeds. The effect of damping and wall contact were not considered in their single span BHA model. The effect of fluid damping, added fluid mass, stabilizer clearance and the friction coefficient on the critical rotary frequencies was investigated by Jansen [22]. It was verified that unstable lateral motion will not converge to a circular trajectory. The effect of torque, gravity and axial-lateral coupling were neglected in his model and the implementation of these terms was suggested for future studies.

In the present paper, the axial and orthogonal lateral resonance frequencies of a drillstring, assuming a multi-span BHA, will be calculated. The first four modes will be retained for the two orthogonal lateral directions and one axial direction (12 generalized coordinate systems in Lagrangian equation). After implementing the solution method, the FFT analysis will be applied on each generalized coordinate system to extract the first

four natural frequencies in each direction. Considering a multi-span BHA will give results that are more accurate than those from a single span BHA model.

In addition to natural frequencies, the axial or lateral time responses of the drillstring or BHA are desirable. FEM and modal analysis are two major methods used to study the time response of the drillstring. Yigit *et al.* [11] investigated the axial-transverse behavior of the non-rotating BHA and verified nonlinear axial-lateral coupling due to nonlinear strain. Mud damping, rotation and the other orthogonal lateral modes were not considered in their model. They implemented a force mode in their one-mode approximation assumed mode method to accelerate the convergence rate. Since the axial load in the BHA was assumed constant in their study, one static axial deformation mode was added to the assumed mode approximation. Spanos *et al.* [23] addressed the effect of contact and added fluid mass generating the deformed shape of the BHA in the lateral modes, based on natural mode analysis. Based on the transfer function of the BHA lateral vibration in the single orthogonal plane, frequency and mud density-dependent damping was proposed. Torque, axial force and axial displacement were not included. Li *et al.* [24] established a mathematical model, based on a simple beam, for axial vibration of the drillstring in air and gas drilling for both bit force and bit displacement excitations and verified that these two excitations do not agree with each other. Comparing the results with the field data verified that the bit-displacement excitation is the appropriate excitation method. Khulief *et al.* [21] implemented the Lagrangian approach with the finite element method to study lateral instabilities. Modal transformations were applied to obtain the reduced order form. The developed model was integrated into a computational

scheme to extract time response analysis of the drillstring. The gyroscopic effect, torsional-bending coupling and gravitational field were considered in the developed model. Drillstring-wellbore contact was not considered in the model.

The model developed in this study, enables the axial and orthogonal lateral-lateral multi-mode time response analysis of any desired point on the entire drillstring, including multiple contact points on the multi-span BHA in presence of the VARD tool.

Due to the higher stiffness, higher mass, and lower natural frequencies of the BHA compared to the pipe section, the vibration behavior of the drillstring is strongly influenced by BHA vibration, especially vibration resulting from contact with the wellbore. Modeling the impact is a crucial task to precisely evaluate the lateral dynamic response. Modeling the contact behavior of the drillstring has been approached in different ways by various researchers. Hakimi *et al.* [14] modelled drillstring-wellbore contact as a series of springs between the drillstring and the wellbore with a constant stiffness. Khulief *et al.* [20] implemented a continuous force-displacement law at the contact point in their multi-body FEM model for axial-bending and torsional-bending. Jansen [22] modeled the contact point of a rotating drillstring as a two DOF lumped element model in two orthogonal transverse planes. Coulomb friction and nonlinear mud drag force was assumed at the contact point. Liao *et al.* [10] developed a reduced order FEM model at the contact point of the drillstring and wellbore. Based on a qualitative analysis, an optimum friction coefficient value for the stable drillstring behavior at the contact point was suggested. The effect of mud damping on the lateral motion at the

contact point was neglected and the model was only capable of predicting lateral motion at the contact point. Christoforou *et al.* [25] modeled the lateral behavior of the drillstring at the contact point for parametric resonance studies. Hamilton's principle was implemented to derive the equations assuming mud damping and constant axial force along the drillstring for the axial-transverse coupling. A single-mode assumed mode approximation was used just for the BHA with a Hertzian contact force at the contact point. Impact was assumed at mid-span of a single-span BHA, and a multi-span BHA analysis was recommended to achieve more accurate results.

In the present study, the Hertzian contact theory is implemented at the contact points of multiple spans. The Dirac delta function of the radial deflection is applied to ensure that at the contact time (when the radial deflection exceeds the borehole clearance), the impact force will be applied to the multiple contact points. Successive contact or single impacts can be accurately predicted. The effect of friction at the contact point is not considered in this study [8,20,7,11]. When the radial deflection does not exceed the borehole clearance, the Dirac delta function will be calculated automatically in the analytical code and no impulsive force will be applied in no-contact instants.

The choice of equation implementation and solution method determines the extent to which symbolic variables can be used, and the ease with which nonlinearity can be included. Contact with the wellbore, mud damping, coupled transverse modes via torque, nonlinear strain energy and axial stiffening are the major nonlinear contributions to drillstring vibrations assumed in this study. Lagrange's equation for the continuous

drillstring is developed and solved using the “Bypassing PDEs” method. This method, which has been proven accurate for nonlinear problems [26], is based on combining the expanded Galerkin's technique with the Lagrange's equation for continuous structures, instead of the conventional Hamiltonian approach. The fast convergence rate without the use of a number of force modes to accelerate the convergence, as compared to other numerical models [11], enables sensitivity analysis for each controllable parameter in the model with the selected solution scheme. Another advantage of the “Bypassing PDEs” is the use of conventional energy terms, rather than the variational form of the energy equations, which further simplifies numerical solution of the developed model at the final step. Outcomes of the model and analysis method of this paper include: multi-mode analysis of the equations (up to the fourth mode), coupled lateral equations in two orthogonal planes along with the axial motion, symbolic model solution, and inclusion of all interacting forces on the drillstring. The developed model can be numerically solved to predict modal characteristics and evaluate dynamic response analysis of the entire drillstring, including multiple contact points on the BHA.

5.4 Derivation of Governing Equations

The drillstring is a beamlike structure with a high slenderness ratio. In this study, the structure is under the effect of gravity, mud hydrostatic force, contact with the wellbore, mud damping and the VARD force. The Euler-Bernoulli beam theory is used to model coupled lateral-axial vibration of the drillstring, which is considered as a beam with a high aspect ratio [27]. The drillstring in this study includes a three span BHA (with a different length for each span) with a long pipe section. The driving torque is applied on

the rotary table and the VARD force generator is applied on the BHA. The drillstring is inside a wellbore filled with mud. Two orthogonal lateral directions, u and v with the axial motion w are assumed. A schematic diagram of the drillstring is shown in Figure 5.1.

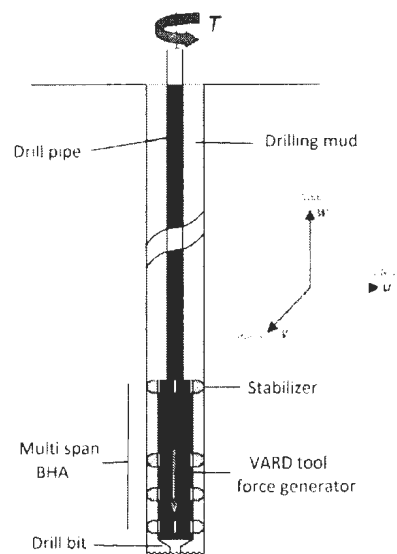


Figure 5.1: Schematic of the multi span drillstring under the effect of the VARD tool

The effects of the hook load, WOB , mud hydrostatic force and self weight are presented as a spatially varying axial force along the drillstring. The buoyant force in the drillstring should not be treated with the Archimedes's rule and the effective tension point of view should be implemented for more precise results [28,29]. Therefore, at the last point of the collar section, there are two axial upward forces, namely the WOB and the hydrostatic force at the lower cross section. At the neutral point (intersection of the pipes and collars) the axial compression in the collars changes to tension in the pipe section. The varying axial force in the collar section is:

$$F_{collar} = \rho_{collar} A_{collar} g z - WOB - \rho_{mud} g l A_{collar} \quad (5.1)$$

The total length of the drillstring is l in the above equation and the reference point is assumed at the bottom of the collar section. The force in the pipe section could be expressed as:

$$F_{pipe} = F_{hook} - \rho_{pipe} A_{pipe} g (l - z) \quad (5.2)$$

This force is depicted in Figure 5.2 for a drillstring with 800 m pipe section and a 60 m collar section.

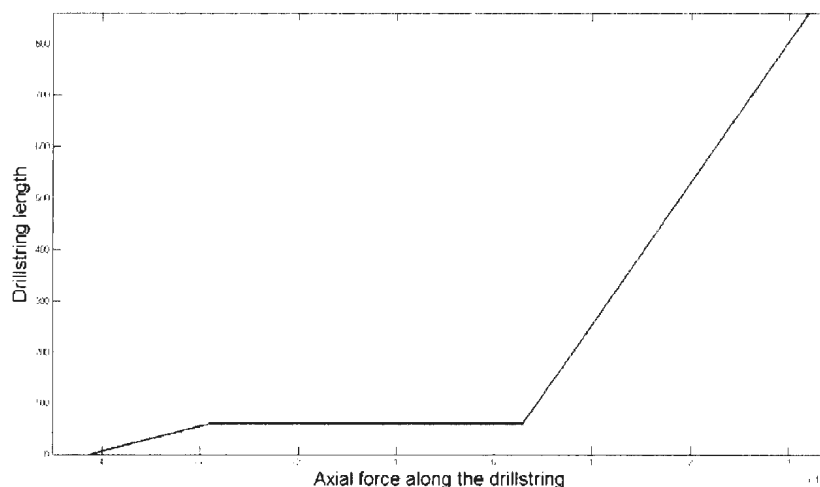


Figure 5.2: Spatially varying axial force along an 860 m drillstring

The Bypassing PDEs method is implemented in this study to derive equations. This method is based on using the Lagrange's equation with the expanded Galerkin's method, instead of the conventional Hamilton's approach for continuous systems. This method has shown accurate results for nonlinear problems [26]. The expanded Galerkin's method will be used in the first step of the energy equations. Therefore, the variational form of the

energy equations is not required in this method. In the next section, the energy terms for the drillstring are derived, to be used in combination with this method.

5.4.1 Energy Equations for the BHA and the Pipe Sections

Since the method of Bypassing PDEs is implemented, the conventional energy terms are derived rather than the variational form. The kinetic energy for the first span is:

$$K_{energy} = \frac{1}{2} \int_0^{l_1} \rho A_{collar} \left(\left(\frac{\partial}{\partial t} u(z,t) \right)^2 + \left(\frac{\partial}{\partial t} v(z,t) \right)^2 + \left(\frac{\partial}{\partial t} w(z,t) \right)^2 \right) dz \quad (5.3)$$

where u and v are two orthogonal lateral motions and w is the axial motion. The strain energy due to axial and lateral deformations is:

$$P_{energy} = \frac{1}{2} \int_0^{l_1} \left(EI_{collar} \left(\left(\frac{\partial^2}{\partial z^2} u(z,t) \right)^2 + \left(\frac{\partial^2}{\partial z^2} v(z,t) \right)^2 \right) + EA_{collar} \left(\frac{\partial}{\partial z} w(z,t) + \frac{1}{2} \left(\frac{\partial}{\partial z} u(z,t) \right)^2 + \frac{1}{2} \left(\frac{\partial}{\partial z} v(z,t) \right)^2 \right) \right) dz \quad (5.4)$$

The first term represents the elastic stiffening, while the second term captures axial stiffening due to the gravitational field ($EA \frac{\partial w}{\partial z}$ represents the gravitational force) and shows the coupling between the axial and flexural deformations. The nonlinear axial stiffening term accounts for the stiffening effect of the tension field over the pipe section and softening effect of the compression fields on the collar section. The quadratic nonlinear term retained in the equation is due to geometric nonlinearity. The work done by the driving torque can be expressed as [30]:

$$W_{torque} = \frac{1}{2} T \left(\int_0^{l_1} \left(\left(\frac{\partial^2}{\partial z^2} u(z,t) \right) \left(\frac{\partial}{\partial z} v(z,t) \right) + \left(\frac{\partial^2}{\partial z^2} v(z,t) \right) \left(\frac{\partial}{\partial z} u(z,t) \right) \right) dz \right) \quad (5.5)$$

The torque appears as the third order derivative of u in the v direction and vice versa. Therefore, this term causes coupling between two orthogonal transverse directions via torque. The work done by the VARD force is:

$$W_{VARD-force} = -\frac{1}{2} \int_0^{l_1} F_{VARD} \sin(\omega t) \left(\left(\frac{\partial}{\partial z} u(z,t) \right)^2 + \left(\frac{\partial}{\partial z} v(z,t) \right)^2 \right) dz \quad (5.6)$$

ω is the excitation frequency of the VARD force generator, which is an important controllable parameter to achieve higher ROPs. The VARD force is assumed sinusoidal. Any span on the collar section is under a spatially varying axial force as stated in Equation 5.1. The energy term due to the compressive axial force can be expressed as:

$$W_{axial-force} = -\frac{1}{2} \int_0^{l_1} F_{collar} \left(\left(\frac{\partial}{\partial z} u(z,t) \right)^2 + \left(\frac{\partial}{\partial z} v(z,t) \right)^2 \right) dz \quad (5.7)$$

The mud damping force as a result of the hydrostatic drag force is in the opposite direction of motion and is a quadratic velocity related force [22]. The dissipated energy of this force is:

$$W_{mud-damping} = \rho_{mud} C_D R_{collar} \left(\int_0^{l_1} \sqrt{\left(\frac{\partial}{\partial t} u(z,t) \right)^2 + \left(\frac{\partial}{\partial t} v(z,t) \right)^2} \left(\frac{\partial}{\partial t} u(z,t) + \frac{\partial}{\partial t} v(z,t) \right) dz \right) \quad (5.8)$$

The contact energy in the first span is approximated based on the Hertzian contact theory using a piecewise function [11]. In the following equation, b_{cl} is the borehole clearance and K_h is the contact stiffness which is related to the material and geometry at the contact point. r is the radial displacement which is related to two orthogonal lateral deflections:

$$contactenergy = - \begin{cases} K_h (r - b_{cl})^{3/2} & b_{cl} \leq |r| \\ 0 & otherwise \end{cases} r \quad (5.9)$$

The other two spans of the BHA are under the same effects. Thus the energy terms are the same, except a change in the integration limits, namely $l_1 - l_2$ for the mid span and $l_2 - l_3$ for the top span. The contact locations are different in each span. The equations for the other two spans are not shown here due to space limitations.

The first few lateral vibration modes in the lower frequencies will not be excited in the pipe section [14]. Therefore, the pipe is assumed to undergo axial vibrations. The kinetic and potential energy terms of the pipe section are:

$$\text{energy of pipe} = \frac{1}{2} \int_{l_3}^{l_4} \rho A_{\text{pipe}} \left(\frac{\partial}{\partial t} w(z,t) \right)^2 dz + \frac{1}{2} \int_{l_3}^{l_4} EA_{\text{pipe}} \left(\frac{\partial}{\partial z} w(z,t) \right)^2 dz \quad (5.10)$$

The energy of the VARD force and the tensional axial load in the pipe section are:

$$W_{\text{pipe VARD-force}} = \frac{1}{2} \int_{l_3}^{l_4} F_{\text{VARD}} \sin(\omega t) \left(\frac{\partial}{\partial z} w(z,t) \right) dz \quad (5.11)$$

$$W_{\text{pipe axial-force}} = \frac{1}{2} \int_{l_3}^{l_4} (F_H - \rho A_{\text{pipe}} g(l-z)) \left(\frac{\partial}{\partial z} w(z,t) \right) dz$$

The Lagrangian of the three-span BHA and the pipe section are as below:

$$\begin{aligned} \text{Lagrangian}_{\text{span1}} = & \frac{1}{2} \int_0^{l_1} \rho A_{\text{collar}} \left[\left(\frac{\partial}{\partial t} u(z,t) \right)^2 + \left(\frac{\partial}{\partial t} v(z,t) \right)^2 + \left(\frac{\partial}{\partial t} w(z,t) \right)^2 \right] dz \\ & - \frac{1}{2} \int_0^{l_1} \left[EI_{\text{collar}} \left(\left(\frac{\partial^2}{\partial z^2} u(z,t) \right)^2 + \left(\frac{\partial^2}{\partial z^2} v(z,t) \right)^2 \right) + EA_{\text{collar}} \left(\frac{\partial}{\partial z} w(z,t) + \frac{1}{2} \left(\frac{\partial}{\partial z} u(z,t) \right)^2 + \frac{1}{2} \left(\frac{\partial}{\partial z} v(z,t) \right)^2 \right) \right] dz \\ & - \frac{1}{2} T \int_0^{l_1} \left[\left(\frac{\partial^2}{\partial z^2} u(z,t) \right) \left(\frac{\partial}{\partial z} v(z,t) \right) + \left(\frac{\partial^2}{\partial z^2} v(z,t) \right) \left(\frac{\partial}{\partial z} u(z,t) \right) \right] dz + \frac{1}{2} \int_0^{l_1} F_{\text{VARD}} \sin(\omega t) \left[\left(\frac{\partial}{\partial z} u(z,t) \right)^2 + \left(\frac{\partial}{\partial z} v(z,t) \right)^2 \right] dz \\ & + \frac{1}{2} \int_0^{l_1} (\rho A_{\text{collar}} g z - WOB - \rho_{\text{mud}} g l A_{\text{collar}}) \left[\left(\frac{\partial}{\partial z} u(z,t) \right)^2 + \left(\frac{\partial}{\partial z} v(z,t) \right)^2 \right] dz \end{aligned} \quad (5.12)$$

$$\begin{aligned}
Lagrangian_{span2} &= \frac{1}{2} \int_{l_1}^{l_2} \rho A_{collar} \left(\left(\frac{\partial}{\partial t} u(z,t) \right)^2 + \left(\frac{\partial}{\partial t} v(z,t) \right)^2 + \left(\frac{\partial}{\partial t} w(z,t) \right)^2 \right) dz \\
&- \frac{1}{2} \int_{l_1}^{l_2} \left(EI_{collar} \left(\left(\frac{\partial^2}{\partial z^2} u(z,t) \right)^2 + \left(\frac{\partial^2}{\partial z^2} v(z,t) \right)^2 \right) + EA_{collar} \left(\frac{\partial}{\partial z} w(z,t) + \frac{1}{2} \left(\frac{\partial}{\partial z} u(z,t) \right)^2 + \frac{1}{2} \left(\frac{\partial}{\partial z} v(z,t) \right)^2 \right) \right) dz \\
&- \frac{1}{2} T \left(\int_{l_1}^{l_2} \left(\left(\frac{\partial^2}{\partial z^2} u(z,t) \right) \left(\frac{\partial}{\partial z} v(z,t) \right) + \left(\frac{\partial^2}{\partial z^2} v(z,t) \right) \left(\frac{\partial}{\partial z} u(z,t) \right) \right) dz \right) + \frac{1}{2} \int_{l_1}^{l_2} F_{VARD} \sin(\omega t) \left(\left(\frac{\partial}{\partial z} u(z,t) \right)^2 + \left(\frac{\partial}{\partial z} v(z,t) \right)^2 \right) dz \\
&+ \frac{1}{2} \int_{l_1}^{l_2} (\rho A_{collar} g z - WOB - \rho_{mud} g l A_{collar}) \left(\left(\frac{\partial}{\partial z} u(z,t) \right)^2 + \left(\frac{\partial}{\partial z} v(z,t) \right)^2 \right) dz
\end{aligned} \tag{5.13}$$

$$\begin{aligned}
Lagrangian_{span3} &= \frac{1}{2} \int_{l_2}^{l_3} \rho A_{collar} \left(\left(\frac{\partial}{\partial t} u(z,t) \right)^2 + \left(\frac{\partial}{\partial t} v(z,t) \right)^2 + \left(\frac{\partial}{\partial t} w(z,t) \right)^2 \right) dz \\
&- \frac{1}{2} \int_{l_2}^{l_3} \left(EI_{collar} \left(\left(\frac{\partial^2}{\partial z^2} u(z,t) \right)^2 + \left(\frac{\partial^2}{\partial z^2} v(z,t) \right)^2 \right) + EA_{collar} \left(\frac{\partial}{\partial z} w(z,t) + \frac{1}{2} \left(\frac{\partial}{\partial z} u(z,t) \right)^2 + \frac{1}{2} \left(\frac{\partial}{\partial z} v(z,t) \right)^2 \right) \right) dz \\
&- \frac{1}{2} T \left(\int_{l_2}^{l_3} \left(\left(\frac{\partial^2}{\partial z^2} u(z,t) \right) \left(\frac{\partial}{\partial z} v(z,t) \right) + \left(\frac{\partial^2}{\partial z^2} v(z,t) \right) \left(\frac{\partial}{\partial z} u(z,t) \right) \right) dz \right) + \frac{1}{2} \int_{l_2}^{l_3} F_{VARD} \sin(\omega t) \left(\left(\frac{\partial}{\partial z} u(z,t) \right)^2 + \left(\frac{\partial}{\partial z} v(z,t) \right)^2 \right) dz \\
&+ \frac{1}{2} \int_{l_2}^{l_3} (\rho A_{collar} g z - WOB - \rho_{mud} g l A_{collar}) \left(\left(\frac{\partial}{\partial z} u(z,t) \right)^2 + \left(\frac{\partial}{\partial z} v(z,t) \right)^2 \right) dz
\end{aligned} \tag{5.14}$$

$$\begin{aligned}
Lagrangian_{pipe} &= \frac{1}{2} \int_{l_3}^{l_4} \rho_{st} A_{pipe} \left(\frac{\partial}{\partial t} w(z,t) \right)^2 dz - \frac{1}{2} \int_{l_3}^{l_4} EA_{pipe} \left(\frac{\partial}{\partial z} w(z,t) \right)^2 dz \\
&- \frac{1}{2} \int_{l_3}^{l_4} F_{VARD} \sin(\omega t) \left(\frac{\partial}{\partial z} w(z,t) \right) dz - \frac{1}{2} \int_{l_3}^{l_4} (F_H - \rho_{st} A_{pipe} g (l-z)) \left(\frac{\partial}{\partial z} w(z,t) \right) dz
\end{aligned} \tag{5.15}$$

At this step of the Bypassing PDEs method, the expanded Galerkin's method is applied to the equations. So, u , v and w are assumed as comparison functions multiplied by mode participation factors. Since the comparison functions for each span are different, the Lagrangian should be assumed for each span separately and after substituting the comparison functions, they will be added together as the total Lagrangian of the system. Thus, u , v and w could be expressed separately for each span. Therefore, for the first span:

$$\begin{aligned}
w(z,t) &= \sum_{r=1}^4 \chi_r(z) \cdot p_r(t) \\
u(z,t) &= \sum_{r=1}^4 \varphi_r(z) \cdot \eta_r(t) \\
v(z,t) &= \sum_{r=1}^4 \phi_r(z) \cdot \lambda_r(t)
\end{aligned}
\tag{5.16}$$

The subscript r depends on the desired mode shapes according to the frequency range of interest. For this problem the first four modes will be retained to conduct the multi-mode analysis. The expanded Galerkin's method for the second span is:

$$\begin{aligned}
w(z,t) &= \sum_{r=1}^4 \chi_r(z) \cdot p_r(t) \\
u(z,t) &= \sum_{r=1}^4 \psi_r(z) \cdot \eta_r(t) \\
v(z,t) &= \sum_{r=1}^4 \psi_r(z) \cdot \lambda_r(t)
\end{aligned}
\tag{5.17}$$

For the last span of the BHA it is:

$$\begin{aligned}
w(z,t) &= \sum_{r=1}^4 \chi_r(z) \cdot p_r(t) \\
u(z,t) &= \sum_{r=1}^4 \theta_r(z) \cdot \eta_r(t) \\
v(z,t) &= \sum_{r=1}^4 \theta_r(z) \cdot \lambda_r(t)
\end{aligned}
\tag{5.18}$$

In the above expressions χ, φ, ψ and θ are comparison functions for axial and orthogonal lateral motions of the first, second and last span of the BHA, respectively. $p_r(t), \eta_r(t)$ and $\lambda_r(t)$ are mode participation factors for axial motion (w), and lateral motions (u) and (v), respectively. The boundary condition for the axial motion of the drillstring is assumed as fixed at the top and free at the bottom, and the spans are assumed

as pinned-pinned boundary conditions (location of the stabilizers) in the lateral direction. Jogi *et al.* [31] verified the natural frequency analysis of several modeling packages with field results. They proved that the simplification of boundary conditions in mathematical models agrees well with the field results for almost all modes, especially for pinned-pinned boundary conditions in the lateral mode. The comparison function for the axial motion, considering the above mentioned boundary condition, is expressed as:

$$\chi_r(z) = \sin\left(\frac{(2r-1)\pi z}{2l}\right) \quad (5.19)$$

where l is the length of the drillstring. Since, the BHA is assumed as a three span beam, the comparison function of each span is required. The exact mode shapes of a three span beam will be derived in the following section and they will be implemented in the Lagrangian equation as the corresponding comparison functions.

5.4.2 Eigenfunctions and Eigenfrequencies of a Three Span Beam with Different Lengths

As it was discussed in the previous section, the mode shapes of a simply supported three span beam are required to proceed with the Bypassing PDEs method. A schematic of a 3 span beam is shown in Figure 5.3.

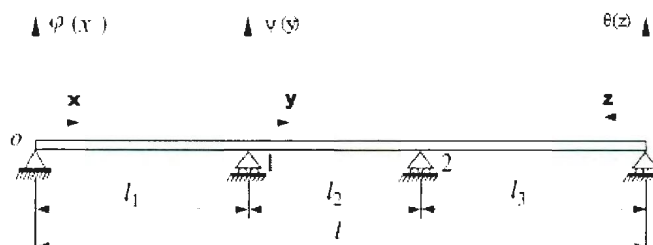


Figure 5.3: Schematic of a 3 span BHA

Separate coordinate systems are assumed for each span and the normal mode for each span could be written as:

$$\begin{aligned}\phi(x) &= a \cos(\beta x) + b \sin(\beta x) + c \cosh(\beta x) + d \sinh(\beta x) \\ \psi(y) &= e \cos(\beta y) + f \sin(\beta y) + g \cosh(\beta y) + h \sinh(\beta y) \\ \theta(z) &= i \cos(\beta z) + j \sin(\beta z) + k \cosh(\beta z) + l \sinh(\beta z)\end{aligned}\quad (5.20)$$

There are 12 unknowns in the equations. Six boundary conditions are zero deflections at the supports, while 2 boundary conditions are zero bending moments at both ends. The remaining four boundary conditions are slope and bending compatibility equations at the two middle supports. For the nontrivial solution of the system of equations, the determinant of the coefficient matrix is set to zero. The result is the frequency equation:

$$\begin{aligned}& \frac{1}{\sin(10\beta)\sinh(10\beta)} \left\{ -2 \sin(10\beta) \cos(10\beta) \sinh(10\beta) \left[\frac{\sinh(10\beta)}{\sin(10\beta)} \right] - 3 \cos(10\beta) \sinh(10\beta)^2 \right. \\ & + \sin(10\beta)^2 \cosh(10\beta) \left[\frac{\sinh(10\beta)}{\sin(10\beta)} \right] + 2 \sin(10\beta) \cosh(10\beta) \sinh(10\beta) \\ & + \sin(10\beta) \sinh(10\beta) \left[\frac{\sinh(10\beta)}{\sin(10\beta)} \right] \cosh(10\beta) + \sin(10\beta) \cos(10\beta) \sinh(10\beta) \\ & \left. + \sin(10\beta) \sinh(10\beta)^2 \left[\frac{\cos(10\beta) - \cosh(10\beta)}{\sin(10\beta)} \right] - \sin(10\beta)^2 \sinh(10\beta) \left[\frac{\cos(10\beta) - \cosh(10\beta)}{\sin(10\beta)} \right] \right\} = 0\end{aligned}\quad (5.21)$$

The equation was solved numerically using the Newton–Raphson algorithm. The first four values for β are 7.171, 12.57, 13.77 and 16.64. The values of β will be substituted in 12 equations (these 12 equations are the results of applying 12 boundary conditions to Equation 5.20) to find the first four mode shapes of each span, and the origin of the second and the last span will be transferred to the very left point of the first span. The first four mode shapes of the first span are:

$$\begin{aligned}
\phi_1 &= \sin(0.119516z) - 0.3340965884 \sinh(0.119516z) \\
\phi_2 &= \sin(0.2095z) + 0.00007849517412 \sinh(0.2095z) \\
\phi_3 &= \sin(0.22616z) + 0.01671568731 \sinh(0.22616z) \\
\phi_4 &= \sin(0.274z) + 0.02704677997 \sinh(0.274z)
\end{aligned} \tag{5.22}$$

The first four mode shapes of the second span can be expressed as:

$$\begin{aligned}
\psi_1 &= -2.461446386 \sin(0.119516z - 0.119516l_1) \\
&\quad + 1.927004330 \sinh(0.119516z - 0.119516l_1) \\
&\quad + 0.9754692378 \cos(0.119516z - 0.119516l_1) \\
&\quad - 0.9754692378 \cosh(0.119516z - 0.119516l_1) \\
\psi_2 &= -1.093320970 \sin(0.2095z - 0.2095l_1) \\
&\quad - 0.001075050855 \sinh(0.2095z - 0.2095l_1) \\
&\quad - 0.0009073462857 \cos(0.2095z - 0.2095l_1) \\
&\quad + 0.0009073462857 \cosh(0.2095z - 0.2095l_1) \\
\psi_3 &= -0.7786943701 \sin(0.22616z - 0.22616l_1) \\
&\quad - 0.2780537428 \sinh(0.22616z - 0.22616l_1) \\
&\quad - 0.2482829965 \cos(0.22616z - 0.22616l_1) \\
&\quad + 0.2482829965 \cosh(0.22616z - 0.22616l_1) \\
\psi_4 &= 0.2184545015 \sin(0.274z - 0.274l_1) \\
&\quad - 0.8338446736 \sinh(0.274z - 0.274l_1) \\
&\quad - 0.8239843412 \cos(0.274z - 0.274l_1) \\
&\quad + 0.8239843412 \cosh(0.274z - 0.274l_1)
\end{aligned} \tag{5.23}$$

The eigenfunctions of the last span are:

$$\begin{aligned}
\theta_1 &= -6.090745568 \sin(-0.119516z + 0.119516l) \\
&\quad - 0.1451462187 \sinh(-0.119516z + 0.119516l) \\
\theta_2 &= -1.046660710 \sin(-0.2095z + 0.2095l) \\
&\quad + 0.000007081079825 \sinh(-0.2095z + 0.2095l)
\end{aligned} \tag{5.24}$$

$$\theta_3 = -0.9019326856 \sin(-0.22616z + 0.22616l) \\ + 0.0009810187433 \sinh(-0.22616z + 0.22616l)$$

$$\theta_4 = -0.3072276254 \sin(-0.274z + 0.274l) \\ + 0.0001544631224 \sinh(-0.274z + 0.274l)$$

The above mode shapes are shown in Figure 5.4 for a three span BHA with 15, 15 and 30 m lengths for the first to the third spans, respectively.

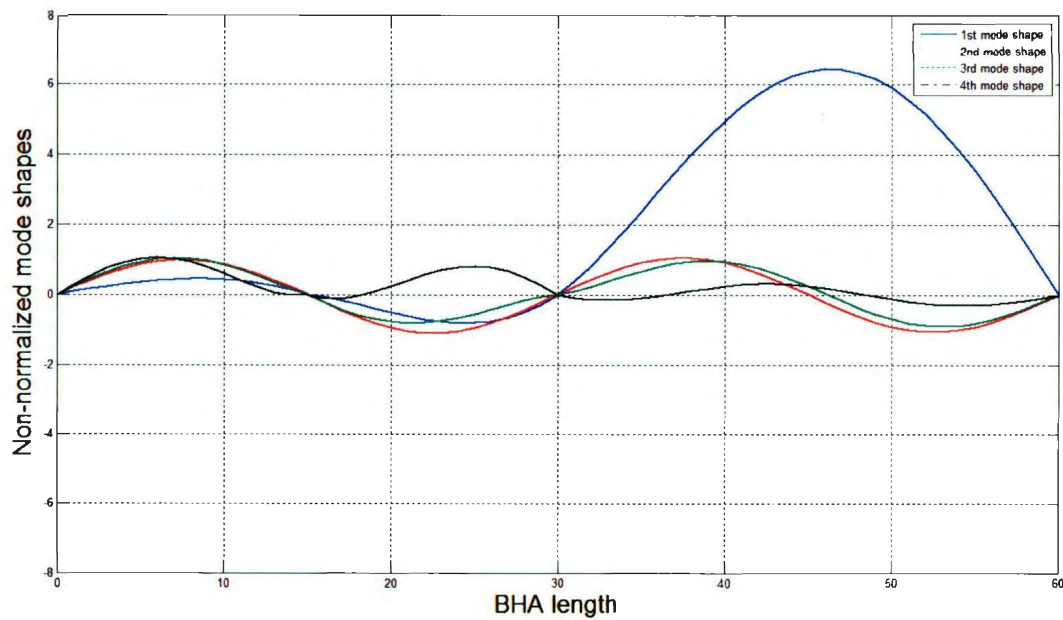


Figure 5.4: The first four mode shapes of a three span beam

5.5 Lagrangian and Equations of Motion

Substituting the corresponding mode shapes in the Lagrangian of each span and adding the corresponding terms, the total Lagrangian of the system is derived. The Lagrange's equation is implemented for each mode participation factor. Substituting the comparison functions and integrating the resulting equations over the drillstring length domain, using the mode orthogonality relations, will give twelve second order coupled nonlinear time

differential equations. One of the major advantages of the current model is that the equations are kept symbolical, up to this step. This symbolic approach allows a high speed sensitivity analysis for each controllable parameter, especially the VARD force amplitude and frequency, which are of great interest for VARD drilling studies. The mathematical model and the above procedure have been implemented in Maple[®].

5.6 Numerical Results

This system was numerically solved using a Fehlberg fourth-fifth order Runge-Kutta method with degree four interpolant, which is an adaptive numeric procedure for solving the initial value problems combining fourth-order and fifth-order Runge-Kutta techniques. The main advantage of this method is the dynamic step reduction strategy compared to the fixed-step fourth-order Runge-Kutta method. In order to avoid discontinuities in the time response, the initial time step was set to 10^{-9} s which is well below the smallest natural period in the system. The characteristics and numerical values used this study are shown in Table 5.1.

The FFT of each specific generalized coordinate system was derived, which reveals the first four natural frequencies for the two orthogonal lateral planes and the axial direction. The results are shown in Table 5.2.

Since lateral constraints (stabilizers) are assumed for the BHA, the flexural frequencies are higher than in other studies that don't assume multi-mode contact at the BHA [20]. There is a small variation between resonance frequencies in the u and v directions as a result of the numerical solution. The maximum difference is 0.05 Hz, which is a

negligible difference in rotary drilling (around 3 rpm). From a practical drilling standpoint, the rotational speed should be adjusted so that it does not correspond to one of the eigenfrequencies. The time history of any desired point is achieved using the numerical solutions of the generalized coordinate systems (12 mode participation factors in this study) and the expanded Galerkin's equations. The lateral behavior at the contact points is of significant interest to the experts in the field. Phase plane qualitative analysis is performed to determine the severity of contact at the contact points, and to avoid wellbore washouts and joint failures.

Table 5.1: Parameters used in the simulations

$T = 4000$	Driving torque (N.m)	$l_4 = 800$	Length of the pipe section (m)
$\rho_{mud} = 1500$,	Mud density (Kg/m ³)	$F_{VARD} = 20000$	VARD force amplitude (N)
$C_D = 1$	Hydrodynamic drag coefficient	$\omega_{VARD} = 600$	VARD tool frequency (rad/s)
$K_h = 6.78 \cdot 10^{11}$	Hertzian stiffness (N.m ^{-1.5})	$A_{collar} = 0.02639$	Collar cross sectional area (m ²)
$WOB = 100000$	Weight on bit (N)	$E = 210 \cdot 10^9$	Young's modulus (Pa)
$A_{pipe} = 0.00471$	Pipe cross sectional area (m ²)	$b_{cl} = 0.1$	Borehole clearance (m)
$l_1 = 15$	Length of the BHA first span (m)	$F_H = 320000$	Hook load (N)
$l_2 = 15$	Length of the BHA second span (m)	$\rho_{st} = 7860$	Pipe and collar density (kg/m ³)
$l_3 = 30$	Length of the BHA last span (m)		

Axial deflection of the drillstring is an especially important response due to implementation of the VARD force generator in the axial direction. Axial deflection at a point on the pipe, very close to the hook point (where the draw-works cable is attached to the pipe), is shown in Figure 5.5. The initial fluctuations are due to the imposed initial

conditions to the BHA. The deformation settles to a stable region with a peak-to-peak value of 5mm .

Table 5.2: The first four natural frequencies for coupled axial-transverse modes

Direction	First mode (Hz)	Second mode (Hz)	Third mode (Hz)	Fourth mode (Hz)
Lateral "u"	1.34	1.95	2.35	3.15
Lateral "v"	1.37	1.92	2.30	3.10
Axial "w"	7.65	22.25	38.59	60.30

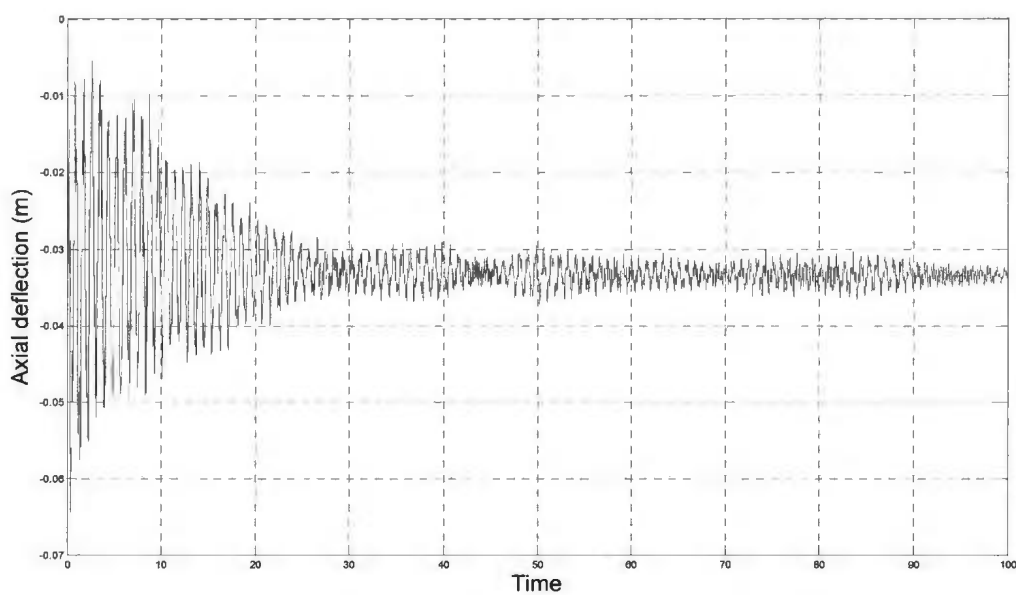


Figure 5.5: Axial deflection near the hook point

The axial deflections of the midpoint of the first and second spans are shown in Figures 5.6 and 5.7.

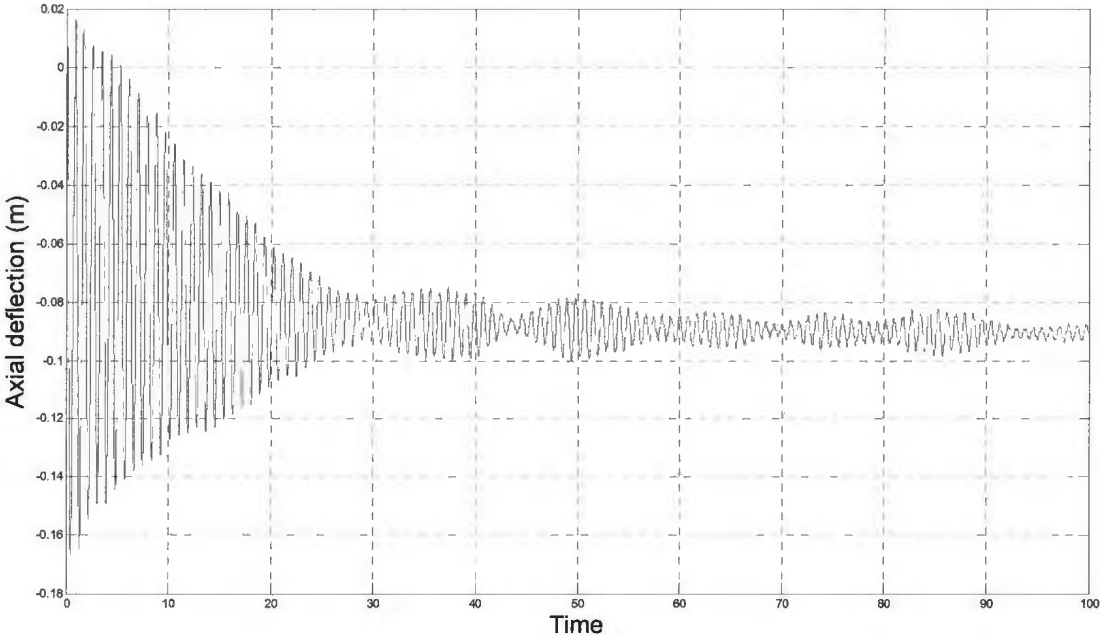


Figure 5.6: Axial deflection, midpoint on span 1 of the BHA

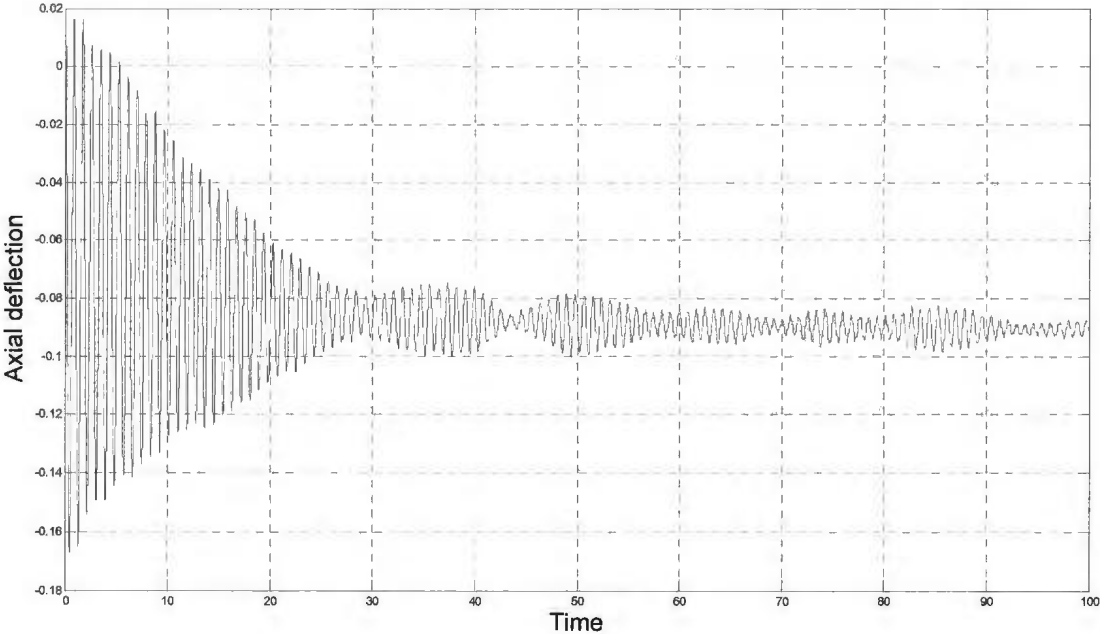


Figure 5.7: Axial deflection, midpoint on span 2 of the BHA

The axial deflection of a point on the last span, close to the bit, is shown in Figure 5.8.

The mean deflection magnitude is below zero, as a result of the interaction of all axial forces and the assumed reference coordinate system, and converges to a 0.01 *m* peak-to-peak region after entering the stability region.

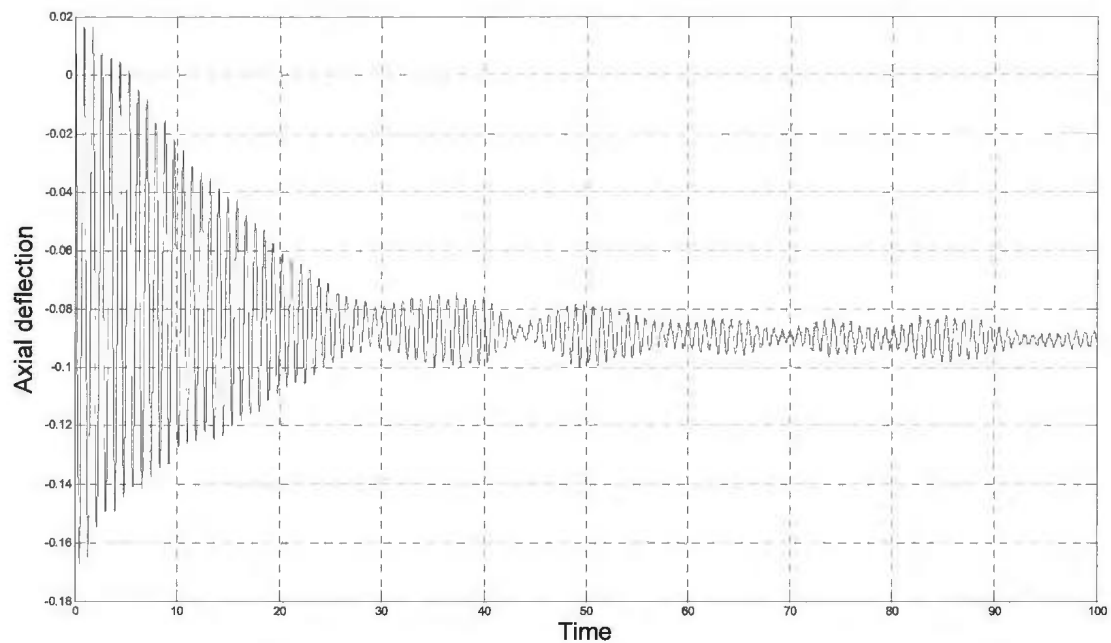


Figure 5.8: Axial deflection, a point close to the bit on span 3 of the BHA

The corresponding axial velocity of that point is depicted in Figure 5.9. The phase portrait of this point is shown in Figure 5.10, which demonstrates stable behavior in the axial mode. The amplitude and frequency of the VARD tool, as well as spatially varying axial force affect this behavior.

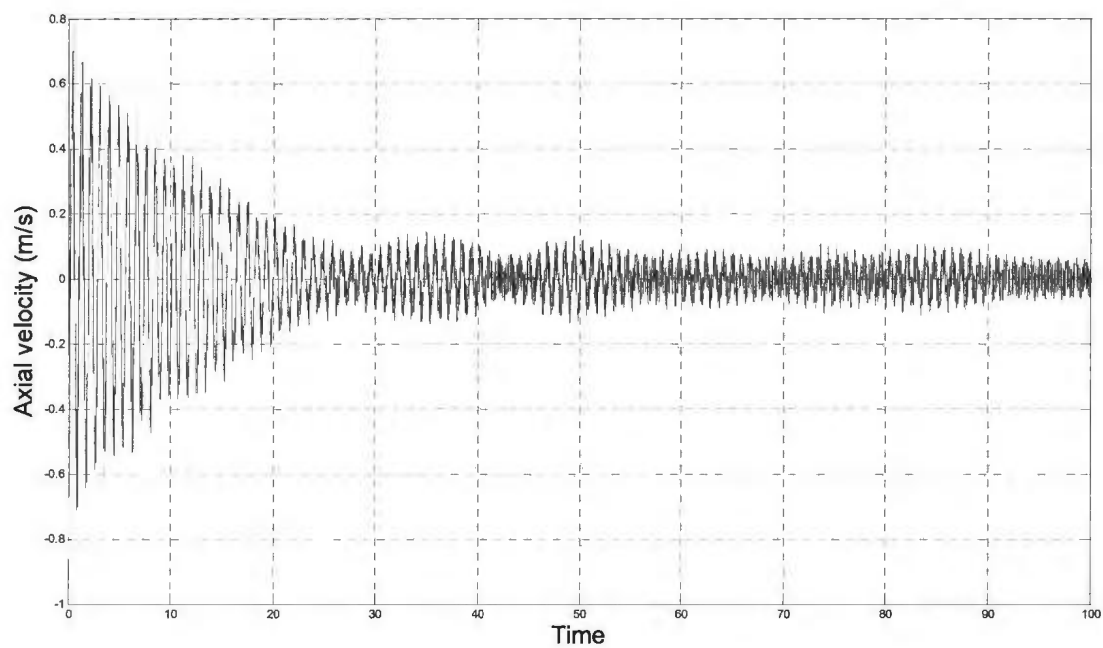


Figure 5.9: Axial velocity, a point close to the bit on span 3 of the BHA

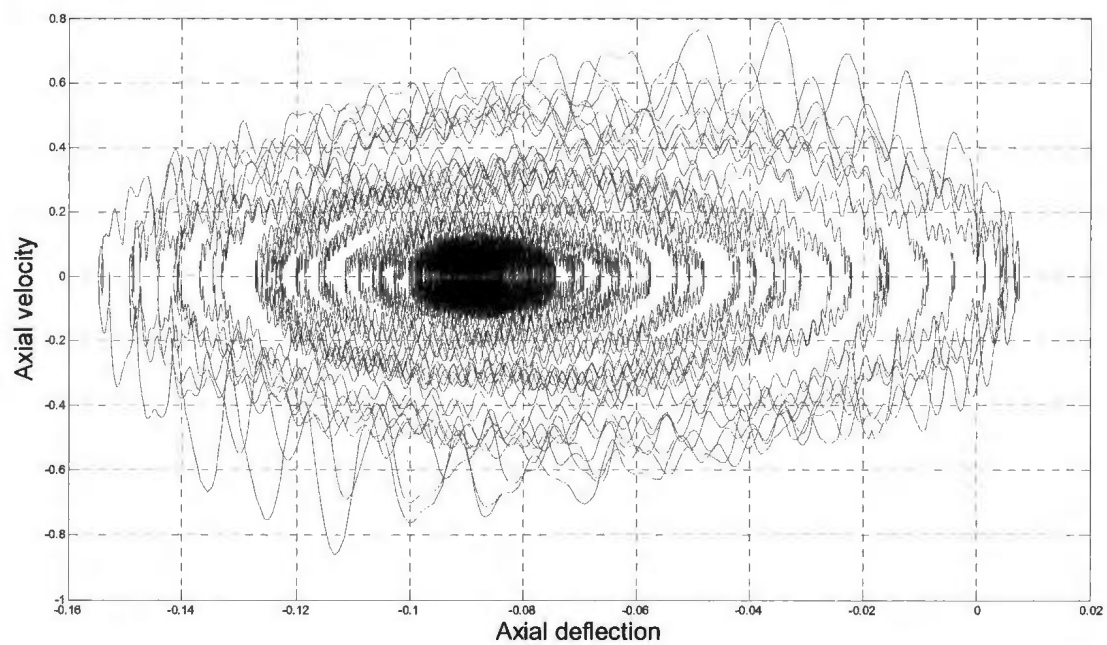


Figure 5.10: Phase plane, a point close to the bit on span 3 of the BHA

The lateral vibration behavior of any point on the BHA is well explained by the radial deflection plots. The borehole-drillstring clearance is defined in the Hertzian contact equation and radial displacement cannot exceed the borehole clearance. At the time of hitting, the Hertzian force impacts the contact point on the drillstring. The procedure to derive the radial deflection is explained for a point without contact on the top span in the following discussion. Figure 5.11a and 5.11c present the lateral deflections of the point in two orthogonal planes. Figures 5.11b and 5.11d show the corresponding lateral velocities.

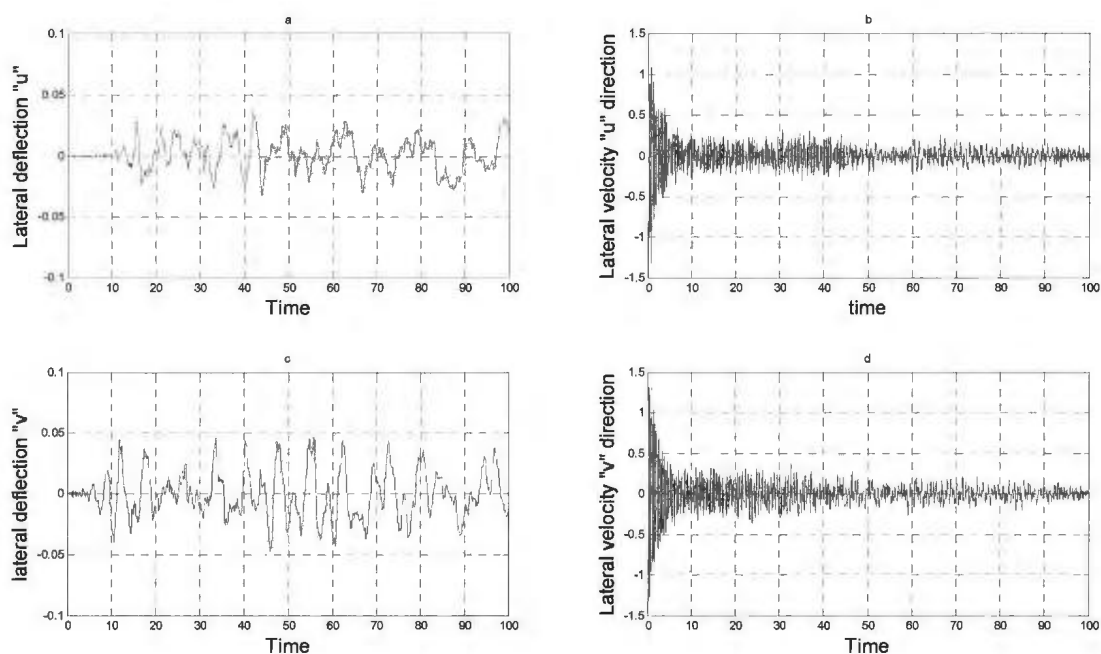


Figure 5.11: Lateral deflection and velocities, a no-contact point on the top span of the BHA

Figures 5.12a and 5.12c demonstrate the phase planes of this point in the u and v directions. These figures verify a stable behavior at the center of the wellbore. Figure 5.12c shows the trajectory of that point. As it is clear from this figure, the point spends a

considerable amount of time near the wellbore center. Figure 5.12d shows the corresponding radial deflection of that point. The maximum radial deflection is around 0.05 m , which is in between the wellbore wall and the center of the wellbore.

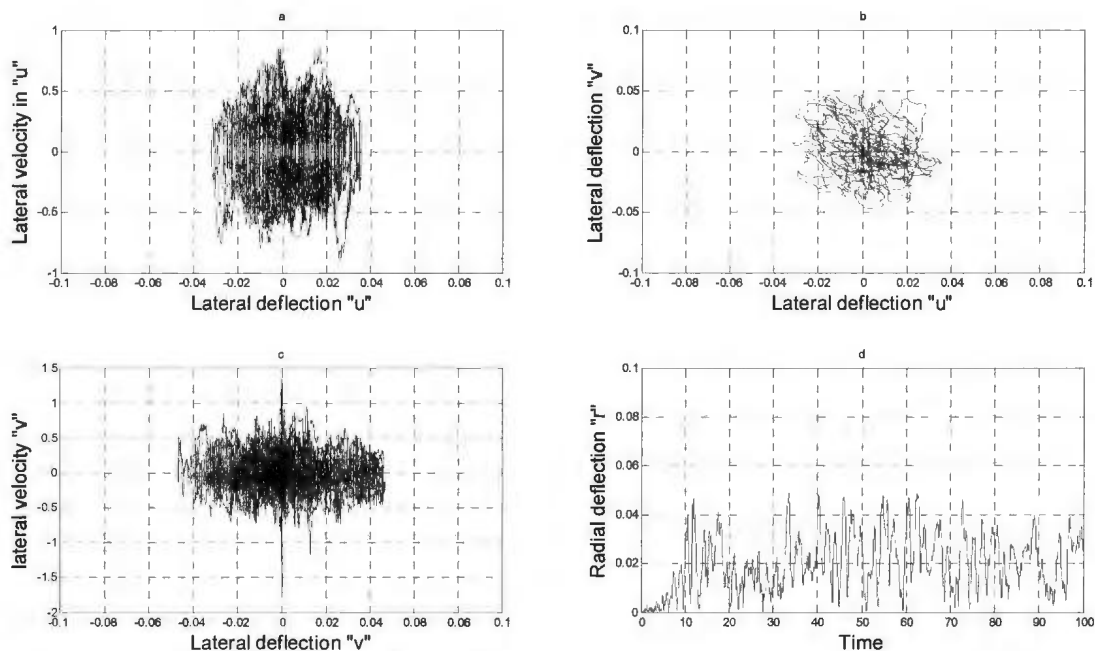


Figure 5.12: Lateral phase planes, trajectory and radial deflection, a no-contact point on the top span of the BHA

Figure 5.13 shows the radial deflection at the contact point on the top span. At this point, the drillstring hits the wellbore irregularly with a bouncing contact behavior.

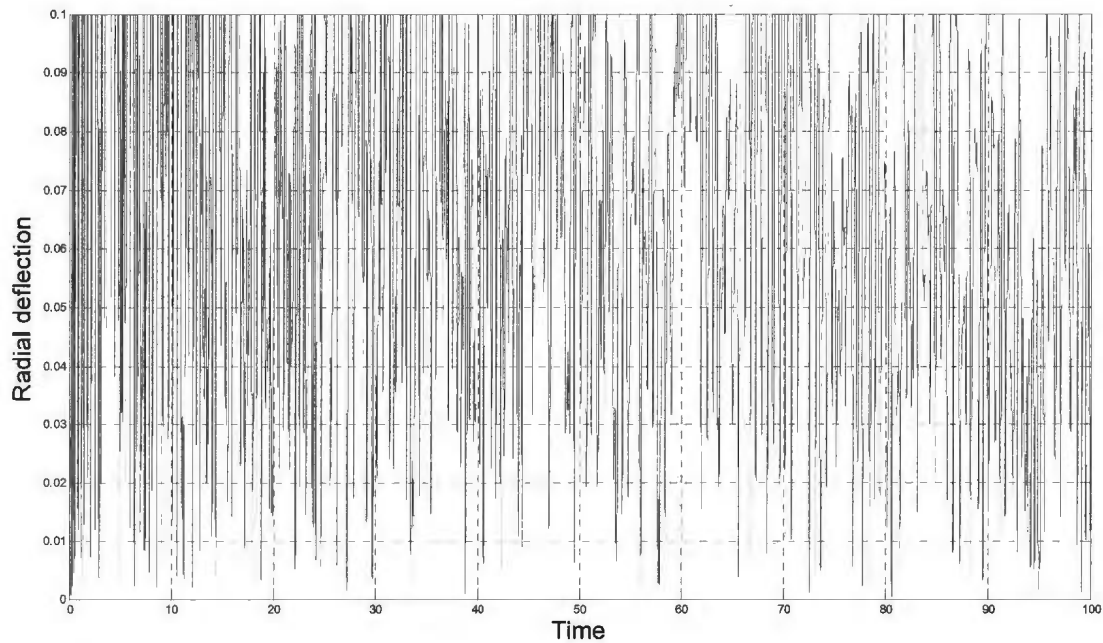


Figure 5.13: Radial deflection of the contact point, first span of the BHA

A phase portrait of the contact point is shown in Figure 5.14, which verifies highly irregular behavior at this location.

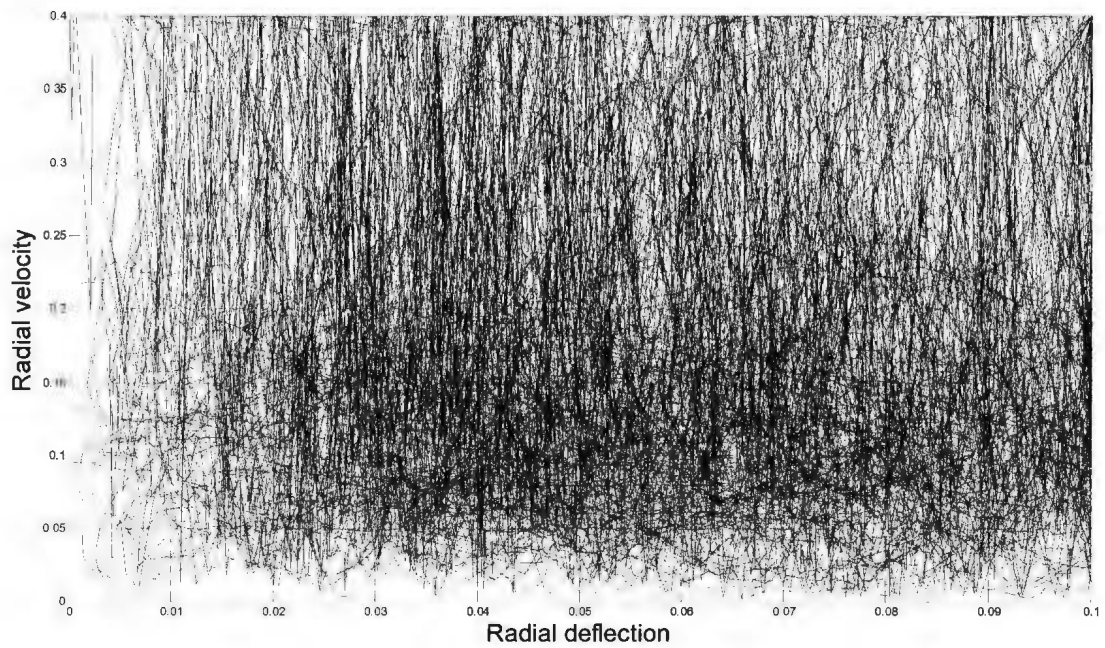


Figure 5.14: Phase portrait of the contact point on the first span of the BHA

The radial deflection of the contact point at the middle of the second span is shown in Figure 5.15. The contact is not as severe as for the top span. After hitting the wellbore for a period of time, the drillstring spends a period near the center, and then hits the wellbore again.

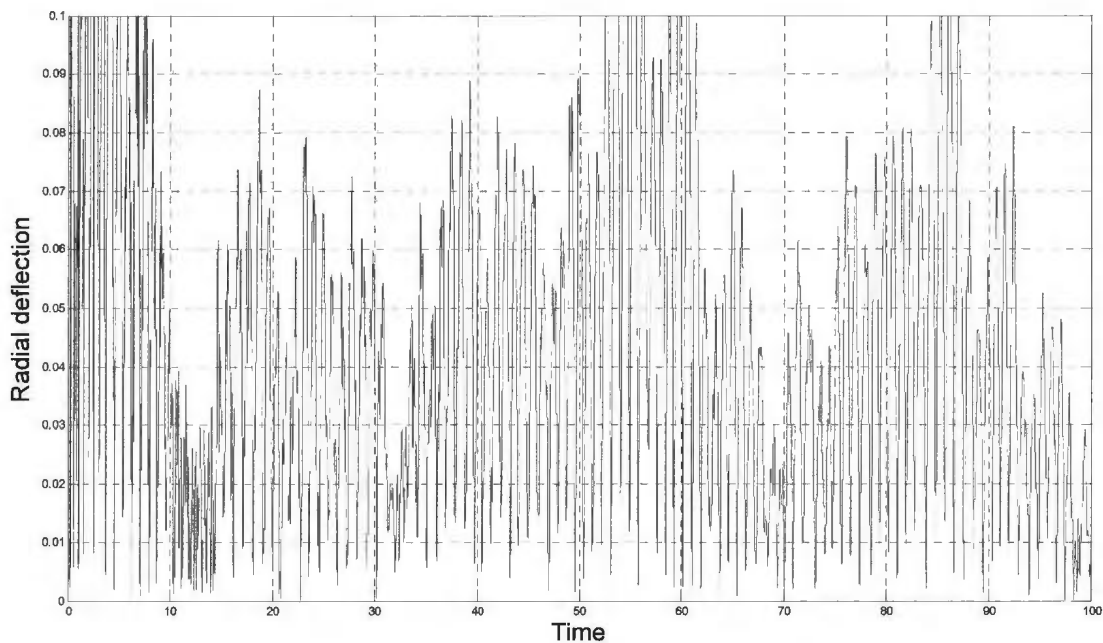


Figure 5.15: Radial deflection of the contact point, second span of the BHA

The phase plane in Figure 5.16 demonstrates that at this location, the drillstring is not traveling strictly near the wellbore.

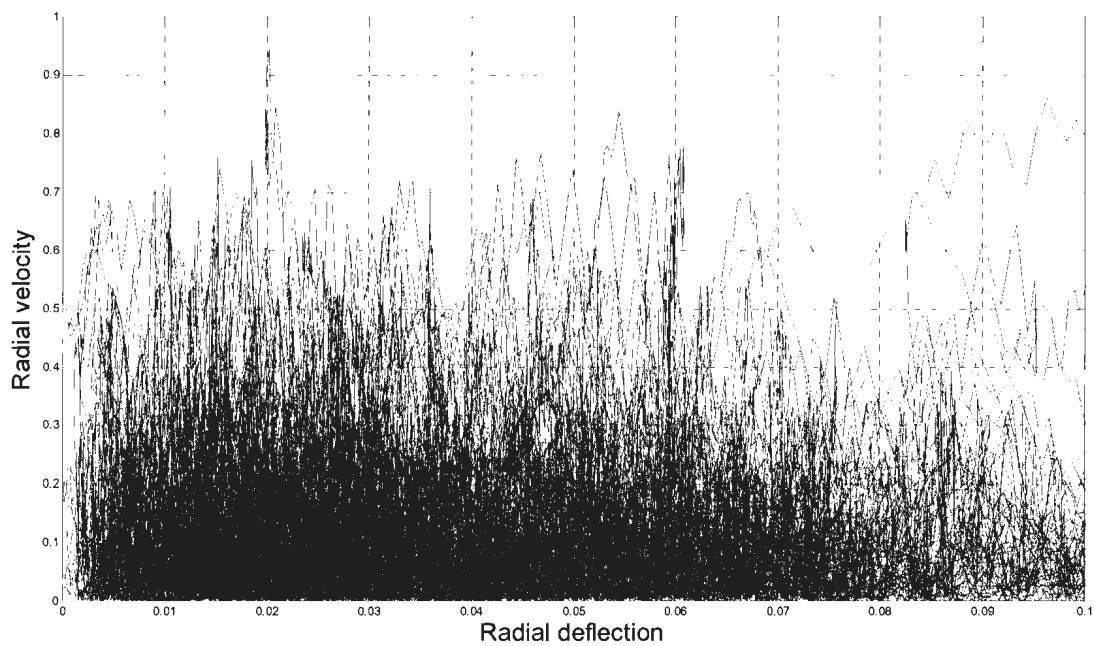


Figure 5.16: Phase portrait of the contact point on the second span of the BHA

The contact behavior at the span closest to the bit is depicted in Figures 5.17 and 5.18.

The radial deflection shows less contact compared to previous spans. It seems that the damping behavior of the mud is affecting the contact at this point; however, the length of the span is half that of the top span. The radial phase plane also shows a less irregular behavior compared to the other two spans.

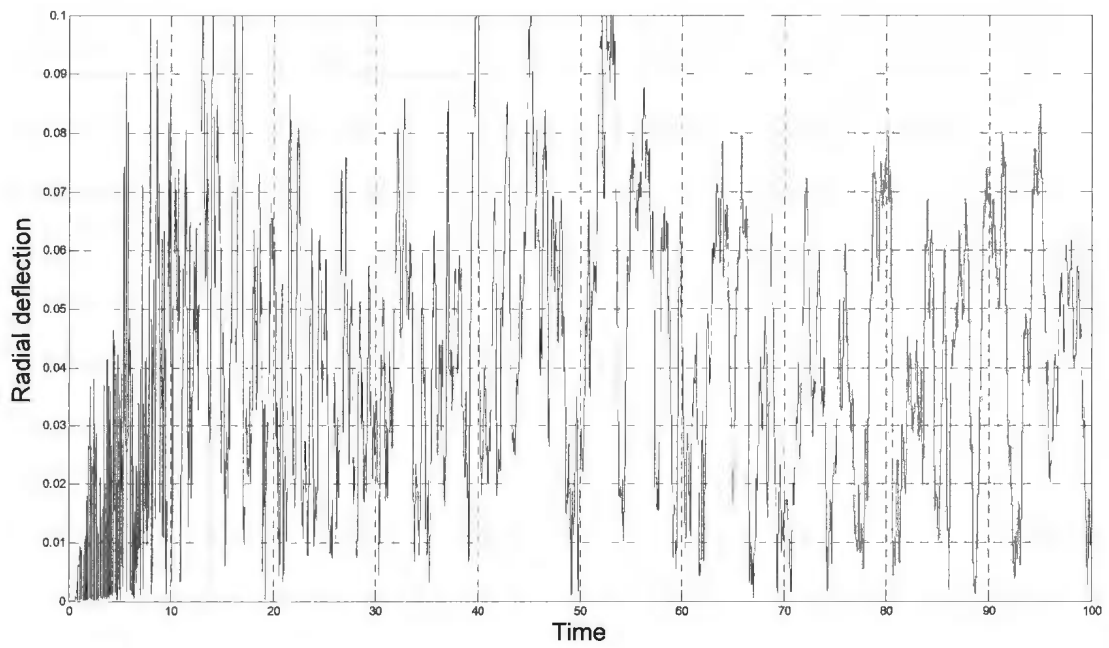


Figure 5.17: Radial deflection of the contact point, last span of the BHA

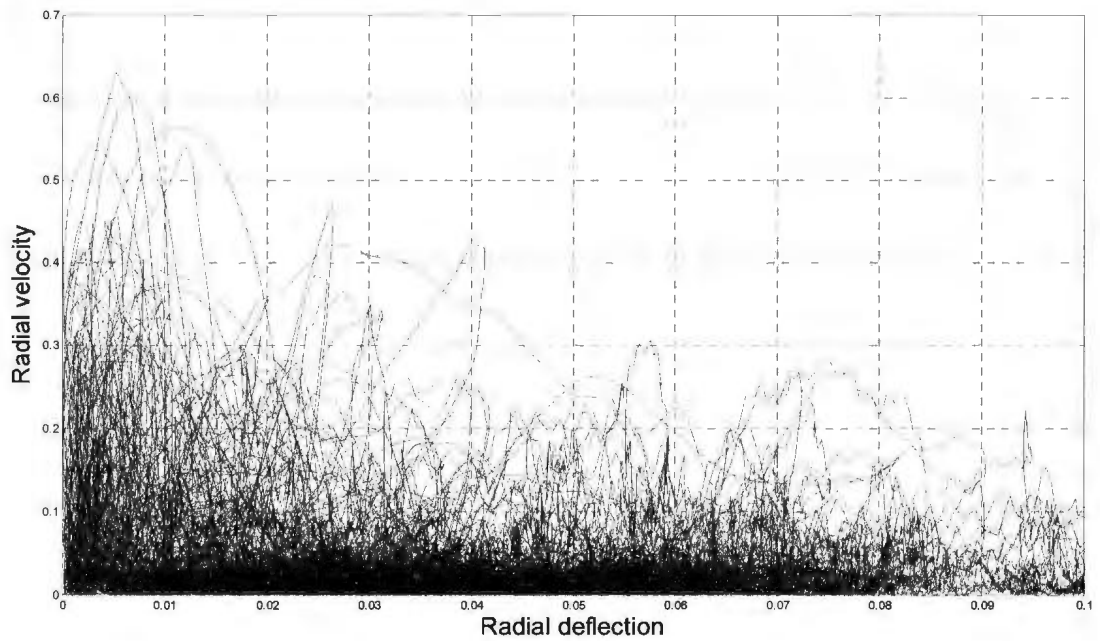


Figure 5.18: Phase portrait of the contact point on the last span of the BHA

This model is capable of predicting dynamic behavior at any point on the drillstring, either on the pipe section or BHA. Additionally, the symbolical code enables sensitivity analysis of the controllable parameters. The VARD tool is always tuned for different geotechnical formations, which is a requirement to investigate the behavior of the drillstring in the wellbore before drilling new formations. The symbolical Maple code allows running the equations with the new set of VARD tool parameters, as well as: span length, pipe length, mud properties, pipe and collar section and material properties.

5.7 Conclusions

The vibration behavior of the drillstring under the effect of the axial force generators such as VARD tools, jars, and agitators in rotary drilling is of significant interest in the field of drilling. Predicting the dynamic behavior is an essential step in designing suppression tools and guidelines. The coupled nonlinear axial-transverse behavior and lateral instabilities of the drillstring under an applied axial force were studied in this paper. The Bypassing PDEs method, along with the Lagrange's equation, was implemented to derive the nonlinear equations. As well, the expanded Galerkin's method, with the first four retained modes for each span, enables a multi-point contact analysis. Mud damping, spatially varying axial force, multi-span contact and torque are assumed in the nonlinear model and the nonlinear coupling terms due to the contact, axial stiffening and torque were retained. The equations were solved symbolically. The multi-span analysis of the BHA provided more realistic results for the resonant rotary speeds. The rotary speed of the drillstring should be kept far enough from the natural frequencies to avoid excessive deflections and contact with the wellbore, both of which can cause premature failure of

bottom-hole assembly components. Phase plane analysis of the contact points demonstrated a highly irregular contact at the top span of the BHA, while the contact at the span closest to the bit was not as severe. The symbolical model of this paper can be used to conduct a sensitivity analysis of controllable parameters for tuning the VARD force generator, determining working guidelines and designing suppression methods, either for the axial or transverse directions.

5.8 Acknowledgment

This research was conducted at the Advanced Drilling Technology Laboratory at Memorial University of Newfoundland and was funded by the Atlantic Canada Opportunities Agency (AIF Contract No. 781-2636-1920044), the Research and Development Corporation of Newfoundland and Labrador, Husky Energy, and Suncor Energy. Also, the authors would like to acknowledge the valuable contributions to the software implementation made by Dr. Muzychka at Memorial University.

5.9 References

- [1] Barton, S., Baez, F., and Al Ali, A., 2011, "Drilling Performance Improvement in Gas Shale Plays Using a Novel Drilling Agitator Device," SPE#144416, SPE North American Unconventional Gas Conference and Exhibition, The Woodlands, Texas.
- [2] Babatunde, Y., Butt, S. D., Molgard, J., and Arvani, F., 2011, "Investigation of the Effects of Vibration Frequency on Rotary Drilling Penetration Rate Using Diamond Drag Bit," ARMA#11-527, 45th US Rock Mechanics/Geomechanics Symposium (ARMA), San Francisco, California.

- [3] Manko, K. I., Pilipenko, V. V., and Zapols'ky, L. G., 2003, "Use Hydrodynamic Cavitation For Increase of Efficiency of Process of Well Drilling," Fifth International Symposium on Cavitation, Osaka, Japan.
- [4] Chin, W. C., 1994, *Wave Propagation in Petroleum Engineering*, Gulf Publishing Company, Texas, USA.
- [5] Ghasemloonia, A., Rideout, D. G., and Butt, S. D., 2012, "Coupled Transverse Vibration Modeling of Drillstrings Subjected to Torque and Spatially Varying Axial Load," *Journal of Mechanical Engineering Science (IMEchE, part C)*, **227**(5), pp. 946-960.
- [6] Sotomayor, G. P. G., Placido, J. C., and Cunha, J. C., 1997, "Drillstring Vibration: How to Identify and Suppress," SPE#39002, Latin American and Caribbean Petroleum Engineering Conference, Rio de Janeiro, Brazil.
- [7] Spanos, P. D., Chevallier, A. M., and Politis, N. P., 2002, "Nonlinear Stochastic Drillstring Vibrations," *ASME Journal of Vibration and Acoustics*, **124**(4), pp. 512-519.
- [8] Berlioz, A., Der Hagopian, J., Dufour, R., and Draoui, E., 1996, "Dynamic Behavior of a Drillstring: Experimental Investigation of Lateral Instabilities," *ASME Journal of Vibration and Acoustics*, **118**(3), pp. 292-298.
- [9] Gulyayev, V. I., Gaidaichuk, V. V., Solovjov, I. L., and Gorbunovich, I. V., 2009, "The Buckling of Elongated Rotating Drillstrings," *Journal of Petroleum Science and Engineering*, **67**(3-4), pp. 140-148.

- [10] Liao, C., Balachandran, B., Karkoub, M., and Abdel-Magid, Y. L., 2011, "Drillstring Dynamics: Reduced-Order Models and Experimental Studies," *ASME J. Vib. Acoust.*, **133**(4), pp. 041008-1041008-8.
- [11] Yigit, A. S., and Christoforou, A. P., 1996, "Coupled Axial and Transverse Vibrations of Oilwell Drillstrings," *Journal of Sound and Vibration*, **195**(4), pp. 617-627.
- [12] Yigit, A. S., Christoforou, A. P., 1998, "Coupled Torsional and Bending Vibrations of Drillstrings Subject to Impact With Friction," *Journal of Sound and Vibration*, **215**(1), pp. 167-181.
- [13] Chen, S. L., Geradin, M., 1995, "An Improved Transfer Matrix Technique as Applied to BHA Lateral Vibration Analysis," *Journal of Sound and Vibration*, **185**(1), pp. 93-106.
- [14] Hakimi, H., Moradi, S., 2009, "Drillstring Vibration Analysis Using Differential Quadrature Method," *Journal of Petroleum Science and Engineering*, **70**(3-4), pp. 235-242.
- [15] Heisig, G., Neubert, M., 2000, "Lateral Drillstring Vibrations in Extended-Reach Wells," IADC/SPE# 59235, IADC/SPE Drilling Conference, New Orleans, Louisiana.
- [16] Dareing, D. W., 1984, "Drill Collar Length Is a Major Factor in Vibration Control," *Journal of Petroleum Technology*, **36**(4), pp. 637-644.
- [17] Gulyayev, V. I., Borshch, O. I., 2011, "Free Vibrations of Drillstrings in Hyper Deep Bore-Wells," *Journal of Petroleum Science and Engineering*, **78**(3-4), pp. 759-764.
- [18] Dareing, D. W., 1984, "Guidelines for Controlling Drillstring Vibrations," *ASME Journal of Energy Resources Technology*, **106**(2), pp. 272-277.

- [19] Gulyaev, V. I., Lugovoi, P. Z., Gaidaichuk, V. V., and Solov'ev, I. L., 2007, "Effect of the Length of a Rotating Drillstring on the Stability of Its Quasistatic Equilibrium," *International Applied Mechanics*, **43** (9), pp. 1017-1023.
- [20] Khulief, Y. A., Al-Sulaiman, F. A., and Bashmal, S., 2008, "Vibration Analysis of Drillstrings With String-Borehole Interaction," *International Journal of Mechanical Engineering Science, (IMechE Part C)*, **222**(11), pp. 2099-2110.
- [21] Khulief, Y. A., and Al-Naser, H., 2005, "Finite Element Dynamic Analysis of Drillstrings," *Finite Element in Analysis and Design*, **41**(13), pp. 1270-1288.
- [22] Jansen, J. D., 1991, "Nonlinear Rotor Dynamics as Applied to Oil Well Drillstring Vibrations," *Journal of Sound and Vibration*, **147** (1), 115-135.
- [23] Spanos, P. D., Payne, M. L., and Secora, C. K., 1997, "Bottom-Hole Assembly Modeling and Dynamic Response Determination," *ASME Journal of Energy Resources Technology*, **119**(3), pp. 153-158.
- [24] Li, Z., Yanshan, U., and Guo, B., 2007, "Analysis of Longitudinal Vibration of Drillstring in Air and Gas Drilling," SPE#107697, SPE Rocky Mountain Oil and Gas Technology Symposium, Denver, Colorado.
- [25] Christoforou, A. P., and Yigit, A. S., 1997, "Dynamic Modeling of Rotating Drillstrings With Borehole Interactions," *Journal of Sound and Vibration*, **206** (2), pp. 243-260.
- [26] Thomsen, J. J., 2003, *Vibrations and Stability*, 2nd ed., Springer, Berlin, Germany.
- [27] Beck, A. T., da Silva Jr., C.R.A., 2010, "Timoshenko Versus Euler Beam Theory: Pitfalls of a Deterministic Approach," *Structural Safety*, **33**(1), pp. 19-25.

- [28] Bourgoyne, A. T., Chenevert, M. E., Millheim, K. K., and Young, F. S., 1986, *Applied Drilling Engineering*, SPE Text Book Series, Society of Petroleum Engineers, Texas, USA.
- [29] Mitchell, R. F., and Miska, S. Z., 2011, *Fundamentals of Drilling Engineering*, SPE textbook series, Texas, USA.
- [30] Simitses, G., Hodges, D., 2005, *Fundamentals of Structural Stability*, Elsevier, Oxford, UK, Chap. 8.
- [31] Jogi, P. N., Macpherson, J. D., and Neubert, M., 2002, "Field Verification of Model-Derived Natural Frequencies of a Drillstring," *ASME Journal of Energy Resources technology*, **124**(3), pp. 154-162.

6 Vibration Analysis of a Drillstring in Vibration-Assisted Rotary Drilling-Finite Element Modeling With Analytical Validation

Ahmad Ghasemloonia, Ph.D. Candidate

D. Geoff Rideout, Associate Professor

Stephen D. Butt, Professor

Advanced Drilling Group, Faculty of Engineering and Applied Science, Memorial University, St. John's, NL, Canada

This chapter is based on the modeling step 4 defined in section 1.4 of this thesis and is published as a full research paper in the ASME Journal of Energy Resources Technology, vol. 135(3), pp. 032902-1-032902-18.

6.1 Abstract

Introducing sources of axial vibration into an oilwell drillstring has the potential to improve the drilling efficiency. Vibration generator tools, such as drillstring agitators, are under development or in current use to excite the bottom-hole assembly (BHA) axially in order to increase power and weight at the bit, improve the rate of penetration (ROP), reduce drillstring-wellbore friction, and accelerate the cutting removal process. Enhanced drilling under the effect of intentional imposed vibration is called “vibration-assisted rotary drilling” or VARD. While potentially enhancing the drilling process, VARD tools

can also excite many unwanted vibration modes of the drillstring. These unwanted vibrations can cause fatigue damage and failure of BHA components such as “measurement while drilling” (MWD) tools, bit and mud motors, and consequently, inefficient drilling. This motivates a study of the complex dynamic behavior of an axially excited drillstring. Transverse vibration is the most destructive type of drillstring vibration, and the coupling between transverse and axial vibration of a drillstring subjected to an applied VARD force is of great interest to the experts in the field. In this study, the coupled axial-transverse vibration behavior of the entire drillstring under the effect of a VARD tool is investigated. A dynamic finite element method (FEM) model of the vertical drillstring assuming a multi-span BHA is generated and validated with a coupled nonlinear axial-transverse elastodynamic mathematical model. The effects of mud damping, driving torque, multi-span contact and spatially varying axial load are included. Geometry, axial stiffening and Hertzian contact forces are sources of nonlinearity in the model. A mesh sensitivity analysis is conducted to reduce computational time. The accuracy of the retained modes in the analytical equations is verified by extracting the total effective mass derived by the FEM model. There is agreement between the FEM and analytical models for coupled-transverse and axial vibration velocities, displacements, resonance frequencies and contact locations and behavior. While the analytical model has fast running time and symbolic solution, the FEM model enables easy reconfiguration of the drillstring for different boundary conditions, inclusion of additional elements such as shock subs, and changing the number and locations of stabilizers.

Key words: Drillstring; Vibration-assisted rotary drilling; Coupled axial-transverse vibration; Finite element method, Model order reduction; Mesh analysis; Wellbore contact

6.2 Introduction

Drilling is one of the most costly and risky activities for both exploration and development of oil fields. Enhanced drilling techniques are rapidly growing for faster and more efficient drilling. Several classes of recent drilling tools apply axial vibration intentionally to the drillstring. "Vibration-assisted rotary drilling", or VARD, can be defined as the intentional introduction of controlled vibration into the drillstring to increase drilling performance. Tools such as "agitators" are currently used to overcome friction and assist with advancing the drillstring [1], especially in horizontal or deviated wells. This imposed vibration significantly reduces drillstring-wellbore friction [1] and speeds up the cuttings flushing process. Improved weight transfer, increased power at the bit and consequently higher rate of penetration (ROP) compared to conventional rotary drilling [2] are other potential advantages of vibration-assisted rotary drilling. However, VARD forces can increase the risk of hole deviation, wellbore washout, and premature failure of the bottom-hole assembly (BHA) and its components, including measurement-while-drilling (MWD) tools, since the drillstring can undergo undesirable vibrations excited by the VARD tool. In addition to the above negative consequences, a great portion of the energy that was supposed to be delivered at the bit can be lost if VARD parameters are not compatible with the overall drillstring and formation properties. Therefore, modeling of the vibration behavior of the total drillstring in the presence of

imposed dynamic forces is an essential step in generating drilling guidelines and designing control strategies to optimize vibration-assisted rotary drilling. Several parameters such as weight on bit (WOB), rotary speed, natural frequencies, and quality of the hole are related to the behavior of the drillstring.

The drillstring includes a long, thin-walled interval called the pipe section, and a heavier, thick-walled bottom section called the collar section. The bit is attached to the end point of the collar section. The collar section is centralized inside the wellbore, with stabilizers located at many points over the BHA. The stabilizers increase the buckling load-carrying capacity of the collar section and are used to control well trajectories for directional drilling. BHA vibrations play a dominant role in the transverse vibration behavior of the drillstring and can give rise to multiple locations for contacts with the borehole wall. The annulus between the BHA and the wellbore is filled with drilling mud, which cools the bit and flushes the cuttings out of the hole. Moreover, the mud helps to overcome formation pressure and transmit hydraulic power to the bit. The role of mud on the stability of drillstring dynamics, especially in the lateral direction, is also important. The drillstring is under the effect of several axial forces: WOB, mud hydrostatic load, drillstring self weight and the VARD force. Under normal drilling condition, it is desirable to have the pipe section under tension, and the collar section under axial compression.

The beam-like drillstring structure can be subjected to three major modes of vibration: axial, lateral and torsional. Moreover, the drillstring can undergo coupled states of vibration, i.e., axial-lateral, axial-torsional and torsional-lateral vibrations. Stick-slip,

whirling and bit bounce are extreme states of the aforementioned vibration modes. While transverse vibration is typically the most severe form of vibration in conventional drilling, axial vibration becomes very important in VARD drilling. The axial frequencies and behavior of the drillstring are major concerns when configuring a VARD tool. Transverse vibrations of the drillstring cause wellbore washout, premature failure of the components and loss of energy [3,4]. BHA-wellbore contact is the main excitation source for the lateral vibration, while the VARD force excites the axial mode. These two coupled modes are present simultaneously and are both potentially harmful if not controlled.

The first step in configuring a VARD tool to be compatible with a drillstring is to model the dynamic behavior of the drillstring and analyze the sensitivity of its behavior to commonly-adjusted drilling parameters. The following section is a review of dynamic FEM vibration models of drillstrings. The dynamic FEM model is then developed and subjected to mesh analysis and model reduction. The results show excellent agreement with the analytical model, which is summarized in Appendices 6.1-6.4 and also described in a recent publication [5]. Finally, conclusions are made and future research directions are suggested.

6.3 Literature Review

Drillstring modeling to predict and understand vibrations can be approached in a number of ways. Several methodologies including static modeling, elastodynamic modeling, dynamic numerical modeling (e.g. finite element, finite difference models and dynamic stiffness method) and laboratory scale test rigs have been used to investigate this

phenomenon. Dykstra *et al.*, [6] investigated the effect of dynamic modeling on improving the drilling performance through comparing some developed dynamic models and case studies. They discussed fixed and rolling cutter polycrystalline diamond compact (PDC) bit dynamic models and their capabilities in dynamic load and stability predictions, and these models were validated through comparing them with several case studies in the UK, North Sea and onshore US. Drillstring dynamic simulations were verified by comparing their results with downhole measurements and using these dynamic models provided insight into drilling system performance.

Static models were developed in the 1950's to investigate the BHA forces under static conditions. These models were mainly implemented to investigate the buckling limit of the BHA (using Euler column theory), to determine interacting static contact forces, to design mud type, bit and BHA; and to develop top rotary drive systems. Stability studies of the drillstring and prediction of the deformed shape of the drillstring were also conducted through these models [7]. These models were not capable of extracting natural frequencies, transient and steady state behavior of the drillstring and the dynamic contact behavior. Static models gave way to dynamic modeling, especially elastodynamic models and numerical models, such as dynamic finite element models.

Basic dynamic models (non-rotating beam-like models) were first developed in the 1960's by Bailey *et al.* [8]. In the beginning, simplified beam elastodynamic models were used to predict natural frequencies, after which models were enhanced to study the transient response [9] or steady state response [10]. These models could be categorized in

three major categories: axial models [11], transverse models [12] and torsional models [13]. Later on, coupling effects were investigated: axial-transverse [9,14], axial-torsional [15] and torsional-transverse modes [16]. Recently, enhanced models have included contact behavior between the drillstring and wellbore [17], the parametric resonance phenomenon [16], buckling analysis of the BHA [14] and bit-rock interaction effects on the drillstring vibration behavior [18,19]. The motivation for these studies was to investigate vibration suppression methods and working guidelines, i.e., the combination of proper weight on bit (WOB), torque on bit (TOB), rotary speed, mud characteristics and pump working parameters.

The difficulties and limitations of analytical models to model complex boundary conditions and forces, and the need to reconfigure such models for new interactions, coupled with the development of fast processing computers, have attracted investigators to the use of recognized powerful numerical methods, such as finite element method (FEM) and the finite difference method (FDM). One of the early attempts at FEM analysis of the drillstring was conducted by Millheim *et al.* [20], where the drillstring was modeled as a straight beam with beam and gap elements using an FEM package called MARC-CDC. The nodal displacement was derived using the variational principle to study drillstring deflection and bit forces. Straight and curved beam elements were compared in their model and the results were verified by field data. Transient response of the rotating BHA, assuming bit-rock interaction force, was modeled by Baird *et al.* using the FEM technique [21]. Apostol [22] studied the forced frequency response of the non-rotating BHA with a 3D finite element model. Three types of damping were assumed in their

model. Burgess *et al.* [23] modeled the lateral vibration of the drillstring by FEM. They only modeled the length of the drillstring which was not lying along the wellbore. A static nonlinear analysis was performed previously to find out this length. Uncoupled transverse-torsional behavior of the drillstring was modeled by Axisa *et al.* with FEM [24]. The drillstring was modeled as a straight rod and a sensitivity analysis for the fluid elastic effect was conducted. The nonlinear gravitational axial stiffening effect was not considered in their model. Parametric instability of the rotating drillstring was studied by Berlioz *et al.* [12], where the FEM equations were derived for a 6 DOF shaft element using rotor dynamics equations. The axial stiffening was neglected in their model. The results were verified by test rig data. Spanos *et al.* [25] modeled the BHA assuming the added fluid mass with a frequency dependent mass matrix. The excitation forces were modeled as monochromatic functions of time and nonlinear contact force at the stabilizers location were assumed. The frequency response model was suggested as a powerful tool to understand the complex behavior of the BHA. In another work by Spanos *et al.* [3] a transfer function representation for the BHA based on modal superposition was derived. Lateral vibrations of the drillstring were studied, while the lateral displacement of the drill bit was defined as an equivalent linear system and predicted subsequently by Monte Carlo simulation. Model uncertainties of the bit-rock nonlinear interaction were studied by Ritto *et al.* [26], using a non-parametric probabilistic approach. They found that the uncertainties in the bit-rock interaction model play an important role in the coupling between the axial and torsional responses. Khulief *et al.* [27] used Lagrange's equation to derive an FEM model of a rotating drillstring. Shaft elements with 12 DOF were used in

their model, capturing torsional-bending inertia coupling and gyroscopic effects, while the contact with the wellbore was not considered. The reduced order model, derived with the modal transformation, was compared with the full order model. Time response analysis of the BHA and transverse natural frequencies were produced. Other numerical techniques, such as differential quadrature method (DQM), finite difference method (FDM), dynamic stiffness method and transfer matrix technique were also used to study the vibration behavior of the drillstring.

Treatment of the contact behavior of the drillstring and wellbore is an ongoing challenge for the drillstring modeling community. If the working conditions stay close to the resonance state, lateral vibrations are amplified and impact with the wellbore results. Catastrophic collisions of the BHA with the wellbore lead to wear of the drillstring, reduction in ROP and reduction of "mean time between failures" (MTBF). MWD tools can also be catastrophically damaged by the successive side contacts. Hsu [28] was the first to model contact behavior using Hertzian contact theory in studying the lateral behavior of the drillstring. Jansen [10] used a lumped representation at the contact point of the drillstring and wellbore, assuming a mud damping force exerted in two orthogonal directions. The effects of fluid damping and stabilizer clearance on the resonance lateral frequencies were studied. Stability at the contact point was also studied using the concept of phase planes. Christoforou *et al.* [17] used the classical Hertzian contact law with the Dirac delta function to model the contact behavior of the drillstring and wellbore with a constant axial force along the drillstring. The assumed mode method with a single mode was used and the contact was modeled at the middle of a single-span BHA. Further

investigation using multi-span multi-mode assumptions was suggested. Yigit *et al.* [16] modeled the contact behavior in coupled torsional-bending motion, using the momentum balance method. Their impulse friction model included a compression phase and restitution phase, with assumed friction and restitution coefficients. The model was capable of analyzing both rolling and slip-rolling behavior. The nonlinear coupling significantly affected response and at some resonance rotary speeds, where there was significant energy transfer between two modes. Mitchell *et al.* [29] presented case studies of BHA vibration failure and suggested a sophisticated 3D model capturing successive contact behavior.

Contact behavior presents challenges specific to finite element modeling. Melakhessou *et al.* [30] modeled only the contact point of the drillstring. Four independent degrees of freedom were assumed in their drillstring model (unbalanced rotor within two bearings). Contact was modeled by the Coulomb friction law and a qualitative sensitivity analysis for the friction coefficient was conducted. Their model was capable of considering both rolling and sliding motions. The location of the contact was also found in their model. The initial position of the string in the well was reported to be an important parameter in its future behavior. Khulief *et al.* [31] implemented the continuous force-displacement law to model impulsive contact force in their FEM model. The material stiffness and damping coefficients were determined at the contact zone according to the energy balance relation. This type of contact modeling was suggested to prevent jump discontinuities in numerical solution of discontinuous models. Impact was provoked by increasing the WOB, and time histories at the contact point were qualitatively studied. The FEM model

derived by Khulief *et al.* was verified and tuned by a laboratory scale test rig [32]. The rig was able to excite the drillstring both for the stick-slip and lateral contact. The WOB was implemented by a shaker and the axial, lateral and torsional natural frequencies for different damping media inside the wellbore were compared. The transient response was not compared between the FEM and the rig data.

Approaches to deal with the impulsive motion of elastodynamic systems with contact, in a finite element environment such as ABAQUS, fall into two categories. The first approach is based on the smooth impulsive force distribution during the impact interval. In this approach the impact force is presented by the force-displacement law, where the material stiffness is estimated or assumed using approximate energy relationships (e.g. [31]). In other words, in this method the contact location could be modeled by an interface spring (the same as the penalty algorithm in ABAQUS). The other approach which is numerically more efficient [33] is based on an impulse-momentum balance equation, since the impulsive forces cause an abrupt change in system velocities or momentum. The kinematic contact algorithm in ABAQUS strictly enforces contact constraints to conserve momentum of all bodies in the system and follows the second algorithm [34,35].

In this study, since the ABAQUS *Explicit* FEM package is used, there are two options for setting up the contact condition between the drillstring and the wellbore, as stated above. The kinematic friction algorithm is preferred to the penalty algorithm, since the residual overclosure in the latter one deteriorates the results as this is a Hertzian type contact

problem with small deformations. The other reason for selecting the kinematic friction algorithm is its lower sensitivity to reduced time steps and mesh size compared to the penalty algorithm. The reader is referred to section 4 for a complete discussion and comparison of these two algorithms.

To summarize, this paper addresses the need for a numerical model to investigate the effect of the imposed vibration of a VARD force generator on the nonlinear coupled axial-transverse dynamics of a vertical drillstring, in the frequency or the time domains. The model includes nonlinear coupling terms due to strain energy, driving torque, multi span contact, and two orthogonal planes in which lateral motion occurs. A finite element model is developed and compared to a symbolical mathematical model [5] capturing the first four modes (the sufficiency of retaining the first four modes is verified by the FEM model). Multiple BHA spans provide more realistic results for the natural frequencies. Gyroscopic effect due to the rotation is not assumed in this study, since the rotary speed of drillstring is not very high (50-150 rpm). While the analytical model offers fast convergence rate for sensitivity analysis, the finite element model is easier to reconfigure for new boundary conditions, force or displacement excitations and BHA geometry, and allows extraction of nodal force, displacement, stress and reactions at any desired points as outputs without extra computations. Having two distinct verified models enables implementation for any set of drillstring parameters, along with sensitivity and design studies once a configuration has been selected.

6.4 Review of the Analytical Drillstring Model- Deriving the Governing Equations

This section provides a summary of analytical model results; however, more details can be found in Appendix 6.1-6.4 and also in [5]. The Euler-Bernoulli beam theory is used to analytically model coupled lateral-axial vibration of the drillstring, which is considered as a beam with a high aspect ratio [36]. A schematic diagram of the drillstring is shown in Figure 6.1. The developed analytical model includes a three span BHA (with a different length for each span) (Figure 6.2) with a long pipe section. The driving torque is applied on the rotary table and the VARD force generator is applied on the BHA. The drillstring is inside a wellbore filled with mud. Two orthogonal lateral directions, u and v with the axial motion w are assumed.

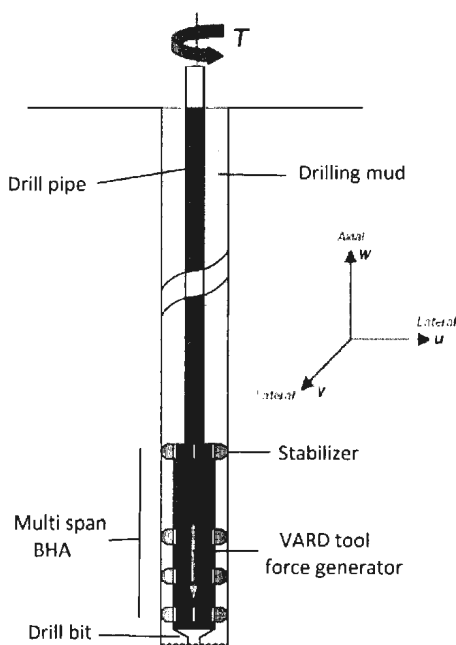


Figure 6.1: Schematic of the multi span drillstring under the effect of the VARD tool

The effects of the hook load (a resultant axial force under static equilibrium), WOB, mud hydrostatic force and self weight are presented as spatially varying axial forces along the drillstring. The buoyant force in the drillstring should not be treated with Archimedes's rule and the effective tension point of view should be implemented for more precise results [37]. Therefore, at the last point of the collar, there are WOB and the hydrostatic force. The varying axial force in the collar and pipe sections are (l is the total length of the drillstring):

$$\begin{aligned}
 F_{collar} &= \rho_{collar} \cdot A_{collar} \cdot g \cdot z - WOB - \rho_{mud} \cdot g \cdot l \cdot A_{collar} \\
 F_{pipe} &= -WOB - \rho_{mud} \cdot g \cdot l \cdot A_{collar} + \rho_{mud} \cdot g \cdot l_p (A_{collar} - A_{pipe}) + \\
 &+ \rho_{collar} \cdot A_{collar} \cdot g \cdot l_c + \rho_{pipe} \cdot A_{pipe} \cdot g \cdot (z - l_c)
 \end{aligned} \tag{6.1}$$

It should be noted that the effect of mud hydrostatic pressure acting over the projected area of the pipe-collar junction has been assumed in the second equation, since the static equilibrium has been assumed for the entire drillstring. Figure 6.3 shows the spatially varying axial force along the drillstring. The change in the axial force at the pipe-collar junction is due to the hydrostatic pressure acting at that location.

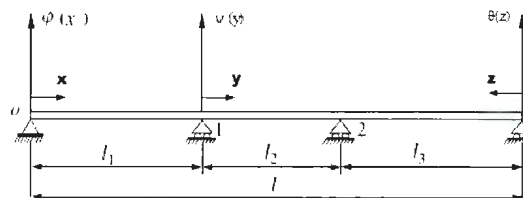


Figure 6.2: schematic of a 3 span BHA

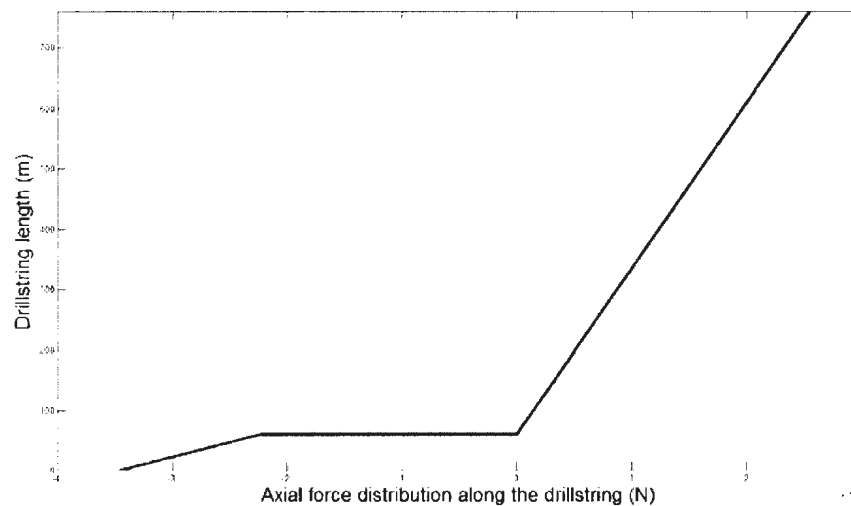


Figure 6.3: Spatially varying axial force along the drillstring

The “Bypassing PDEs” method was implemented to derive elastodynamic equations. This method is based on Lagrange's equation with the expanded Galerkin's method, instead of the conventional Hamilton's approach for continuous systems. The expanded Galerkin's method was applied in the first step of the energy equations. Since the method of Bypassing PDEs was implemented, the conventional energy terms were derived instead of the variational form. The reader is referred to [38] for more details on the Bypassing PDEs method. Although the pipe lateral vibration modes are excited, the lateral response is not significant, since it will not contact the wellbore [16]. Therefore, the pipe is assumed to undergo axial vibrations only. The assumed energy terms for the collar section are due to the beam kinetic (Equation 6.7) and strain energy for axial and two orthogonal lateral directions (Equation 6.8) (nonlinear elastic stiffening and axial stiffening are both assumed to capture axial-lateral coupling), the work done by the driving torque (Equation 6.9) which causes lateral coupling in two orthogonal directions,

the implemented VARD force (Equation 6.10), and spatially varying compressive force (Equation 6.11). Dissipation energy of the mud damping in both orthogonal lateral directions (Equation 6.12) and the contact energy terms at multiple contact points (Equation 6.13) in each span of the BHA are also assumed. The energy terms of the pipe section are: kinetic and potential energy of the pipe (Equation 6.14), the energy of the imposed VARD force and the work done by the spatially varying tensile force on the pipe section (Equation 6.15). The energy terms will be added together to generate the Lagrangian of the system. The Lagrangian is an integral equation with different limits for each span and the pipe section (Equations 6.16-6.19).

At the next step of the Bypassing PDEs method, the expanded Galerkin's method is applied to the equations (Equation 6.20). The responses u , v and w are assumed as comparison functions multiplied by mode participation factors. The first four modes were retained to conduct the multi-mode analysis. A modal sensitivity analysis will be conducted by the FEM model to verify this assumption, as described in sections 4-1 and 5-1 of this paper. The boundary condition for the axial motion of the drillstring was assumed as fixed at the top and free at the bottom, and the spans were assumed as pinned-pinned boundary conditions (location of the stabilizers) in the lateral direction. The comparison function in the axial direction was assumed as a sine function, which depends on the length of the drillstring (Equation 6.21).

Since the BHA was assumed as a three span beam, the comparison function of each span was required to apply the expanded Galerkin method of the BHA. The exact mode shapes

of a three span beam were derived symbolically, are plotted in Appendix 6.4 (Figure 6.19) and were implemented in the Lagrangian equation as the corresponding comparison functions.

Substituting the comparison functions and integrating the resulting equations over the drillstring length domain, and considering the mode orthogonality relations, the total Lagrangian of the system in terms of mode participation factors was derived. Then, Lagrange's equation was implemented for each mode participation factor. The result is a set of twelve second-order coupled nonlinear time differential equations in terms of second-order derivatives of mode participation factors. The mathematical model and the above procedure were coded and solved in Maple[®]. This system was numerically solved using a Fehlberg fourth-fifth order Runge-Kutta method with degree four interpolant. The numerical results for each generalized coordinate were stored and substituted back in the assumed expanded Galerkin function for each direction to generate deflection and velocity time history of any desired point, including the contact locations. The FFT of each specific generalized coordinate system was also derived, which revealed the first four natural frequencies for the two orthogonal lateral planes and the axial direction.

6.5 Dynamic Finite Element Model of the Drillstring

The ABAQUS FEM *Explicit* solver package was used to develop the dynamic FEM model. The FEM model is capable of modal characteristic extraction as well as dynamic analysis. The modal characteristics are derived using eigenvalue extraction with the linear

perturbation procedure. The dynamic analysis module is capable of extracting the transient response of the drillstring for any set of initial conditions or forcing functions.

The drillstring is assumed as a beam with two cross sections (collars and pipes). A planar wire shape sketch with hollow pipe profiles is used to model the entire drillstring. The "Hermite cubic" beam element is used, which does not account for the shear flexibility, although axial strain is considered. This is the proper element for modeling slender Euler-Bernoulli beams, in order to be consistent with the derived analytical model. The beam assumption of the drillstring is valid, since the cross section dimensions are less than $1/5$ of the drillstring length [35]. In the beam element equations, it is considered that plane sections perpendicular to the axis of the beam remain planar during the deformations. Therefore, the orientation of the beam cross section must be determined in the global Cartesian system prior to the analysis. A three dimensional extruded shell is assumed for the wellbore. The drillstring and the wellbore are modeled as a single assembly in the global coordinate system.

There are two possible contact algorithms in the *Explicit* solver package: the kinematic friction and the penalty contact algorithms. The kinematic algorithm uses a predictor-corrector algorithm in each time increment. The contact condition in the kinematic state of the model is ignored in the predictor phase of the algorithm, which results in an overclosure. In the corrector phase, a corrective acceleration is applied to both slave and master nodes to resolve this overclosure, while the momentum conservation is satisfied. Therefore, the contact overclosure is eliminated at the end of each increment. In the

penalty algorithm, the corrective phase is not carried out and an interface spring is assumed between slave and master nodes to account for overclosure. Thus, a small penetration always exists, since the spring force is valid for a residual penetration and the contact constraints are not fulfilled exactly at the end of each step.

One of the advantages of the kinematic algorithm is that a constant time increment has no effect on the ongoing solution, while the penalty algorithm requires reducing time steps during contact. In the penalty method, the default penalty stiffness is calculated to minimize the residual penetration and this fact reduces the stable time increment by 4% [35]. The penalty method depends significantly on the mesh size as well, and reducing the mesh size results in deteriorating quality of results. Slow convergence is another drawback of the penalty method.

In large deformation problems, the penalty contact algorithm provides the same results as the other method, while in small deformation-displacement problems driven by Hertzian contact theory, this residual overclosure has a significant effect on the results. In such cases the kinematic algorithm is preferred. Therefore, the kinematic contact algorithm is implemented in this study, since Hertzian contact theory was used in the analytical model. Sliding friction is not included, as it has not significantly impacted the results in other studies [14,31,32] and if included will seriously degrade computation time.

The contact surfaces in the *Explicit* solver package can be defined with two methods: the general kinematic contact and the contact pair algorithms. In the general contact algorithm, the contact is defined between all regions of the model. Therefore, the overall

drillstring and the inner surface of the wellbore are capable of having contact and the contact location can be anywhere on the BHA. This capability of the FEM model will be used to verify the assumption of the contact point locations assumed in the analytical model. The surfaces in the kinematic contact comprise the contact domain that can span any disconnected region in the model. In the contact pair algorithm, the contact surfaces are required to be defined prior to the analysis, which does not account for contact between all surfaces of the model. The general kinematic contact algorithm is used in this study to model the contact between the drillstring and wellbore to account for all possible contact points.

The drillstring-mud interaction effects on the drillstring dynamic analysis are important. The effect of inside-outside drillstring mud flow was investigated by Paidoussis *et al.* [39]. They found that the effect of internal and external mud flow is sensitive to the annular space between the drillstring and wellbore. Zhang *et al.*, [40] studied the effects of mud flow on the load carrying capacity of the drillstring. A two dimensional model for a pinned-pinned vertical pipe without wellbore contact was developed. They found the critical flow rate for pipe buckling and investigated a relationship for the length of the pipe section and flow rate in the drillpipe buckling analysis. Effect of fluid density on the pipe buckling was also studied. However, the role of damping on the stability analysis and multiple lateral contacts was not investigated in their study. Ritto *et al.*, [41] analyzed the influence of mud flow on the natural frequencies and dynamic behavior of the drillstring. They investigated that the axial and torsional behaviors are not sensitive to the mud flow. They found lateral natural frequencies changed by a maximum of 0.53 rpm

when the fluid flow is considered. When the fluid flow was considered in the dynamic equations, the lateral dynamic response was a bit larger initially. However, steady-state response was unchanged. The effect of fluid flow has not been considered in this study; however, the damping effect of mud in the lateral direction was included.

The viscous damping behavior is considered as Rayleigh damping (a quadratic expression for the energy dissipation rate), which is proportional to the mass and stiffness of each mode. In the absence of a major source of dissipation, such as inelastic material or dashpots, Rayleigh damping is appropriate with the *Explicit* dynamic package (e.g., pipes with contact) [15]. It provides a convenient abstraction for damping low-frequency range behavior (mass dependent) and higher-frequency range behavior (stiffness dependent).

The Rayleigh damping depends on two damping factors, namely α_r as the mass proportional damping and β_r as the stiffness proportional damping [35]:

$$C_i = \alpha_i m_i + \beta_i k_i \quad (6.2)$$

During the analysis this value is averaged over the substructure to determine specific values of α_r and β_r . The average is normalized with mass and volume for the first and second factor, respectively. This assumption has been shown to deliver accurate results, especially near natural frequencies [22]. For mode i , the critical damping ratio is defined in terms of the Rayleigh damping factors as [22]:

$$\xi_i = \frac{\alpha_r}{2\omega_i} + \frac{\beta_r \omega_i}{2} \quad (6.3)$$

where ω_i is the natural frequency of mode i . The mass proportional damping factor introduces damping forces that are caused by absolute velocities at each node. This

phenomenon could model a structure moving through a viscous fluid (such as drillstring inside mud), in a way such that any point in the model triggers damping forces [15].

Appropriate mass-proportional damping does not have a great effect on the stability limit, while the other factor significantly reduces the stability limit. The Rayleigh damping factors are determined and tuned in the developed FEM model.

Two solver packages are available in ABAQUS: the *Implicit* and *Explicit* solver packages. For both solvers, equilibrium is based on external load, internal element forces and the nodal accelerations. In the *Implicit* procedure, a set of linear equations is solved by the direct integration method. The *Explicit* solver package implements the central difference operator for integration of the set of nonlinear equations through small time increments. The time increments must be capable of resolving the highest frequency of interest. The computation cost is proportional to the number of elements and roughly inversely proportional to the smallest element dimension. The computational cost for the *Implicit* package, in the case of large structures with nonlinearities, rises rapidly. The *Explicit* method is especially efficient in high-speed dynamic events that require many small increments to obtain a high-resolution solution. In the case of contact, the *Explicit* solver package has shown a more efficient integration time compared to the *Implicit* package, even though stress wave propagation is considered in the *Explicit* package. Therefore, the *Explicit* solver package was implemented in this study to achieve more efficient computation.

Time increments should be defined properly to achieve efficient computation and capture dynamics in the highest frequency range of interest. The stability limit dictates the maximum time increment used by ABAQUS *Explicit*. The stability limit is defined in terms of the highest frequency of the system. The stable time increment in the model is twice the inverse of the highest frequency of the system. It is not feasible to calculate this exact value. Therefore, the estimate is carried out based on the highest frequency of each individual element in the model, which is always associated with the dilatational mode. The highest frequency determined on an element-by-element basis is always higher than the highest frequency in the assembled finite element model. In terms of the element-by-element estimate, the stability limit will be defined based on the element length and the wave speed inside the material ($\Delta t_{stable} = \frac{L^e}{c_d}$). The numerator is the element length and the denominator is the current effective, dilatational wave speed of the material, which is related to the effective hypo-elastic material modulus from the material's constitutive response [33]. The drawback of this calculation is that the effect of contacts and constraints on computing the eigenvalue spectrum is not considered in the element-by-element estimation. To resolve this problem, the *Explicit* package implements an adaptive algorithm to determine conservative bounds for the highest frequency component, using the maximum element dilatational mode of the mesh. This stability limit is conservative compared to the stability limit extracted based on the maximum frequency of the entire model. The advantage of this algorithm is the continuous update for estimation of the highest natural frequency. At the start of each step, the element by element algorithm is used. As the step proceeds, the stability limit will be determined from the global

estimator, once the algorithm determines that the accuracy of the global estimation is acceptable.

The natural frequencies are extracted through the linear perturbation step. "Lanczos" and "subspace iteration" have been widely used for obtaining a certain number of eigen-pair solutions for practical engineering problems. The Lanczos algorithm falls into the class of transformation methods (transformation of the normalized eigenvectors through the displacement). This method is faster than the subspace algorithm for structures with many degrees of freedom [42]. Both methods have been compared in this study and the results were in agreement. The solution follows with the dynamic *Explicit* step. Nodal dynamic time responses are derived in this step and the results are compared with the analytical model in the next section. Geometric nonlinearity effects were assumed in the *Explicit* step to account for the same nonlinear terms as are in the analytical model.

6.5.1 Appropriate Model Order and Mesh Sensitivity Analysis (h-method)

The size of elements influences the convergence of the solution and accuracy of the results. A smaller-sized element means more computational time. A mesh sensitivity analysis verifies that having 150 elements over the BHA and 350 elements on the pipe section ensures convergence of the analysis. The distribution of the elements on the collar section is denser compared to the pipe section, where the contact analysis requires smaller elements.

In order to ensure that enough modes have been used in the analysis, the participation factor, the effective mass and the total modal effective mass are extracted for the

drillstring. The participation factor ($\Gamma_{\alpha i}$) indicates the predominant degree of freedom in which each mode acts in the model. In other words, this parameter indicates the strength of the motion (global translations in this model) in the three assumed directions (two lateral and one axial) in the eigenvector of that mode:

$$\Gamma_{\alpha i} = \frac{1}{m_{\alpha}} \chi_{\alpha}^N M^{NM} Y_i^M \quad (6.4)$$

where M^{NM} is the structural matrix and χ_{α}^N is the eigenvector for mode α . “ M ” and “ N ” are degrees of freedom of the FEM model and Y_i^M defines the magnitude of the rigid body response of the degree of freedom M in the model. m_{α} is the generalized mass, associated with the mode α and is defined as:

$$m_{\alpha} = \chi_{\alpha}^N M^{NM} \chi_{\alpha}^M \quad (6.5)$$

In the case of eigenvector normalization, m_{α} is defined as unity. The effective mass indicates the value of active mass in each degree of freedom at a specific mode [4]:

$$m_{\alpha i}^{eff} = \Gamma_{\alpha i}^2 \cdot m_{\alpha} \quad (6.6)$$

The total modal mass of the model is the sum of effective masses of all modes in any particular direction. The masses that are constrained by some nodes due to model constraints are approximately a quarter of the total mass of the element attached to the constrained node. The modes that are contributing a high mass compared to the mass of the model are kept in the analysis [4]. The results for mesh sensitivity analysis and total effective modal mass will be discussed in the last section of the paper.

6.6 Numerical Results and Discussion

The analytical and FEM models are solved to derive the natural frequencies and response of the drillstring at certain points of interest. The characteristics and numerical values used in this study are shown in Table 6.1.

Table 6.1: Parameters used in the simulations

$T = 4000$	Driving torque (N.m)	$l_4=700$	Length of the pipe section (m)
$\rho_{mud} = 1500$	Mud density (Kg/m ³)	$l=760$	Length of the drillstring (m)
$C_D = 1$	Hydrodynamic drag coefficient	$F_{VARD}=20000$	VARD force amplitude (N)
$K_h = 6.78 * 10^{11}$	stiffness (N.m ^{-1.5})	$\omega_{VARD}=600$	VARD tool frequency (rad/s)
$WOB = 50000$	Weight on bit (N)	$A_{pipe} = 0.02639$	Collar cross sectional area (m ²)
$A_{pipe} = 0.00471$	Pipe cross sectional area (m ²)	$E = 210 * 10^9$	Young's modulus (Pa)
$l_1=15$	Length of the BHA first span (m)	$b_{cl} = 0.1$	Borehole clearance (m)
$l_2=15$	Length of the BHA second span (m)	$F_H = 2.545 * 10^5$	Hook load (N)
$l_3=30$	Length of the BHA last span (m)	$\rho_{st} = 7860$	Pipe and collar density (kg/ m ³)

Predicting the resonance frequencies at the early stage of designing a drillstring and before each run is a crucial task to avoid the unwanted resonance states. If the working conditions stay close to the resonance state, the BHA absorbs energy, which amplifies lateral motions. These amplified motions, as a result of the transferred resonance energy, result in potentially catastrophic collisions of the BHA with the wellbore. Therefore, the very first step to reduce lateral motions and avoid successive contacts is to find resonance

natural frequencies of the drillstring. In order to extract natural frequencies by the FEM model and compare the results with the ones extracted from the analytical model, the linear perturbation step in the FEM model is set to find natural frequencies of the system with a Lanczos eigensolver. The natural frequencies extracted from both methods are compared in Table 6.2.

The natural frequencies derived in this study are slightly higher than the ones extracted by other studies assuming the BHA as a single-span beam. These higher frequencies are due to assuming a multi-span BHA that has several constraints (stabilizers) on the BHA. Although this assumption adds complexity to the model, it allows for more realistic results. There is a small variation between resonance frequencies in the u and v directions as a result of the numerical solution. The maximum difference is 0.05 Hz, which is a negligible difference in rotary drilling operations (around 3 rpm). The resonance frequency values are in agreement between both implemented methods.

As mentioned in the literature review, the axial and lateral deflections are important indicators of drillstring behavior in the presence of a VARD force generator. Axial deflection at a point very close to the hook (where the draw-works cable is attached to the pipe) is compared in Figure 6.4 for both FEM and analytical methods. The overall deflection is below zero as a result of all applied axial forces and it converges to a region between 1-2 *cm* of compression. The FEM and analytical steady-state results are in agreement with a difference of 0.03 *cm*, which is an acceptable difference in terms of

practical drilling. The small discrepancies could be due to the assumed axial comparison function in the analytical model and numerical computational scheme.

Table 6.2: Extracted resonance rotary speeds

Direction	First mode (Hz)		Second mode (Hz)		Third mode (Hz)		Fourth mode (Hz)	
	FEM	Analytical	FEM	Analytical	FEM	Analytical	FEM	Analytical
Lateral "u"	1.34	1.30	1.95	1.93	2.35	2.30	3.15	3.13
Lateral "v"	1.37	1.32	1.92	1.89	2.30	2.27	3.12	3.10
Axial "w"	7.65	7.60	22.25	22.17	38.59	38.54	60.3	60.28

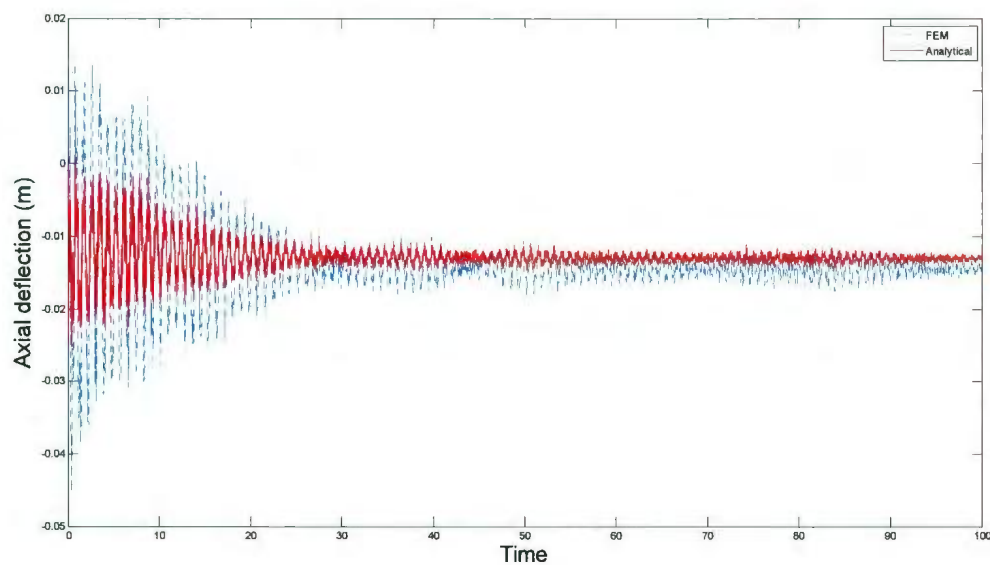


Figure 6.4: Axial deflection near the hook point

The axial deflections of the top, middle and last span of the BHA are shown in Figures 6.5, 6.6 and 6.7, respectively. The corresponding axial velocity of the point on the last span is depicted in Figure 6.8 for both the FEM and the analytical model which are in agreement. The analytical code is also capable of deriving the velocity of any desired

point, since the first derivative of the mode participation factors are computed after the numerical solution. The FEM and analytical results are in good agreement for all three spans and the axial deflection shows stable behavior. This fact is verified using a phase portrait as shown in Figure 6.9.

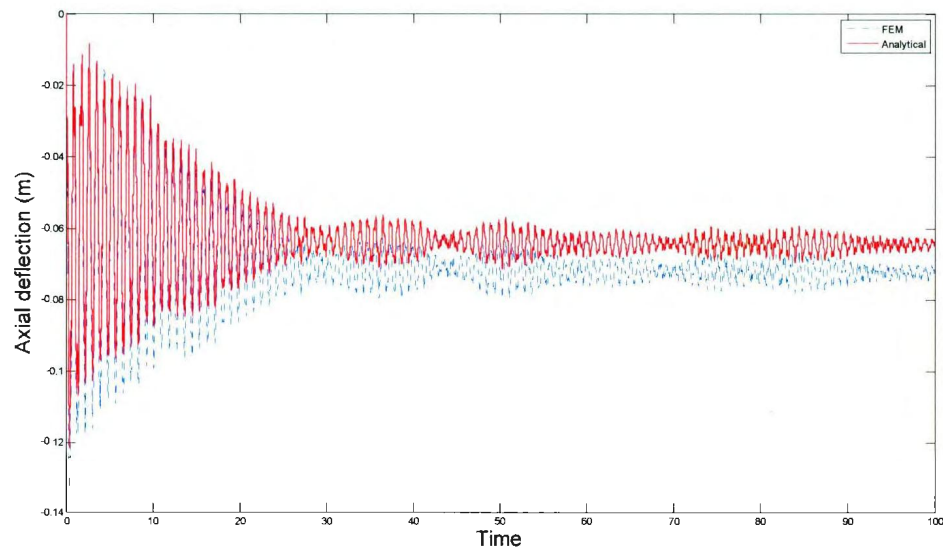


Figure 6.5: Axial deflection of a point on the top span

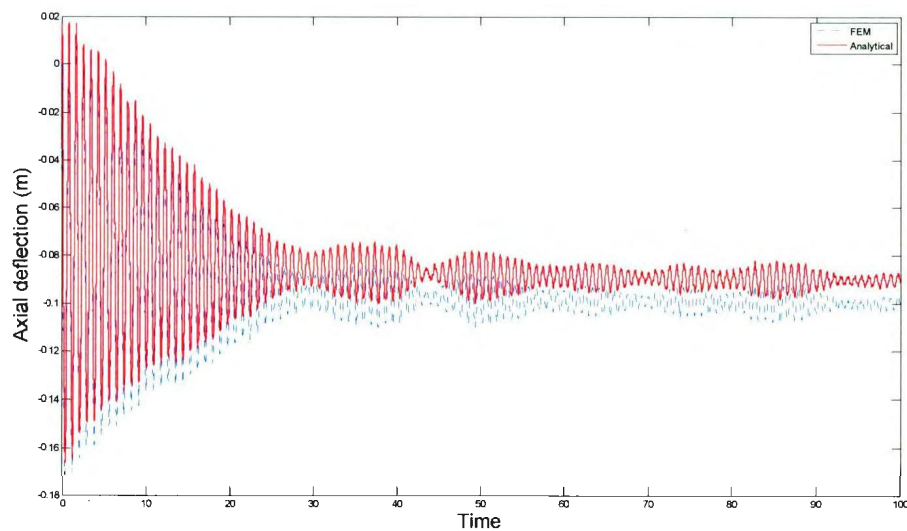


Figure 6.6: Axial deflection of a point on the middle span

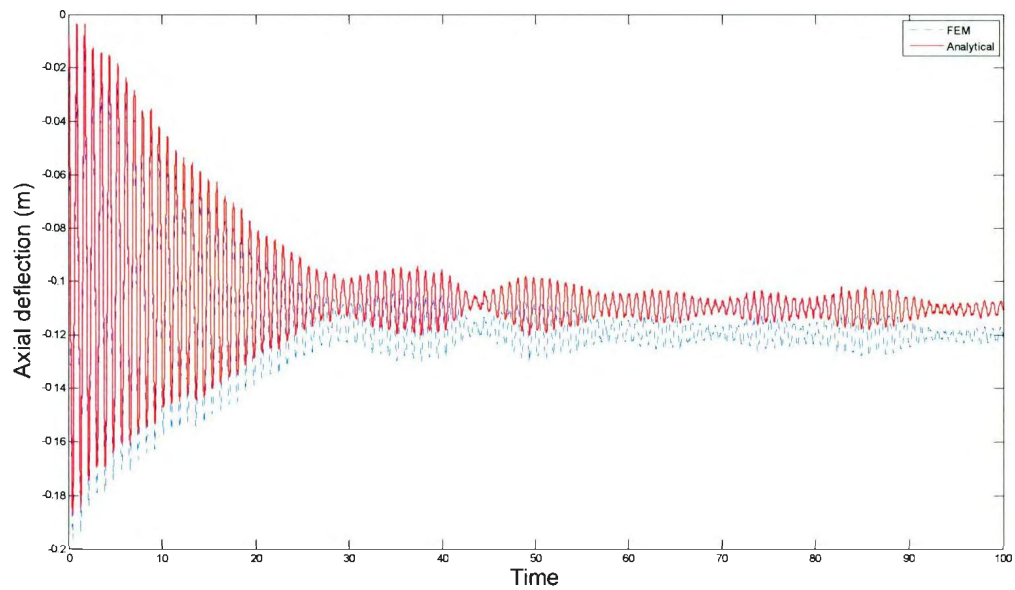


Figure 6.7: Axial deflection of a point on the last span, close to the bit

The axial deflection in the last span close to the bit is an important parameter for studying the rock failure mechanism. It is clear from these figures that the axial deflection has its maximum value on the last span.

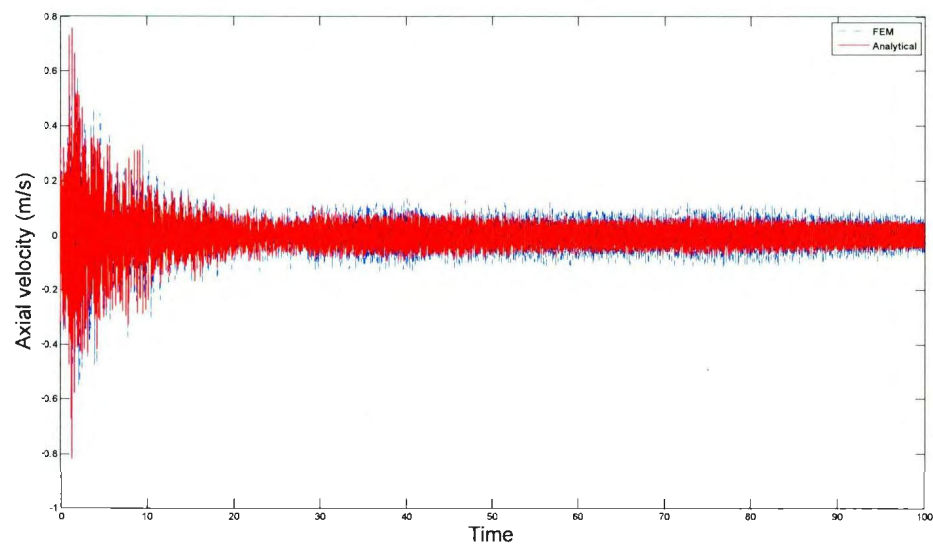


Figure 6.8: Axial velocity of a point on the last span, close to the bit

The phase portrait of the last span, shown in Figure 6.9, verifies stable axial behavior, which ends in circular trajectories [10]. Since the FEM and analytical results are in agreement, the FEM values are used to draw the phase plane.

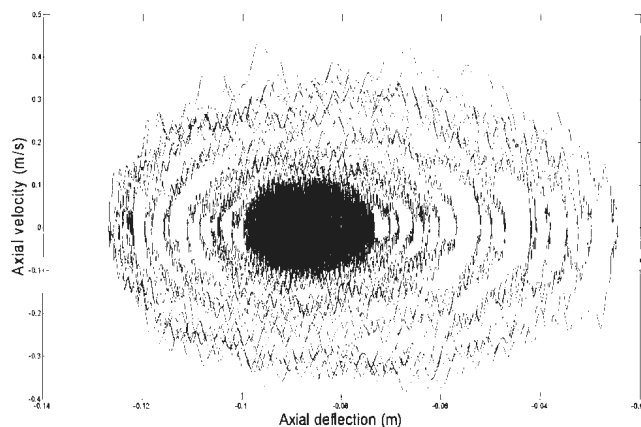


Figure 6.9: Phase plane, a point on the last span, close to the bit

The lateral behavior of any point on the drillstring can be studied using the concept of radial deflection. The borehole-drillstring clearance is considered in the analytical equations for the Hertzian contact force. If the lateral deflection of the drillstring exceeds this clearance, the drillstring hits the borehole and the result is the Hertzian contact force at the contact point. The pipes are assumed to laterally deflect less than the BHA and since the borehole diameter is the same, the pipes are assumed not to hit the wellbore. Since general contact is defined in the FEM model, the entire model is capable of being in contact, if the drillstring radial deflection exceeds the clearance. A point on the middle of the pipe section is considered and the lateral deflection for both u and v directions are derived and plotted. The analytical and FEM results are in agreement and the FEM results verify the contact point location assumption made in the analytical equations. All

elements on the drillstring were checked for contact and the no-contact assumption of the pipe section in the analytical model is verified. Figures 6.10a and 6.10b show the lateral deflection of this point in the u and v orthogonal directions. Figures 6.10c and 6.10d show the corresponding lateral velocities. The velocities and deflections are in agreement in both methods.

Figures 6.11a and 6.11b depict the phase planes of the corresponding point in both lateral directions, which verifies the stable behavior of the point on the pipe section. Figure 6.11c shows the phase trajectory of the same point, which shows that this point remains nearly close to the borehole center and far away from the wellbore. Figure 6.11d shows the radial deflection of this point. The maximum radial deflection is 6 cm for both the FEM and the analytical model, which verifies that this point never hits the wellbore wall.

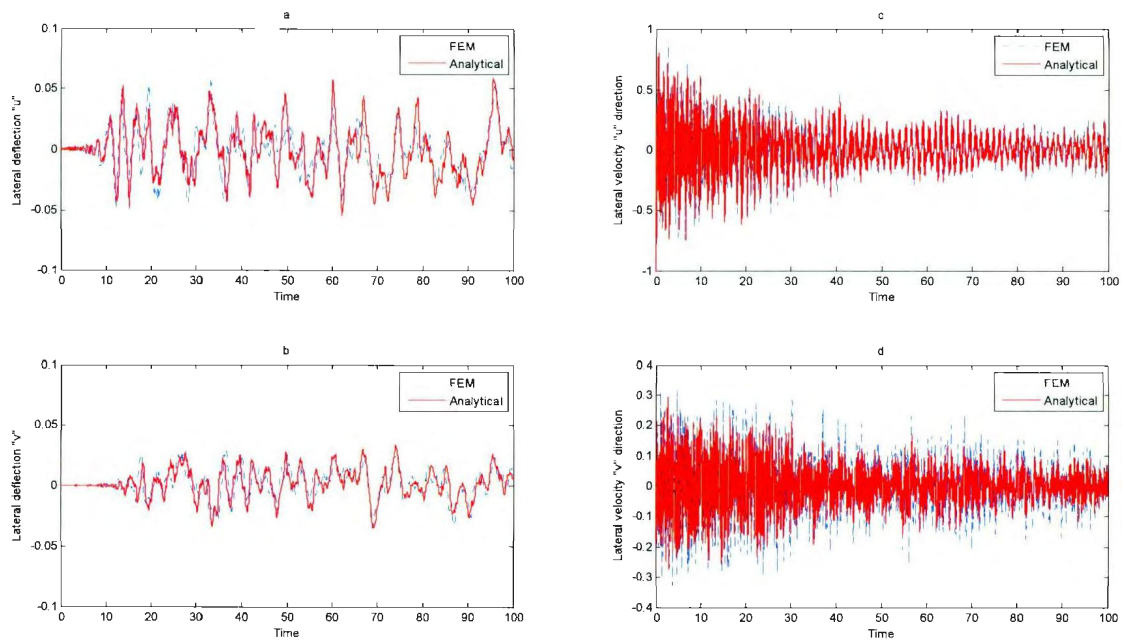


Figure 6.10: Lateral deflection and velocities for a point on the pipe section

Figure 6.12 shows the radial deflection of the contact point on the top span. This figure depicts a highly irregular behavior at this point with bouncing contact. It is clear in this figure that in most cases both FEM and analytical models hit the wellbore at the same time and remain close to the midpoint of the clearance.

The radial deflection at the contact point of the second span is shown in Figure 6.13. The contact behavior is not as severe as in the top span, as the effect of initial conditions dies out. The second BHA span does not hit the wellbore successively as in the top span. This result shows the importance of using multiple spans in a BHA model.

The contact behavior at the span close to the bit is shown in Figure 6.14. There is less contact between the drillstring and wellbore at this location and a bouncing back behavior is seen at this point. The mud damping seems to have an effect at this point. The FEM and analytical models verify each other, except for a few mismatches. The length of this span is half of the top span. A less irregular behavior is also obvious at this span.

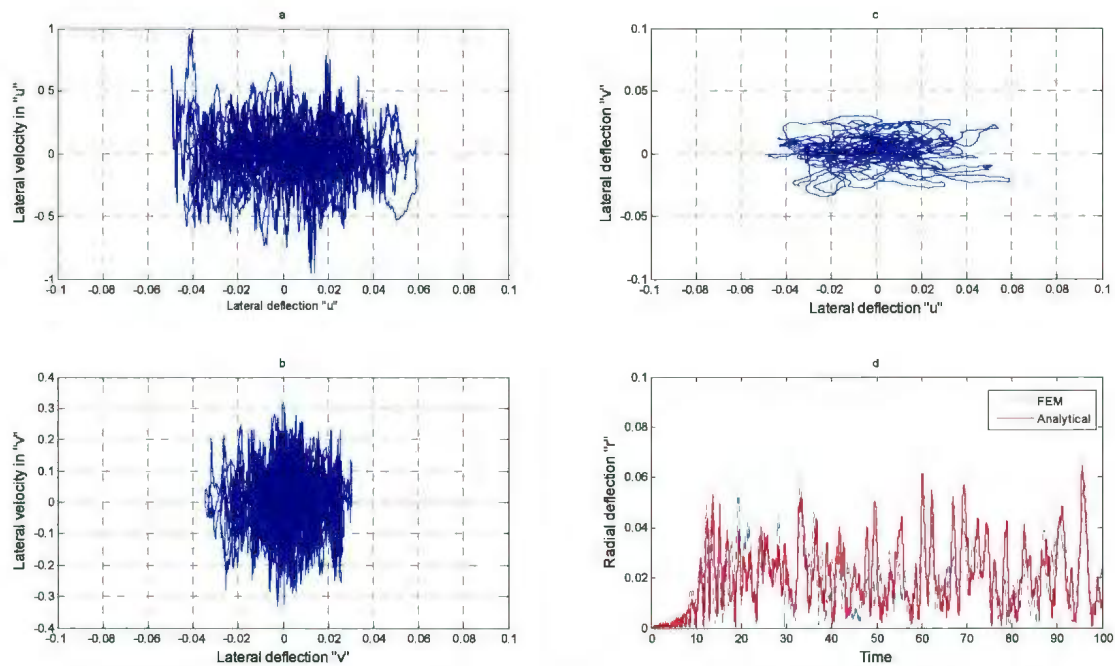


Figure 6.11: Phase plane, phase trajectory and radial deflection for a point on the pipe

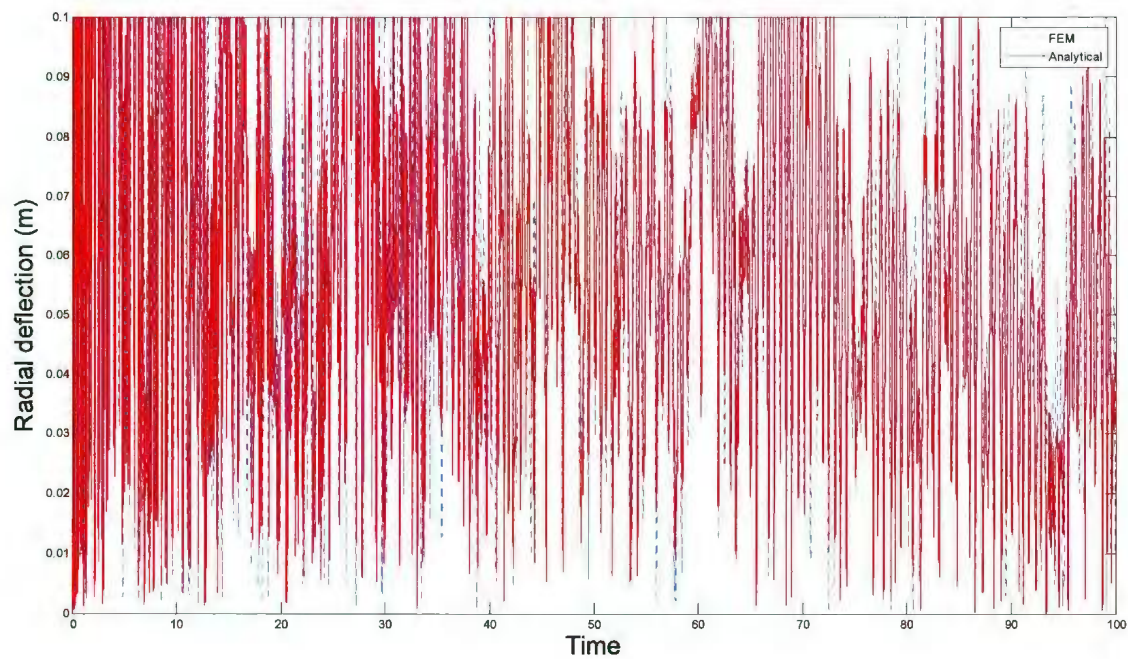


Figure 6.12: Radial deflection of the contact point, first span

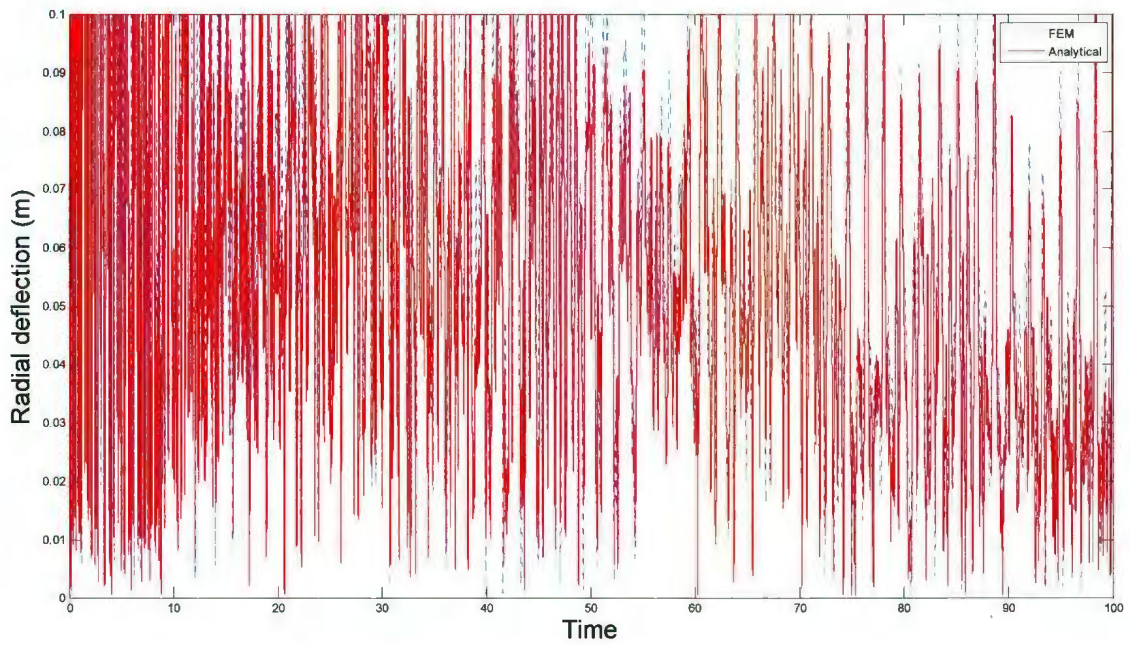


Figure 6.13: Radial deflection of the contact point, second span

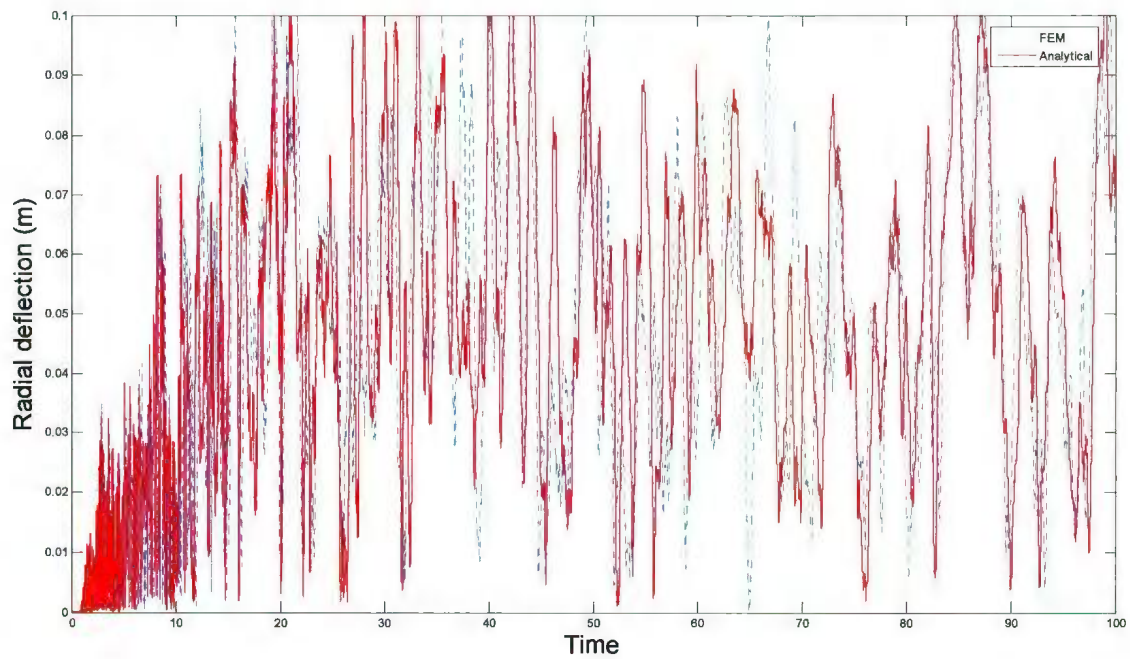


Figure 6.14: Radial deflection of the contact point, third span

The lateral velocities at the top span are shown in Figure 6.15 in both u and v directions. There is a good agreement between both models. The results of lateral velocities of other spans show similar agreement but are omitted for brevity.

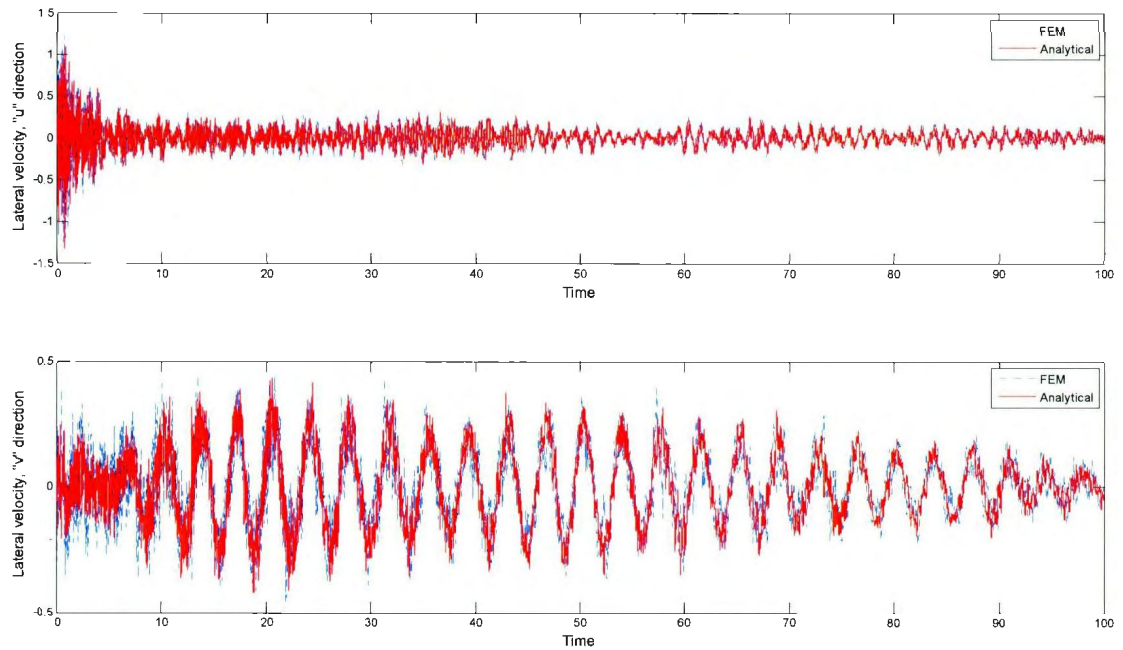


Figure 6.15: Lateral velocities of a point on the top span

6.6.1 Modal Order Detection and Mesh Sensitivity Analysis Results

In an analytical model, determining the significant modes that account for the majority of the system's kinetic energy is important to ensure that model complexity, and thus computation time, is not needlessly high. The FEM model is a valuable tool for computing the required analytical model complexity. In order to verify that the retained number of modes is enough in the analytical model, the total effective mass in each direction was computed using the FEM model. The required number of modes was assumed to be that for which 90% of the total modal mass was captured. The mass of the

constrained elements by boundary conditions is assumed as one quarter of the mass of the corresponding element. The total effective mass quantities (normalized) in the axial and two lateral directions are shown in Figure 6.16. It is clear that retaining up to the fourth mode captures dynamics of interest. The total effective mass in the u direction is 82% for the first mode, which verifies that in this direction the first mode contributes a high value compared to the rest of the modes, while in the v direction the third mode is the predominant mode. The predominance of the modes in each direction also can be verified by the mass participation factor.

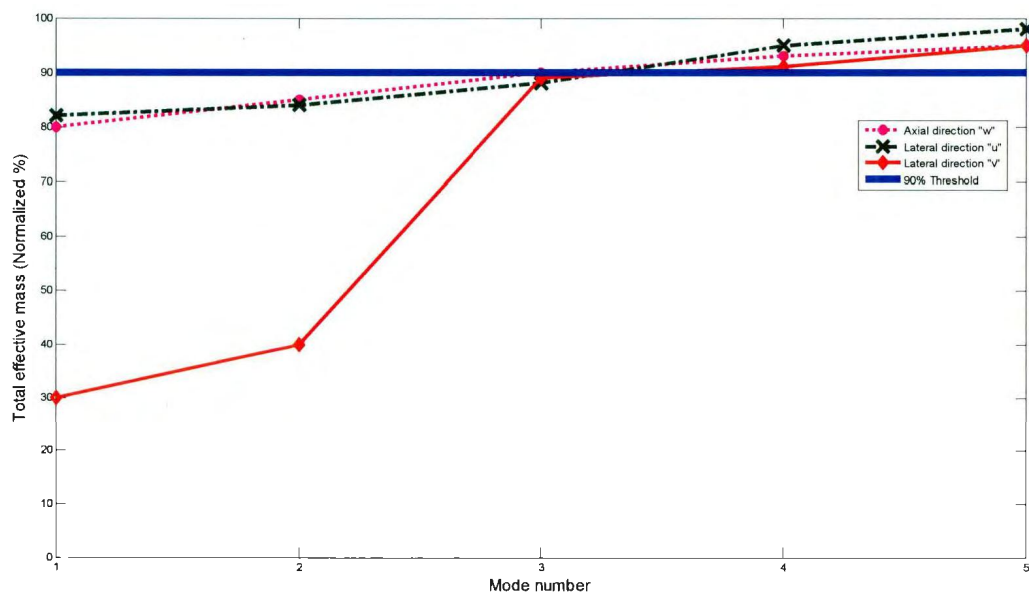


Figure 6.16: Normalized total effective mass in each direction

A mesh sensitivity analysis was carried out for both the collar and pipe sections using the h -method. Since the contact location will be compared with the analytical model, the elements on the collar section are finer compared to the ones on the pipe section. The

mesh sensitivity analysis was based on the h-method and conducted for axial motion of a point on the pipe section to find the appropriate number of meshes on the pipe (Figure 6.17). There is insignificant change between 350 and 400 elements on the pipe section. Therefore, the 800m pipe is divided into 350 elements. To find out the appropriate number of elements on the collar section, the h-method analysis was carried out in the lateral direction for a point on the collar section (Figure 6.18). Convergence is achieved while meshing the collar section with 150 elements. The density of the elements per unit length is higher on the collar section, compared to the pipe section. The computational cost of the *Explicit* package in contact analysis highly depends on the number of elements and this analysis results in less computational cost.

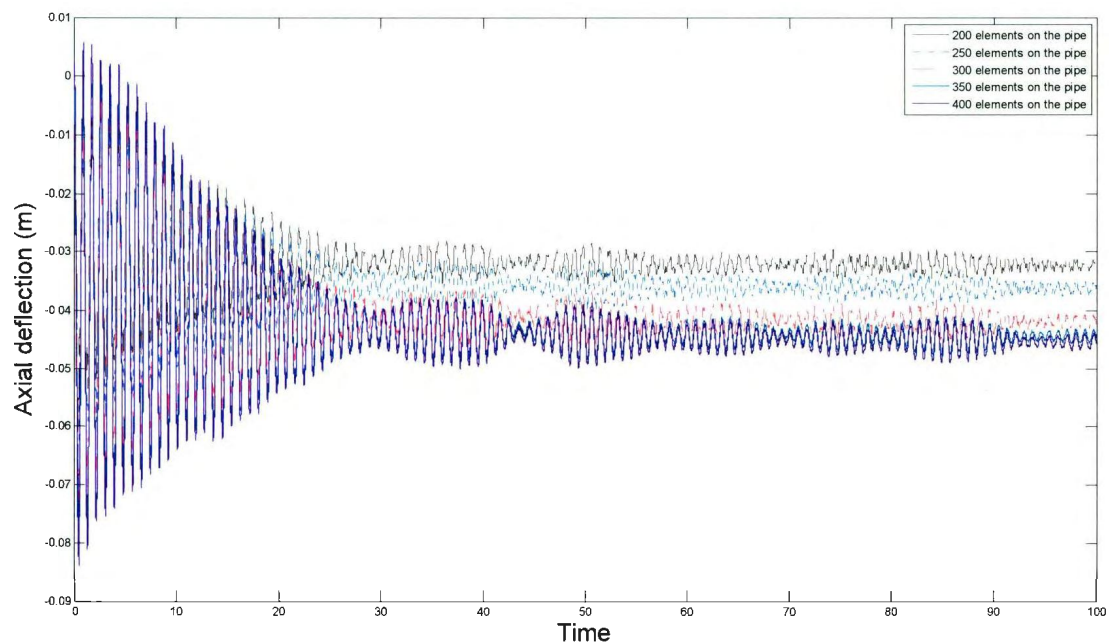


Figure 6.17: Mesh sensitivity analysis, pipe section

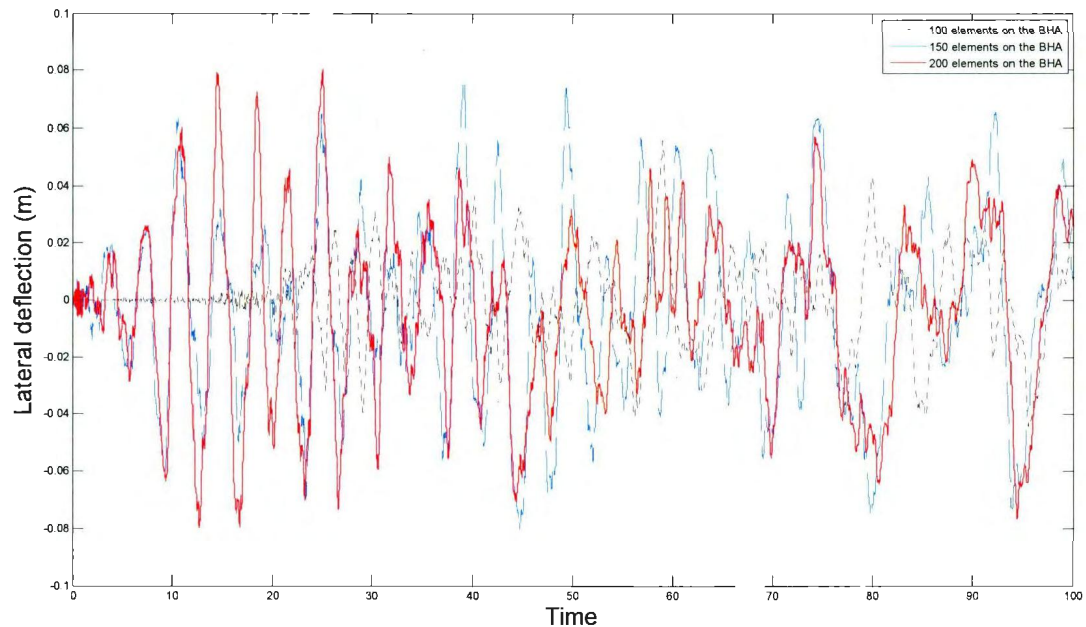


Figure 6.18: Mesh sensitivity analysis, collar section

6.7 Conclusions

The vibration behavior of a drillstring under the effect of an axial force generator in vibration assisted rotary drilling was studied with a dynamic finite element model and validated with a developed analytical model. The mud damping, driving torque, vibration generator force, hydrostatic effects, self weight, WOB and hook load were included. Additional nonlinear phenomena in the model were Hertzian contact forces at multiple locations, axial stiffening and geometric nonlinearity. A bottom-hole assembly with multiple spans due to multiple stabilizers was modeled. The model was used to extract natural frequencies. The rotary speed of the drillstring should be kept far enough from the natural frequencies to avoid excessive deflections and contact with the wellbore, both of which can cause premature failure of bottom-hole assembly components. Time histories

and phase plane plots of the axial and two orthogonal lateral displacements and velocities were generated for several points. The time response allows the modeller to assess severity and stability of wellbore contact. The most severe lateral vibration occurred in the uppermost of the three bottom-hole assembly spans, with axial motion being most severe near the bit. Total effective mass was used to determine a sufficient number of modes to be retained in the analytical model, and mesh analysis was conducted to improve computational efficiency.

The finite element model was validated against a four-mode analytical model using the “Bypassing PDEs method”. The resonant frequencies and time responses from both models showed excellent agreement. The contact locations assumed in the analytical equations were verified by the FEM model. Both models demonstrated the same contact severities at the contact locations.

While the analytical model runs quickly, and in a software environment that requires less specialized knowledge, the FEM model is more easily reconfigurable for different drillstring geometries, and can accommodate more complex, nonlinear phenomena. Expansion of the models to capture torsional vibration is ongoing. The models in their current form will be an important tool in specifying force generators, and designing vibration suppression systems, in pursuit of vibration-assisted drilling systems that increase rate of penetration and efficiency without negative consequences for component life.

6.8 Acknowledgment

This research was conducted at the Advanced Drilling Technology Laboratory at Memorial University of Newfoundland and was funded by Husky Energy, Suncor Energy, The Atlantic Canada Opportunities Agency and The Research and Development Corporation of Newfoundland and Labrador under AIF Contract No. 781-2636-1920044.

6.9 References

- [1] Barton, S., Baez, F., and Al Ali, A., 2011, "Drilling Performance Improvement in Gas Shale Plays Using a Novel Drilling Agitator Device," SPE#144416, SPE North American Unconventional Gas Conference and Exhibition, , The Woodlands, Texas.
- [2] Babatunde, Y., Butt, S. D., Molgard, J., and Arvani, F., 2011, "*Investigation of the Effects of Vibration Frequency on Rotary Drilling Penetration Rate Using Diamond Drag Bit*," ARMA#11-527, 45th US Rock Mechanics/Geomechanics Symposium (ARMA), San Francisco, California.
- [3] Spanos, P. D., Chevallier, A. M., and Politis, N. P., 2002, "Nonlinear Stochastic Drillstring Vibrations," ASME Journal of Vibrations and Acoustics, **124**, pp. 512-518.
- [4] Ghasemloonia, A., Rideout, D. G., and Butt, S. D., 2012, "Coupled Transverse Vibration Modeling of Drillstrings Subjected to Torque and Spatially Varying Axial Load," Journal of Mechanical Engineering Science (IMechE, part C), **227**(5), pp. 946-960.
- [5] Ghasemloonia, A. Rideout, D. G., and Butt, S. D., 2012, "Analysis of Multi-Mode Nonlinear Coupled Axial-Transverse Drillstring Vibration in Vibration Assisted Rotary Drilling," Journal of Petroleum Science and Engineering, under review.

- [6] Dykstra, M. W., Chen, D. C. K., Warren, T. M. and Zannoni, S. A., 1994, "Experimental evaluations of drill bit and drill string dynamics," 69th SPE Annual Technical Conference and Exhibition, SPE#28323, New Orleans, Louisiana.
- [7] Walker, B. H., and Friedman, M. B., 1977, "Three Dimensional Force and Deflection Analysis of a Variable Cross Section Drillstring," ASME Journal of pressure Vessels, **99**(5), pp. 367-373.
- [8] Bailey, J. J., and Finnie, I., 1960, "An Analytical Study of Drillstring Vibration," ASME Journal of Engineering for Industry, **82**(2), pp. 122 – 128.
- [9] Trindade, M. A., Wolter, C., and Sampaio, R., 2003, "Karhunen-Loeve Decomposition of Coupled Axial-Bending Vibrations of Beams Subject to Impacts," Journal of Sound and Vibration, **279**, pp.1015-1036.
- [10] Jansen, J. D., 1991, "Nonlinear Rotor Dynamics as Applied to Oil Well Drillstring Vibrations," Journal of Sound and Vibration, **147** (1), 115-135.
- [11] Elsayed, M. A, Wells, R. L., Dareing, D. W., and Nagirimadugu, K., 1994, "Effect of Process Damping on Longitudinal Vibrations in Drillstrings," ASME Journal of Energy Resources Technology, **116**, pp. 129-135.
- [12] Berlioz, A., Der Hagopian, J., Dufour, R., and Draoui, E., 1996, "Dynamic Behavior of a Drillstring: Experimental Investigation of Lateral Instabilities," ASME Journal of Vibration and Acoustics, **118**, pp. 292-298.
- [13] Aminfar, O., and Khajepour, A., 2008, "Torsional Vibration Analysis of Drillstring in Blasthole Drilling," ASME International Mechanical Engineering Congress (IMECE), Boston, Massachusetts.

- [14] Yigit, A. S., and Christoforou, A. P., 1996, "Coupled Axial and Transverse Vibrations of Oilwell Drillstrings," *Journal of Sound and Vibration*, **195**(4), pp. 617-627.
- [15] Sampaio, R., Piovan, M. T., and Lozano, G. V., 2007, "Coupled Axial Torsional Vibrations of Drillstring by Means of Nonlinear Model," *Journal of Mechanics Research Communications*, **34**, pp. 497-502.
- [16] Yigit, A. S., and Christoforou, A. P., 1998, "Coupled Torsional and Bending Vibrations of Drillstrings Subject to Impact with Friction," *Journal of Sound and Vibration*, **215**(1), pp. 167-181.
- [17] Christoforou, A. P., and Yigit, A. S., 1997, "Dynamic Modeling of Rotating Drillstrings with Borehole Interactions," *Journal of Sound and Vibration*, **206** (2), pp. 243-260.
- [18] Elsayed, M. A., Washington, L. F., 2009, "Drillstring Stability Based on Variable Material Specific Force and Using a Sharp Three-Insert Polycrystalline Diamond Compact (PDC) Bit," *ASME Journal of Energy Resources Technology*, **123**, pp 138-142.
- [19] Spanos, P. D., Sengupta, A. K., Cunningham, R. A., and Palsey, P. R., 1995, "Modeling of Roller Cone Bit Lift-Off Dynamics in Rotary Drilling," *ASME Journal of Energy Resources Technology*, **117**, pp 197-207.
- [20] Millheim, K., Jordan, S., and Ritter, C. J., 1978, "Bottom Hole Assembly Analysis Using the Finite Element Method," *Journal of Petroleum Technology*, **30**(2), pp. 265-274.
- [21] Baird, J. A., Caskey, B. C., Wormley, D.N., and Stone, C. M., 1985, "GEODYN2: A Bottomhole Assembly Geological Formation Dynamic Interaction Computer Program," SPE#14328, SPE Annual Technical Conference and Exhibition, Las Vegas, Nevada.

- [22] Apostal, M. C., Haduch, G. A., and Williams, J. B., 1990, "A Study to Determine the Effect of Damping on Finite Element Based Forced Frequency Response Models for Bottomhole Assembly Vibration Analysis," SPE Annual Technical Conference and Exhibition, New Orleans, Louisiana.
- [23] Burgess, T. M., McDaniel, G. L., and Das, P. K., 1987, "Improving BHA Tool Reliability with Drillstring Vibration Models: Field Experience and Limitations," SPE#16109, SPE/IADC Drilling Conference, New Orleans, Louisiana.
- [24] Axisa, F., and Antunes, J., 1992, "Flexural Vibration of Rotors Immersed in Dense Fluids: Part I- Theory," *Journal of Fluids and Structures*, **6**(1), pp 3-21.
- [25] Spanos, P. D., Payne, M. L., and Secora, C. K., 1997, "Bottom-hole Assembly Modeling and Dynamic Response Determination," *ASME Journal of Energy Resources Technology*, **119**, pp. 153-158.
- [26] Ritto, T. G., Soize, C. and Sampaio, R., 2009, "Non-linear dynamics of a drill-string with uncertain model of the bit-rock interaction," *International Journal of Non-linear Mechanics*, **44**, pp. 865-876.
- [27] Khulief, Y. A., and Al-Naser, H., 2005, "Finite Element Dynamic Analysis of Drillstrings," *Finite Element in Analysis and Design*, **41**, pp. 1270-1288.
- [28] Hsu, F., Wilhoit, J., and James, C., 1965, "Lateral Vibration of Drill Pipe Including Wall Reaction," SPE#1046, Conference on Drilling and Rock Mechanics, Austin, Texas.
- [29] Mitchell, R. F., and Allen, M. B., 1987, "Case Studies of BHA Vibration Failure," SPE#16675, SPE Annual Technical Conference and Exhibition, Dallas, Texas.

- [30] Melakhessou, H., Berlioz, A., and Ferraris, G., 2003, "A Nonlinear Well-Drillstring Interaction Model," *ASME Journal of Vibration and Acoustics*, **125**, pp. 46-52.
- [31] Khulief, Y. A., Al-Sulaiman, F. A., and Bashmal, S., 2008, "Vibration Analysis of Drillstrings with String-Borehole Interaction," *International Journal of Mechanical Engineering Science, IMechE Part C*, **222**, pp. 2099-2110.
- [32] Khulief, Y. A., and Al-Sulaiman, F. A., 2009, "Laboratory Investigation of Drillstring Vibrations," *International Journal of Mechanical Engineering Science, IMechE Part C*, **223**(10), pp. 2249-2262.
- [33] Khulief, Y. A., 2000, "Spatial Formulation of Elastic Multibody Systems with Impulsive Constraints," *Multibody System Dynamics*, **4**(4), pp. 383-406.
- [34] Wong, S. V., Hamuda, A. M. S., and Hasmi, M. S. J., 2001, "Kinematic Contact-Impact Algorithm with Friction," *International Journal of Crashworthiness*, **6**(1), pp. 65-82.
- [35] ABAQUS Theory Manual (version 6.10), 2012, Dassault Systèmes Simulia Corp., RI, USA.
- [36] Beck, A. T., da Silva Jr., C.R.A., 2010, "Timoshenko Versus Euler Beam Theory: Pitfalls of a Deterministic Approach," *Structural Safety*, **33**(1), pp. 19-25.
- [37] Mitchell, R. F., and Miska, S. Z., 2011, *Fundamentals of Drilling Engineering*, SPE textbook series, Texas, USA, Chap. 10.
- [38] Thomsen, J. J., 2003, *Vibrations and Stability*, 2nd ed., Springer, Berlin, Germany, Chap. 3.

- [39] Paidoussis, M. P., Luu, T. P. and Prabhakar, S., 2008, "Dynamics of a Long Tubular Cantilever Conveying Fluid Downwards, Which Then Flows Upwards Around the Cantilever as a Confined Annular Flow," *Journal of Fluids and Structures*, **24**, pp. 111-128.
- [40] Zhang, Q. and Miska, S., 2005, "Effects of Flow-Pipe Interaction on Drill Pipe Buckling and Dynamics," *ASME Journal of Pressure Vessels*, **127**, pp. 129-136.
- [41] Ritto, T. G., Sampaio, R. and Soize, C., 2009, "Drill-String Nonlinear Dynamics Accounting for Drilling Fluid," 30^o CILAMCE-Iberian-Latin-American Congress on Computational Methods in Engineering, Armação dos Búzios, Rio de Janeiro.
- [42] Nour-Omid, B., Parlett, B. N. and Taylor, R. L., 1983, "Lanczos versus Subspace Iteration for Solution of Eigenvalue Problems," *International Journal for Numerical Methods in Engineering*, **19**(6), pp. 859-871.
- [43] Simitse, G., and Hodges, D., 2005, *Fundamentals of Structural Stability*, Elsevier, Oxford, UK, Chap. 8.

6.10 Appendix 6.1: Energy terms for the first span of the BHA

The energy terms for the first span of the BHA are derived and shown below. The other two spans of the BHA are under the same effects. Thus, the energy terms are the same, except a change in the integration limits, namely $l_1 - l_2$ for the mid span and $l_2 - l_3$ for the top span. Kinetic energy for the first span:

$$K_{energy} = \frac{1}{2} \int_0^{l_1} \rho A_{collar} \left(\left(\frac{\partial}{\partial t} u(z,t) \right)^2 + \left(\frac{\partial}{\partial t} v(z,t) \right)^2 + \left(\frac{\partial}{\partial t} w(z,t) \right)^2 \right) dz \quad (6.7)$$

where u and v are two orthogonal lateral motions and w is the axial motion.

Strain energy due to axial and lateral deformations:

$$P_{energy} = \frac{1}{2} \int_0^{l_1} \left(EI_{collar} \left(\left(\frac{\partial^2 u(z,t)}{\partial z^2} \right)^2 + \left(\frac{\partial^2 v(z,t)}{\partial z^2} \right)^2 \right) + EA_{collar} \left(\frac{\partial w(z,t)}{\partial z} + \frac{1}{2} \left(\frac{\partial u(z,t)}{\partial z} \right)^2 + \frac{1}{2} \left(\frac{\partial v(z,t)}{\partial z} \right)^2 \right) \right) dz \quad (6.8)$$

Work done by the deriving torque [43] is:

$$W_{torque} = \frac{1}{2} T \left(\int_0^{l_1} \left(\left(\frac{\partial^2 u(z,t)}{\partial z^2} \right) \left(\frac{\partial v(z,t)}{\partial z} \right) + \left(\frac{\partial^2 v(z,t)}{\partial z^2} \right) \left(\frac{\partial u(z,t)}{\partial z} \right) \right) dz \right) \quad (6.9)$$

Work done by the VARD force (ω is the excitation frequency of the VARD generator):

$$W_{VARD-force} = -\frac{1}{2} \int_0^{l_1} F_{VARD} \sin(\omega t) \left(\left(\frac{\partial u(z,t)}{\partial z} \right)^2 + \left(\frac{\partial v(z,t)}{\partial z} \right)^2 \right) dz \quad (6.10)$$

Energy term due to spatially-varying compressive axial force:

$$W_{axial-force} = -\frac{1}{2} \int_0^{l_1} F_{collar} \left(\left(\frac{\partial u(z,t)}{\partial z} \right)^2 + \left(\frac{\partial v(z,t)}{\partial z} \right)^2 \right) dz \quad (6.11)$$

Dissipated energy of mud damping force [10]:

$$W_{mud-damping} = \rho_{mud} C_D R_{collar} \left(\int_0^{l_1} \sqrt{\left(\frac{\partial u(z,t)}{\partial t} \right)^2 + \left(\frac{\partial v(z,t)}{\partial t} \right)^2} \left(\frac{\partial u(z,t)}{\partial t} + \frac{\partial v(z,t)}{\partial t} \right) dz \right) \quad (6.12)$$

The contact energy in the first span is approximated based on the Hertzian contact theory using a piecewise function [14]:

$$contactenergy = - \begin{cases} K_h (r - b_{cl})^{3/2} & b_{cl} \leq |r| \\ 0 & otherwise \end{cases} r \quad (6.13)$$

where b_{cl} is the borehole clearance, K_h is contact stiffness and r is radial displacement.

6.11 Appendix 6.2: Energy terms for the pipe section

Kinetic and potential energy terms of the pipe section:

$$energy_{pipe} = \frac{1}{2} \int_{l_3}^{l_4} \rho A_{pipe} \left(\frac{\partial}{\partial t} w(z,t) \right)^2 dz + \frac{1}{2} \int_{l_3}^{l_4} EA_{pipe} \left(\frac{\partial}{\partial z} w(z,t) \right)^2 dz \quad (6.14)$$

Energy of the VARD force and the tensional axial load in the pipe section:

$$W_{pipe_VARD-force} = \frac{1}{2} \int_{l_3}^{l_4} F_{VARD} \sin(\omega t) \left(\frac{\partial}{\partial z} w(z,t) \right) dz \quad (6.15)$$

$$W_{pipe_axial-force} = \frac{1}{2} \int_{l_3}^{l_4} (F_H - \rho A_{pipe} g(l-z)) \left(\frac{\partial}{\partial z} w(z,t) \right) dz$$

6.12 Appendix 6.3: Lagrangian of the BHA and the pipe section

The Lagrangian of the three-span BHA and the pipe section are as below:

$$\begin{aligned} Lagrangian_{span1} = & \frac{1}{2} \int_0^l \rho A_{collar} \left[\left(\frac{\partial}{\partial t} u(z,t) \right)^2 + \left(\frac{\partial}{\partial t} v(z,t) \right)^2 + \left(\frac{\partial}{\partial t} w(z,t) \right)^2 \right] dz \\ & - \frac{1}{2} \int_0^l \left[EI_{collar} \left[\left(\frac{\partial^2}{\partial z^2} u(z,t) \right)^2 + \left(\frac{\partial^2}{\partial z^2} v(z,t) \right)^2 \right] + EA_{collar} \left[\left(\frac{\partial}{\partial z} w(z,t) \right)^2 + \frac{1}{2} \left(\frac{\partial}{\partial z} u(z,t) \right)^2 + \frac{1}{2} \left(\frac{\partial}{\partial z} v(z,t) \right)^2 \right] \right] dz \\ & - \frac{1}{2} T \int_0^l \left[\left(\frac{\partial^2}{\partial z^2} u(z,t) \right) \left(\frac{\partial}{\partial z} v(z,t) \right) + \left(\frac{\partial^2}{\partial z^2} v(z,t) \right) \left(\frac{\partial}{\partial z} u(z,t) \right) \right] dz + \frac{1}{2} \int_0^l F_{VARD} \sin(\omega t) \left[\left(\frac{\partial}{\partial z} u(z,t) \right)^2 + \left(\frac{\partial}{\partial z} v(z,t) \right)^2 \right] dz \\ & + \frac{1}{2} \int_0^l (\rho A_{collar} g z - WOB - \rho_{mud} g l A_{collar}) \left[\left(\frac{\partial}{\partial z} u(z,t) \right)^2 + \left(\frac{\partial}{\partial z} v(z,t) \right)^2 \right] dz \end{aligned} \quad (6.16)$$

$$\begin{aligned}
Lagrangian_{span2} &= \frac{1}{2} \int_{l_1}^{l_2} \rho A_{collar} \left(\left(\frac{\partial}{\partial t} u(z,t) \right)^2 + \left(\frac{\partial}{\partial t} v(z,t) \right)^2 + \left(\frac{\partial}{\partial t} w(z,t) \right)^2 \right) dz \\
&- \frac{1}{2} \int_{l_1}^{l_2} \left(EI_{collar} \left(\left(\frac{\partial^2}{\partial z^2} u(z,t) \right)^2 + \left(\frac{\partial^2}{\partial z^2} v(z,t) \right)^2 \right) + EA_{collar} \left(\frac{\partial}{\partial z} w(z,t) + \frac{1}{2} \left(\frac{\partial}{\partial z} u(z,t) \right)^2 + \frac{1}{2} \left(\frac{\partial}{\partial z} v(z,t) \right)^2 \right)^2 \right) dz \\
&- \frac{1}{2} T \int_{l_1}^{l_2} \left(\left(\frac{\partial^2}{\partial z^2} u(z,t) \right) \left(\frac{\partial}{\partial z} v(z,t) \right) + \left(\frac{\partial^2}{\partial z^2} v(z,t) \right) \left(\frac{\partial}{\partial z} u(z,t) \right) \right) dz + \frac{1}{2} \int_{l_1}^{l_2} F_{VARD} \sin(\omega t) \left(\left(\frac{\partial}{\partial z} u(z,t) \right)^2 + \left(\frac{\partial}{\partial z} v(z,t) \right)^2 \right) dz \\
&+ \frac{1}{2} \int_{l_1}^{l_2} (\rho A_{collar} g z - WOB - \rho_{mud} g l A_{collar}) \left(\left(\frac{\partial}{\partial z} u(z,t) \right)^2 + \left(\frac{\partial}{\partial z} v(z,t) \right)^2 \right) dz
\end{aligned} \tag{6.17}$$

$$\begin{aligned}
Lagrangian_{span3} &= \frac{1}{2} \int_{l_2}^{l_3} \rho A_{collar} \left(\left(\frac{\partial}{\partial t} u(z,t) \right)^2 + \left(\frac{\partial}{\partial t} v(z,t) \right)^2 + \left(\frac{\partial}{\partial t} w(z,t) \right)^2 \right) dz \\
&- \frac{1}{2} \int_{l_2}^{l_3} \left(EI_{collar} \left(\left(\frac{\partial^2}{\partial z^2} u(z,t) \right)^2 + \left(\frac{\partial^2}{\partial z^2} v(z,t) \right)^2 \right) + EA_{collar} \left(\frac{\partial}{\partial z} w(z,t) + \frac{1}{2} \left(\frac{\partial}{\partial z} u(z,t) \right)^2 + \frac{1}{2} \left(\frac{\partial}{\partial z} v(z,t) \right)^2 \right)^2 \right) dz \\
&- \frac{1}{2} T \int_{l_2}^{l_3} \left(\left(\frac{\partial^2}{\partial z^2} u(z,t) \right) \left(\frac{\partial}{\partial z} v(z,t) \right) + \left(\frac{\partial^2}{\partial z^2} v(z,t) \right) \left(\frac{\partial}{\partial z} u(z,t) \right) \right) dz + \frac{1}{2} \int_{l_2}^{l_3} F_{VARD} \sin(\omega t) \left(\left(\frac{\partial}{\partial z} u(z,t) \right)^2 + \left(\frac{\partial}{\partial z} v(z,t) \right)^2 \right) dz \\
&+ \frac{1}{2} \int_{l_2}^{l_3} (\rho A_{collar} g z - WOB - \rho_{mud} g l A_{collar}) \left(\left(\frac{\partial}{\partial z} u(z,t) \right)^2 + \left(\frac{\partial}{\partial z} v(z,t) \right)^2 \right) dz
\end{aligned} \tag{6.18}$$

$$\begin{aligned}
Lagrangian_{pipe} &= \frac{1}{2} \int_{l_3}^{l_4} \rho_{pipe} A_{pipe} \left(\frac{\partial}{\partial t} w(z,t) \right)^2 dz - \frac{1}{2} \int_{l_3}^{l_4} EA_{pipe} \left(\frac{\partial}{\partial z} w(z,t) \right)^2 dz \\
&- \frac{1}{2} \int_{l_3}^{l_4} F_{VARD} \sin(\omega t) \left(\frac{\partial}{\partial z} w(z,t) \right) dz - \frac{1}{2} \int_{l_3}^{l_4} (F_H - \rho_{st} A_{pipe} g (l-z)) \left(\frac{\partial}{\partial z} w(z,t) \right) dz
\end{aligned} \tag{6.19}$$

To apply the expanded Galerkin's method u , v and w were assumed as comparison functions multiplied by mode participation factors. For the first span:

First span	Second span	Third span	
$w(z,t) = \sum_{r=1}^4 \chi_r(z) \cdot p_r(t)$	$w(z,t) = \sum_{r=1}^4 \chi_r(z) \cdot p_r(t)$	$w(z,t) = \sum_{r=1}^4 \chi_r(z) \cdot p_r(t)$	(6.20)
$u(z,t) = \sum_{r=1}^4 \varphi_r(z) \cdot \eta_r(t)$	$u(z,t) = \sum_{r=1}^4 \psi_r(z) \cdot \eta_r(t)$	$u(z,t) = \sum_{r=1}^4 \theta_r(z) \cdot \eta_r(t)$	
$v(z,t) = \sum_{r=1}^4 \phi_r(z) \cdot \lambda_r(t)$	$v(z,t) = \sum_{r=1}^4 \psi_r(z) \cdot \lambda_r(t)$	$v(z,t) = \sum_{r=1}^4 \theta_r(z) \cdot \lambda_r(t)$	

The subscript r depends on the desired mode shapes according to the frequency range of interest. For this problem the first four modes were retained to conduct the multi-mode analysis. In the above expressions χ, φ, ψ and θ are comparison functions for axial and orthogonal lateral motions of the first, second and last span of the BHA, respectively.

$p_r(t), \eta_r(t)$ and $\lambda_r(t)$ are mode participation factors for axial motion (w), and lateral motions (u) and (v), respectively. For the fixed at top-free at the bottom boundary conditions, the axial comparison function is:

$$\chi_r(z) = \sin\left(\frac{(2r-1)\pi z}{2l}\right) \quad (6.21)$$

6.13 Appendix 6.4: Eigenfunctions and eigenfrequencies of a three span beam with different lengths

Separate coordinate systems are assumed for each span (Figure 6.2) and the normal mode for each span can be written as:

$$\begin{aligned} \phi(x) &= a \cos(\beta x) + b \sin(\beta x) + c \cosh(\beta x) + d \sinh(\beta x) \\ \psi(y) &= e \cos(\beta y) + f \sin(\beta y) + g \cosh(\beta y) + h \sinh(\beta y) \\ \theta(z) &= i \cos(\beta z) + j \sin(\beta z) + k \cosh(\beta z) + l \sinh(\beta z) \end{aligned} \quad (6.22)$$

There are 12 unknowns in the equations. Six boundary conditions are zero deflections at the supports, while two boundary conditions are zero bending moments at both ends. The remaining four boundary conditions are slope and bending compatibility equations at the two middle supports. For the nontrivial solution of the system of equations, the determinant of the coefficient matrix is set to zero. The result is the frequency equation:

$$\begin{aligned}
 & \frac{1}{\sin(10\beta)\sinh(10\beta)} \left\{ -2 \sin(10\beta) \cos(10\beta) \sinh(10\beta) \left[\frac{\sinh(10\beta)}{\sin(10\beta)} \right] - 3 \cos(10\beta) \sinh(10\beta)^2 \right. \\
 & + \sin(10\beta)^2 \cosh(10\beta) \left[\frac{\sinh(10\beta)}{\sin(10\beta)} \right] + 2 \sin(10\beta) \cosh(10\beta) \sinh(10\beta) \\
 & + \sin(10\beta) \sinh(10\beta) \left[\frac{\sinh(10\beta)}{\sin(10\beta)} \right] \cosh(10\beta) + \sin(10\beta) \cos(10\beta) \sinh(10\beta) \\
 & \left. + \sin(10\beta) \sinh(10\beta)^2 \left[\frac{\cos(10\beta) - \cosh(10\beta)}{\sin(10\beta)} \right] - \sin(10\beta)^2 \sinh(10\beta) \left[\frac{\cos(10\beta) - \cosh(10\beta)}{\sin(10\beta)} \right] \right\} = 0
 \end{aligned} \tag{6.23}$$

The equation was solved numerically using the Newton–Raphson algorithm. The first four values for β are 7.171, 12.57, 13.77 and 16.64. The values of β were substituted in 12 equations to find the first four modes of each span, namely 12 mode shapes. The mode shapes are derived symbolically [5] and shown in Figure 6.19 for a three span BHA with 15, 15 and 30 m span Lengths for the first to the third spans, respectively.

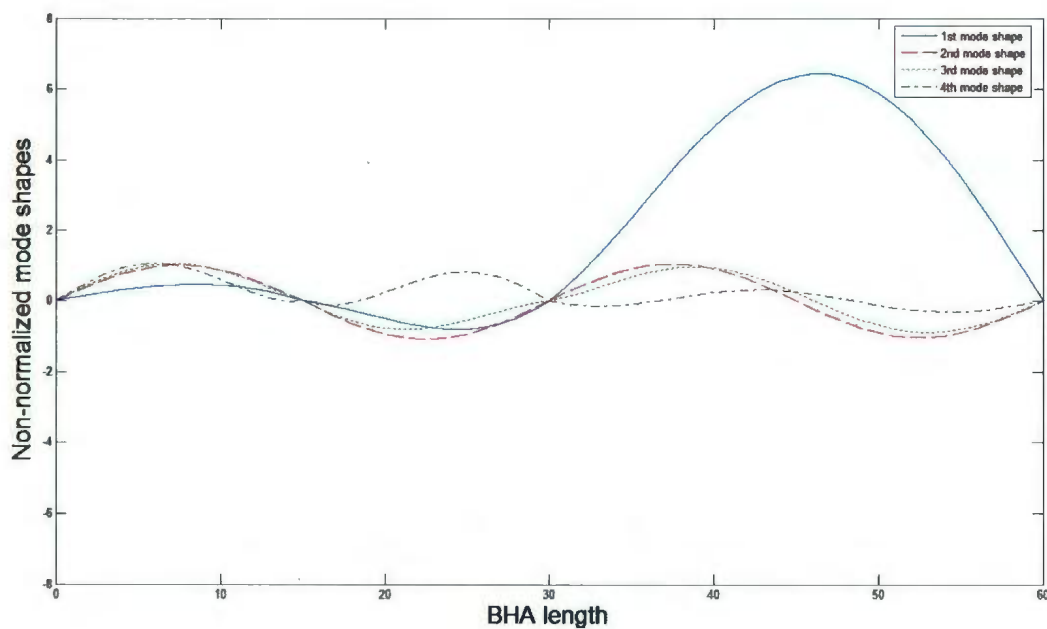


Figure 6.19: The first four mode shapes of a three span BHA

6.14 Nomenclature

F_{collar}	Compressive force along the collars	F_{pipe}	Tensile force along the pipes
ρ_{collar}	Density of the collars	ρ_{pipe}	Density of the pipes
A_{collar}	Cross sectional area of the collars	A_{pipe}	Cross sectional area of the pipes
l	Total length of the drillstring	T	Driving torque
WOB	Weight-on-bit	F_{hook}	Hook load
ρ_{mud}	Mud density	C_D	Hydrodynamic drag coefficient
E	Young's modulus	g	Acceleration due to gravity
l_1, l_2, l_3	Length of the first, second and the last span of the BAH, respectively	β	Natural frequencies of the three-span BHA
I_{collar}	Area moment of inertia of the collars	R_{collar}	Outer radius of the collars
F_{VARD}	Amplitude of the VARD force	ω	Frequency of the VARD force

K_h	Hertzian contact stiffness	b_{ct}	Borehole clearance
$u(z,t)$	Deflection in the first orthogonal transverse direction	$\varphi_r(z)$	The comparison function in the first orthogonal transverse direction (u)
$v(z,t)$	Deflection in the second orthogonal transverse direction	$\varphi_r(z)$	The comparison function in the second orthogonal transverse direction (v)
$w(z,t)$	Axial deflection	$\chi_r(z)$	The axial comparison function
$p_r(t)$	Axial mode participation factor	$\eta_r(t)$	Lateral (u) mode participation factor
$\lambda_l(t)$	Lateral (v) mode participation factor	$\theta(z)$	Mode shape of the third span of BHA
$\phi(x)$	Mode shape of the first span of BHA	$\psi(y)$	Mode shape of the second span of BHA
<i>contact energy</i>	Contact energy due to the Hertzian contact forces	<i>energy of pipe</i>	kinetic and potential energies of the pipes
K_{energy}	Kinetic energy of the collars	$W_{VARD-force}$	Work due to VARD force
P_{energy}	Strain energy of the collars	$W_{axial-force}$	Work due to the drillstring axial force
W_{torque}	Work due to the driving torque	$W_{mud-damping}$	Mud damping dissipated energy

7 Elastodynamic and Finite Element Vibration Analysis of a Drillstring with a Downhole Vibration Generator Tool and a Shock Sub

Ahmad Ghasemloonia, Ph.D. Candidate

D. Geoff Rideout, Associate Professor

Stephen D. Butt, Professor

Advanced Drilling Group, Faculty of Engineering and Applied Science, Memorial University, St. John's, NL, Canada

Ali Hajnayeb, Assistant Professor

Department of Mechanical Engineering, Faculty of Engineering, Chamran University, Ahvaz, Iran

This chapter is based on the modeling step 5 defined in section 1.4 of this thesis and is submitted as a full research paper to the ASME Journal of Vibration and Acoustics on May 2013 and currently is under review.

7.1 Abstract

Applying high frequency axial oscillation into an oilwell drillstring above the bit has the potential to enhance drilling efficiency in extended reach wells. Downhole vibration

generator tools such as jars and agitators reduce the drillstring-wellbore friction and enhance the rate of penetration (ROP), ultimately improving weight transfer from the drillstring to the rock and facilitating the cutting removal process. However, introducing controlled vibrations into the drillstring can result in undesired vibration waves propagating along the drillstring, leading to inefficient drilling and catastrophic fatigue failure of the "bottom-hole assembly" (BHA) components, "measurement-while-drilling" (MWD) tools, and mud motors. A dynamic model of the entire drillstring, including vibration generators and shock subs, is required to study the effect of vibration generators on the complex nonlinear coupled axial-lateral dynamics of a drillstring inside a wellbore, to study the effect of vibration tools on the developed cutting force at the bit, and to facilitate simulation-based design of shock subs. A dynamic finite element model (FEM) and an analytical elastodynamic model, both including the vibration generator tool and a shock sub, have been developed. The "Bypassing PDEs" method was implemented on the Lagrangian of the system to develop the analytical equations. A multi-mode expanded Galerkin's approximation, in conjunction with a multi-span BHA and Hertzian contact assumption, allowed analysis of multiple BHA contact points and thus more realistic estimates of drilling rotary speeds that can cause excessive vibration. The models also include torque, mud damping, spatially varying axial force, geometric nonlinearity, and axial stiffening. While the analytical model has fast running time and symbolic solution, the FEM model enables easy reconfiguration and future extensions of model geometry, interactions, and modified BHA configurations. There is agreement between the analytical and FEM simulation results for the vibration suppression ability of the shock

sub, dynamic amplification of the vibrating tool force, critical rotary speeds, axial force along the drillstring, axial and lateral displacements, and the contact locations and severity.

Keywords: Drillstring; Downhole vibration generator; Shock sub; Coupled axial-transverse; Finite element analysis; Multi-span BHA; "Bypassing PDEs"; Wellbore contact; Multi-mode analysis

7.2 Introduction

As worldwide drilling for exploration and exploitation of energy reservoirs increases, so too does the need for enhanced techniques for faster and more efficient drilling.

Downhole axial vibration generators, such as agitators and jars, are a recent class of high-frequency tools, which have been demonstrated to increase the rate of penetration in extended reach wells. Based on the idea of reducing static friction between the drillstring and wellbore, these tools generate high-frequency axial oscillation above the bit, resulting in an improved weight transfer, and thus less required "weight-on-Bit" (WOB). Reduced stick-slip, improved steering, more efficient cutting removal, and improved load buckling capacity are other potential benefits of these tools. Nevertheless, implementing vibration generator tools in conventional rotary drilling raises questions about the side effects of the imposed vibration on the drilling rig itself and, in particular, on the drillstring.

Vibration generator tools act as a source of axial excitation of the drillstring, and due to the coupling effect, lateral modes are also excited by installing these tools above the bit. Unwanted lateral vibration can offset some of the benefit of vibrating tools. A large

portion of the provided power at the surface can be lost if the undesired vibrations of the drillstring are not suppressed. As well, if the working parameters of the vibration generator (load and frequency) are not compatible with the configuration of the drillstring and formation properties, this will not only result in reducing the ROP, but also in hole deviation, wellbore washout, and premature failure of drillstring components, including the MWD tools. Premature failures of MWD tools on BHA's with vibrating tools have been reported by industry, and the only effective way to benefit from the positive consequences of these tools is to isolate the imposed vibration from the rest of the drillstring.

A shock sub consisting of a spring and damper in parallel, if properly located and tuned, can enhance the effect of the vibration generator tool at the bit, while preventing the generated axial vibration from propagating up the drillstring and exciting lateral vibration that can lead to excessive wellbore contact. The most efficient way to configure the shock sub parameters and investigate its decoupling efficacy is through simulation-based design, using a dynamic model of the entire drillstring incorporating the vibrating tool, shock sub and all relevant interactions and forces. In this paper, both an elastodynamic analytical model and a dynamic numerical (finite element) model are constructed to extract modal characteristics and dynamic time response of the entire drillstring. These models can predict drillstring motion inside the wellbore, and study contact behavior and bit reaction force in various drilling conditions.

The vibration models are useful not only for shock sub design, but also for determining BHA geometry, stabilizer location, working parameters of the vibration generator tools, and guidelines for adjusting the main drilling parameters at the surface, such as rotary speed, torque, and WOB. Such dynamic models are the first essential step towards developing control strategies for faster and more efficient drilling without premature failures of the drill rig components. Complexity of the models depends on the assumptions about interacting forces, linear and non-linear excitation sources, damping effects, contact behavior with the wellbore, and boundary conditions such as multiple stabilizers located along the BHA and the hoisting system (derrick cables).

The drillstring is composed of a long, thin-walled interval (drill pipes) – which can be up to 5 kilometres long – and a heavier, thick-walled bottom section (drill collars and BHA) with a typical length of up to several hundred metres, constrained by stabilizers inside the wellbore. The BHA plays the dominant role in the vibration behavior of the drillstring [1]. The top point of the drillstring passes through the kelly and rotary table and is attached to the derrick cables, while the bit is attached to the bottom point. The stabilizers are fins placed outside of the drill collars at multiple locations to centralize the drillstring inside the wellbore, to increase the load carrying capacity of the BHA, and to control well trajectories in deviated wells. Here, the annulus between the BHA and the wellbore is up to 10 centimetres and filled with the drilling mud, which is used to cool down the bit, flush out the cuttings, and transmit the hydraulic power to the bit. Moreover, the mud plays an important role in well kick-out control through a balance with the formation pressure and in stabilizing the lateral vibrations of the BHA as a nonlinear damping

medium. The drillstring is under interaction of several axial forces, such as WOB (to provide the cutting force), hook load, self weight, mud hydrostatic effects (both upward and downward), and excitation forces (e.g. bit-formation interaction, multiple contact loads, and the vibration generator tool) [2]. The tendency in drilling engineering is to keep the pipe section under tension, while keeping the stiff BHA under compression. The length and material properties of the BHA, alongside with WOB and mud density, are controllable parameters to keep the BHA under compression [2]. The rotary speed of the drillstring is typically between 20 and 200 rpm, and this excitation frequency can cause an unwanted vibration to propagate through the drillstring and cause premature failure of BHA components and MWD tools, bit and stabilizer wear, deterioration of well trajectory, dissipation of the provided energy, and lower penetration rate [3].

A typical drillstring vibrates in three major coupled modes: axial [4], transverse [5], and torsional [6]. Extreme manifestations of these modes are bit-bounce, whirling, and stick-slip, respectively. Bit-formation interaction, multiple point drillstring-wellbore contacts, mass imbalance, and vibration generation tools are the main sources of excitation. The axial vibration causes lateral vibration in the BHA, while severe downhole lateral vibration causes axial and torsional vibrations that can be monitored at the surface. Rotary speed, driving torque, and curvature of the drillstring are causes of the coupling phenomenon, as will be observed in the developed analytical equations. Axial vibration excited by the bit-formation interaction can lead to bit bounce, which results in the bit cutting tooth wear and bearing failure. Lateral vibration, as the most destructive type of vibration excited by unbalance or successive drillstring-wellbore contacts, causes large

high-frequency bending moment fluctuations in the BHA, which ends in premature fatigue failure of the BHA components, wellbore washout, and wear of stabilizers. Torsional vibration, especially stick-slip, can cause fatigue failure of pipe joints and damage to the bit. While lateral vibrations are very severe in vertical wells and result in catastrophic BHA failures [7,8], axial vibrations become very important when downhole vibrating tools are used. Simultaneous axial-lateral vibration is potentially harmful if not controlled. The developed models must capture these two modes.

Basic vibration models can reveal the resonant frequency of the drillstring and BHA. Based on that, the surface rotary speed and the vibration-generator tool frequency can be adjusted to not coincide with these critical speeds. However, complex dynamic models are required to predict the time response of the drillstring and stresses on downhole tools with greater fidelity.

Section 7.3 reviews prior drillstring modeling work, and Sections 7.4 and 7.5 describe the new analytical and FEM models. The developed models are used in Section 7.6 to extract natural frequencies, to study the effect of vibrating tools on the developed cutting force at the bit and to design a shock sub, and to analyze the lateral instabilities at multiple contact points in the presence of vibrating tools and shock subs.

7.3 Literature Review

7.3.1 Downhole Vibration Generator Tools

Interest in implementing high-frequency axial vibration tools in conventional rotary drilling has increased over the past decade. Manko *et al.* [9] introduced a hydrovibrator

tool which superimposes axial vibrations to a drillstring by transforming a stationary mud flow to a high frequency pulsating flow, resulting in a hydrodynamic cavitation impact on the drillstring. Al Ali *et al.* [3] investigated axial oscillation generator (AGT) tools for which a 60% increase in ROP with 63% less required WOB, extended bit life and less stick-slip were reported in vertical wells. However, drillstring vibration levels increased. Newman *et al.* [10] presented a theoretical torque-drag model to verify the experimental results of friction reduction through the use of vibration generator tools, while implementing the National Oilwell CT AG-imatorTM tool. The use of this tool increased the depth of penetration by approximately 1000 feet and the developed model and field test results were in agreement in predicting the amount of friction forces eliminated by the tool. Babatunde *et al.* [11] and Li *et al.* [12] investigated the effect of introducing various levels of vibration in diamond drag and coring bits, and concluded that at controlled frequencies the imposed vibration has a significant positive effect on ROP. Khorshidian *et al.* [13] investigated the effect of introducing vibration force in a single cutter "Polycrystalline Diamond Compact" (PDC) bit, using the "Distinct Element Methodology" (DEM). They verified that imposing energized impact on the rock-cutter surface improves the value of the drilling mechanical specific energy (MSE), and this factor was then used to find an optimum level of the cutter vertical vibrations for a faster ROP. However, alongside the considerable potential improvement in drilling efficiency, the implementation of downhole vibration generator tools introduces some adverse effects: complexity in adjustment of operating parameters of the vibration tools and possibly high levels of vibration induced to the drillstring.

7.3.2 Shock Subs and Drillstring Axial Vibration Decoupling

Axial vibration generated due to the bit-rock interaction and the downhole vibration generator should be decoupled from the drillstring as much as possible. A shock sub is a passive spring in parallel with a damper that is installed above the bit to reduce the displacement or force amplitude transmitted to the BHA and drill pipes, through frequency detuning and phase shift. Elsayed *et al.* [14] investigated the effect of shock sub-parameters on vibration isolation in hard rock drilling through an experimental setup, and an optimum range for the stiffness and damping values of the shock sub to reduce the bit bouncing phenomenon was investigated. Warren *et al.* [15] investigated the role of shock sub on the reduction of axial vibrations, and suggested to install the shock subs with softer springs below the collars for a more efficient isolation; a reduction in lateral vibration levels with the use of shock subs was also reported. Skaugen *et al.* [16] proposed a linear simple axial model for designing shock sub parameters and recommended a nonlinear model for a precise design of shock subs. Moreover, it is concluded that decreasing the stiffness value of a shock sub to an optimum point increases its efficiency in reducing axial vibration amplitudes above the shock sub. Kreisle *et al.* [17] investigated the effect of a shock sub on the axial vibration of the drillstring through an uncoupled axial model and the Laplace solution scheme. A sinusoidal displacement boundary condition at the bit location was implemented for the excitation of the axial mode, and it was proven that the efficacy of the shock sub is due to the change in the phase angle rather than a change in natural frequency of the system, and a softer spring was recommended to increase the efficiency of the shock sub. Prior work

on shock subs indicates that optimum shock sub tuning depends on many factors such as drillstring configuration, bit-rock boundary condition, and the presence of coupled axial-lateral modes. Comprehensive drillstring dynamic models containing shock subs and vibrating tools, that allow multiple simulation runs to be done inexpensively and efficiently, are thus a potentially valuable design tool.

7.3.3 Analytical Modeling

Static modeling, analytical elastodynamic modeling, and numerical modeling (e.g., finite element or finite difference) are common approaches towards analyzing the dynamic behavior of the drillstring. Static models were first developed in the 1950's to investigate the stability and load carrying capacity of the drillstring, reaction loads at the bit, BHA-wellbore side forces, and mud hydrostatic forces. These models were mostly implemented to design the length and geometry of the entire drillstring, and to predict the deformed shape of the drillstring inside the wellbore [18]; however, they were not able to reveal any information about the modal content of the drillstring, dynamic response of the BHA, and contact behavior.

Basic elastodynamic models were first developed in the 1960's to investigate the natural frequencies and mode shapes of the drillstring. Classical uncoupled, non-rotating lateral, axial, and torsional-beam vibration equations were used with simplified boundary conditions and without major excitations (e.g., bit-rock excitation, contact forces). One of the early works which determined the critical rotary speed of the drillstring with a simplified model was conducted by Dareing [1], in which he suggested basic equations in

terms of the drillstring length and natural frequencies to control unwanted vibrations of a non-rotating drillstring. However, the basic models were not capable of predicting the precise motion trend of the drillstring inside the wellbore, contact behavior, or sensitivity analysis of the input parameters.

Then, enhanced uncoupled dynamic models were developed to investigate precise critical rotary speeds, the transient and steady state response of the drillstring, contact behavior and the developed forces, cutting forces at the bit, and reaction forces at the surface. The motivation for the enhanced dynamic models was to adjust the primary working parameters during drilling (combination of WOB, driving torque, rotary speed, pump pressure and mud characteristics), to develop remedial guidelines for severe vibration levels of the drillstring, and to design controllers for in-time suppression actions based on investigation of the transient and steady-state response of the drillstring.

Vibration coupling effects have been considered recently: axial-transverse [19,20], axial-torsional [21], and torsional-transverse modes [22]. Based on an enhanced model, Hakimi *et al.* [23] investigated the single plane lateral-axial natural frequencies of a single span BHA. Gulyayev *et al.* [24] studied the effect of length of the BHA on its stability through a coupled lateral model, while Yigit *et al.* [19] investigated the axial-transverse behavior of the non-rotating BHA. The parametric resonance phenomenon [22] and buckling analysis of the BHA [19] were also research goals of the coupled enhanced models.

In order to investigate the dynamic behavior of the drillstring, either in the frequency domain or the time domain, it is essential to derive the equations of motion of the

drillstring. The Newtonian approach and the energy variational approach (Hamilton's principle with the variational approach) are extensively used by researchers in the field. Ghasemloonia *et al.* [25,26], Yigit *et al.* [22], and Hakimi *et al.* [23] implemented the force-balance equation concept (Newtonian modeling) and derived the equations of motion of the drillstring. An energy variational approach with Hamilton's principle was applied by Jafari *et al.* [27], Melakhessou *et al.* [28], Sampaio *et al.* [21], Heisig *et al.* [29], Christopherrou *et al.* [30] and Khulief *et al.* [31]. Energy methods are preferred to the Newtonian approach for analyzing complicated systems, due to the energy being a scalar quantity (in contrast to force vectors) and the availability of energy equations for all interacting sources of excitations on the drillstring. In the current paper, the Lagrangian of the drillstring motion in the coupled axial-lateral (two orthogonal lateral) directions is developed and equations of motions are derived using the "Bypassing PDEs" method. This method, which has been proven to be accurate for nonlinear problems [32], is based on combining the expanded Galerkin's technique with Lagrange's equation, instead of using the conventional Hamiltonian approach. The expanded Galerkin's method, then, is applied at the first step of the Lagrange's equation, while setting up the energy equations.

Closed-form solution of the coupled nonlinear equations of motion is not possible. Approximate methods such as Galerkin's method [33], expanded Galerkin's method [26], and assumed modes method [30] have been implemented to convert time-space domain "eigenvalue problems" (EVPs) to a set of nonlinear coupled ordinary differential equations (ODEs). This idea is based on integrating the developed equations over the

space domain in EVPs, and assumption of the approximate space domain functions (mode shapes) to eliminate the space variable, while considering the orthogonality of the mode shapes. Due to the complexity of the geometric configuration and boundary conditions, deriving the exact mode shapes of the drillstring problem is not feasible and approximate shape functions, e.g. comparison functions [26] and admissible functions [19], are instead implemented. In this study, the expanded Galerkin's method with realistic comparison functions for both axial and lateral directions is implemented to convert the EVPs to ODEs, and then a fixed-step Runge-Kutta method is used to solve the resulting set of ODEs. The axial mode shapes in this paper include the discrete elements associated with the shock sub and hoisting system, and not just the continuous pipe and collar sections.

The lateral vibration behavior of the drillstring is strongly influenced by the BHA vibrations, especially vibrations resulting from contact with the wellbore [7,8]. Modeling the impact is a crucial task to precisely evaluate the lateral dynamic response, and the contact behavior has been approached in different ways: Hakimi *et al.* [23] modelled the drillstring-wellbore contact as a series of constant stiffness springs; Jansen [34] modeled the contact point of a rotating drillstring as a two DOF lumped element model in two orthogonal transverse planes; and Christoforou *et al.* [30] and Hsu *et al.*, [35] modeled the lateral behavior of the drillstring at the contact point through a Hertzian contact force. In this study, the Hertzian contact model is implemented at multiple contact points along the multi-span BHA. The location of the contact points is verified by the developed FEM model, through the general kinematic contact algorithm, which is capable of detecting any contact point for the entire drillstring.

The proper assumption and simplification of boundary conditions (BC) for different modes is an important step towards getting a precise approximate function – and thus a precise solution. Fixed at top-free at the bottom BC [19,27], fixed-fixed BC [36], and free at top-fixed at the bottom BC [37] are commonly used BCs for the axial mode of the drillstring vibration. Jogi *et al.* [38] suggested that the free-fixed axial BC does not match well with major axial frequencies observed at the field and that the free end assumption is closer to the field data. Clayer *et al.* [39] suggested an equivalent mass-spring-damper at the top and verified that this model is sufficiently accurate for the rig surface modeling. Arrestad *et al.* [40] also suggested an equivalent mass-spring-damper for the top boundary condition, but recommended a nonlinear coupled axial model to study the role of this boundary condition on the axial vibration of the drillstring. Bit displacement functions have been suggested as an accurate lower boundary condition in the axial direction, which depends on the rock formation properties and the bit type. Kreisle *et al.* [17] was the first one who applied a sinusoidal bit displacement as the lower BC for axial motion. The frequency of displacement was assumed to be three times the rotary speed for tricone bits and the same as the rotary speed for PDC bits [30]. Macpherson *et al.* [41] suggested the same boundary condition proposed by Kreisle *et al.* [17], with a phase shift related to the drillstring rotary speed. Dareing [36] also suggested a constant amplitude sinusoidal function as the bit displacement. On the other hand, however, in a number of studies the bit in the axial direction was assumed as a free BC, and an excitation force (not a BC) was assumed instead. Elsayed *et al.* [42] proposed a force excitation at the bit which depends on the width of the cut and cutting stiffness of the rock. Yigit *et al.* [22]

and Dunyaevsky *et al.* [43] assumed that WOB has a constant component and a varying component with the same frequency as the drillstring rotary speed for PDC bits. To decide between these two excitation and boundary conditions at the bit, Li *et al.* [44] used a mathematical model of the drillstring and field data and recommended the bit displacement BC for axial vibration modeling. Skaugen *et al.* [16] also recommended a bit displacement BC for shock sub design. Meanwhile, simply-supported BCs for lateral vibrations at the stabilizer locations were suggested by Khulief *et al.* [31], Dareing [1], Heisig *et al.* [29], and Yigit *et al.* [19,22]. Field investigation by Jogi *et al.* [38] supported the assumption of simply supported BCs at the locations of stabilizers. The top BC in the lateral direction is suggested to be fixed at the location of the rotary table [37]. In the present study, a bit-displacement BC with an equivalent mass-spring-damper at the rig surface is assumed as the proper BC's for the axial motion. Lateral BC's are pinned-pinned at the stabilizers, and fixed at the rig surface.

To summarize the analytical model, a nonlinear coupled axial-lateral (two orthogonal lateral directions) elastodynamic model of the entire drillstring, including a multi-span BHA and a shock sub is developed. The kinetic energy, nonlinear strain energy (axial stiffening), multiple contacts, mud damping, torque, vibration generator tool, axially distributed force along the drillstring, rotary gyroscopic effect and discrete mass spring dampers for realistic boundary conditions and shock sub are considered. Then, axial and lateral comparison function based on realistic boundary conditions are developed and substituted in the expanded Galerkin's method. The lateral comparison functions were derived analytically for the entire drillstring, assuming a multi-span BHA with different

span length. The axial comparison functions were determined analytically for a system of hybrid continuous and discrete elements, including the shock sub and equivalent mass-spring-damper as the top hoisting system. The retained first four modes in the expanded Galerkin's method, based on the results of an effective modal mass study in the FEM model, enable a multi-mode analysis of the critical rotary speeds and steady state response of any point on the drillstring, including the contact points. The effect of a shock sub on the vibration suppression is also investigated by the analytical model and the results are compared with the developed dynamic FEM model.

7.3.4 Dynamic Finite Element Modeling (FEM)

The difficulties and limitations of analytical models to model complex boundary conditions and forces, and the need to reconfigure such models for new extensions, coupled with the development of fast processing computers, have attracted investigators to numerical methods, such as finite element method (FEM), finite difference method (FDM), and differential quadrature method (DQM). These techniques are based on discretization of the drillstring continuous media, setting up equilibrium compatibility equations, and their numerical solutions. This procedure is coded in software such as ABAQUS[®] and Ansys[®], and an extensive library of beam elements, dashpot elements, time varying forces, different contact algorithms, and the ability to record nodal time histories and account for higher modes are the great advantages of such software packages [45]. As with analytical modeling, FEM modeling of the drillstring started with simple models [46] to extract natural frequencies, mode shapes, and developed force

along the drillstring. Later on, enhanced models captured contact phenomena, bit-rock interaction force, and complicated geometric configurations of the BHA.

Transient and steady state responses of the drillstring with the FEM technique were investigated by Apostol *et al.* [47], Burgess *et al.* [7], Spanos *et al.* [48,49] and Khulief *et al.* [50]. Berlioz *et al.* [5] studied the critical rotary speed of the drillstring using parametric instability of the rotating drillstring.

Wellbore contact must be predicted to fully understand the severity of coupled axial-lateral vibrations. Modeling schemes for impulsive motion of elastodynamic systems in FEM analysis fall into two categories. The first approach is based on a smooth impulsive force distribution during the impact interval, where the impact force is presented by the force-displacement law and contact location is modeled by an interface spring [51]. The other approach, which is numerically more efficient [52], is based on an impulse-momentum balance equation, since the impulsive force causes an abrupt change in system velocities or momentum [20]. Melakhessou *et al.* [28] modeled only the contact point of the drillstring using the Coulomb friction law. Khulief *et al.* [51] implemented a continuous force-displacement law and the energy balance relation at the contact point in their multi-body FEM model for axial-bending and torsional-bending drillstring vibrations. He suggested this method as an efficient way to prevent jump discontinuities in numerical solution of the continuous models. As well, Liao *et al.* [53] developed a reduced order FEM model at the contact point of the drillstring and wellbore. Based on a

qualitative analysis, an optimum friction coefficient value for the stable drillstring behavior at the contact point was suggested.

The damping effect of the mud on the drillstring dynamic analysis is an important parameter in the transverse vibration of the drillstring. The effect of drillstring mud flow on the lateral response, load carrying capacity, and critical rotary speeds were investigated by Zhang *et al.* [54] and Ritto *et al.* [55], respectively. Zhang *et al.* [54] found the critical flow rate for pipe buckling and investigated a relationship for the length of the pipe section and flow rate in the drillpipe buckling analysis. Effect of fluid density on the pipe buckling was also studied. Ritto *et al.* [55] analyzed the influence of mud flow on the natural frequencies and dynamic behavior of the drillstring. They investigated that the axial and torsional behaviours are not sensitive to the mud flow. When the fluid flow was considered in the dynamic equations, the lateral dynamic response was a bit larger initially. However, steady-state response was unchanged. Khulief *et al.* [31] modeled the fluidelastic effects of the mud on the drillstring, using a previously developed semi-analytical approach. The early model was modified, since it was valid for annulus gap ratios less than 0.1 (the annulus gap ratio is greater than 0.1 in drilling applications). They developed the fluidelastic force equations in two directions (normal and tangential) for the element of the drillstring. The force equations were based on the density of mud, radial clearance, deflection of the string element and the rotary speed. The developed equations were then implemented in an FEM model and the model was tuned based on a laboratory test rig results. The viscous lateral damping behavior is mainly considered as Rayleigh damping in FEM models, which implements damping in both low and high

frequency ranges. The damping factor in this method is related to the mass and stiffness matrix developed in the FEM model of a structure [21]. Apostol *et al.* [47] developed an equation which converts the Rayleigh damping to the critical damping in each mode, by relating the mass and stiffness proportional damping values to the natural frequency of each mode. Spanos *et al.* [56] developed another equation for finding the critical damping ratio based on the frequency of each mode and the density of the mud and verified the equation with test results. The mass proportional damping causes damping at each node in the FEM models which is related to the absolute velocity of that node. This is in agreement with the hydrodynamic drag damping model which is used in analytical studies of the drillstring vibrations, since both of them are velocity proportional damping models.

In the FEM model developed in this study, mud damping, torque, spatially varying axial load, and gyroscopic rotary effects are considered, and the boundary conditions are the same as in the analytical model. Having two distinct models (analytical and numerical) allows them to be validated against each other. While the analytical model offers a fast convergence rate for sensitivity analysis, the finite element model is easier to reconfigure for new boundary conditions, force or displacement excitations, and BHA geometry, and also allows extraction of nodal force, displacement, stress, and reactions at any desired points as outputs without extra computations.

7.4 Analytical Modeling: Derivation of Governing Equations

The beamlike drillstring structure with a high slenderness ratio is modeled using Euler-Bernoulli beam theory. The drillstring in this study includes a span close to the bit (three

metres) with the vibration-generator tool, a three-span BHA (with different length for each span), a shock sub between the bit span and the BHA, a long pipe section and an equivalent mass-spring- damper on top, representing derrick, cables, and the traveling block. A wellbore is assumed around the drillstring and the annulus between the drillstring and wellbore is filled with mud. Two orthogonal lateral directions ("v" and "w"), in addition to the axial motion "u" are also assumed. A schematic diagram of the drillstring is shown in Figure 7.1.

The effects of the hook load, WOB, mud hydrostatic force and self weight are presented as a spatially-varying axial force along the drillstring [20,26]. The varying axial force in the collar and pipe sections are (variables are defined in Table 7.2):

$$\begin{aligned}
 F_{collar} &= \rho_{collar} \cdot A_{collar} \cdot g \cdot z - WOB - \rho_{mud} \cdot g \cdot l \cdot A_{collar} \\
 F_{pipe} &= -WOB - \rho_{mud} \cdot g \cdot l \cdot A_{collar} + \rho_{mud} \cdot g \cdot l_p (A_{collar} - A_{pipe}) + \\
 &\rho_{collar} \cdot A_{collar} \cdot g \cdot l_c + \rho_{pipe} \cdot A_{pipe} \cdot g \cdot (z - l_c)
 \end{aligned} \tag{7.1}$$

Since the method of the "Bypassing PDEs" will be implemented, the conventional form of the energy equations is required. In the following equations, the energy terms for the first span of the BHA will be shown and for the remaining BHA spans and the pipe section, they will be the same, except for a change in the integration domain (the reference point for all equations and comparison functions is at the bit). The nomenclature for motion of each span and the corresponding comparison function is shown in Table 7.1, where "i" represents the mode number:

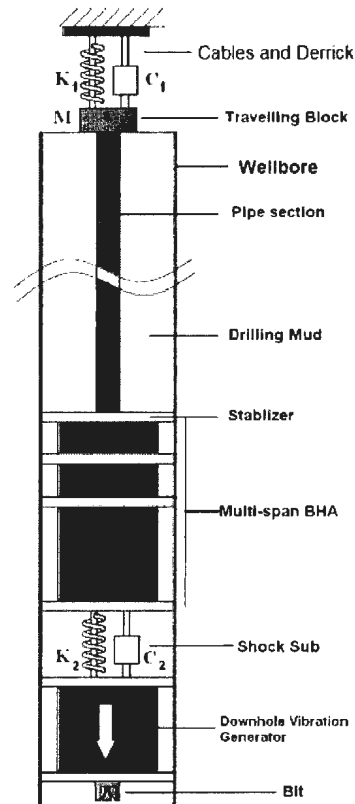


Figure 7.1: Schematic of the drillstring inside the wellbore

Table 7.1: Nomenclature of motion and comparison functions for each section of the drillstring

Direction of motion	Axial		Lateral		Lateral	
	motion	Comparison function	motion	Comparison function	motion	Comparison function
3 m span	$u_1(z, t)$	$\theta_i(z)$	$v_1(z, t)$	$\varphi_i(z)$	$w_1(z, t)$	$\varphi_i(z)$
1st span of BHA	$u_2(z, t)$	$\psi_i(z)$	$v_2(z, t)$	$\sigma_i(z)$	$w_2(z, t)$	$\sigma_i(z)$
2nd span of BHA	$u_3(z, t)$	$\psi_i(z)$	$v_3(z, t)$	$X_i(z)$	$w_3(z, t)$	$X_i(z)$
3rd span of BHA	$u_4(z, t)$	$\psi_i(z)$	$v_4(z, t)$	$\Gamma_i(z)$	$w_4(z, t)$	$\Gamma_i(z)$
Pipe section	$u_5(z, t)$	$\Delta_i(z)$	$v_5(z, t)$	$\epsilon_i(z)$	$w_5(z, t)$	$\epsilon_i(z)$

The kinetic and strain energy for the first span of the BHA is:

$$\begin{aligned}
 \text{Kinetic} + \text{potential} = & \frac{1}{2} \int_{l_1}^{l_2} \rho_{\text{collar}} A_{\text{collar}} \left[\left(\frac{\partial}{\partial t} u_2(z,t) \right)^2 + \left(\frac{\partial}{\partial t} v_2(z,t) \right)^2 + \left(\frac{\partial}{\partial t} w_2(z,t) \right)^2 \right. \\
 & \left. + \omega \left(v_2(z,t)^2 + w_2(z,t)^2 \right)^2 \right. \\
 & \left. + 2\omega \left(v_2(z,t) \left(\frac{\partial}{\partial t} w_2(z,t) \right) - w_2(z,t) \left(\frac{\partial}{\partial t} v_2(z,t) \right) \right) \right] dz \quad (7.2) \\
 & + \frac{1}{2} \int_{l_1}^{l_2} \left[EI_{\text{collar}} \left(\left(\frac{\partial^2}{\partial z^2} v_2(z,t) \right)^2 + \left(\frac{\partial^2}{\partial z^2} w_2(z,t) \right)^2 \right) + EA_{\text{collar}} \left(\frac{\partial}{\partial z} u_2(z,t) + \frac{1}{2} \left(\frac{\partial}{\partial z} v_2(z,t) \right)^2 \right)^2 \right. \\
 & \left. + \frac{1}{2} \left(\frac{\partial}{\partial z} w_2(z,t) \right)^2 \right] dz
 \end{aligned}$$

where v_2 and w_2 are two orthogonal lateral motions and u_2 is the axial motion of the first span of the BHA. The first three terms in the first integral are the kinetic energy terms due to the translational motion and the next three terms are rotational kinetic energy associated with the gyroscopic effect. The first term in the second integral (strain energy) represents the elastic stiffening, while the second term captures axial stiffening due to the gravitational field, which accounts for the stiffening effect of tension in the pipe section and compression on the collar section and shows the coupling between the axial and flexural deformations. The quadratic nonlinear term retained in the equation is due to geometric nonlinearity.

The work done by the driving torque can be expressed as [20]:

$$W_{\text{torque}} = \frac{1}{2} T \left(\int_{l_1}^{l_2} \left(\left(\frac{\partial^2}{\partial z^2} v_2(z,t) \right) \left(\frac{\partial}{\partial z} w_2(z,t) \right) + \left(\frac{\partial^2}{\partial z^2} w_2(z,t) \right) \left(\frac{\partial}{\partial z} v_2(z,t) \right) \right) dz \right) \quad (7.3)$$

which shows the coupling role of the driving torque in two orthogonal lateral directions.

The energy term due to the spatially varying axial force in the first span of the collar section is:

$$W_{axial-force} = -\frac{1}{2} \int_{l_1}^{l_2} F_{collar} \left(\left(\frac{\partial}{\partial z} v_2(z,t) \right)^2 + \left(\frac{\partial}{\partial z} w_2(z,t) \right)^2 \right) dz \quad (7.4)$$

The F_{collar} term will be changed to F_{pipe} while finding the corresponding energy term due to the axial force in the pipe section (using the formulation of Equation 7.1). The mud damping force as a result of the hydrostatic drag force is in the opposite direction of motion and is a quadratic function of velocity [34]. The dissipation energy of the mud is:

$$W_{mud-damping} = \rho_{mud} C_D R_{collar} \int_{l_1}^{l_2} \sqrt{\left(\frac{\partial}{\partial t} v_2(z,t) \right)^2 + \left(\frac{\partial}{\partial t} w_2(z,t) \right)^2} \cdot \left(\frac{\partial}{\partial t} v_2(z,t) + \frac{\partial}{\partial t} w_2(z,t) \right) dz \quad (7.5)$$

The contact energy in the first span is approximated based on Hertzian contact theory using a piecewise function [19]. In the following equation, b_{cl} is the borehole clearance and K_h is the contact stiffness which is related to the material and geometry of the contact point. " r " is the radial displacement at the contact point:

$$W_{contact-energy} = - \begin{pmatrix} K_h (r - b_{cl})^{3/2} & b_{cl} \leq |r| \\ 0 & otherwise \end{pmatrix} r \quad (7.6)$$

The energy term due to the vibration generator on the three-metre span close to the bit is:

$$W_{vibration} = \frac{1}{2} \int_0^{l_1} 2F_{vibration} \sin(\Omega t) \left(\frac{\partial}{\partial z} u_1(z, t) + \left(\frac{\partial}{\partial z} w_1(z, t) \right)^2 + \left(\frac{\partial}{\partial z} v_1(z, t) \right)^2 \right) dz \quad (7.7)$$

where $F_{vibration}$ is the amplitude and Ω is the working frequency of the force generated by the downhole vibration tool. The energy equations for the discrete mass and springs of the system are:

$$Energy_{spring-mass} = \frac{1}{2} K_2 (u_2(l_1, t) - u_1(l_1, t))^2 + \frac{1}{2} K_1 (u_5(l_5, t))^2 + \frac{1}{2} M \left(\frac{\partial^2}{\partial t^2} u_5(l_5, t) \right) \quad (7.8)$$

K_1 and K_2 are spring stiffness values of the hoisting cable and the shock sub, respectively, and M is the mass of the traveling block. The damping energy of the system due to discrete dashpot elements is:

$$Energy_{damping} = \frac{1}{2} C_1 \left(\frac{\partial}{\partial t} u_5(l_5, t) \right)^2 + \frac{1}{2} C_2 \left(\frac{\partial}{\partial t} u_2(l_1, t) - \left(\frac{\partial}{\partial t} u_1(l_1, t) \right) \right)^2 \quad (7.9)$$

The Lagrangian ($L=T-V$) of the system is:

$$\begin{aligned}
& \left\{ \frac{1}{2} \int_{l_{i-1}}^{l_i} \rho_{collar} A_{collar} \left(\left(\frac{\partial}{\partial t} u_i(z,t) \right)^2 + \left(\frac{\partial}{\partial t} v_i(z,t) \right)^2 + \left(\frac{\partial}{\partial t} w_i(z,t) \right)^2 \right. \right. \\
& \left. \left. + \omega \left(v_i^2(z,t) + w_i^2(z,t) \right) + 2\omega \left(v_i(z,t) \frac{\partial}{\partial t} w_i(z,t) \right) \right\} dz \\
& - \frac{1}{2} \int_{l_{i-1}}^{l_i} (EI_{collar} \left(\left(\frac{\partial^2}{\partial z^2} v_i(z,t) \right)^2 + \left(\frac{\partial^2}{\partial z^2} w_i(z,t) \right)^2 \right) \\
L = & \sum_{i=1}^5 \left(EA_{collar} \left(\left(\frac{\partial}{\partial z} u_i(z,t) + \left(\frac{\partial}{\partial z} v_i(z,t) \right)^2 \right) + \frac{1}{2} \left(\frac{\partial}{\partial z} w_i(z,t) \right)^2 \right) dz \right. \\
& \left. - \frac{1}{2} T \int_{l_{i-1}}^{l_i} \left(\left(\frac{\partial^2}{\partial z^2} v_i(z,t) \right) \left(\frac{\partial}{\partial z} w_i(z,t) \right) + \left(\frac{\partial^2}{\partial z^2} w_i(z,t) \right) \left(\frac{\partial}{\partial z} v_i(z,t) \right) \right) dz \right. \\
& \left. - \frac{1}{2} \int_{l_{i-1}}^{l_i} F_{collar} \left(\left(\frac{\partial}{\partial z} v_i(z,t) \right)^2 + \left(\frac{\partial}{\partial z} w_i(z,t) \right)^2 \right) dz \right\} \\
& - \frac{1}{2} \int_0^{l_i} 2F_{vibration} \sin(\Omega t) \left(\frac{\partial}{\partial z} u_i(z,t) + \left(\frac{\partial}{\partial z} v_i(z,t) \right)^2 + \left(\frac{\partial}{\partial z} w_i(z,t) \right)^2 \right) dz \\
& + \frac{1}{2} K_2 (u_2(l_1,t) - u_1(l_1,t)) + \frac{1}{2} K_1 (u_5(l_5,t))^2 + \frac{1}{2} M \left(\frac{\partial^2}{\partial z^2} u_5(l_5,t) \right)
\end{aligned} \tag{7.10}$$

The damping energy of the system is:

$$\begin{aligned}
Damping\ energy = & \sum_{i=1}^5 \left\{ \rho_{mud} C_D R_{collar} \left(\int_{l_{i-1}}^{l_i} \sqrt{\left(\frac{\partial}{\partial t} v_i(z,t) \right)^2 + \left(\frac{\partial}{\partial t} w_i(z,t) \right)^2} \right. \right. \\
& \left. \left. \left(\frac{\partial}{\partial t} v_i(z,t) - \frac{\partial}{\partial t} w_i(z,t) \right) dz \right\} \right. \\
& \left. + \frac{1}{2} C_1 \left(\frac{\partial}{\partial t} u_5(l_5,t) \right)^2 + \frac{1}{2} C_2 \left(\frac{\partial}{\partial t} u_2(l_1,t) - \frac{\partial}{\partial t} u_1(l_1,t) \right)^2 \right.
\end{aligned} \tag{7.11}$$

where l_0 represents $z=0$ in the lower integration limit when $i=1$. For $i=5$ (Lagrangian and damping of the pipe section) the F_{collar} term will be changed to F_{pipe} and

$\rho_{collar} A_{collar}$, I_{collar} , R_{collar} should be changed to these values for the pipe section.

At this step of the "Bypassing PDEs" method, the expanded Galerkin's method is applied to the equations. Therefore, "u", "v" and "w" are assumed as comparison functions multiplied by mode participation factors for each specific span.

$$\begin{aligned}
 u_1(z, t) &= \sum_{r=1}^4 \theta_r(z) \cdot \lambda_r(t) & u_2(z, t) &= \sum_{r=1}^4 \psi_r(z) \cdot \lambda_r(t) \\
 v_1(z, t) &= \sum_{r=1}^4 \phi_r(z) \cdot \eta_r(t) & v_2(z, t) &= \sum_{r=1}^4 \sigma_r(z) \cdot \eta_r(t) \\
 w_1(z, t) &= \sum_{r=1}^4 \varphi_r(z) \cdot \delta_r(t) & w_2(z, t) &= \sum_{r=1}^4 \tau_r(z) \cdot \delta_r(t) \\
 \\
 u_3(z, t) &= \sum_{r=1}^4 \psi_r(z) \cdot \lambda_r(t) & u_4(z, t) &= \sum_{r=1}^4 \psi_r(z) \cdot \lambda_r(t) \\
 v_3(z, t) &= \sum_{r=1}^4 \chi_r(z) \cdot \eta_r(t) & v_4(z, t) &= \sum_{r=1}^4 \Gamma_r(z) \cdot \eta_r(t) \\
 w_3(z, t) &= \sum_{r=1}^4 \chi_r(z) \cdot \delta_r(t) & w_4(z, t) &= \sum_{r=1}^4 \Gamma_r(z) \cdot \delta_r(t) \\
 \\
 u_5(z, t) &= \sum_{r=1}^4 \Delta_r(z) \cdot \lambda_r(t) \\
 v_5(z, t) &= \sum_{r=1}^4 \varepsilon_r(z) \cdot \eta_r(t) \\
 w_5(z, t) &= \sum_{r=1}^4 \varepsilon_r(z) \cdot \delta_r(t)
 \end{aligned} \tag{7.12}$$

In the above equations, the comparison functions defined in Table 7.1 ($\lambda_r(t)$, $\eta_r(t)$ and $\delta_r(t)$) are 12 mode participation factors for axial motion "u", and lateral motions "v" and "w", respectively. The subscript "r" depends on the retained modes according to the frequency range of interest. For this problem the first four modes will be retained to conduct the multi-mode analysis.

The expanded Galerkin's functions are substituted into the expressions for the Lagrangian and damping energy of the system. Precise comparison functions are required to accurately integrate over the space domain. The axial comparison functions are required to study the effect of the shock sub on the reduction of force and displacement amplitude of the drillstring. In the following section, the derivation of the axial comparison functions based on the assumed realistic BCs is discussed. Moreover, the lateral comparison functions are required in order to precisely study the contact behavior of the BHA. The BHA is assumed as a three-span beam with pinned-pinned boundary conditions at the location of the stabilizer, and the three-metre span close to the bit is assumed as a pinned-pinned single span, since it is constrained by the stabilizers at the top and bottom of the span. Then, classical solution of the transverse vibration are assumed for each span and the resulting 12 unknowns in the assumed functions are found based on the twelve auxiliary boundary equations. Six boundary conditions are zero deflections at the supports, while two boundary conditions are zero bending moments at both ends. The remaining four boundary conditions are slope and bending compatibility equations at the two middle supports. For the nontrivial solution of the system of equations, the determinant of the coefficient matrix is set to zero. The result is the frequency equation, which is solved numerically, using the Newton–Raphson algorithm. The first four roots of the frequency equation are substituted in 12 auxiliary equations to find the first four modes of each span, namely 12 mode shapes. The reader is referred to a recent publication by the authors [20] for a detailed derivation of the exact lateral mode shapes of a three-span beam, which will be implemented as the comparison function for the

three-span BHA. The first four normalized mode shapes of the entire drillstring in the lateral direction are shown in Figure 7.2. The transition from the thick-walled collars to the thin drill pipe occurs at 85 m.

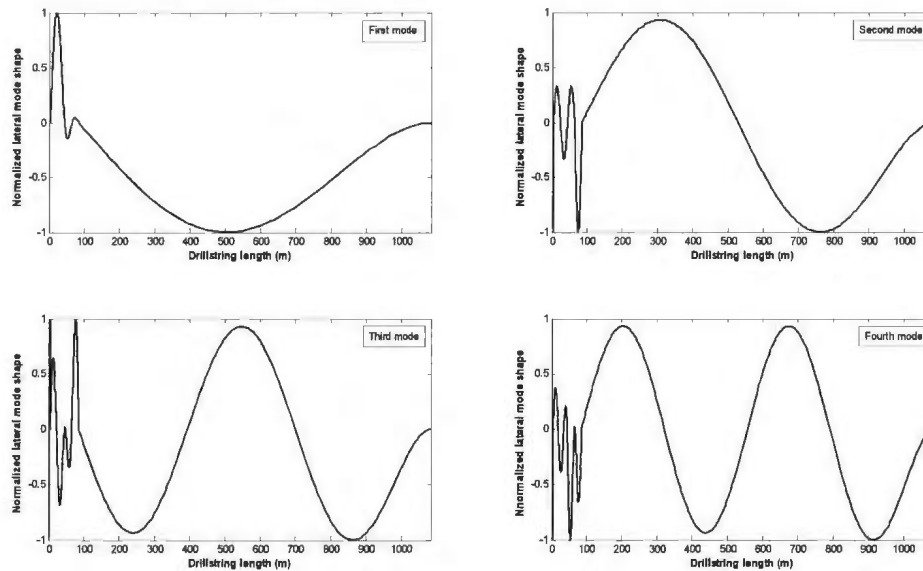


Figure 7.2: Normalized lateral mode shapes for the entire drillstring

7.4.1 Eigenfunctions and Eigenfrequencies of the Axial Motion of the Drillstring

The eigenfunctions of a drillstring are required in order to apply them as comparison functions in the expanded Galerkin's method. These eigenfunctions are computed analytically for a system of hybrid continuous (the entire step-beam drillstring) and discrete elements (shock sub elements and equivalent mass-spring-damper of the top hoisting system). Based on the schematic of Figure 7.2, the axial mode shape of the span close to the bit is assumed as u_1 , while the axial displacement for the BHA is considered as u_2 . The axial displacement for the pipe section is assumed as u_3 , and the origin ($z=0$) is at the bit.

The boundary condition at the bit location is a sinusoidal displacement, with the same frequency as the rotary speed of the drillstring. An equivalent mass-spring damper is used at the rig surface.

The equation governing the longitudinal motion of the bar is:

$$\rho A \frac{\partial^2 u(z, t)}{\partial t^2} = EA \frac{\partial^2 u(z, t)}{\partial z^2} \quad (7.13)$$

A general form of the solution to the above equation for u_1 , u_2 and u_3 in the complex plane are assumed as:

$$\begin{aligned} u_1 &= \left(A \sinh\left(\frac{s \cdot z}{speed_1}\right) + B \cosh\left(\frac{s \cdot z}{speed_1}\right) \right) e^{st} \\ u_2 &= \left(C \sinh\left(\frac{s \cdot z}{speed_1}\right) + D \cosh\left(\frac{s \cdot z}{speed_1}\right) \right) e^{st} \\ u_3 &= \left(E \sinh\left(\frac{s \cdot z}{speed_2}\right) + F \cosh\left(\frac{s \cdot z}{speed_2}\right) \right) e^{st} \end{aligned} \quad (7.14)$$

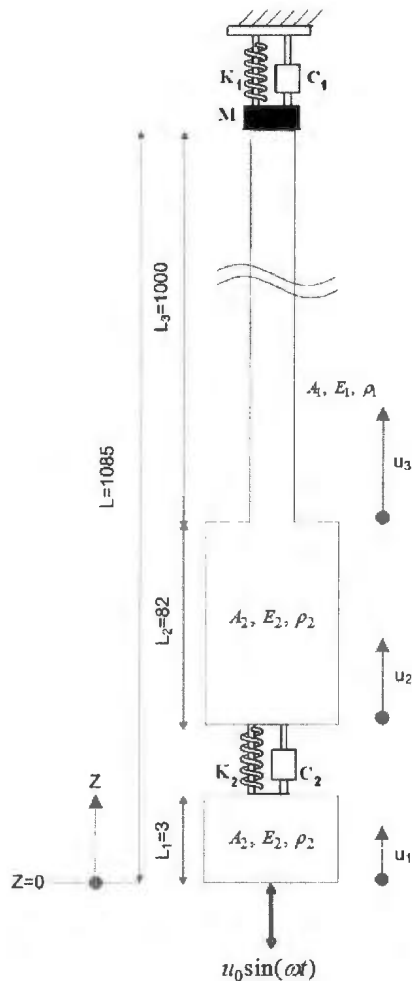


Figure 7.3: Schematic of the drillstring in the axial motion

where $speed_1$ and $speed_2$ are wave speeds in the BHA section and the pipe section, respectively. A, B, C, D, E and F are six complex unknowns which could be determined using the boundary conditions. The real terms are of interest.

At the bit location ($z=0$), the bar is subjected to base motion (bit-rock displacement function). In order to simplify the boundary conditions of u_1 , A new variable ($v(z,t)$) is

defined, that denotes the displacement of any point on the three-meter span relative to the base:

$$v(z, t) = u_1(z, t) - \text{base motion} = u_1(z, t) - u_0 \sin(\omega t) \quad (7.15)$$

If the above equation is implemented in the general form of the bar axial vibration equation (Equation 7.13), then:

$$\rho A \frac{\partial^2 v(z, t)}{\partial t^2} = EA \frac{\partial^2 v(z, t)}{\partial z^2} - \rho A \frac{\partial^2 (u_0 \sin(\omega t))}{\partial t^2} \quad (7.16)$$

The last term on the right-hand side is the equivalent distributed loading, induced by the base motion. Therefore, $v(z, t)$ is assumed instead of $u_1(z, t)$ to solve the set of equations and the equivalent distributed loading is assumed as an energy term in the analytical equations for the three-meter span. The boundary conditions are as follows:

$$\begin{aligned} v(0, t) &= 0 & Z=0 \\ A_2 \cdot E_2 \frac{\partial v(L_1, t)}{\partial z} &= K_2 \cdot (u_2(L_1, t) - v(L_1, t)) + C_2 \left(\frac{\partial u_2(L_1, t)}{\partial t} - \frac{\partial v(L_1, t)}{\partial t} \right) & Z=L_1 \\ A_2 \cdot E_2 \frac{\partial u_2(L_1, t)}{\partial z} &= K_2 \cdot (u_2(L_1, t) - v(L_1, t)) + C_2 \left(\frac{\partial u_2(L_1, t)}{\partial t} - \frac{\partial v(L_1, t)}{\partial t} \right) & Z=L_1 \\ A_2 \cdot E_2 \frac{\partial u_2(L_1 + L_2, t)}{\partial z} &= A_1 \cdot E_1 \frac{\partial u_3(L_1 + L_2, t)}{\partial z} & Z=L_1 + L_2 \\ u_2(L_1 + L_2, t) &= u_3(L_1 + L_2, t) & Z=L_1 + L_2 \\ A_1 \cdot E_1 \frac{\partial u_3(L, t)}{\partial z} &= -K_1 \cdot u_3(L, t) - C_1 \cdot \frac{\partial u_3(L, t)}{\partial t} - M \cdot \frac{\partial^2 u_3(L, t)}{\partial t^2} & Z=L \end{aligned} \quad (7.17)$$

L_1 , L_2 and L are three meters, 82 meters and 1085 meters, respectively. The first BC is the result of change of the variable from $u(z, t)$ to $v(z, t)$, where at the bit location the

displacement is zero. The second and the third BCs are the continuity of the force at the location of the shock sub and the fourth and fifth BCs are continuity of displacement and force at the pipe-collar junction. The last BC is the continuity of the force at the location of discrete mass-spring-damper. Consequently, implementing the above boundary conditions in the general solution equations (Equation 7.14) results in a system of six equations and six unknowns. For the nontrivial solution of the system of equations, the determinant of the coefficient matrix is set to zero. The result is the frequency equation:

$$\begin{aligned}
&((-4.21 \cdot 10^{22} s^2 (s^2 + 0.44 \cdot 10^{-3}) \sinh(0.21s) - 7.70 \cdot 10^{20} s^3 (s^2 + 2.34) \cosh(0.21s)) \\
&\cosh(0.12 \cdot 10^{-1} s)^2 + (-3.54 \cdot 10^{21}) s^3 (s^2 + 0.66) \sinh(0.21s) + (-1.94 \cdot 10^{23} s^4 + 1.51 \cdot 10^{19} s^2) \\
&\cosh(0.21s)) \sinh(0.12 \cdot 10^{-1} s) \cosh(0.12 \cdot 10^{-1} s) + 2.36 \cdot 10^{23} s^2 (s^2 + 0.14 \cdot 10^{-4}) \sinh(0.21s) \\
&+ 4.31 \cdot 10^{21} s^3 (s^2 + 0.96) \cosh(0.21s) \sinh(0.12 \cdot 10^{-1} s)^2 \cosh(0.39 \cdot 10^{-3} s) \\
&+ ((4.31 \cdot 10^{21} s^3 (s^2 + 0.91) \sinh(0.21s) + 2.36 \cdot 10^{23} s^4 \cosh(0.21s) \sinh(0.39 \cdot 10^{-3} s) \cosh(0.12 \cdot 10^{-1} s)^2 \\
&+ (-1.94 \cdot 10^{23} s^4 \sinh(0.21s) - 3.54 \cdot 10^{21} s^3 (s^2 + 0.91) \cosh(0.21s)) \sinh(0.39 \cdot 10^{-3} s) \\
&\sinh(0.12 \cdot 10^{-1} s) \cosh(0.12 \cdot 10^{-1} s) \sinh(0.39 \cdot 10^{-3} s) \sinh(0.12 \cdot 10^{-1} s) \cosh(0.12 \cdot 10^{-1} s) \\
&+ (-7.70 \cdot 10^{20} s^3 (s^2 + 0.91) \sinh(0.21s) - 4.21 \cdot 10^{22} s^4 \cosh(0.21s)) \sinh(0.39 \cdot 10^{-3} s) \sinh(0.12 \cdot 10^{-1} s)^2 \\
&\cosh(0.39 \cdot 10^{-3} s) + (2.01 \cdot 10^{19} s^2 (s^2 + 0.91) \sinh(0.21s) + 1.1 \cdot 10^{21} s^3 \cosh(0.21s)) \sinh(0.39 \cdot 10^{-3} s)^2 \\
&\cosh(0.12 \cdot 10^{-1} s)^2 - 9.04 \cdot 10^{20} s^3 \sinh(0.21s) - 1.65 \cdot 10^{19} s^2 (s^2 + 0.91) \cosh(0.21s)) \sinh(0.39 \cdot 10^{-3} s)^2 \\
&\sinh(0.12 \cdot 10^{-1} s) \cosh(0.12 \cdot 10^{-1} s) + (-3.59 \cdot 10^{18} s^2 (s^2 + 0.91) \sinh(0.21s) \\
&- 1.96 \cdot 10^{20} s^3 \cosh(0.21s)) \sinh(0.39 \cdot 10^{-3} s)^2 \sinh(0.12 \cdot 10^{-1} s)^2 = 0
\end{aligned} \tag{7.18}$$

In order to solve the above equation, since the roots have complex values, s is defined as $s = p + iq$. The first four values of s are determined using the Bisection method and the results are confirmed with the Newton-Raphson algorithm as well. The first four values of s are: $0.24i$, $3.48i$, $11.76i$ and $24.94i$ and are substituted back in the six boundary condition equations to find the first four mode shapes of each segment. The first four axial mode shapes of the entire drillstring are shown in Figure 7.4a. Since the shock

sub is less stiff compared to its equivalent collar length, there is a discontinuity at the location of shock sub ($z=3$). This discontinuity is shown in Figure 7.4b.

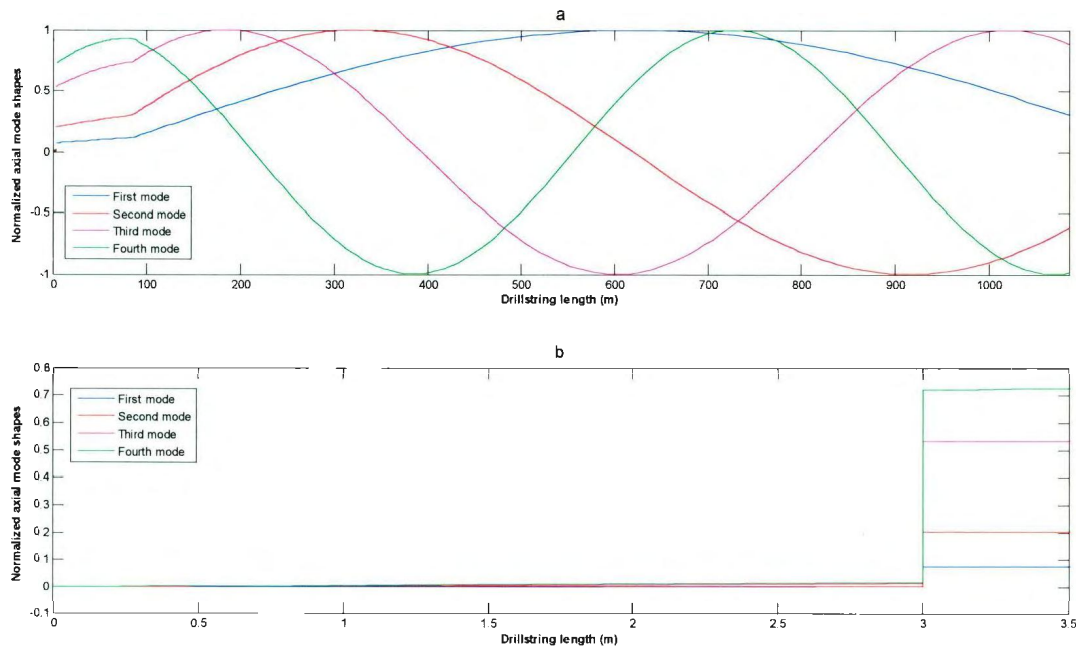


Figure 7.4: Normalized axial mode shapes of the entire drillstring

7.4.2 The Lagrange's Equation and Equations of Motion

The axial and lateral comparison functions are substituted back in the Lagrangian of the system and damping energy equation. Integrating the Lagrangian over the drillstring length, using the mode orthogonality relations, results in a time domain Lagrangian of each span. The Lagrange's equation is then implemented for each mode participation factor.

$$\frac{d}{dt} \left(\frac{\partial L}{\partial \dot{q}_i} \right) - \frac{\partial L}{\partial q_i} + \left(\frac{\partial D.E.}{\partial \dot{q}_i} \right) = 0 \quad (7.19)$$

where L is the Lagrangian of the system, $D.E.$ is the dissipated energy of the system and q_i is the generalized coordinate variable. The result is a set of twelve second-order coupled nonlinear time differential equations. The resulting stiff system is solved using a fixed-step fourth-order Runge-Kutta method and the dynamic time step reduction strategy is not implemented because it became unstable due to discontinuities in the response. The time step was set to 10^{-11} s which is well below the smallest natural period in the system. The numerical results for each generalized coordinate were stored and substituted back into the expanded Galerkin's functions for each direction to generate deflection and velocity time history of any desired point, including the contact locations. The mathematical model and the above procedure have been implemented in Maple[®]. The characteristics and numerical values used in this study are shown in Table 7.2.

Table 7.2: Numerical values used in the simulations

$T = 4000$	Driving torque (N.m)	A_{pipe} $= 0.00471$	Pipe cross sectional area (m^2)
$\rho_{mud} = 1500$	Mud density (Kg/m^3)	A_{collar} $= 0.02639$	Collar cross sectional area (m^2)
$C_D = 1$	Hydrodynamic drag coefficient	$F_{Vibration}=20000$	Vibration generator force (N)
$K_h = 6.78 * 10^{11}$	Hertzian stiffness ($N.m^{-1.5}$)	$E = 210 * 10^9$	Young's modulus (Pa)
$WOB = 50000$	Weight on bit (N)	$b_{cl} = 0.1$	Borehole clearance (m)
I_{pipe} $= 13.31 * 10^{-6}$	Area moment of inertia (pipe section) m^4	I_{collar} $= 76.52 * 10^{-6}$	Area moment of inertia (collar section) m^4
$l_1=3$	Span length of the downhole tool (m)	$\rho_{pipe} = \rho_{collar}$ $= 7860$	Pipe and Collar density (kg/m^3)
$l_2=44$	Z coordinate of the top point of the BHA first span (m)	$g=9.81$	Gravity acceleration (m/s^2)

$l_3=64.5$	Z coordinate of the top point of the BHA second span (m)	$R_{collar} = 0.1$	Collar outside diameter (m)
$l_c=l_4=85$	Z coordinate of the top point of the BHA third span	$l_p=1000$	Length of the pipe section (m)
$l=l_5=1085$	Z coordinate of the top point of the pipe section (m)	$u_0 = 0.003$	Bit displacement amplitude (m)
$\omega = 10.47$	Drillstring rotary speed (rad/s)	$M = 3500$	Mass of the traveling block (kg)
$\Omega = 95.50$	Frequency of the downhole vibration generator tool (Hz)	$speed_1 = speed_2 = 5168.90$	Wave speed in the pipe and collar section ($\sqrt{\frac{N.m}{Kg}}$)
$K_1 = 9.2 * 10^6$	Stiffness of the top cable (N/m)	$K_2 = 7.6 * 10^6$	Stiffness of the shock sub (N/m)
$C_1 = 3 * 10^4$	Damping of the top cable (N.s/m)	$C_2 = 4 * 10^3$	Damping of the shock sub (N.s/m)

7.5 Dynamic Finite Element Model of the Drillstring

The ABAQUS FEM *Explicit* solver package[®] is used to develop the dynamic FEM model. The FEM model is capable of modal characteristic extraction, as well as the dynamic analysis of the entire drillstring. The modal characteristics are derived using eigenvalue extraction with the linear perturbation procedure. The dynamic analysis extracts the displacement and force response of the drillstring for any set of initial conditions or forcing functions.

The drillstring is assumed as a beam with two cross sections (collars and pipes). A three-segment planar wire shape sketch with hollow pipe profiles is used to model the entire drillstring. The "Hermite cubic" beam element is used, which does not account for the shear flexibility, although axial strain is considered. This is the proper element for

modeling slender Euler-Bernoulli beams, in order to be consistent with the derived analytical model. Furthermore, the orientation of the beam cross-section must be determined in the global Cartesian system prior to the analysis. A three-dimensional extruded shell is assumed for the wellbore. The discrete dashpot and spring elements are modeled using the ABAQUS *Explicit* solver package elements "DASHPOTA" and "SPRINGA". These two elements introduce stiffness and damping between two degrees of freedom without any associated mass. The nodes which are attached to the spring element must have some mass contribution from adjacent elements. If a stiff element is selected, then the *Explicit* time step is appropriate for maintaining the stability condition. Since the dashpot is used in parallel with a spring element, the stable time increment is not affected. As well, the drillstring and the wellbore are modeled as a single assembly in the global coordinate system.

The explicit solver package (integration by the central difference operator) is preferred to the implicit solver package (direct time integration) in the developed model. The explicit solver package is computationally more efficient in the case of large structures with nonlinearities, which capture high speed dynamic events such as successive contacts with the wellbore with many small time increments to achieve a high-resolution response.

The kinematic friction is preferred to the penalty contact algorithm in the *Explicit* solver package to model the drillstring-wellbore contact. The kinematic friction algorithm has a corrector algorithm which results in no overclosure at the end of each time increment, while in the penalty algorithm the overclosure always exists at the end of each increment.

This overclosure does not cause any problem in large deformation problems, while in the small deformation problems driven by Hertzian contact theory, the results of the two algorithms are not the same due to the overclosure. In such problems the kinematic contact algorithm is preferred to the other one. Since Hertzian contact was also assumed in the derivation of the analytical model, the kinematic friction algorithm is implemented in the FEM model. Another advantage of the kinematic friction algorithm is that time steps are not reduced during contact, while in the penalty algorithm the stable time increment is reduced. Slow convergence and dependency on the mesh size are other drawbacks of the penalty algorithm. Nonetheless, sliding friction is not included, as it has not significantly impacted the results in other studies [19,31,51] and if included will seriously degrade computation time.

The general kinematic contact and the contact pair algorithms are the commonly used methods to define the surfaces in contact. While in the other algorithms the contact surfaces are required to be determined prior to the analysis, the surfaces in the kinematic contact can span any disconnected region in the model. Hence, the general kinematic contact algorithm is selected in the developed model to account for multiple contact points in the BHA, and any point on the drillstring is capable of having contact with the inner surface of the wellbore. This capability of the FEM model will be used to verify the assumption of the contact point locations assumed in the analytical model.

The mud damping effect plays an important role in the study of lateral vibrations of the BHA and irregularity and severity of motion at the contact points. The mud damping

behavior in this study is considered as Rayleigh damping (a quadratic expression for the energy dissipation rate), which is proportional to the mass and stiffness of each mode. In the absence of a major source of dissipation, such as inelastic material, Rayleigh damping is appropriate with the *Explicit* dynamic package (e.g., pipes with contact). In particular, it provides a convenient abstraction for damping low-frequency range behavior (mass dependent) and higher-frequency range behavior (stiffness dependent). The mass proportional damping factor introduces damping forces that are caused by absolute velocities at each node: this phenomenon could model a structure moving through a viscous fluid (such as drillstring inside mud), in a way such that any point in the model triggers damping forces [21]. This is in agreement with the hydrodynamic drag damping model which is used in analytical studies of the drillstring vibrations, since both of them are velocity proportional damping models. The Rayleigh damping factors are determined and tuned in the developed FEM model. Another advantage of the mass proportional damping is that the stability limit in the final numerical solution step is not sensitive to this factor, while the stiffness proportional damping reduces the stability limit of the numerical solution [45].

The computation cost is proportional to the selected time increments and number of elements, and is roughly inversely proportional to the smallest element dimension. Time increments should be defined properly to achieve efficient computation and capture dynamics in the highest frequency range of interest. The stability limit dictates the maximum time increment used by ABAQUS *Explicit*. The stability limit is defined in terms of the highest frequency of the system. Furthermore, the stable time increment in

the model is twice the inverse of the highest frequency of the system, as determined on an element-by-element basis. The effects of instantaneous contact and constraints are difficult to account for in the element-by-element based time increment. The *Explicit* package implements an adaptive algorithm to determine conservative bounds for the highest frequency component to resolve this issue. This stability limit is conservative and continuously updated compared to the fixed stability limit extracted based on the maximum frequency of the entire model.

As aforementioned, the size of elements influences the convergence of the solution, accuracy of the results and the computational cost. A mesh sensitivity analysis is carried out for both the collar and pipe sections using the "h-method". The "h-method" analysis was conducted for the axial motion of a point on the pipe section and lateral motion of a no-contact point on the collar section to investigate the appropriate mesh size on the pipe and collar sections, respectively. The results verify that having 250 elements over the BHA and the three-metre span and 1000 elements on the pipe section ensures convergence of the analysis. The denser distribution of the elements on the multi-span BHA (finer mesh) enables a determination of the contact points with higher accuracy. These points are used in the analytical model as potential contact points.

In an analytical model, determining the significant modes that account for the majority of the system's kinetic energy (the modes that are contributing a high mass) is important to ensure that model complexity, and thus computation time, is not needlessly high. The FEM model is a valuable tool for computing the required analytical model complexity.

The total effective mass is a tool to achieve this goal. Moreover, the effective mass indicates the value of active mass in each degree of freedom at a specific mode, which is related to the mode participation factor. The mode participation factor indicates the strength of the motion (global translations in this model) in the three assumed directions in the eigenvector of that mode and determines the predominance of the modes in each direction. The total modal mass of the model is the sum of effective masses of all modes in any particular direction [20,26]. In this study the modes that capture 90% of the total modal mass are retained in the analytical model. Here, retaining up to the fourth mode captures dynamics of interest. The total effective mass in the u direction is 80% for the first mode, which verifies that in this direction the first mode contributes a high value compared to the rest of the modes, while in the v direction the second mode is the predominant mode with a total effective mass of 90%.

7.6 Numerical Results and Discussion

The simulation results of both models are used to predict critical rotary speeds, efficacy of the shock sub in vibration decoupling and the enhancing effect of the downhole vibration generator tool on the developed cutting force. Moreover, the axial and lateral time responses for desired locations on the drillstring, contact location and behavior are also determined. Predicting the critical rotary speeds at the early stages of designing a drillstring and before each run is a crucial task to avoid unwanted resonance states. If the working conditions stay close to the resonance state, the BHA absorbs energy, which amplifies lateral, axial and torsional motions. In the analytical model, the frequency equations are solved to determine the first four natural frequencies in the axial and lateral

directions. In order to extract natural frequencies by the FEM model and compare the results with the ones extracted from the analytical model, the linear perturbation step in the FEM model is selected to find natural frequencies of the system with a Lanczos eigensolver [26]. The natural frequencies extracted from both methods are shown in Table 7.3, show good agreement. The maximum differences between analytical and FEM models are 0.0435 Hz in the lateral direction and 0.035 Hz in the axial direction, which is a negligible difference in rotary drilling operations (around 2.6 rpm). The natural frequencies derived in this study are higher than the ones extracted by other studies which assumed the BHA as a single-span beam. These higher frequencies are due to assuming several constraints (stabilizers) on the BHA. Although this assumption adds complexity to the models, it allows for more realistic results.

Table 7.3: Extracted resonance rotary speeds

Direction	First mode (Hz)		Second mode (Hz)		Third mode (Hz)		Fourth mode (Hz)	
	FEM	Analytical	FEM	Analytical	FEM	Analytical	FEM	Analytical
Lateral	0.36	0.33	1.08	1.041	1.28	1.24	1.85	1.82
Axial	0.06	0.03	0.58	0.55	1.90	1.87	4.00	3.96

Axial displacement and developed axial forces above the shock sub are main indicators of the efficacy of the implemented shock sub [17]. Axial response of the drillstring is also an especially important consideration when tuning the vibration generator tool. The time history of any desired point along the drillstring is achieved using the numerical solutions of the generalized coordinate systems (12 mode participation factors in this study) and substituting back the results in the expanded Galerkin's equations (Equation 6.12) in the

analytical model. In the FEM model, the force and displacement time histories of the points of interests are recorded every 20 intervals for each time increment. Axial displacement above the shock sub for the case when there is no shock sub and the case with a shock sub for analytical and FEM models are depicted in Figure 7.5.

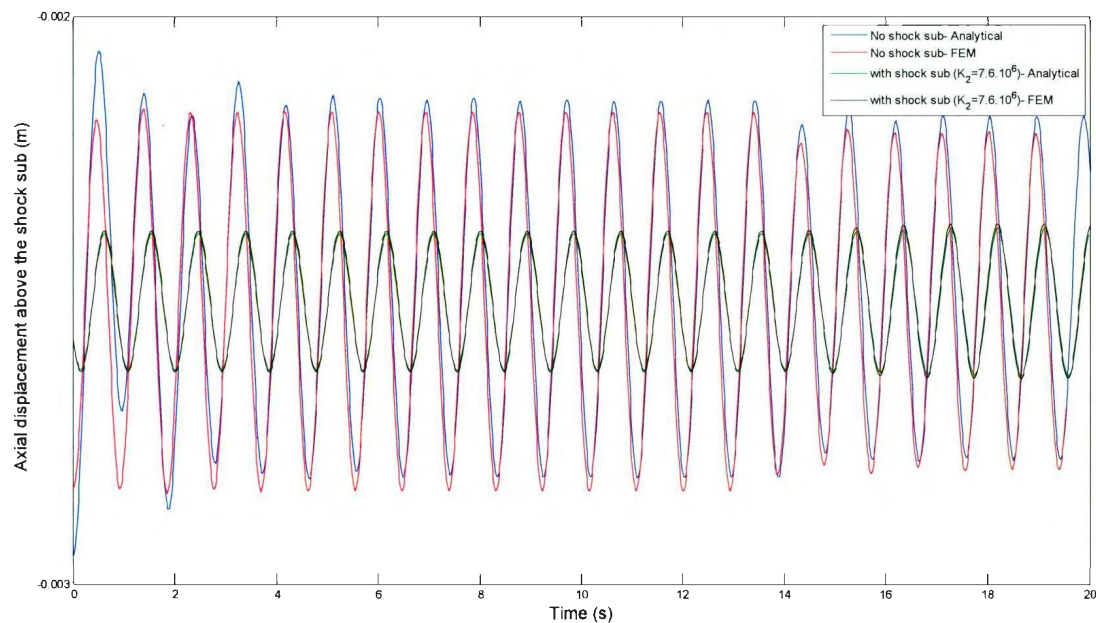


Figure 7.5: Axial displacement above the shock sub (with and without shock sub)

Use of a shock sub significantly reduces the axial displacement above the sub, which means less vibration is transmitted to the drillstring. The FEM and analytical steady-state results are in agreement with a difference of less than 1 *cm*, which is an acceptable difference in terms of practical drilling. The small discrepancies could be due to the assumed axial comparison function in the analytical model and numerical computational scheme. The sensitivity study of the axial displacement above the shock sub for different shock sub stiffness values ($K_2 = 7.6E6, 6E6$ and $4.5E6$) is shown in Figure 7.6, which

verifies the reduction of the displacement by softening the stiffness value of the shock sub. It should be noted that the curves are de-meant and horizontally shifted over the time domain to match the peak locations for the sake of better comparison.

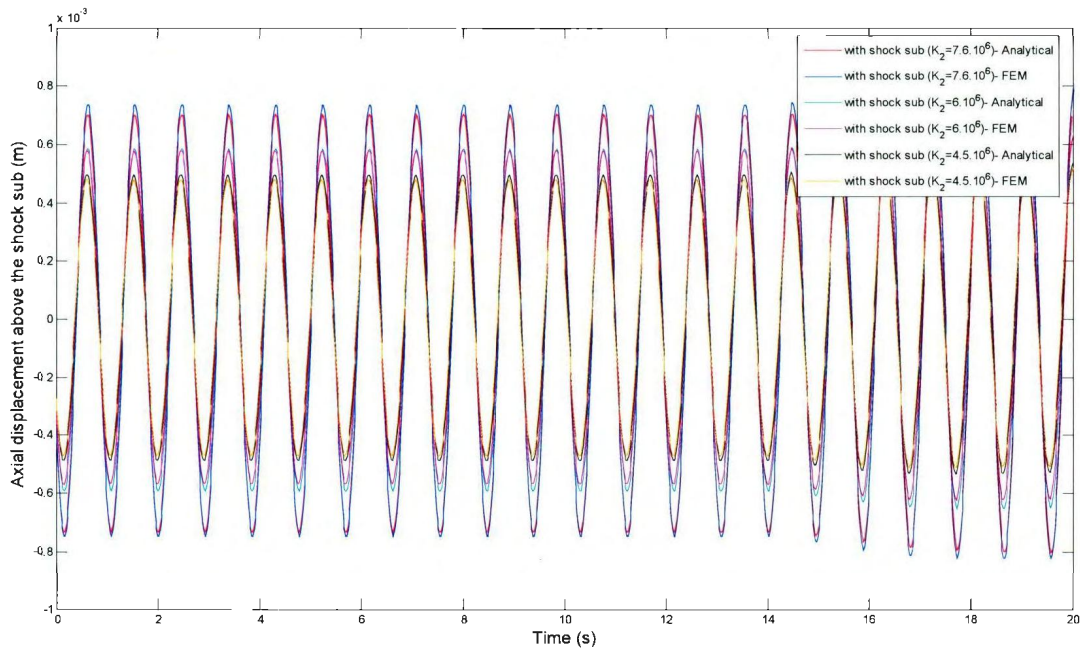


Figure 7.6: Sensitivity analysis of the shock sub to the stiffness value (transmitted axial displacement)

Figure 7.7 depicts the axial force above the shock sub location, with and without a shock sub for both FEM and analytical models. It is clear that the shock sub significantly reduces the transmitted axial force to the BHA and the drillstring as well as the axial vibration displacement.

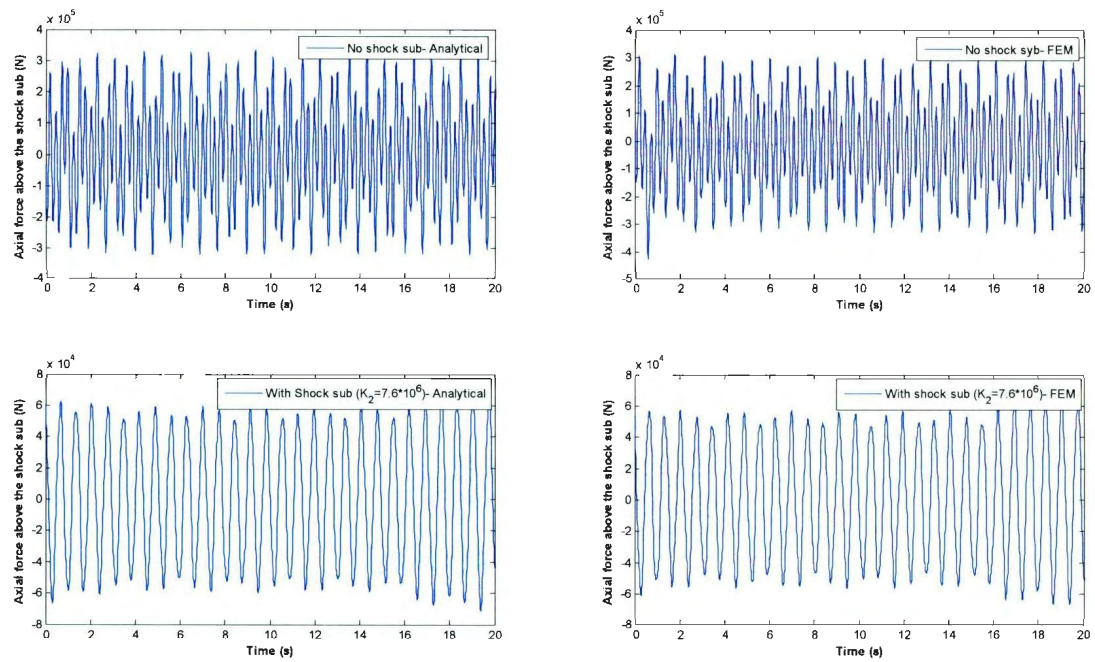


Figure 7.7: Transmitted axial force above the shock sub

Figure 7.8 shows the transmitted force to the BHA versus different stiffness values of the shock sub. With the softening of the shock sub spring, lower values of the force are transmitted to the drillstring for both analytical and FEM models, which are in agreement.

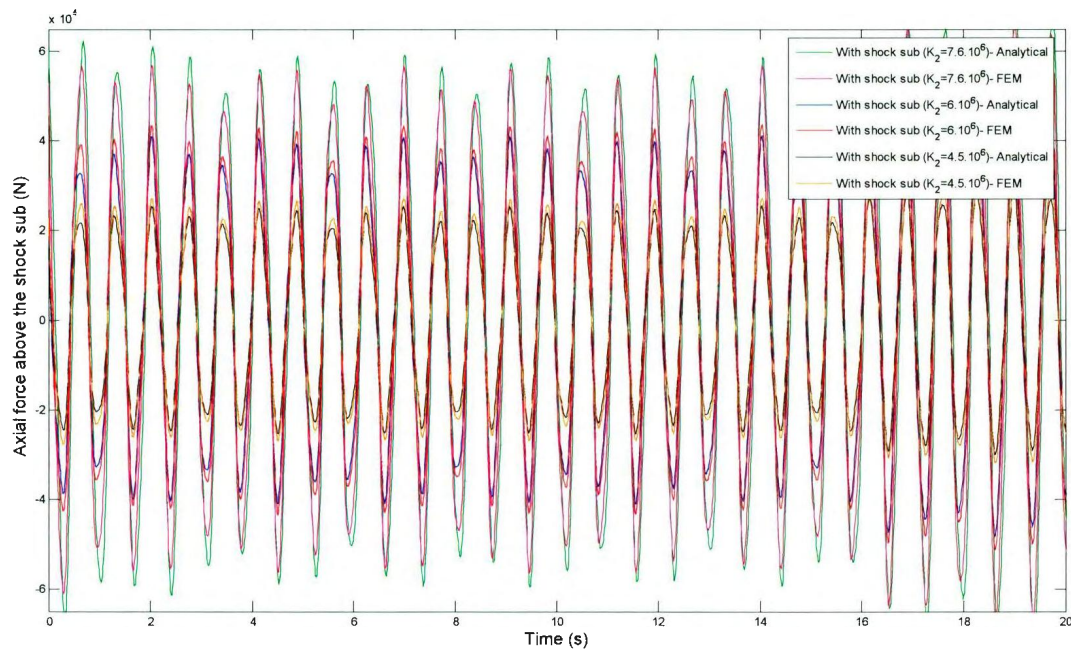


Figure 7.8: Sensitivity analysis of the shock sub to the stiffness value (transmitted axial force)

Axial displacement of the drillstring near the rig surface is also important, since the axial displacement at this location causes fatigue stress for the connections in the rig surface [57]. Figure 7.9 shows a 40% reduction in the transmitted vibration displacement to the surface when using a shock sub.

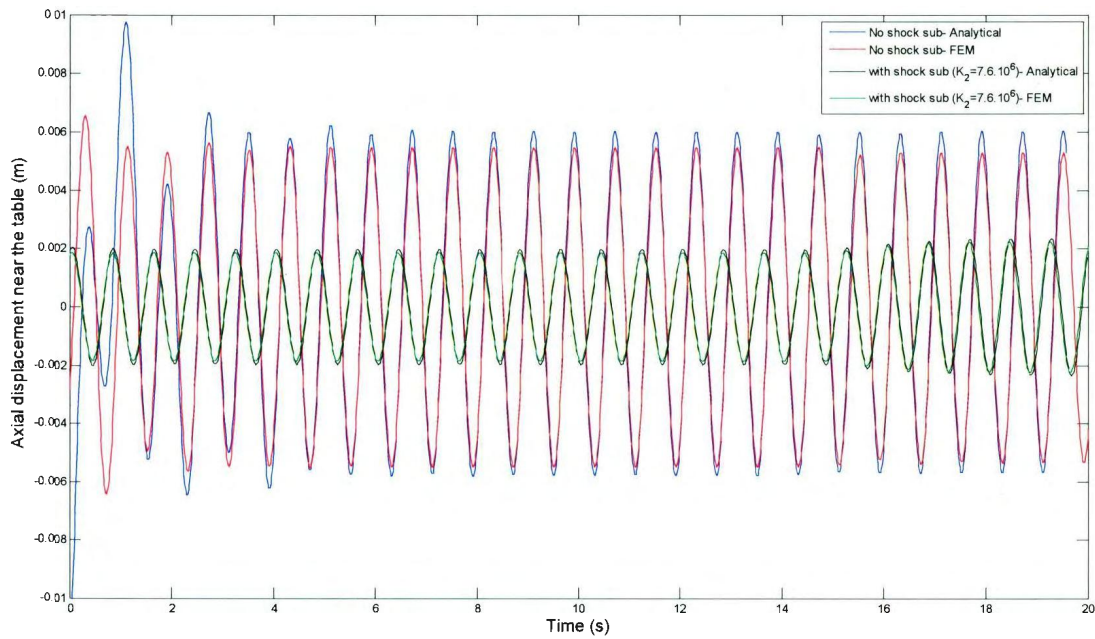


Figure 7.9: Axial displacement near the rig floor (with and without shock sub)

The sensitivity analysis of the displacement at the surface for three different values of the shock sub stiffness is shown in Figure 7.10. Softening the shock sub's spring decreases the transmitted displacement to the rig floor as well.

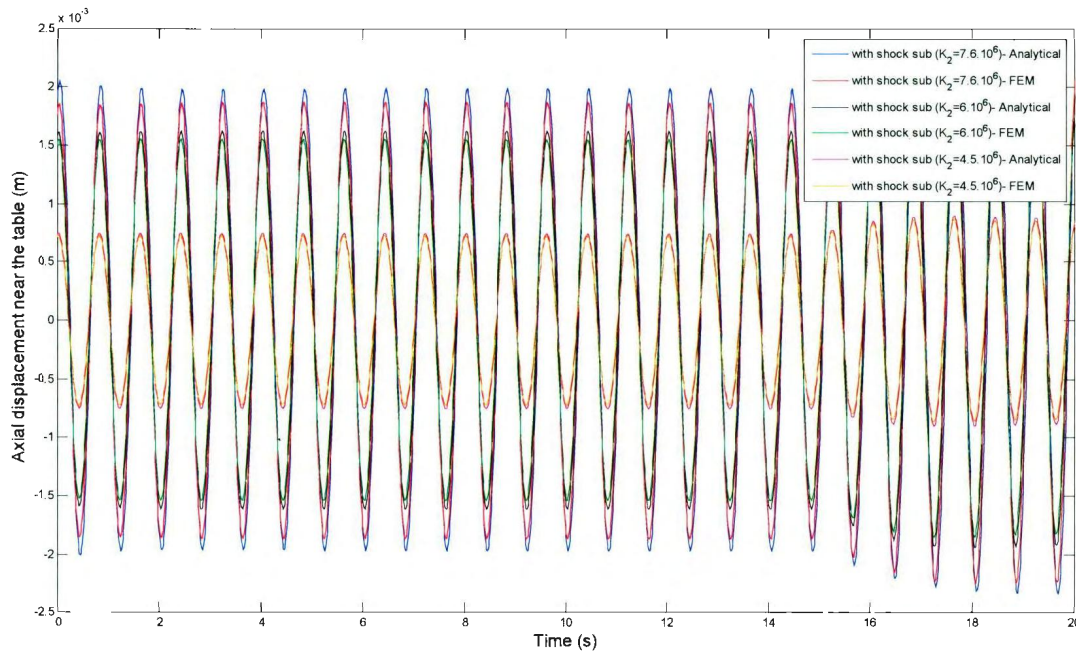


Figure 7.10: Sensitivity analysis of the shock sub to the stiffness value (axial displacement near the rig floor)

The efficiency of the shock sub in decoupling the generated vibration at the bit due to the vibration generator tool also depends on the rotary speed of the drillstring, since the rotary speed is also the frequency of the bit displacement excitation. The rotary speed varies in true drilling applications (normally 20-200 rpm). Figure 7.11 shows the peak-to-peak axial force above the final span with and without a shock sub, as a function of drilling speed. Good agreement is noted between numerical and analytical models.

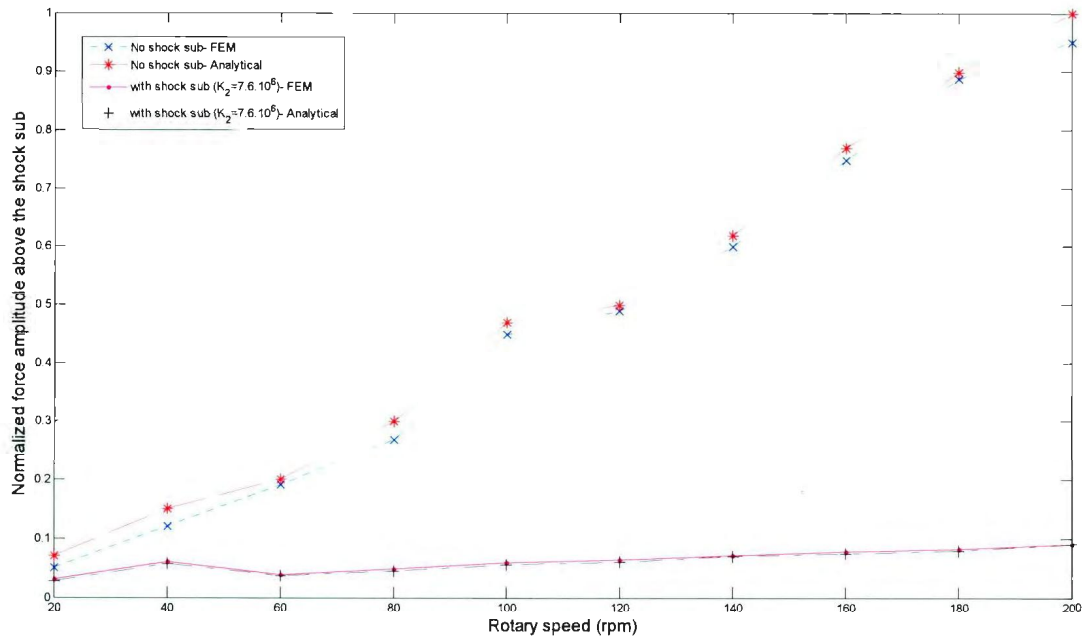


Figure 7.11: Sensitivity analysis of the shock sub to the drillstring rotary speed (axial force above the shock sub)

Hence, the result verifies that the shock sub is effective over an extended range of the rotary speed of the drillstring, with a higher efficiency above 60 rpm. The effect of the shock sub on the peak-to-peak displacement above the shock sub location is shown in Figure 7.12, which also shows benefit over the entire rotary speed range of the drillstring. A higher isolation of the displacement is also noticeable after the rotary speed of 100 rpm in Figure 7.12.

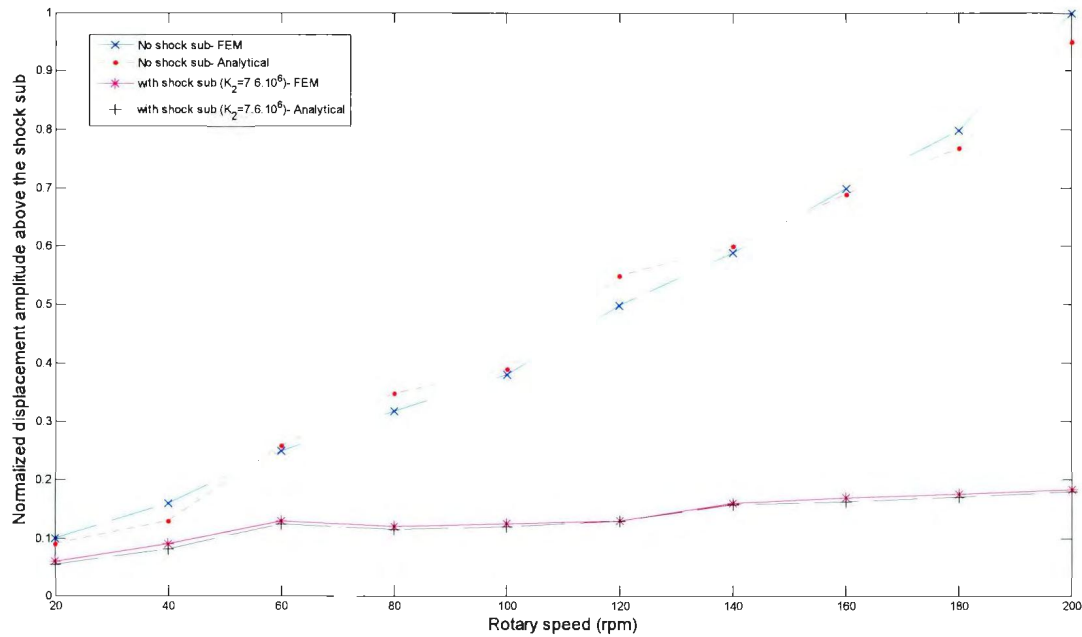


Figure 7.12: Sensitivity analysis of the shock sub to the drillstring rotary speed (axial displacement above the shock sub)

The shock sub, while isolating a vibrating tool from the upper portion of the drillstring, should not attenuate the force transmitted to the rock. Figures 7.13 and 7.14 show that the downhole vibration generator tool increases the developed cutting force at the bit, with and without a shock sub.

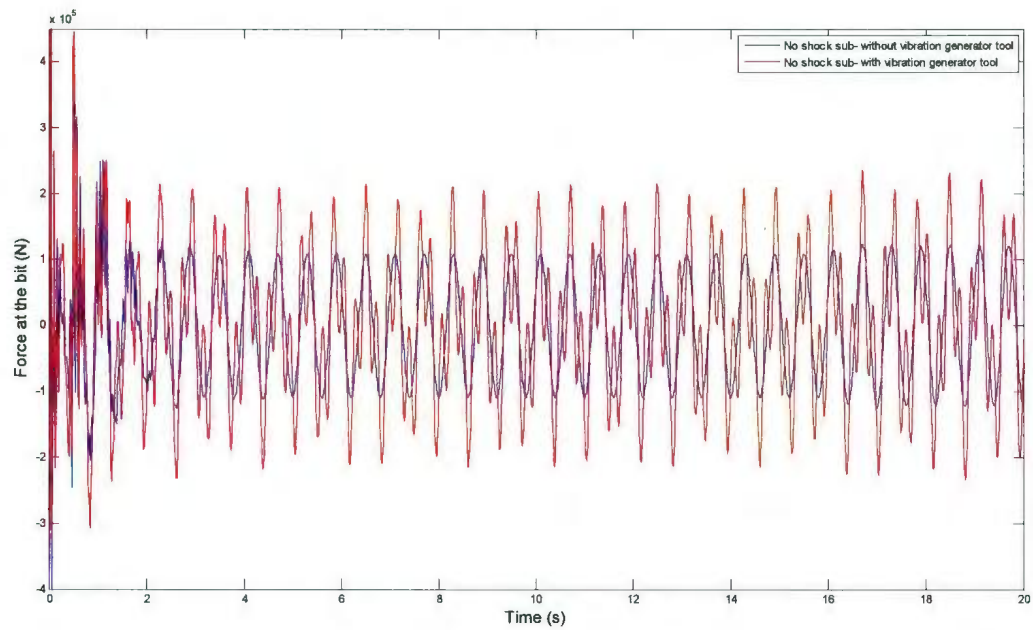


Figure 7.13: Developed cutting force at the bit due to the downhole vibration generator
(without shock sub)

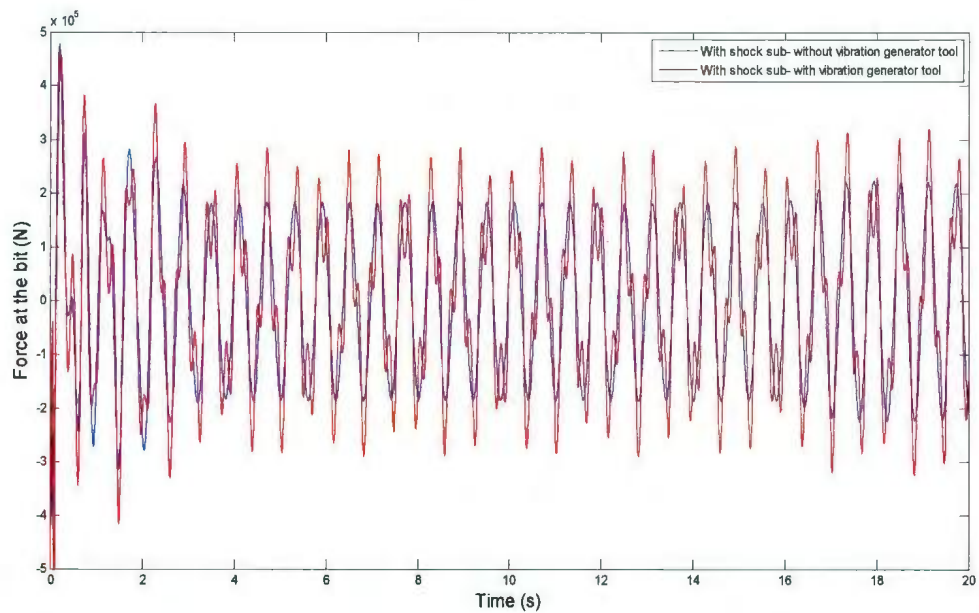


Figure 7.14: Developed cutting force at the bit due to the downhole vibration generator
(with shock sub)

Figure 7.15 compares the last two figures and verifies that if the vibration generator tool is implemented with a shock sub, the bit-rock force amplification is increased by 35%.

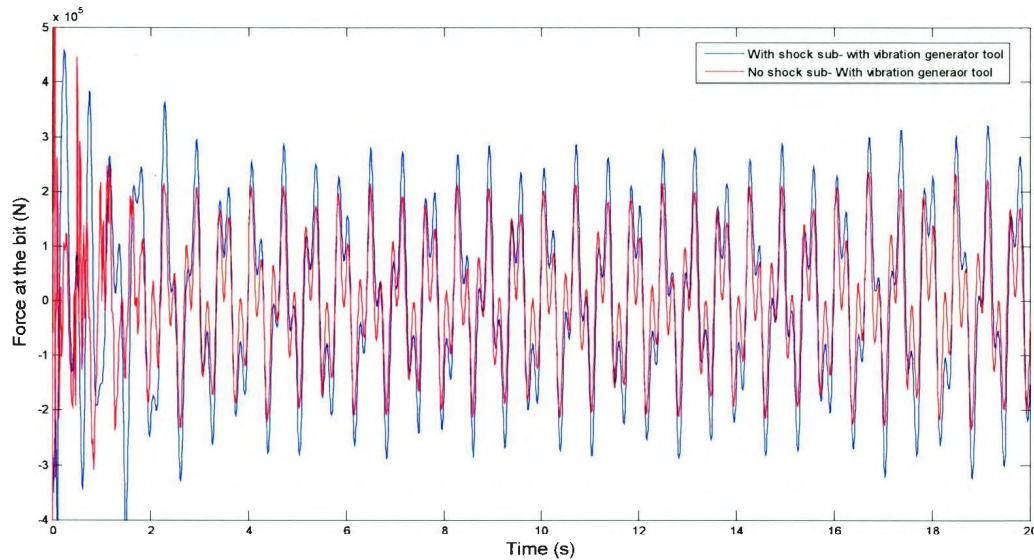


Figure 7.15: Developed cutting force at the bit due to the downhole vibration generator tool (with and without shock sub)

In Figures 7.13-7.15, while the downhole vibration generator tool is in use, a high frequency (vibration generator frequency) component of the force is riding over a low frequency (drillstring rotary speed) force component developed due to the bit displacement.

The contact behavior in the presence of a vibration generator tool and the shock sub is also investigated in this study. Figure 7.16 shows the radial deflection of the contact point on the 41m BHA span. This figure depicts a highly irregular contact trend at this point with multiple contacts. Both FEM and analytical models typically hit the wellbore at the same time. The borehole clearance is set to 10 cm.

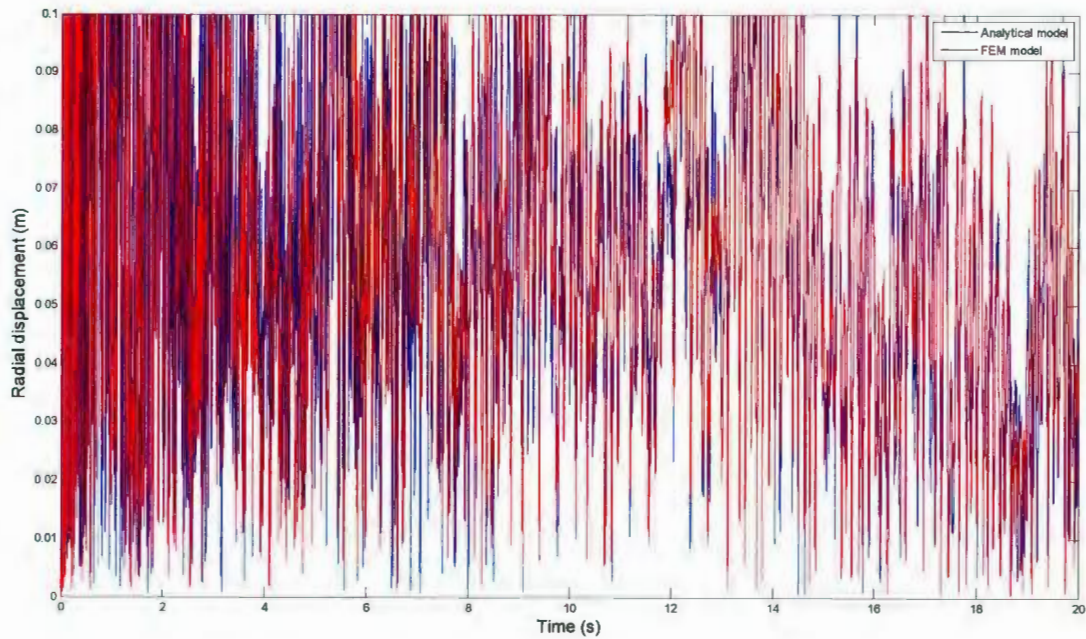


Figure 7.16: Radial deflection at the contact point, first span of the BHA

The radial deflection at the contact point of the mid span is shown in Figure 7.17. The contact behavior is not as severe as the 41m span, as the effect of initial conditions dies out. The system is excited by an initial velocity at the pipe-collar junction and at the midpoint of the middle span of the BHA. The BHA at this span does not hit the wellbore successively as in the previous span. Consequently, this different result shows the importance of using a multiple spans BHA, while modeling the contact behavior between the drillstring and wellbore.

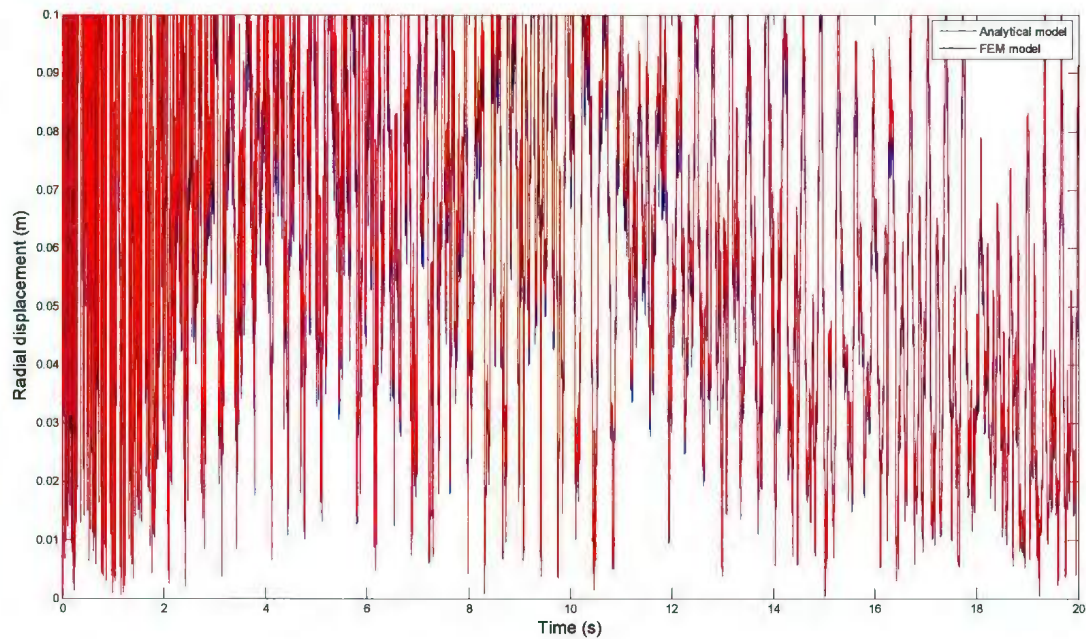


Figure 7.17: Radial deflection at the contact point, second span of the BHA

The contact behavior at the top span of the BHA is shown in Figure 7.18. There is less contact between the drillstring and wellbore at this location and a bouncing back behavior is seen at this point. A less irregular behavior is also obvious at this span.

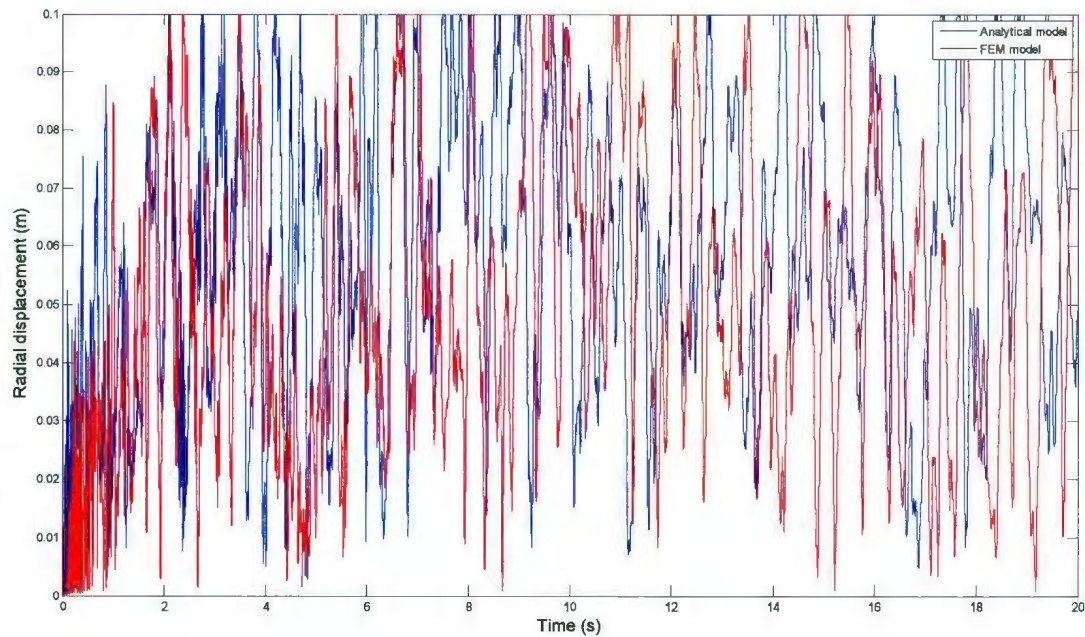


Figure 7.18: Radial deflection at the contact point, last span of the BHA

The effect of setting the rotary speed near the resonance rotary speed is also investigated. The contact behavior of the last span is shown in Figure 7.19, when the rotary speed of the drillstring is set to the first lateral resonant frequency of the drillstring (30 rpm) and the remaining parameters remain the same. The low intensity contact (Figure 7.18) becomes severe and highly irregular.

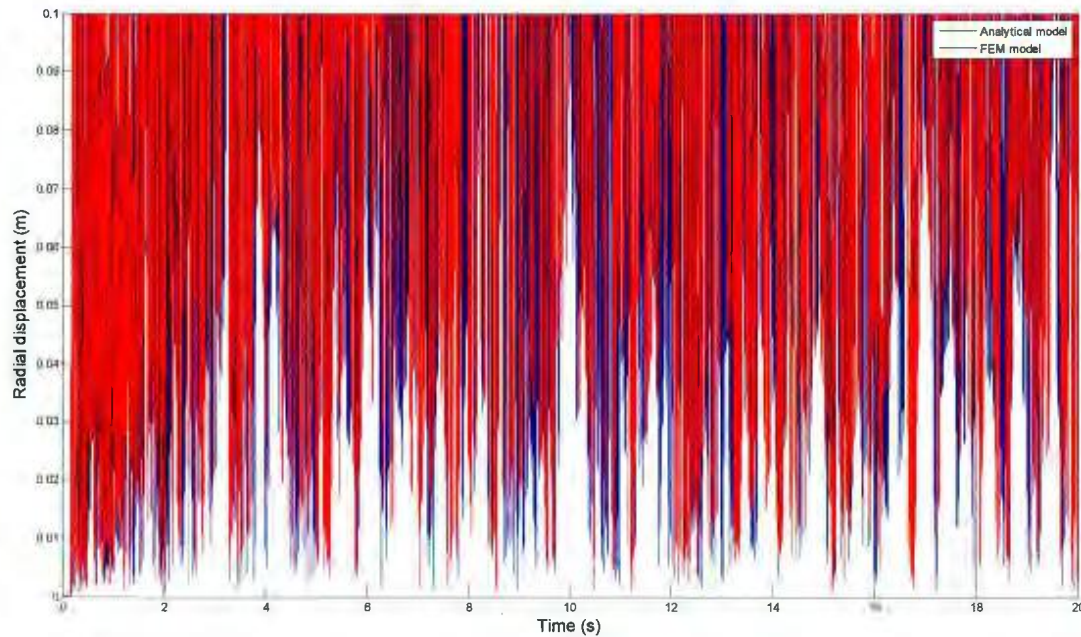


Figure 7.19: Radial deflection at the contact point in the resonance, top span of the BHA

7.7 Conclusions

While downhole vibration generator tools enhance the drilling efficiency, they have also been associated with premature failure of BHA components and MWD tools.

Catastrophic failures can be avoided with increased understanding of the dynamic behavior of the drillstring in the presence of these tools. High-fidelity dynamic models can assist in specifying BHA properties, shock sub parameters, vibrating tool force and frequency, drilling speed, and weight on bit. The nonlinear, coupled axial-lateral vibration behavior of a drillstring, under the effect of an axial force generator, was simulated with an analytical model and validated against a dynamic finite element model. A shock sub was also implemented to decouple the imposed vibration at the bit from the rest of the drillstring. The "Bypassing PDEs" method, along with the expanded Galerkin's method

and the Lagrange's equation, was implemented to derive the analytical model of a drillstring with a multi-span BHA. As well, the multi-mode analysis in the expanded Galerkin's method and more realistic assumed boundary conditions enabled a multi-point contact analysis, multi mode modal dynamic analysis, and prediction of more realistic critical rotary speeds. The lateral comparison functions for a multi-span BHA and the pipe section were determined analytically. Also, the axial comparison functions for a system of hybrid continuous (the entire step-beam drillstring) and discrete elements (shock sub elements and equivalent mass-spring-damper of the top hoisting system) were developed analytically. These precise comparison functions facilitate sensitivity studies of different design parameters, such as drillstring geometrical configurations, equivalent stiffness and damping values of the drillstring hoisting system, and shock sub parameters. The FEM model was specifically developed using the *Explicit* solver package of ABAQUS[®], with "kinematic friction algorithm" and general contact surface detection method. The mud damping, spatially varying axial force, driving torque, downhole axial vibratory tool and a shock sub are captured in both models and the nonlinear coupling terms due to contact, axial stiffening and torque were retained in the analytical model. The geometry, configuration and boundary conditions were the same in both developed models. Time histories of the axial displacement, two orthogonal lateral displacements and the developed forces were extracted for several points along the drillstring. The implementation of the shock sub showed significant decoupling and isolation of the tool vibration. Softer springs gave better vibration suppression, and the shock sub was effective over an extensive range of rotary speeds. The vibration isolation effect was

greater at higher speeds. Simultaneous use of a shock sub with a generator tool results in a more enhanced cutting force at the bit. Study of the lateral instabilities verified that multiple contact point analysis driven by the Hertzian contact theory in the analytical model coincides with the "kinematic friction algorithm" in the FEM model in terms of contact locations and severities. Dynamic time responses and extracted critical rotary speeds in both models were also in agreement. While the analytical model runs quickly, the FEM model is more easily reconfigurable for different drillstring geometries, and can accommodate more complex, nonlinear phenomena. The models in their current form will be an important tool in tuning downhole vibration generators, and configuring vibration suppression systems, in the pursuit of vibration generator tools that increase rate of penetration and efficiency without negative consequences for the drillstring and MWD components.

7.8 Acknowledgment

This research was conducted at the Advanced Drilling Technology Laboratory at Memorial University of Newfoundland and was funded by Husky Energy, Suncor Energy, The Atlantic Canada Opportunities Agency and The Research and Development Corporation of Newfoundland and Labrador under AIF Contract No. 781-2636-1920044. Also, the authors would like to acknowledge the valuable suggestion for the solution of the coupled stiff ODE system made by Dr. Neil Hookey and Dr. Seshu Adluri at Memorial University.

7.9 References

- [1] Dareing, D. W., 1984, "Guidelines for Controlling Drillstring Vibrations," ASME Journal of Energy Resources Technology," **106**(2), pp. 272-277.
- [2] Mitchell, R. F., and Miska, S. Z., 2011, *Fundamentals of Drilling Engineering*, SPE textbook series, Texas, USA, Chap. 10.
- [3] Al Ali, A., Barton, S., and Mohanna, A., 2011, "Unique Axial Oscillation Tool Enhances Performance of Directional Tools in extended Reach Applications," SPE#143216, SPE Brasil Offshore, Macaé, Brazil.
- [4] Elsayed, M. A., Wells, R. L., Dareing, D. W., and Nagirimadugu, K., 1994, "Effect of Process Damping on Longitudinal Vibrations in Drillstrings," ASME Journal of Energy Resources Technology, **116**, pp. 129-135.
- [5] Berlioz, A., Der Hagopian, J., Dufour, R., and Draoui, E., 1996, "Dynamic Behavior of a Drillstring: Experimental Investigation of Lateral Instabilities," ASME Journal of Vibration and Acoustics, **118**, pp. 292-298.
- [6] Aminfar, O., and Khajepour, A., 2008, "Torsional Vibration Analysis of Drillstring in Blasthole Drilling," ASME International Mechanical Engineering Congress (IMECE), Boston, Massachusetts.
- [7] Burgess, T. M., McDaniel, G. L., and Das, P. K., 1987, "Improving BHA Tool Reliability with Drillstring Vibration Models: Field Experience and Limitations," SPE#16109, SPE/IADC Drilling Conference, New Orleans, Louisiana.

- [8] Yaveri, M., Damani, K., and Kalbhor, H., 2010, "Solutions to the Downhole Vibrations during drilling," SPE#136956, 34th Annual SPE International Conference and Exhibition, Tinapa, Nigeria.
- [9] Manko, K. I., Pilipenko, V. V., and Zapol'sky, L. G., 2003, "Use Hydrodynamic Cavitation For Increase of Efficiency of Process of Well Drilling," Fifth International Symposium on Cavitation, Osaka, Japan.
- [10] Newman, K., Burnett, T., Pursell, J., and Ouahab Gouasmia, S., 2009, "Modeling the Affect of a Downhole Vibrator," SPE#121752, SPE/ICO TA Coiled Tubing and Well Intervention Conference, Houston, Texas.
- [11] *Babatunde, Y., Butt, S. D., Molgard, J., and Arvani, F., 2011, "Investigation of the Effects of Vibration Frequency on Rotary Drilling Penetration Rate Using Diamond Drag Bit," ARMA#11-527, 45th US Rock Mechanics/Geomechanics Symposium (ARMA), San Francisco, California.*
- [12] Li, H., Butt, S. D., Munaswamy, K., and Arvani, F., 2010, "Experimental Investigation of Bit Vibration on Rotary Drilling Penetration Rate," ARMA# 10-426, 44th US Rock mechanics symposium (ARMA), Salt Lake City, Utah.
- [13] Khorshidian, H., Mozaffari, M., and Butt, S. D., 2012, "The Role of Natural vibrations in Penetration Mechanism of a Single PDC Cutter," ARMA# 12-9, 46th U.S. Rock Mechanics/Geomechanics Symposium (ARMA), Chicago, Illinois.
- [14] Elsayed, M. A., and Aissi, C., 2006, "Analysis of Shock Absorber Characteristics for Drillstrings," ESDA# 2006-95141, ASME 8th Biennial Conference on Engineering System Design and Analysis (ESDA 2006), Torino, Italy.

- [15] Warren, T. M., Oster, J. H., Hughes, C., and Chen, D. C. K., 1998, "Shock Sub Performance Tests," IADC/SPE# 39323, IADC/SPE Drilling Conference, Dallas, Texas.
- [16] Skaugen, E., Kyllingstad, A., Aarrestad, T. V., and Tonnesen, H. A., 1987, "Experimental and Theoretical Studies of Vibrations in Drillstrings Incorporating Shock Absorbers," 12th World Petroleum Congress, Houston, Texas.
- [17] Kreisle, L. F., and Vance, J. M., 1970, "Mathematical Analysis of the Effect of Shock Sub on the Longitudinal Vibrations of an Oilwell Drillstring," SPE Journal, **10**(4), pp. 349-356.
- [18] Walker, B. H., and Friedman, M. B., 1977, "Three Dimensional Force and Deflection Analysis of a Variable Cross Section Drillstring," ASME Journal of Pressure Vessels, **99**(5), pp. 367-373.
- [19] Yigit, A. S., and Christoforou, A. P., 1996, "Coupled Axial and Transverse Vibrations of Oilwell Drillstrings," Journal of Sound and Vibration, **195**(4), pp. 617-627.
- [20] Ghasemloonia, A, Rideout D. G. and Butt, S. D., 2013, "Vibration Analysis of a Drillstring in Vibration-Assisted Rotary Drilling: Finite Element Modeling With Analytical Validation," ASME Journal of Energy Resources Technology, **135**(3), pp. 032902-1-032902-18.
- [21] Sampaio, R., Piovan, M. T., and Lozano, G. V., 2007, "Coupled Axial Torsional Vibrations of Drillstring by Means of Nonlinear Model," Journal of Mechanics Research Communications, **34**, pp. 497-502.

- [22] Yigit, A. S., and Christoforou, A. P., 1998, "Coupled Torsional and Bending Vibrations of Drillstrings Subject to Impact With Friction," *Journal of Sound and Vibration*, **215**(1), pp. 167-181.
- [23] Hakimi, H., and Moradi, S., 2009, "Drillstring Vibration Analysis Using Differential Quadrature Method," *Journal of Petroleum Science and Engineering*, **70**(3-4), pp. 235-242.
- [24] Gulyaev, V. I., Lugovoi, P. Z., Belova, M. A., and Solov'ev, I. L., 2007, "Effect of the Length of a Rotating Drillstring on the Stability of its Quasistatic Equilibrium," *International Journal of Applied Mechanics*, **43**(9), pp. 1017-1023.
- [25] Ghasemloonia, A., Rideout, D. G., and Butt, S. D., 2010, "The Effect of Weight-On-Bit on the Contact Behavior of Drillstring and Wellbore," 9th International Conference on Bond Graph Modeling (ICBGM2010), Orlando, Florida.
- [26] Ghasemloonia, A., Rideout, D. G., and Butt, S. D., 2012, "Coupled Transverse Vibration Modeling of Drillstrings Subjected to Torque and Spatially Varying Axial Load," *Journal of Mechanical Engineering Science (IMEchE, part C)*, **227**(5), pp. 946-960.
- [27] Jafari, A. A., Kazemi, R. and Faraji Mahyari, M., 2012, "The Effects of Drilling Mud and Weight Bit on Stability and Vibration of a Drillstring," *ASME Journal of Vibration and Acoustics*, **134**, pp. 0111014-1-0111014-9.
- [28] Melakhessou, H., Berlioz, A., and Ferraris, G., 2003, "A Nonlinear Well-Drillstring Interaction Model," *ASME Journal of Vibration and Acoustics*, **125**, pp. 46-52.

- [29] Heisig, G., and Neubert, M., 2000, "Lateral Drillstring Vibrations in Extended-Reach Wells," IADC/SPE# 59235, IADC/SPE Drilling Conference, New Orleans, Louisiana.
- [30] Christoforou, A. P., and Yigit, A. S., 1997, "Dynamic Modeling of Rotating Drillstrings With Borehole Interactions," *Journal of Sound and Vibration*, **206** (2), pp. 243-260.
- [31] Khulief, Y. A., and Al-Sulaiman, F. A., 2009, "Laboratory Investigation of Drillstring Vibrations," *Journal of Mechanical Engineering Science, IMechE Part C*, **223**(10), pp. 2249-2262.
- [32] Thomsen, J. J., 2003, *Vibrations and Stability*, 2nd ed., Springer, Berlin, Germany, Chap. 3.
- [33] Vaz, M. A., and Patel, M. H., 1995, "Analysis of Drillstrings in Vertical and Deviated Holes Using the Galerkin Technique," *Engineering Structures*, **17**(6), pp. 437-442.
- [34] Jansen, J. D., 1991, "Nonlinear Rotor Dynamics as Applied to Oil Well Drillstring Vibrations," *Journal of Sound and Vibration*, **147** (1), 115-135.
- [35] Hsu, F., Wilhoit, J., and James, C., 1965, "Lateral Vibration of Drill Pipe Including Wall Reaction," SPE#1046, Conference on Drilling and Rock Mechanics, Austin, Texas.
- [36] Dareing, D. W., and Livesay, B. J., 1968, "Longitudinal and Angular Drillstring Vibrations with Damping," *ASME Journal of Manufacturing Engineering*, **90**(4), 671-679.
- [37] Bailey, J. J., and Finnie, I., 1960, "An Analytical Study of Drillstring Vibration," *ASME Journal of Engineering for Industry*, **82**(2), pp. 122 – 128.

- [38] Jogi, P. N., Macpherson, J. D., and Neubert, M., 2002, "Field Verification of Model-Derived Natural Frequencies of a Drillstring," *ASME Journal of Energy Resources Technology*, **124**(3), pp. 154-162.
- [39] Clayer, F., Vandiver, J. K., and Lee, H. Y., 1990, "The Effect of Surface and Downhole Boundary Conditions on the Vibration of Drillstrings," SPE#20447, SPE Annual Technical Conference, New Orleans, Louisiana.
- [40] Aarrestad, T. V., and Kyllingstad, A., 1993, "Rig Suspension Measurements and Theoretical Models and the Effect on Drillstring Vibrations," *SPE Drilling and Completion*, **8**(3), pp. 201-206.
- [41] Macpherson, J. D., Jogi, P. N., and Kingman, J. E. E., 2001, "Application and Analysis of Simultaneous Near Bit and Surface Dynamics Measurements," *SPE Drilling and Completion*, **16**(4), pp. 230-238.
- [42] Elsayed, M. A., Dareing, D. W., and Vonderheide, M. A., 1997, "Effect of Torsion on Stability, Dynamic Forces and Vibration Characteristics in Drillstrings," *ASME Journal of Energy Resources Technology*, **119**(1), pp. 11-19.
- [43] Dunyaevsky, V. A., Abbassian, F., and Judzls, A., 1993, "Dynamic Stability of Drillstrings Under Fluctuating Weight on Bit," *SPE Drilling and Completion*, **8**(2), pp. 84-92.
- [44] Li, Z., Yanshan, U., and Guo, B., 2007, "Analysis of Longitudinal Vibration of Drillstring in Air and Gas Drilling," SPE#107697, SPE Rocky Mountain Oil and Gas Technology Symposium, Denver, Colorado.

- [45] ABAQUS Theory Manual (version 6.10), 2012, Dassault Systèmes Simulia Corp., RI, USA.
- [46] Millheim, K., Jordan, S., and Ritter, C. J., 1978, "Bottom Hole Assembly Analysis Using the Finite Element Method," *Journal of Petroleum Technology*, **30**(2), pp. 265-274.
- [47] Apostol, M. C., Haduch, G. A., and Williams, J. B., 1990, "A Study to Determine the Effect of Damping on Finite Element Based Forced Frequency Response Models for Bottomhole Assembly Vibration Analysis," SPE#20458, SPE Annual Technical Conference and Exhibition, New Orleans, Louisiana.
- [48] Spanos, P. D., Payne, M. L., and Secora, C. K., 1997, "Bottom-Hole Assembly Modeling and Dynamic Response Determination," *ASME Journal of Energy Resources Technology*, **119**(3), pp. 153-158.
- [49] Spanos, P. D., Chevallier, A. M., and Politis, N. P., 2002, "Nonlinear Stochastic Drillstring Vibrations," *ASME Journal of Vibration and Acoustics*, **124**(4), pp. 512-518.
- [50] Khulief, Y. A., and Al-Naser, H., 2005, "Finite Element Dynamic Analysis of Drillstrings," *Finite Element in Analysis and Design*, **41**(13), pp. 1270-1288.
- [51] Khulief, Y. A., Al-Sulaiman, F. A., and Bashmal, S., 2008, "Vibration Analysis of Drillstrings With String-Borehole Interaction," *International Journal of Mechanical Engineering Science, IMechE Part C*, **222**(11), pp. 2099-2110.
- [52] Khulief, Y. A., 2000, "Spatial Formulation of Elastic Multibody Systems with Impulsive Constraints," *Multibody System Dynamics*, **4**(4), pp. 383-406.

- [53] Liao, C., Balachandran, B., Karkoub, M., and Abdel-Magid, Y. L., 2011, "Drillstring Dynamics: Reduced-Order Models and Experimental Studies," ASME Journal of Vibration and Acoustics, **133**(4), pp. 041008-1041008-8.
- [54] Zhang, Q. and Miska, S., 2005, "Effects of Flow-Pipe Interaction on Drill Pipe Buckling and Dynamics," ASME Journal of Pressure Vessels, **127**(2), pp. 129-136.
- [55] Ritto, T. G., Sampaio, R. and Soize, C., 2009, "Drill-String Nonlinear Dynamics Accounting for Drilling Fluid," 30^o CILAMCE-Iberian-Latin-American Congress on Computational Methods in Engineering, Armação dos Búzios, Rio de Janeiro.
- [56] Spanos, P. D., and Payne, M. L., 1992, "Advances in Dynamic Bottomhole Assembly Modeling and Dynamic Response Determination," SPE/IADC# 23905, SPE/IADC Drilling Conference, New Orleans, Louisiana.
- [57] Evans, J. T., and McGrail, J., 2011, "An Evaluation of the Fatigue Performance of Subsea Wellhead Systems and Recommendations for Fatigue Enhancements," OTC#21400, Offshore Technology Conference, Houston, Texas.

7.10 Nomenclature

F_{collar}	Axial force along the collar section	$X_i(z)$	Lateral comparison function for the second span of the BHA
ρ_{collar}	Collar density	$F_i(z)$	Lateral comparison function for the third span of the BHA
$A_{collar} = A_2$	Collar cross sectional area	$\epsilon_i(z)$	Lateral comparison function for the pipe section
g	Gravity acceleration	L_1	Length of the span close to the bit
z	Coordinate along the drillstring axis	L_2	Length of the BHA
WOB	Weight-on-Bit	L_3	Length of the pipe section

ρ_{mud}	Mud density	L	Length of the drillstring
l	Drillstring length	C_D	Hydrodynamic drag coefficient
F_{pipe}	Axial force along the pipe section	R_{collar}	Collar outside diameter
l_p	Length of the pipe section	K_h	Hertzian stiffness
$A_{pipe} = A_1$	Pipe cross sectional area	r	Radial deflection of the drillstring
l_c	Length of the collar section	b_{cl}	Borehole clearance
$u_i(z, t)$	Axial motion in different sections	$F_{vibration}$	Vibration generator force
$v_1(z, t)$	First lateral motion in different sections	Ω	Frequency of the downhole vibration generator tool
$w_1(z, t)$	Second lateral motion in different sections	K_1	Stiffness of the top cable
$\theta_i(z)$	Axial comparison function for 3 m span	K_2	Stiffness of the shock sub
$\psi_i(z)$	Axial comparison function for the spans of the BHA	M	Mass of the traveling block
$\Delta_i(z)$	Axial comparison function for the pipe section	C_1	Damping of the top cable
$\varphi_i(z)$	Lateral comparison function for the 3 m span	C_2	Damping of the shock sub
$\sigma_i(z)$	Lateral comparison function for the first span of the BHA	E_1	Young's modulus of the pipe section
$\lambda_r(t)$	Generalized coordinates system in the axial direction	E_2	Young's modulus of the collar and collar section
$\delta_r(t)$	Generalized coordinates system in the second lateral direction	$\eta_r(t)$	Generalized coordinates system in the first lateral direction

8 Concluding Remarks

“These oscillations arise freely, and I have determined various conditions, and have performed a great many beautiful experiments on the position of the knot points and the pitch of the tone, which agree beautifully with the theory.”

Daniel Bernoulli (from a letter to Leonhard Euler)

8.1 Summary

With the increasing demand for petroleum products, drilling of oil and gas reservoirs has evolved, becoming faster and more efficient. One of the newest techniques in the drilling industry is the use of downhole axial vibration generators above the bit, which have been shown to enhance rate of penetration, and thus drilling cost. However, with the implementation of these tools, the rate of failure of the "Bottomhole Assembly" (BHA) and downhole tools, such as "Measurement-While-Drilling" (MWD) tools has increased. The only effective way to benefit from the positive consequences of these tools is to isolate the imposed vibration from the rest of the drill rig, and in particular the drillstring. Vibration modeling of the drillstring provides an effective tool towards maximizing the positive effect of vibrating tools on bit-rock force, and minimizing unwanted vibration that is transmitted to the rest of the drillstring.

In this thesis, the nonlinear coupled axial-lateral vibration of the drillstring in presence of a downhole vibration generator tool was simulated through analytical and numerical modeling schemes. Also, a shock sub was simulated as a means of isolating the induced vibration by the downhole vibration generator tool. The developed and validated models

were used to extract modal contents and time response of points of interest along the drillstring. The contact behavior of the drillstring was also investigated. As aforementioned in the introduction section, due to the complexity of the drillstring vibration modeling, the research was divided into five steps and the models were enhanced at each step by considering more interactions, adding more degrees of freedom and considering more drilling components. In this chapter a summary of all of the modeling work conducted in chapters 3, 4, 5, 6 and 7 is presented.

8.2 Concluding Remarks

The first model which was developed in this study was a bond graph model of a non-rotating BHA under a constant compressive load, developed using the modal expansion method. A Newtonian approach was implemented to derive the mode shapes and natural frequencies of the BHA, required for the modal expansion method in bond graph modeling. Nonlinear Hertzian contact was defined at midspan. The effect of the "Weight-on-Bit" (WOB) on the lateral instabilities were qualitatively analyzed through phase planes of the contact points and it was verified that lower WOB values results in a less chaotic contact behavior, while increasing WOB to the buckling limit of the BHA results in a highly successive irregular contact trend. The effect of torque, mud damping, varying axial force along the drillstring and coupling between lateral and axial modes were not included in the first model.

The second developed model was an analytical model of the coupled lateral modes of a non-rotating BHA in the presence of driving torque and spatially varying axial load. The

Newtonian approach was used to derive the partial differential equations (PDEs) of motion and then, the expanded Galerkin's method with the first four retained modes was applied to convert the PDEs to coupled ordinary differential equations (ODEs) in terms of general coordinates. The resulting set of ODEs was solved to extract the lateral resonant frequencies, with which the rotary speed should not coincide. For validation of the analytical model, a Finite Element Model (FEM) with the same loads, interactions and boundary conditions was developed. The concept of mass participation factor was used to verify that retaining the first four modes in the analytical model captures most of the system kinetic energy. The critical rotary speeds were also verified by the FEM model. It was also concluded that transverse coupled natural frequencies are more sensitive to changes in the WOB than to the driving torque. The mud damping effect and lateral contact, which are major parameters affecting lateral motion of the drillstring, were not captured in this step. In order to investigate the effect of the axially-vibrating downhole tools, it is required to capture the axial mode in the drillstring. Also, the entire drillstring needs to be modeled to study the pipe axial and lateral motions as well.

In the next modeling step, the entire non-rotating drillstring, including a downhole vibration generator tool, mud damping, driving torque, spatially varying axial load and Hertzian contact forces was simulated using a nonlinear coupled axial-lateral elastodynamic model. The BHA section was assumed as a three-span BHA, which results in more accurate lateral contact and lateral resonant frequency prediction. Lateral mode shapes of a three-span beam were derived analytically and implemented in the expanded Galerkin's method with the first four modes retained. The "Bypassing PDEs" method was

applied to derive the equations of motion and the equations were solved symbolically, which simplifies sensitivity analysis. The resonant frequencies and the time response of points of interest along the entire drillstring were studied. The severity of the contact at each BHA span was studied through the radial displacements and phase planes at multiple contact points. In order to validate the developed model in this step, another model with the same characteristics, dimensions, boundary conditions and interacting loads, but with a different modeling scheme was required. This directed the research towards the next modeling step.

A dynamic finite element model of the drillstring with the same characteristics of the model developed in the previous step was created. The ABAQUS FEM Explicit solver package[®] with the "kinematic friction contact" algorithm and Rayleigh damping model for the mud was used. The h-method mesh sensitivity analysis was conducted to determine the proper element length and minimize the computational time. The effective modal mass was applied in the axial and two orthogonal lateral directions to validate the number of modes retained in the analytical model of the previous step. The resonant frequencies and time responses from both models showed excellent agreement. Also, the contact locations assumed in the analytical model were verified by the FEM model and both models demonstrated the same contact severities at the contact locations. The FEM model is easily reconfigurable for different drillstring geometries, and can accommodate more complex, nonlinear phenomena and more interactions. In order to decouple the imposed vibration induced by the downhole axially vibrating tools, a shock sub must be

implemented. Also, the bit rock-interaction needs to be addressed in the model for proper selection of shock sub parameters.

In the last modeling step, analytical and numerical modeling schemes were used to develop an elastodynamic and an FEM model of the coupled axial-lateral vibrations of a rotating drillstring with a multi-span BHA in presence of the downhole vibration generator tool and a shock sub. The "Bypassing PDEs" method, along with the expanded Galerkin's method and the Lagrange's equation, was implemented to derive the analytical model. The lateral comparison functions for the mode shapes approximation technique were derived analytically. Also, the axial comparison functions for a system of hybrid continuous (the entire step-beam drillstring) and discrete elements (shock sub elements and equivalent mass-spring-damper of the top hoisting system) were developed analytically. The FEM model was specifically developed using the *Explicit* solver package of ABAQUS[®], with "kinematic friction algorithm" and "general contact surface detection" method. The mud damping, spatially varying axial force, driving torque, downhole axial vibratory tool, bit-rock interaction and a shock sub were captured in both models and the nonlinear coupling terms due to contact, axial stiffening and torque were retained in the analytical model. Time histories of the axial displacement, two orthogonal lateral displacements, contact locations and severities, critical rotary speeds and the developed forces were extracted for several points along the drillstring and they were in agreement in both models. The shock sub showed significant decoupling and isolation of the tool vibration over an extensive range of the drillstring rotary speeds and with the softening of the shock sub's spring, the vibration suppression was more efficient. It was

also conducted that the simultaneous use of a shock sub with a downhole vibration generator tool results in a more enhanced cutting force at the bit.

8.3 Dissertation Highlights and Contributions

- Development of a nonlinear elastodynamic model of the coupled axial-lateral vibrations of the entire rotating drillstring with the following features
 - Downhole axial vibration generator tool and shock sub
 - Mud damping, driving torque, spatially varying axial force along the drillstring
 - Bit-rock interaction as a displacement boundary condition at the bit location
 - Nonlinearities due to strain energy, geometry and axial stiffening
 - Hertzian contact at the contact points
 - Multi-span BHA
 - Application of the “Bypassing PDEs” method to derive the equations of motion
 - Multi-mode approximation with the expanded Galerkin's approximation
 - Symbolic solution of all analytical equations to facilitate sensitivity analysis
- Deliverables of the analytical model
 - Modal contents (mode shapes and natural frequencies)

- Time history of any point on the drillstring, including multiple contact points
- Prediction of contact at multiple possible points on the multi-span BHA
- Demonstrating the vibration suppression ability of the implemented shock sub
- Development of a nonlinear dynamic finite element model of the of the entire rotating drillstring with the following features
 - Downhole axial vibration generator tool and shock sub
 - Driving torque, spatially varying axial force along the drillstring
 - Bit-rock interaction as a displacement boundary condition at the bit location
 - Drillstring-wellbore contact model with the "kinematic friction algorithm"
 - "General kinematic contact algorithm" was used to determine all contact points
 - Mud damping model as Rayleigh damping model
 - Mesh sensitivity analysis to minimize the computational cost
 - *Explicit* solver package for conducting the simulations
- Deliverables of the FEM model
 - Determining modal contents of the drillstring

- Mass participation factor, modal mass and effective modal mass values
- Dynamic response of any point on the drillstring, including the contact point
- Capturing the developed axial bit-rock force in the presence of all interacting loads
- Prediction of contact at multiple possible points on the multi-span BHA
- Demonstrating the vibration suppression ability of the implemented shock sub

8.4 Future Research Recommendations

The following extensions and enhancement are suggested to extend the current models for further applications:

- Capturing the torsional mode of the drillstring and considering the frictional torque developed between the drillstring and the borehole to study the forward and backward whirl phenomena:

The mass unbalance in a rotating drillstring causes centrifugal forces, and bowing of the drillstring, which causes whirling. If the torsional mode is captured in the drillstring vibration study and frictional torque (rolling contact) between the drillstring and borehole included in the equations, it allows for whirling study of the drillstring. In order to capture this

phenomenon, the torsional mode needs to be captured and the impact model needs to be modified to include rolling contact.

- Tuning the bit-rock interaction model based on field test or laboratory experiments:

The amplitude and frequency of the bit-displacement boundary condition assumed in this study is based on values reported in the literature. In order to implement this model for further laboratory tests or field trials in a certain formation, it is recommended to tune the assumed amplitude and frequency using data provided by experimental facilities.

- Assumption of fluid flow inside and outside of the drillstring:

The internal and external mud flow does not have a considerable effect on the axial and torsional natural frequencies and steady state response of the drillstring in these modes in vertical wells. However, capturing the mud flow can result in a more realistic model.

- Modifying the models for directional drilling applications and investigation of appropriate friction models for inclined wellbores:

In deviated wellbores, modeling the contact between the lower side of the drillstring and the wellbore (friction modeling), and implementing torque and drag forces are the most challenging concepts. Many studies by others have undertaken to develop torque-drag models in vibration modeling of the drillstring in inclined wellbores. The developed torque-drag models are static models, useful for pulling pipe out, lowering it down, or drilling

without vibration. These models would need to be modified for capturing dynamic nonlinear friction effects in vibrating drillstrings, and the modified models would need to be incorporated into the FEM and analytical models of this thesis.

- Tuning the models for further field application based on MWD data from field tests:

MWD tools provide useful information about the vibration trend of the drillstring down the hole. The assumptions and simplifications made in the developed models in this thesis could potentially be verified and tuned using data provided by MWD tools.

Appendix 1: Buoyant Force Treatment in the Drillstring

A1.1: Introduction

There are two different points of views to treat the static loads resulting from the buoyant force of the mud on the drillstring: The Archimedes's law and the concept of effective tension.

If the buoyant force due to the mud is treated with the Archimedes's law, there will be a distributed buoyant force acting on the entire body equal to the weight of the drilling mud displaced by the drillstring.

On the other hand, the effective tension is based on the submerged weight of the body. In the effective tension point of view "the drillstring does experience a vertical force at the bottom end which is equal to $\rho_{mud} gAL$. This concentrated vertical upward force combines with the distributed weight of the drillstring" [1].

If the buoyant force is treated with the Archimedes's law, there will be no axial force in the drillstring at a specific elevation above the bottom which is not correct in the applied drilling. For further explanation of this fact, consider the following example:

"Consider a solid body which has the same density as water; an athletic swimmer is a reasonable approximation of this. Considering buoyancy as a distributed force (in the Archimedean sense) would now yield an effective tension in this swimmer's body that would be zero, independent of the depth to which he or she might happen to dive. As anyone who has suddenly plunged into a pool has probably discovered, this is not the

case. Indeed, as one dives rapidly deeper into the water the external pressure trying to crush one's body only gets larger. This observation supports the external pressure form of buoyancy argument rather than Archimedes' approach. Apparently, the external pressure form is better for revealing the actual true stress in the submerged body, just as with the rapidly diving swimmer." [1]

This fact is also verified by Bourgoyne *et al.* [2] in the SPE drilling handbook. After comparing two points of views for treating the hydrostatic force, they have concluded that: "When axial force must be determined, the effective point of application of the hydrostatic pressure must be considered and Archimedes's relation cannot be used." [2]

The presence of the concentrated force is also verified by Mitchell *et al.* [3] in the SPE's newly published textbook. They have drawn the free body diagram of the drillstring (Figure A1-1). Two concentrated forces, namely F_1 and F_2 are considered at the top and bottom of the drill collars cross sectional area, respectively. These two forces are stated as "hydrostatic pressures acting on surfaces perpendicular to drillstring axis".

A1-2: Derivation of the Spatially Varying Axial Force along the Drillstring

Using the effective tension point of view as discussed above, the equilibrium equation is written for the entire drillstring for the FBD diagrams shown in Figure A1-2. The abbreviations are explained in Table A1-1.

If the entire drillstring is assumed under equilibrium (FBD #1), the following equilibrium equation is written along the z axis:

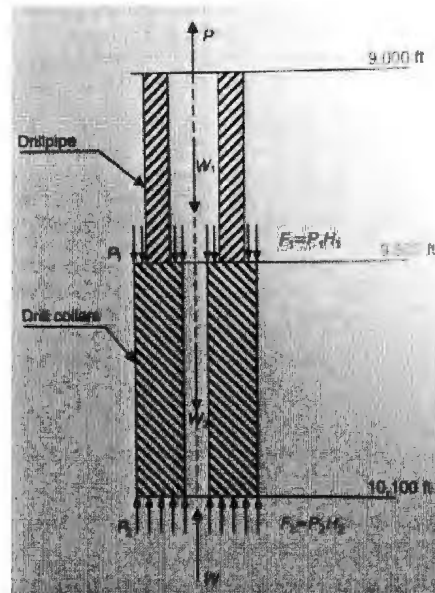


Figure A1.1: Free body diagram of the drillstring [3]

Table A1-1: Abbreviations used in Figure A1.2

$F_{\text{Hydrostatic1}}$	Hydrostatic force at the bottom of collar section	L_p	Length of the pipe section
$F_{\text{Hydrostatic2}}$	Hydrostatic force at the pipe-collar junction	L_c	Length of the collar section
WOB	Weight on bit	L	Entire length of drillstring
W_c	Weight of the collar section	F_{pipe}	Axial force in the pipe section
W_p	Weight of the pipe section	F_{collar}	Axial force in the collar section
F_{hook}	Hook load	z	Longitudinal axis along the drillstring

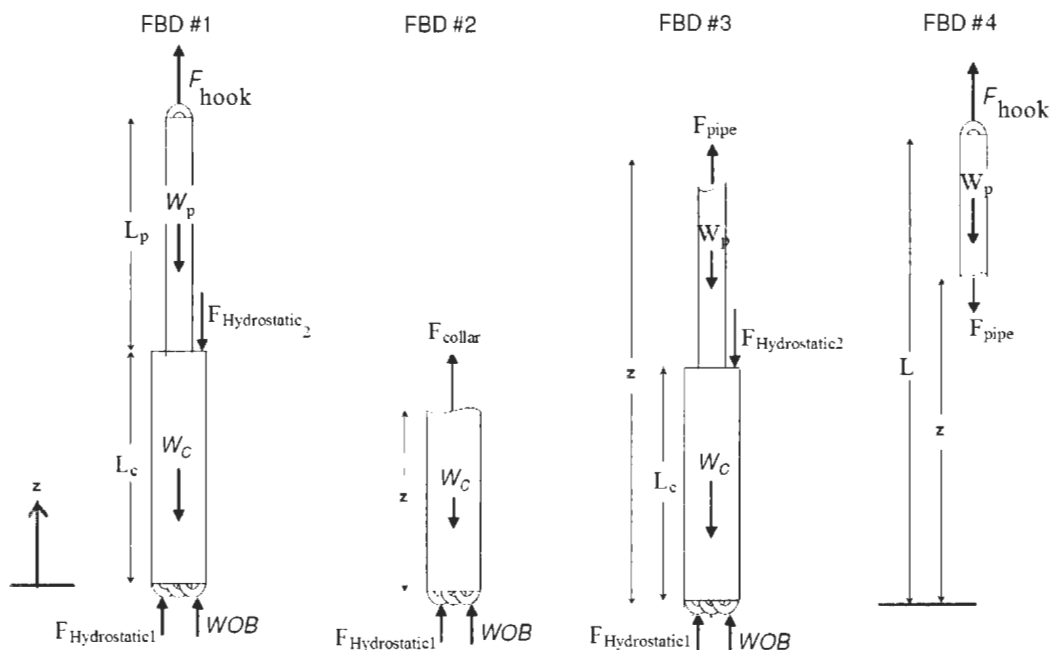


Figure A1-2: Free body diagram of the drillstring

$$\sum F_z = WOB + F_{Hydrostatic1} + F_{hook} - W_p - W_C - F_{Hydrostatic2} = 0 \quad (A1.1)$$

In order to find the axial force along the collar section, FBD #2 is assumed and the equilibrium equation in the z direction for this section is:

$$F_{collar} = -WOB - F_{Hydrostatic1} + W_C \quad (A1.2)$$

Considering this fact that the $F_{Hydrostatic1}$ is the resultant force due to the mud column pressure at the bottom of the collar section and assuming the weight of the collar section up to the section cut, these two forces are expanded and Equation A1.2 is written as:

$$F_{collar} = -WOB - \rho_{mud}gLA_{collar} + \rho_{collar}A_{collar}gz \quad (A1.3)$$

In order to find the axial force distribution in the pipe section, FBD #3 is considered and the equilibrium equation is written in the z direction as:

$$F_{ppe} = -WOB - F_{Hydrostatic1} + F_{Hydrostatic2} + W_c + W_p \quad (A1.4)$$

Knowing this fact that $F_{Hydrostatic2}$ is applied at the drill pipe-collar junction and is computed from the cross sectional area difference between the drill pipe and drill collar, multiplied by the hydrostatic pressure in the mud column at that depth, Equation A1.4 is expanded as:

$$F_{pipe} = -WOB - \rho_{mud}gL A_{collar} + \rho_{mud}gL_p(A_{collar} - A_{pipe}) + \rho_{collar}A_{collar}gL_c + \rho_{pipe}A_{pipe}g(z - L_c) \quad (A1.5)$$

This is one notation for the axial force distribution in the pipe section derived from considering the lower section (FBD #3) at the pipe section. Another section which could be assumed to find the axial force in the pipe section is the remaining top section (FBD #4). Considering the subject of internal force in the sections, the internal forces in both top and bottom sections have the same magnitude and are in the opposite directions.

Writing the equilibrium equation for the top section in the z direction:

$$F_{pipe} = F_{hook} - \rho_{pipe}A_{pipe}g(L - z) \quad A1.6$$

If F_{hook} is substituted in this equation from static equilibrium for the entire drillstring

(Equation A1.1), then Equation A1.6 will be the same as Equation A1.5:

$$F_{pipe} = (-WOB - F_{Hydrostatic1} + W_c + W_p + F_{Hydrostatic2}) - \rho_{pipe}A_{pipe}g(L - z) \quad (A1.7)$$

Expanding the terms in the above equation:

$$F_{pipe} = (-WOB - \rho_{mud}gL A_{collar} + \rho_{collar}A_{collar}gL_c + \rho_{pipe}A_{pipe}gL_p + \rho_{mud}gL_p(A_{collar} - A_{pipe})) - \rho_{pipe}A_{pipe}g(L - z) \quad (A1.8)$$

Rearranging the above equation and knowing that $L = L_p + L_c$, Equation A1.7 is simplified as:

$$F_{pipe} = -WOB - \rho_{mud}gL A_{collar} + \rho_{mud}gL_p(A_{collar} - A_{pipe}) + \rho_{collar}A_{collar}gL_c + \rho_{pipe}A_{pipe}g(z - L_c) \quad (A1.9)$$

which is exactly the same as Equation A1.5. Since the static equilibrium has been assumed for the entire drillstring, there is no difference between Equation A1.5 and Equation A1.6.

References

- [1] Journée J. M. J., Massie, W. W., 2001, *Offshore hydromechanics*, 1st edition, Delft University of Technology Press, Delft, Netherlands.
- [2] Bourgoyne, A. T., Chenevert, M. E., Millheim, K. K., and Young, F. S., 1986, *Applied Drilling Engineering*, SPE Text Book Series, Society of Petroleum Engineers, Texas, USA.
- [3] Mitchell, R. F., and Miska, S. Z., 2011, *Fundamentals of Drilling Engineering*, SPE textbook series, Texas, USA, Chap. 10.

Appendix 2: Hamilton's Principle and Lagrange's Equation

A2.1: The Principle of Virtual Work

The principle of virtual work is essentially a statement of static equilibrium of a mechanical system. Before any further discussion, it is necessary to introduce the concept of virtual displacements. Assuming that the position of a point in a N dimensional space is given by $r_i (i = 1, 2, \dots, N)$, the virtual displacement is defined as imagined infinitesimal changes $\delta r_i (i = 1, 2, \dots, N)$ in the position, which are consistent with the constraints of the system. The virtual displacements are not true displacements, but small variations in the system coordinates resulting from imagining the system in a slightly displaced position. In contrast to true displacement, this process does not involve any changes in time. Therefore, the forces and constraints do not change during this process.

A2.2: Lagrange's Equation

For most discrete mechanical systems, the potential energy can be expressed in terms of the generalized coordinates, $q = (q_1, q_2, \dots, q_N)$, while the kinetic energy can be expressed in terms of the generalized coordinate vector, q , and its first time derivative. In addition, the virtual work which is performed by non conservative forces as they act through the virtual displacements, caused by arbitrary set of variations in the generalized coordinates, can be expressed as a linear function of those variations. Once these scalar functions are expressed in terms of generalized coordinates, the well-known Lagrange's equation is [1]:

$$\frac{\partial}{\partial t} \left(\frac{\partial T}{\partial \dot{q}_i} \right) - \frac{\partial T}{\partial q_i} + \frac{\partial V}{\partial q_i} = Q_i \quad i = 1, 2, \dots, n \quad (\text{A2.1})$$

where T is the kinetic energy, V is the potential energy of the system including both strain and potential of any conservative external force. Q_1 , Q_2 and Q_n are the generalized forces corresponding to the coordinates q_1 , q_2 and q_n .

However, the situation is more complicated in the case of distributed systems, because there are at least two independent variables instead of one. In addition, the potential energy of the distributed systems is usually a function of not only the generalized coordinates alone, but also the spatial derivatives.

For distributed systems kinetic and potential energies, in terms of generalized coordinates, can be written as [1]:

$$\begin{aligned} T &= \int_0^L \hat{T}(\dot{q}) dx \\ V &= \int_0^L \hat{V}(q, q', q'') dx \end{aligned} \quad (\text{A2.2})$$

where \hat{T} and \hat{V} are kinetic and potential energy intensities, respectively. Moreover, the virtual work is simply:

$$\delta W_{nc} = \int_0^L f(x, t) \delta q dx \quad (\text{A2.3})$$

where $f(x, t)$ is a vector of generalized forces corresponding to generalized coordinate, q . Notice that concentrated forces can be expressed as distributed by means of spatial Dirac

delta functions. The extended Hamilton's principle, requires variation of the Lagrangian $L = T - V$. Therefore [1]:

$$\delta L = \int_0^l \delta \hat{L} dx = \int_0^l \left(\frac{\partial \hat{L}}{\partial q} \delta q + \frac{\partial \hat{L}}{\partial q'} \delta q' + \frac{\partial \hat{L}}{\partial q''} \delta q'' + \frac{\partial \hat{L}}{\partial \dot{q}} \delta \dot{q} \right) dx \quad (\text{A2.4})$$

It is essential to carry out integration by parts with respect to x and t . First, integration with respect to t will be:

$$\int_{t_1}^{t_2} \frac{\partial \hat{L}}{\partial \dot{q}} \delta \dot{q} dt = \frac{\partial \hat{L}}{\partial \dot{q}} \delta q \Big|_{t_1}^{t_2} - \int_{t_1}^{t_2} \frac{\partial}{\partial t} \left(\frac{\partial \hat{L}}{\partial \dot{q}} \right) \delta q dt = - \int_{t_1}^{t_2} \frac{\partial}{\partial t} \left(\frac{\partial \hat{L}}{\partial \dot{q}} \right) \delta q dt \quad (\text{A2.5})$$

Note that the assumption that δq is zero at $t=t1-t2$ is used here. The next step is to carry out integration by parts with respect to x . It is assumed that differentiation and variation are interchangeable; Hence [1]:

$$\begin{aligned} \int_0^l \frac{\partial \hat{L}}{\partial q'} \delta q' dx &= \int_0^l \frac{\partial \hat{L}}{\partial q'} \frac{\partial}{\partial x} \delta q dx = \frac{\partial \hat{L}}{\partial q'} \delta q \Big|_0^l - \int_0^l \frac{\partial}{\partial x} \left(\frac{\partial \hat{L}}{\partial q'} \right) \delta q dx \\ \int_0^l \frac{\partial \hat{L}}{\partial q''} \delta q'' dx &= \frac{\partial \hat{L}}{\partial q''} \delta q' \Big|_0^l - \frac{\partial}{\partial x} \left(\frac{\partial \hat{L}}{\partial q''} \right) \delta q \Big|_0^l + \int_0^l \frac{\partial^2}{\partial x^2} \left(\frac{\partial \hat{L}}{\partial q''} \right) \delta q dx \end{aligned} \quad (\text{A2.6})$$

Introducing the above equations into Hamilton's principle (this subject will be discussed right after this section):

$$\begin{aligned} \int_{t_1}^{t_2} \left\{ \left[\frac{\partial \hat{L}}{\partial q'} \delta q \Big|_0^l + \frac{\partial \hat{L}}{\partial q''} \delta q' \Big|_0^l - \frac{\partial}{\partial x} \left(\frac{\partial \hat{L}}{\partial q''} \right) \delta q \Big|_0^l \right] + \right. \\ \left. \int_0^l \left[\frac{\partial \hat{L}}{\partial q} - \frac{\partial}{\partial x} \left(\frac{\partial \hat{L}}{\partial q'} \right) + \frac{\partial^2}{\partial x^2} \left(\frac{\partial \hat{L}}{\partial q''} \right) - \frac{\partial}{\partial T} \left(\frac{\partial \hat{L}}{\partial \dot{q}} \right) + f(x, t) \right] \delta q dx \right\} dt = 0 \end{aligned} \quad (\text{A2.7})$$

At this point, the arbitrariness of the virtual displacement is invoked. Let

$\delta q(0,t) = \delta q(L,t) = 0$ and $\delta q'(0,t) = \delta q'(L,t) = 0$, and conclude that the above equation is satisfied for all values of δq with $x \in (0, L)$ if and only if [1]:

$$\frac{\partial \hat{L}}{\partial q} - \frac{\partial}{\partial x} \left(\frac{\partial \hat{L}}{\partial q'} \right) + \frac{\partial^2}{\partial x^2} \left(\frac{\partial \hat{L}}{\partial q''} \right) - \frac{\partial}{\partial t} \left(\frac{\partial \hat{L}}{\partial \dot{q}} \right) + f(x,t) = 0 \quad (\text{A2.8})$$

Boundary conditions may be derived from:

$$\frac{\partial \hat{L}}{\partial q'} \delta q \Big|_0^L + \frac{\partial \hat{L}}{\partial q''} \delta q' \Big|_0^L - \frac{\partial}{\partial x} \left(\frac{\partial \hat{L}}{\partial q''} \right) \delta q \Big|_0^L = 0 \quad (\text{A2.9})$$

Boundary conditions are obtained by considering that either $\delta q(0,t)$ or its coefficients are zero and either $\delta q'(0,t)$ or its coefficient is zero. Similar statements can be made about conditions at $x=L$. The above equation represents the Lagrange's equation of motion for distributed parameter systems with Lagrangian given by $L = T - V$, where T and V are defined above.

It is worth noting that the Lagrange's equation was derived for systems with Lagrangian given by T and V . Possible sources of potential energy at the boundaries, such as springs, were not considered in this equation. In cases where such devices are attached to the boundaries, the potential energy due to these devices can be included to the expression for potential energy. Inclusion of these terms will not affect the Lagrange's equation, but changes the boundary conditions for that particular system.

A2.3: Hamilton's Principle

Hamilton's principle holds for any mechanical system subjected to monogenic forces and *holonomic* constraints. By contrast to the Lagrange's equation, it applies for systems characterized by infinitely many degrees of freedom, such as continuous or distributed systems. By Hamilton's principle [2]:

$$\delta H = 0 \quad \text{where} \quad H = \int_{t_1}^{t_2} L dt = \int_{t_1}^{t_2} \delta(T - V + W_{nc}) dt = 0 \quad (\text{A2.10})$$

This approach has the advantage of being independent of the coordinates used, when contrasted with other approaches, such as the Lagrangian. In addition, Hamilton's principle permits the derivation of equations of motion from scalar energy quantities in a variational form. In the above equation, W_{nc} denotes work done by non conservative forces acting on system, including damping and any arbitrary external loads. The symbol δ indicates variation taken during indicated time interval.

This principle states that the variation of the potential and kinetic energy plus the variation of work done by the non conservative force during any time interval $[t_1, t_2]$ must be equal to zero. Application of this principle leads to the equation of motion for any given system. This approach enjoys the advantage of dealing solely with scalar quantities such as kinetic and potential energies.

In other words, this principle states that the motion of a mechanical system, from an initial configuration at time t_1 to a final configuration at time t_2 , occurs in such a manner that the integral action attains a stationary value with respect to arbitrary admissible

variations of system configurations. At static equilibrium, the kinetic energy vanishes and the potential energy becomes independent of time. Hamilton's principle then reduces the principle of minimum potential energy. Also, one can deduce Lagrange's equation from Hamilton's principle. Some definitions which are required are:

Monogenic forces are derivable from a scalar quantity. This scalar is typically some work or energy function. For example the spring force kx in a linear spring is monogenic, since it could be derived from energy function $\frac{kx^2}{2}$ by differentiation. Forces that cannot be derived from a scalar quantity (such as frictional force) are polygenic.

Holonomic constraints express relations between the system coordinates in a finite form. That is $a_1q_1 + a_2q_2 = 0$ is a *holonomic constraint*, whereas $a_1dq_1 + a_2dq_2 = 0$ is a *non-holonomic constraint* since non-finite differentials dq_j are involved [3].

A variational of a function is a virtual infinitesimal change of all function values. This change, by contrast to the infinitesimal d-process of ordinary calculus, is not caused by an actual change of an independent variable, but is imposed on a set of independent variables as kind of mathematical experiment. For a deformation pattern $u(x)$, if all values of u are changed by a slight amount $\delta u(x)$, the result is the variation of $u(x)$. An admissible variation satisfies the boundary condition of the problem. Thus $\delta u = 0$ at boundaries, when $\delta u(x)$ is an admissible variation of $u(x)$.

Certain rules apply for the calculus of variation of functionals. For example, the first variation δf of a functional $F(x, y(x), y'(x), y''(x), \dots, y^{(n)}(x))$ is given by a simple chain rule [2]:

$$\delta F = \frac{\partial F}{\partial y} \delta y + \frac{\partial F}{\partial y'} \delta y' + \frac{\partial F}{\partial y''} \delta y'' + \dots + \frac{\partial F}{\partial y^{(n)}} \delta y^{(n)} \quad (\text{A2.11})$$

Expressions for strain energy are required, when using Hamilton's principle for elastic structures. For one dimensional bending of beams, the strain energy per unit beam length is $\frac{M^2}{2EI}$.

In the next Appendix, an illustrative example will be solved using Hamilton's principle and Lagrange's equation.

References

- [1] Meirovitch, L., 1967, *Analytical methods in vibration*, 1st edition, The McMillan Company, New York, USA.
- [2] Thomsen, J. J., 2003, *Vibrations and Stability*, 2nd ed., Springer, Berlin, Germany.
- [3] Meirovitch, L., 2001, *Fundamentals of vibration*, 1st edition, McGraw-Hill higher education Company, New York, USA.

Appendix 3: Hamilton's Principle versus the "Bypassing PDEs"

Method for Continuous Systems- A Case Study

In the following section, two different energy methods, namely the conventional Hamilton's principle and the "Bypassing PDEs" method will be discussed through a comprehensive example and the results of both methods will be compared.

A3.1: Hamilton's Principle

The equations of motion governing the single-plane transverse vibration of a beam with a point load time-varying force and a concentrated mass will be derived, using the conventional Hamilton's principle. The beam is shown in Figure A3.1:

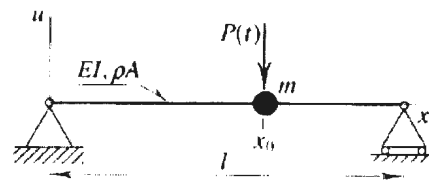


Figure A3.1: Simply supported beam in transverse motion [1]

The beam is pin supported at both ends and a time varying point load ($P(t)$) is applied at point x_0 along the beam. A concentrated mass is also located at the same point. The lateral motion is in the u direction and the coordinate along the beam length is x . The stiffness of the beam is EI , the density of the beam is ρ and the length of the beam is denoted by l . In order to derive the Lagrangian of the system, the kinetic and potential energy equations of the system needs to be derived first. The kinetic energy of the system is:

$$T = \frac{1}{2} \int_0^l \rho A \dot{u}^2 + m \delta(x - x_0) (\dot{u}(x_0, t))^2 dx = \frac{1}{2} \int_0^l \rho A + m \delta(x - x_0) \dot{u}^2 dx \quad (\text{A3.1})$$

And the potential energy of the system is defined as:

$$V = \int_0^l \frac{1}{2} EI (u'')^2 + P(t) \delta(x - x_0) u dx \quad (\text{A3.2})$$

In the above equations, $\delta(x)$ is the Dirac's delta function. The Lagrangian is defined as

$L=T-V$ and in the variational form as:

$$L = \int_0^l h(x, t, u, \dot{u}, u'') dx \quad (\text{A3.3})$$

The Hamiltonian for the time span of t_1 to t_2 is defined as $H = \int_{t_1}^{t_2} L dt$. Therefore, h for

the above system can be defined as $h = \frac{d}{dt} (T - V)$:

$$h = \frac{1}{2} (\rho A + m \delta(x - x_0) \dot{u}^2) - \frac{1}{2} EI (u'')^2 - P(t) \delta(x - x_0) u \quad (\text{A3.4})$$

In order to implement the Hamilton's principle, the variational form of Hamiltonian (H) is required:

$$\delta H = \int_{t_1}^{t_2} \delta L dt = \int_{t_1}^{t_2} \delta \int_0^l h dx dt \quad (\text{A3.5})$$

$$= \int_{t_1}^{t_2} \int_0^l \delta h dx dt = \int_{t_1}^{t_2} \int_0^l \left(\frac{\partial h}{\partial u} \delta u + \frac{\partial h}{\partial \dot{u}} \delta \dot{u} + \frac{\partial h}{\partial u''} \delta u'' \right) dx dt$$

Integration of part is used to express all the terms in Equation A3.5 in terms of virtual displacement $\delta(u)$. For the terms inside the above integral containing δu :

$$\begin{aligned}
\int_0^l \int_{t_1}^{t_2} \frac{\partial h}{\partial \dot{u}} \delta \dot{u} dx dt &= \int_0^l \left(\int_{t_1}^{t_2} \frac{\partial h}{\partial \dot{u}} \delta \dot{u} dt \right) dx = \int_0^l \left(\left[\frac{\partial h}{\partial \dot{u}} \delta u \right]_{t_1}^{t_2} - \int_{t_1}^{t_2} \frac{\partial}{\partial t} \left(\frac{\partial h}{\partial \dot{u}} \right) \delta u dt \right) dx \\
&= \int_0^l \left(\left[\rho A + m \delta (x - x_0) \dot{u} \delta u \right]_{t_1}^{t_2} - \int_{t_1}^{t_2} (\rho A + m \delta (x - x_0)) \ddot{u} \delta u dt \right) dx
\end{aligned} \tag{A3.6}$$

And the integration for $\delta u''$ is similarly conducted using the integration by part:

$$\begin{aligned}
\int_{t_1}^{t_2} \int_0^l \left(\frac{\partial h}{\partial u''} \delta u'' \right) dx dt &= \int_{t_1}^{t_2} \left(\left[\frac{\partial h}{\partial u''} \delta u' \right]_0^l - \int_0^l \frac{\partial}{\partial x} \left(\frac{\partial h}{\partial u''} \right) \delta u' dx \right) dt \\
&= \int_{t_1}^{t_2} \left(\left[\frac{\partial h}{\partial u''} \delta u' \right]_0^l - \left[\frac{\partial}{\partial x} \left(\frac{\partial h}{\partial u''} \right) \delta u \right]_0^l + \int_0^l \frac{\partial^2}{\partial x^2} \left(\frac{\partial h}{\partial u''} \right) \delta u dx \right) dt \\
&= \int_{t_1}^{t_2} \left([-EIu'' \delta u']_0^l - [-EIu''' \delta u]_0^l + \int_0^l -EIu'''' \delta u dx \right) dt
\end{aligned} \tag{A3.7}$$

The above two integrals can be simplified, using the boundary conditions of the beam.

Since δu is zero for any time interval, the first term of Equation A3.6 is zero. The first term inside the integral of Equation A3.7 is also zero, since EIu'' (bending moment) is zero for both integral interval limits. Moreover, the second term in Equation A3.7 is zero, because the virtual deformation (δu) is zero for any time interval. Simplified Equations A3.6 and A3.7 are substituted back in Equation A3.5 and the result is:

$$\delta H = \int_{t_1}^{t_2} \int_0^l \left(-P(t) \delta (x - x_0) - (\rho A + m \delta (x - x_0)) \ddot{u} - EIu'''' \right) \delta u dx dt \tag{A3.8}$$

Since $\delta(H)$ is zero for any virtual displacement ($\delta(u)$), Equation A3.8 can be simplified to the following form:

$$(\rho A + m \delta (x - x_0)) \ddot{u} + EIu'''' + P(t) \delta (x - x_0) = 0 \tag{A3.9}$$

The above equation is the equation of motion of the system in the transverse direction u .

For solution of the above PDE equation, an approximate method is required to convert the PDE to ODE. In the approximation technique, the dependent variable of the PDE ($u(x,t)$) in the above equation, is approximated by the following equation:

$$u(x,t) = \sum_{j=1}^N q_j(t) * \varphi_j(x) \quad (\text{A3.10})$$

where $\varphi_j(x)$ is a trial function, which could be an eigenfunction, a test function (also the called the comparison function) or an admissible function, determined based on the solution of the free vibration equation. $q_j(t)$ is called the mode participation factor or normal coordinates. A detailed review of the approximate solution techniques also can be found in section 2.9 of the thesis. Let's set the concentrated mass m to zero for simplicity in the trial function assumption and add a viscous damping term to equation A3.9:

$$\rho A \ddot{u} + c \rho A \dot{u} + E I u'''' + P(t) \delta(x - x_0) = 0 \quad (\text{A3.11})$$

If Equation A3.10 is substituted in Equation A3.11 and all the terms are multiplied by $\varphi_i(x, t)$, using the mode orthogonality characteristic and conducting the integration, then the result is the following equation:

$$\rho A \int_0^l \varphi_i \sum_j \ddot{q}_j \varphi_j dx + c \rho A \int_0^l \varphi_i \sum_j \dot{q}_j \varphi_j dx + E I \int_0^l \varphi_i \sum_j q_j \varphi_j'''' dx + P(t) \int_0^l \varphi_i \delta(x - x_0) dx = 0 \quad (\text{A3.12})$$

For the system of Figure A3.1 (simply supported beam), $\varphi_j(x)$ can be set to $\sin(\frac{j\pi x}{l})$.

Therefore, this approximate function is substituted in Equation A3.12 and the result is:

$$\begin{aligned}
& \rho A \sum_j \int_0^l \varphi_i \varphi_j dx \ddot{q}_j + c \rho A \sum_j \int_0^l \varphi_i \varphi_j dx \dot{q}_j + \\
& EI \sum_j \int_0^l \varphi_i \varphi_j'''' dx q_j + P(t) \varphi_i(x_0) = 0 \\
& = \rho A \sum_j \frac{1}{2} l \delta_{ij} \ddot{q}_j + c \rho A \sum_j \frac{1}{2} l \delta_{ij} \dot{q}_j + EI \sum_j \frac{l}{2} \left(\frac{j\pi}{l} \right)^4 \delta_{ij} q_j + P(t) \varphi_i(x_0) = 0 \\
& \ddot{q}_i + c \dot{q}_i + \left(\frac{i\pi}{l} \right)^4 \frac{EI}{\rho A} q_i = -2(\rho A l)^{-1} P(t) \sin \left(\frac{i\pi x_0}{l} \right) \quad i = 1, 2, 3, \dots, N
\end{aligned} \tag{A3.13}$$

The above equation is a set of N coupled ODEs, which can be solved using a numerical solver algorithm, such as Runge-Kutta method.

A3.2: The Bypassing PDEs Method

In order to bypass the PDEs for continuous systems and acquire the time domain ordinary differential equations, the mode shape approximation technique along with the Lagrange's equation is implemented. This method is called the "Bypassing PDEs" method. In this method, trial functions in the mode shape approximation technique are substituted in the energy equations at the first step. For the system of Figure A3.1, the conventional energy terms are determined as:

$$\begin{aligned}
T &= \frac{1}{2} \int_0^l \rho A \dot{u}^2 dx = \frac{1}{2} \int_0^l \rho A \left(\sum_j \dot{q}_j \varphi_j \right)^2 dx \\
V &= \frac{1}{2} \int_0^l EI (u'')^2 dx - (-P(t) \cdot u(x_0, t)) \\
D &= \frac{1}{2} \int_0^l c \rho A \dot{u}^2 dx
\end{aligned} \tag{A3.14}$$

Where T is the kinematic energy, V is the potential energy and D is the dissipated energy.

The Lagrange's equation for the above energy terms is applied, knowing that the

Lagrangian is defined as $L=T-V$ and the Lagrange's equation is $\frac{d}{dt} \left(\frac{\partial L}{\partial \dot{q}_i} \right) - \left(\frac{\partial L}{\partial q_i} \right) + \left(\frac{\partial D}{\partial \dot{q}_i} \right) =$

0 for $i = 1$ to N . The result is:

$$\int_0^l \rho A (\varphi_i \sum_j \ddot{q}_j \varphi_j) dx + \int_0^l EI (\varphi_i'' \sum_j q_j \varphi_j'') dx + P(t) \varphi_i(x_0) + c \int_0^l \rho A (\varphi_i \sum_j \dot{q}_j \varphi_j) dx = 0 \quad (\text{A3.15})$$

If the mode shape approximation technique is applied at this step ($\varphi_i(x, t) = \sin(\frac{i\pi x}{l})$)

and the orthogonality of modes is considered, the following equation is derived:

$$\ddot{q}_i + c\dot{q}_i + \left(\frac{i\pi}{l}\right)^4 \frac{EI}{\rho A} q_i = -2(\rho Al)^{-1} P(t) \sin\left(\frac{i\pi x_0}{l}\right) \quad i = 1, 2, 3, \dots, N \quad (\text{A3.16})$$

which is the same as Equation A3.13, which was derived using the conventional Hamilton's principle in the last section. This method is accurate and workable for complicated nonlinear problems [1].

References

- [1] Thomsen, J. J., 2003, *Vibrations and Stability*, 2nd ed., Springer, Berlin, Germany

Appendix 4: FEM Modeling of the Drillstring-A Case Study

As an alternative method to derive the equations of motion of the drillstring in the complicated coupled vibration states, and investigate its vibration behavior, the FEM method can be used. In the following, a general formulation method for the FEM model of the drillstring in the transverse vibration state (without contact) will be discussed. In the following equations, the drillstring is assumed elastic, homogenous and isotropic.

The XYZ is a Cartesian coordinate system with its origin on the un-deformed element.

The xyz is the Cartesian coordinate system after deformation (Figure A4.1).

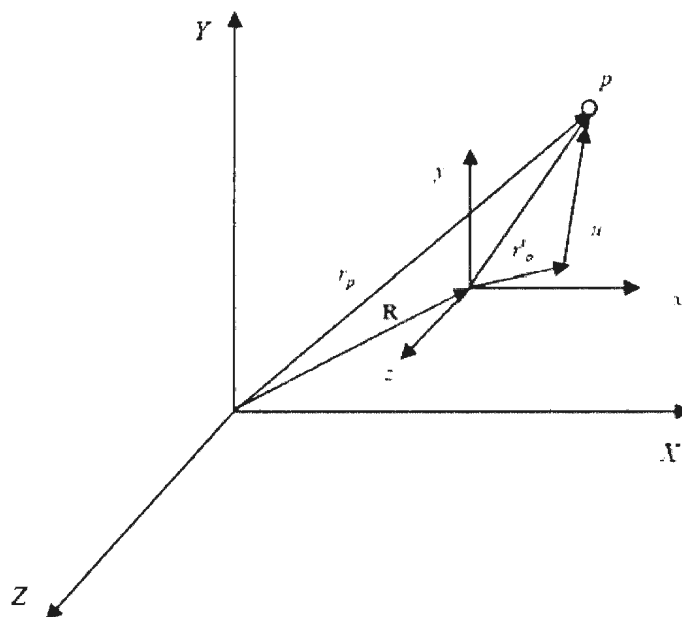


Figure A4.1: Generalized coordinates [1]

The rotation of the latter coordinate system is through rotation angles as in Figure A4.2.

The instantaneous angular velocity of the xyz frame can be stated as:

$$\omega = \dot{\varphi}I + \dot{\theta}_y j_1 + \dot{\theta}_z k_2 \quad (\text{A4.1})$$

The I , j_1 and k_2 are unit vectors along the X , y_1 and z_2 axis. If the angular velocity is transformed to the XYZ coordinate system, the following equation will be achieved [1]:

$$\omega = \begin{bmatrix} \omega_x \\ \omega_y \\ \omega_z \end{bmatrix} = \begin{bmatrix} \dot{\varphi} - \dot{\theta}_z \theta_y \\ \dot{\theta}_y \cos(\varphi) - \dot{\theta}_z \sin(\varphi) \\ \dot{\theta}_z \cos(\varphi) + \dot{\theta}_y \sin(\varphi) \end{bmatrix} \quad (\text{A4.2})$$

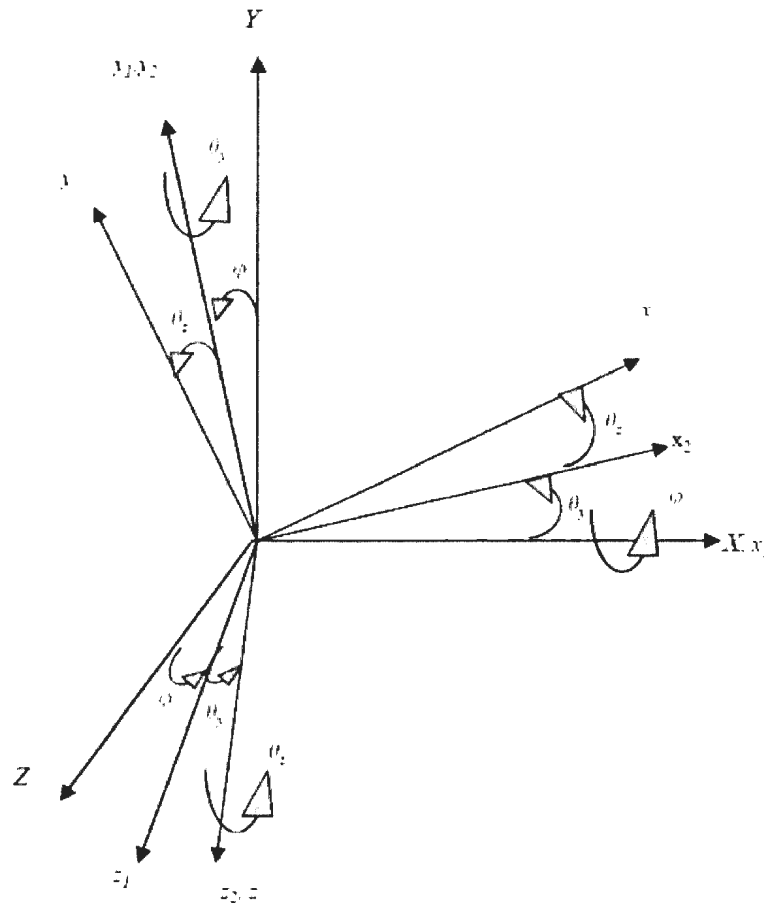


Figure A4.2: Rotation angles [1]

If the point p is on the undeformed shaft element, the global position of the point p can be stated as:

$$r_p = R + r_o + u \quad (\text{A4.3})$$

u is the deformation vector of p . the first derivative of the above equation with respect to time is:

$$\frac{dr_p}{dt} = \dot{r}_p + \omega \cdot r_p = \dot{r}_p + [\omega] \{r_p\} = [N_v] \{\dot{e}\} + [\omega] \{r_p\} \quad (\text{A4.4})$$

N is the shape matrix and e is the matrix for nodal coordinate of the finite element. The kinetic energy of the element is [1]:

$$T = \frac{1}{2} \int_v \mu \{\dot{e}\}^T [N_v]^T [N_v] \{\dot{e}\} + \{\dot{e}\}^T [N_v]^T [\omega] \{r_p\} + \{r_p\}^T [\omega]^T [N_v] \{\dot{e}\} + \{r_p\}^T [\omega]^T [\omega] \{r_p\} dV \quad (\text{A4.5})$$

The second and the third terms are zero, because of stating the moment of inertia with respect to the center of the mass of the element. The first term in the above equation is due to the translation and the last term is the result of rotation. Equation of the Kinetic energy can be simplified as [1]:

$$T = \frac{1}{2} \{\dot{e}\}^T [M_t] \{\dot{e}\} + \frac{1}{2} C \dot{\phi}^2 + \frac{1}{2} \{\dot{e}\}^T [M_\phi] \{\dot{e}\} - \dot{\phi} \{\dot{e}\}^T [G] \{e\} - \{\dot{e}\}^T [M_e] \{\dot{e}\} + \frac{1}{2} \{\dot{e}\}^T [M_r] \{\dot{e}\} \quad (\text{A4.6})$$

M_t is the translational mass matrix, M_r is the rotary inertia mass matrix, M_ϕ is the torsional-transverse inertia coupling mass matrix and G is the gyroscopic matrix [1]:

$$\begin{aligned}
[M_r] &= \int_0^l [N_r]^T \mu A [N_r] dx \\
[M_r] &= \int_0^l [N_\theta]^T I_\theta [N_\theta] dx \\
[M_\varphi] &= \int_0^l I_\rho [N]^T [N] dx \\
[M_e] &= \int_0^l (I_\rho [N_\varphi]^T [N_{\theta z}] \{e\} [N_{\theta \varphi}] - [N_\varphi]^T [N_{\theta \varphi}] \{e\} [N_{\theta z}]) dx \\
[G] &= [G^*] - [G^*]^T, \quad [G^*] = \int_0^l I_\rho [N_{\theta \varphi}]^T [N_{\theta z}] dx
\end{aligned} \tag{A4.7}$$

The strain energy of the element can be written as follows for one axial, two lateral and three rotations [1]:

$$\begin{aligned}
U_e &= U_1 + U_2 + U_3 \\
&= \frac{1}{2} \int_0^l [EA \left(\frac{du}{dx}\right)^2 + EI_z \left(\frac{\partial^2 v}{\partial x^2}\right)^2 + EI_y \left(\frac{\partial^2 w}{\partial x^2}\right)^2 + GJ \left(\frac{\partial \varphi}{\partial x}\right)^2] dx
\end{aligned} \tag{A4.8}$$

The strain energy due to the gravity effect is [1]:

$$U_s = \frac{1}{2} \int_0^l EA \left(\frac{\partial u}{\partial x}\right) \left[\left(\frac{\partial v}{\partial x}\right)^2 + \left(\frac{\partial w}{\partial x}\right)^2\right] dx \tag{A4.9}$$

Adding equations of the strain energy and knowing that for the circular cross section of the drillstring, $I_z = I_y$ [1]:

$$\begin{aligned}
U &= \frac{E}{2} \int_0^l I(x) \left[\left(\frac{\partial \theta_x}{\partial x}\right)^2 + \left(\frac{\partial \theta_z}{\partial x}\right)^2\right] dx + \frac{EA}{2} \int_0^l \left(\frac{du}{dx}\right)^2 dx + \frac{GJ}{2} \int_0^l \left(\frac{\partial \varphi}{\partial x}\right)^2 dx \\
&\quad + \frac{1}{2} \int_0^l F(x) \left[\left(\frac{\partial v}{\partial x}\right)^2 + \left(\frac{\partial w}{\partial x}\right)^2\right] dx
\end{aligned} \tag{A4.10}$$

Or in the matrix form as $U = \frac{1}{2} \{e\}^T [K] \{e\}$.

K is the stiffness matrix, which is the sum of axial stiffness matrix (K_a), torsional stiffness matrix K_q , bending stiffness matrix K_b and K_{gs} as the axial stiffening matrix

due to the gravity. K_{gs} can be divided to two separate parts according to the axial force distribution along the drillstring from tension at the upper part to the compression at the lower part [1]:

$$[K_{gs}] = \int_0^{l_i} F[B_s]^T [B_s] dx \quad \text{and} \quad [B_s] = \frac{\partial}{\partial x} [N_v] \quad (\text{A4.11})$$

The axial force along the element can be stated as [1]:

$$F_i(x) = - \left(\int_{L_p-L_i}^{L_p} \rho g A dx + \int_x^{l_i} \rho g A dx \right) \quad (\text{A4.12})$$

L_p is the length of the pipe section. Therefore, the axial force in the pipe section is [1]:

$$F_i(x) = -\rho g A [L_i + (l_i - x)] \quad (\text{A4.13})$$

And for the collar section under compression, the axial force is [1]:

$$F_c(x) = \int_0^{L_i} \rho g A dx + \int_{L_i}^{L_{i+1}} \rho g A dx \quad (\text{A4.14})$$

Utilizing the energy expressions to the variational form of the Lagrange's equation and using the conventional assembly procedure, the equation of motion of the drillstring for the finite element method can be written as $[M]\{\ddot{e}\} + [G]\{\dot{e}\} + [K]\{e\} = \{Q\}$. M is the global mass matrix, G is the gyroscopic matrix, K is the assembled global stiffness matrix and e is the deformation vector.

Reference

- [1] Khulief, Y. A., Al-Naser, H., 2005, "Finite Element Dynamic Analysis of Drillstrings," *Finite Element in Analysis and Design*, **41**(13), pp. 1270-1288.

Appendix 5: List of Assumptions in the Developed Models

The following assumptions have been made in the modeling steps 1 to 5, defined in section 1.4 of this thesis. The justification of these assumptions can be found in the body of the thesis.

- The drillstring is assumed vertical in this study and inclined drilling has not been assumed
- Euler-Bernoulli beam theory is assumed as the drillstring beam element
- Stabilizers are assumed as pinned-pinned boundary conditions in the lateral direction
- Hertzian contact theory is assumed as the impact force between the drillstring and wellbore
- Spatially varying axial load is assumed as the axial force along the drillstring
- Driving torque, hook load and WOB are assumed constant during the analysis
- The frequency and amplitude of the downhole vibration generator tool are constant values
- Mud damping in the lateral direction is modeled through the hydrodynamic drag concept
- In chapters 5 and 6, the boundary condition is assumed as fixed at top-free at the bottom in the axial direction
- In chapter 6, kinematic friction algorithm is assumed as the lateral interaction force between the drillstring and wellbore and sliding friction is neglected

- The rotation of the drillstring is neglected in chapters 3, 4, 5 and 6, but is considered in chapter 7
- The torsional mode of the drillstring and the sliding friction are neglected in this research
- Rayleigh damping model is assumed in chapter 6 and 7 for mud damping modeling in the developed FEM model
- The top point of the drillstring is assumed as an equivalent mass-spring damper boundary condition in the axial direction in chapter 7
- The bottom point of the drillstring in the axial direction is assumed as a displacement boundary condition through a sinusoidal function with constant amplitude and a constant frequency (the same as the drillstring rotary speed)

